AN INVESTIGATION OF STRETCH FORMING IN RELATION TO DEEP-DRAWING AND TESTING SHEET METAL

by

BİLGİN KAFTANOĞLU, B.Sc. (Eng.)

VOLUME - I

Thesis presented for the Awards of

DOCTOR OF PHILOSOPHY

Degree

in the

Faculty of Engineering

of

University of London

and

DIPLOMA OF IMPERIAL COLLEGE

in the

Department of Mechanical Engineering

Imperial College,

London, S.W.7.

January, 1966

ABSTRACT

A theory has been developed to obtain a general solution for the axisymmetrical stretch forming of sheet metal with clamped boundary. Factors included were plastic anisotropy in the thickness direction, non-linear strain-hardening, pre-strain, variable coefficient of friction, and an approximation to the variation of thickness stress. The effects of strain history, and the moving contact of sheet metal on the punch surface with continued deformation has been incorporated. The numerical solution was programmed for the Atlas computer. Three plastic instability criteria have been studied, one of which is an integral part of the numerical solution and is new in concept.

The theoretical results were compared with the results of stretch forming tests. Agreement was very satisfactory for all but the last few stages of deformation. Near the occurrence of plastic instability greater differences between experiment and theory were observed, but the location of the instability zone and instability strains in most cases could be accurately predicted.

Extensions to the theory to solve the hydraulic bulging and deep-drawing problems have been given, but no numerical results were obtained.

Two methods of estimating the coefficient of friction in stretch forming and in radial drawing were used. It

was found that coefficients of friction in stretch forming are considerably higher than those in radial drawing.

Experimentally obtained strain hardening curves could satisfactorily be curve-fitted to a Swift type empirical law by a computer program.

Limiting Drawing Ratio (L.D.R.) in deep-drawing could be predicted satisfactorily by an empirical method from tests of three oversize blanks.

The effect on the Erichsen number of altering the main variables has been investigated. Equivalent round and strip sizes were determined. Results showed that "drawing-in" could not be completely eliminated when using serrated surfaces on blank-holder and dies. No correlation was found between the appearance of fracture in the Erichsen test and planar plastic anisotropy.

ACKNOWLEDGEMENTS

Firstly I would like to express my gratitude to my supervisor J.M.Alexander, Professor of Engineering Plasticity, Imperial College, London, for his continued attentive interest, encouragement and very useful discussions during the course of the research so freely offered at all times.

I would also like to acknowledge the Department of Technical Co-operation for financing, and The British Council for administring the Award of a CENTO Fellowship without which it would not have been possible to carry out the required study and research.

Many thanks are due to The Institute of Computer Science, University of London for the allocation of a large amount of computer time on the Atlas and the Mercury computers, and for many helpful discussions.

Thanks are also due to I.C.I. Metals Division and the Shell International Petroleum Co., Ltd., for donating some of the sheet metals and lubricant.

CONTENTS

Page No.

Page No.

Page No.

Page No.

Page No.

Copies of the author's six publications (see references 45 to 49 in BIBLIOGRAPHY) are bound with this thesis.

NOTATION

A, B, n	constants in empirical strain-hardening equation, $X = A(B + \varepsilon_\ell)^n$.
a, b	semi-axes of an ellipsoid of revolution.
C_1, C_2	integration constants.
c	constant in equivalent anisotropic plastic strain-increment equation (eqn. 3.21).
E	Young's modulus.
D	die throat diameter.
D_b	diameter of undeformed blank in deep-drawing.
D_{cr}	critical or limiting blank diameter in deep-drawing.
F, G, H, L, M, N and $F_o, G_o, H_o, L_o, M_o, N_o$	parameters of plastic anisotropy (See eqns. 3.12 and 3.13).
F_1, F_2	radial frictional forces on a large segment of sheet metal in radial drawing (Fig.17) acting on upper and lower surfaces of the segment.
f	yield function, also a general mathematical function
F^*, $\bar{F}^*$	general mathematical functions.
g	a scalar in plastic stress-strain relationships (eqn. 3.10).
I	Erichsen number

J_1, J_2, J_3 invariants of the stress tensor σ_{ij}.

J_1', J_2', J_3' invariants of the reduced or deviatoric stress tensor $\sigma_{ij}' = \sigma_{ij} - \sigma\delta_{ij}$.

H blank-holder load.

h bulge depth, and also proportionality parameter for yield stresses for anisotropic materials (eqn. 3.13).

$K_1, K_2, \ldots, K_5$ constants in equations for plastic instability (eqns. 4.8 to 4.20).

k stress ratio $= \sigma_3/\sigma_1$.

$k_{ro}, k_{r1}, k_{r2}, k_{r3}$ intermediate quantities in Runga-Kutta integration.

ℓ steplength in numerical integration, also distance between two gauge markings on a tensile specimen.

M, N constants in empirical equation (12.1) used in determining L.D.R.

P punch load in deep-drawing and stretch forming.

p interfacial pressure between sheet metal and tool in stretch forming and deep-drawing.

p_1 interfacial pressure between sheet metal and die in deep-drawing.

p_2 interfacial pressure between sheet metal and blank-holder in deep-drawing.

Q	total load transmitted in a direction tangential to the mean surface of a bulge per radian
R	parameter of plastic anisotropy in tension = $\frac{\varepsilon_W}{\varepsilon_t}$.
r_a	current radius of rim of the blank (Fig.1).
r_b	radius to innermost point of flat portion of blank (Fig.1).
r_c	radius to centre of cup wall at point of departure from die (Fig.1).
r_d	radius to centre of cup wall at point of junction with punch profile (Fig.1).
r_e	radius of flat portion of punch head (Fig.1).
r	current radius to centre of shell wall (Fig.3).
r'	current radius to inner face of shell wall (Fig.3).
S_1, S_2, S_3	forces on a segment of sheet metal in radial drawing (See section 7.1).
s	principal stress, also degree of a polynomial.
t	current thickness of element of sheet metal.
T	time.
u	radial displacement.
V	any mathematical variable.

V_1, V_2, V_3	constants in equations for plastic bending under tension (See eqns. G.4, G.5 and G.6).
w	one less than the number of points in a tabular set of data, also width of a tensile specimen.
W	work.
X, Y, Z	yield stresses in principal directions of plastic anisotropy.
X_s, Y_s, Z_s	yield stresses in shear in the principal directions of plastic anisotropy.
x, y, z and 1, 2, 3	orthogonal co-ordinates.
x	stress ratio = $\frac{\sigma_2}{\sigma_1}$, and also independent variable.
y	dependent variable, and also co-ordinate through the thickness direction of an element in plastic bending under tension.
y_n	displacement between neutral and central surfaces in plastic bending under tension.
z	vertical co-ordinate.
α	angle, that normal to element of sheet metal makes with the vertical axis at the point of contact with punch (Fig.2).
β	rate of linear strain-hardening.
γ	angle separating two normals to the shell wall in the plane of ρ_2 (Fig.B.1).

Δ	general error function.
$\bar{\varepsilon}$, $d\bar{\varepsilon}$	total and incremental equivalent strains.
ε_ℓ, ε_w, ε_t	true strains in length, width and thickness directions in tensile test.
ε_1, ε_2, ε_3	and
$d\varepsilon_1$, $d\varepsilon_2$, $d\varepsilon_3$	total and incremental principal plastic strains also corresponding to meridional, circumferential, thickness strains in axi-symmetrical sheet metal deformation.
ε_{1b}, ε_{2b}, ε_{3b}	principal strains in plastic bending under tension in meridional, circumferential, and thickness directions.
θ	angle, that normal to an element of shell wall makes with vertical.
$d\lambda$, $d\lambda'$, $d\lambda''$	scalars in plastic stress-strain relationships.
μ	coefficient of friction.
ξ	general function in integration.
ν	Poisson's ratio.
ρ	instantaneous radius of curvature.
ρ_1	meridional radius of curvature of the mean surface of shell wall.
ρ_1'	meridional radius of curvature of the inner surface of shell wall.
ρ_2	radius of curvature in circumferential direction of the mean surface of the shell wall.

ρ'_d radius of curvature of die profile in deep-drawing.

ρ_N radius of curvature of neutral surface in plastic bending under tension.

$\bar{\sigma}$ equivalent stress.

σ_1, σ_2, σ_3 meridional, circumferential, and thickness stresses in axisymmetrical sheet metal deformation.

σ hydrostatic stress ($\sigma = \frac{1}{3}\sigma_{ii}$).

σ_{1b} mean stress in plastic bending under tension (Fig.G.1).

φ angle, that normal to an element of cup wall makes with vertical at contact with die surface in deep-drawing (Fig.1).

ψ angular co-ordinate in horizontal plane (Fig.3).

τ shear stress.

<u>Operators</u>:

δ refers to a finite increment.

d total differential.

∂ partial differential.

δ_{ij} Kronecker delta. $\delta_{ij} = 1$ when $i = j$
$\delta_{ij} = 0$ when $i \neq j$.

Δ increments at a discontinuity.

Abbreviations:

L.D.R.	limiting drawing ratio in deep-drawing.
U.T.S.	ultimate tensile strength in uniaxial tension.
D.R.	drawing ratio in deep-drawing.
F.P.	flat headed punch.
H.P.	hemispherical headed punch.

Suffices:

i, j, k, ℓ	summation convention applies over values 1, 2, and 3.
m, n	designates location of a point in space and time respectively (summation convention does not apply).
u	refers to any discrete point on yield stress curve.
v	refers to total number of points on yield stress curve.
q	number of differential equations in a system.
r	a member of a family of differential equations.

Subscripts:

p	polar values of variables in stretching over punch.

o	initial values of variables.
e	effective values of variables.
m	mean values of variables.
cr	critical values of variables.

<u>Superscripts</u>:

*	increments taken along a strain path following an element.
p	plastic state of stress.

LIST OF FIGURES

PAGE NO.

PAGE NO.

PAGE NO.

In Appendices: PAGE NO.

VOLUME -II.

LIST OF TABLES

INTRODUCTION

In any process of deforming sheet metal, force is applied to the component which is initially in the form of a plate or a shell, until the desired shape of the final or the intermediate product is reached by the plastic deformation. The amount of deformation is generally limited by either the tensile plastic instability, or plastic buckling, in regions of dominating tensile or compressive stress respectively.

The various processes can be classified by consideration of the force transmitting media:

(i) Rigid tools are used quite extensively as dies and punches especially in mass production, and are preferred to the others because of the close tolerances and good surface finish obtained. The main disadvantage is the expense of tool making, and therefore this is uneconomic for small-lot production.

The process of "stretch forming" is one in which the flow or drawing-in of the metal at the edges of a blank is prevented by rigid clamping or gripping by the use of serrated dies, or by the restraint of the undeformed metal in the flange. The punch, in the shape of the desired product, deforms the metal by moving forward.

"Deep-drawing" is different from stretch forming in that the former allows the flow of metal inwards over the die, which induces circumferential compressive stresses in the flange and over the die profile. To prevent "wrinkling", which is a mode of plastic buckling producing a wavy appearance of the flange caused by such compressive stresses, lateral pressure must be applied on the flange by a suitably shaped blank-holder.

"Pressing" is a general term for a process which contains elements of stretching and drawing-in to various degrees in different parts of a component.

(ii) Fluid is used in cases where a generally smaller number of parts with less restrictions on the final geometrical shape is required. The sheet metal is securely clamped around the edges and deformed against an external die by quasistatic or dynamic pressure provided generally by an incompressible fluid such as water. The process, in which the dynamic pressure is produced by an explosion and subsequent shock waves is known as "explosive forming". If no external die is used, then the geometry is uncontrolled and this is termed as "hydraulic bulging". In these processes the fluid acts as a punch analogous to that of item (i). The "Hydroform" process is one in which high-pressure hydraulic fluid contained behind a flexible diaphragm replaces a die.

(iii) Elastomers can be used to replace the metal dies or punches. A development of the deep-drawing process in which the metal die is replaced by a large rubber pad contained within a rigid metal container is the "Marform" process. The pad provides uniform pressure on the deformed component as it is pushed into the rubber by the punch. Although this is a fairly economical process, it requires a careful control of the blank-holding pressure.

Such processes are commonly employed in the production of symmetrical and asymmetrical shells, which do or do not bear load, and find large applications in automotive, aircraft, spacecraft and other conventional industries.

Very useful information can be gleaned by the application of the theory of plasticity to such metal deforming processes. This can be done by the study of stress systems operative in different regions of the deforming shell. In places where the sheet metal is in contact with the force transmitting medium, a tri-axial stress system will exist, the magnitude of the thickness stress being dependent upon the radius of curvature and the thickness of metal, which in many cases is small. The effects of the surface frictional stresses are important, and they modify the mode of deformation significantly, especially in stretch forming. The stresses in the plane of the sheet metal are tensile in stretching over the punch head.

Compressive circumferential stresses are associated with the inward flow of the metal as in deep-drawing. In areas where the sheet metal is exposed to the atmosphere on both sides, the system is generally tensile bi-axial, with meridional stress dominating.

Also bending under tension takes place at points where there is a sudden change of curvature as at points of departure from punch and die, which is accompanied by further thinning.

Localized compressive stresses can occur in places such as beneath the blank-holder plate and at the die throat in ironing of the cup wall in deep-drawing.

The above mentioned stress systems also interact, which increases the complexity of the problems involved. The main properties influencing the stress systems are the initial and current geometry of the shell, fundamental material properties (i.e. pre-strain, strain-hardening rate, and its variation over the range of strains involved), and operating conditions such as the rate of deformation, and lubrication.

An important function of an element of sheet metal in the course of the deformation is to transmit the load to the neighbouring element, so that the deformation can continue. Otherwise the shell will reach plastic instability and subsequently will fracture at this point. Hence the materials with more strain-hardening capacity sustain larger deformations. The converse is true for ones having large pre-strain. This effect can be made use of in deep-drawing if the flange is annealed and the centre of the blank remains strain-hardened, since due to less load being induced by the flange and the high load carrying capacity of the stretching region even larger deformations can be achieved. This heat-treatment process is known as "differential annealing". The same effect can be obtained by using heated dies and cooled punch. Also the technique of "differential lubrication" (i.e. having a higher coefficient of friction over the stretching region compared to that in the drawing region) produces the same result. Plastic anisotropy of the sheet metal has also a significant effect in the deformation process which can be used beneficially.

To understand the behaviour, and to try to predict the performance of sheet metal in any operation, four schools of thought have been adopted by previous investigators:

(i) Theoretical studies have been conducted mainly in deep drawing and hydraulic bulging which gave satisfactory results for stress and strain distributions in the deformed shell, and predicted the maximum pressure instability in hydraulic bulging, using the basic stress-strain characteristics of the materials. No realistic solution has been obtained for stretch forming, or for predicting plastic instability and fracture in this process.

(ii) Fundamental tests, such as the uniaxial tension test, with the aim of determining the basic stress-strain characteristics of the materials, anisotropic parameters, and other derived information, as a guide to "formability",* yield useful information, but they are unable to predict the behaviour of any material in a given process.

(iii) Simulative tests, to the extent possible, try to duplicate the shop-floor conditions in small-scale laboratory experiments. Generally, the choice of the test is made on the basis of the dominating stress system in the actual part, e.g. Erichsen and Swift tests for stretch forming and deep-drawing respectively. Although the ranking of materials obtained this way most often gives the right order of merit for simpler pressings, it is still quite controversial for the more complicated ones.

(iv) Metallurgical investigations were carried out to try and find correlations between the basic metallurgical properties of metals, and their performances in press operations. Recently, the "dislocation theory"

---

* The term "formability" is commonly used to mean "ability to deform".

has been applied to study the mechanism of strain-hardening relevant to sheet metal deformations.

It is, of course, desirable to have methods by which one can predict the behaviour of sheet metal in any operation from its basic stress-strain characteristic, geometrical, and operational conditions. This will reduce wastage, save time, and enable one to tailor materials for processes or change processes to suit materials. Also, better correlation criteria between the tests and practice can be found.

In this report, after a survey of previous work, a theoretical and experimental study of the plastic deformation, and an investigation of instability and fracture in the stretch forming process is presented. More refined theoretical methods are suggested for analysing drawing over the die surface in deep-drawing, and for hydraulic bulging. The determination and formulation of the basic stress-strain characteristics of the materials used (i.e. steel, brass, copper, and aluminium), and two possible methods of determining the coefficient of friction in sheet metal deformation processes are given. Also, an empirical method of estimating L.D.R. in deep-drawing, an experimental investigation of the factors influencing the Erichsen number, and some deep-drawing experiments are presented.

The Atlas and Mercury computers were extensively used for the numerical solutions obtained for stretch forming, curve-fitting to the tensile stress-strain characteristics of metals, calculations of the coefficients of friction, and processing of experimental results. The relevant methods and corresponding computer programs are included.

CHAPTER 1 - SURVEY AND DISCUSSION OF THE SUBJECT AND PREVIOUS WORK

The manufacturing methods employing sheet metal deformation processes are of great antiquity, and have been used by jewellers and armourers since the early times of history. Materials were pressed into metal dies with repeated blows from appropriately shaped punches, mainly constituting stretch forming operations. With the development of power presses, sheet metal fabrication, and automation, which led to a vast improvement of such processes, they became a vital part of today's industry. The "art" of deforming sheet metal gradually gave way to better and more efficient methods since the last century. The scientific and technological studies of such processes really started soon after the complete formulation and rediscovery of the theory of plasticity, and advances in the metallurgical sciences in the 1920's.

The pertinent investigations after this date are discussed under the appropriate section headings.

1.1. Deep-Drawing

Due to the complexity of the problem no complete investigation of deep-drawing has been yet recorded. Researches studying different aspects, mainly of the deep-

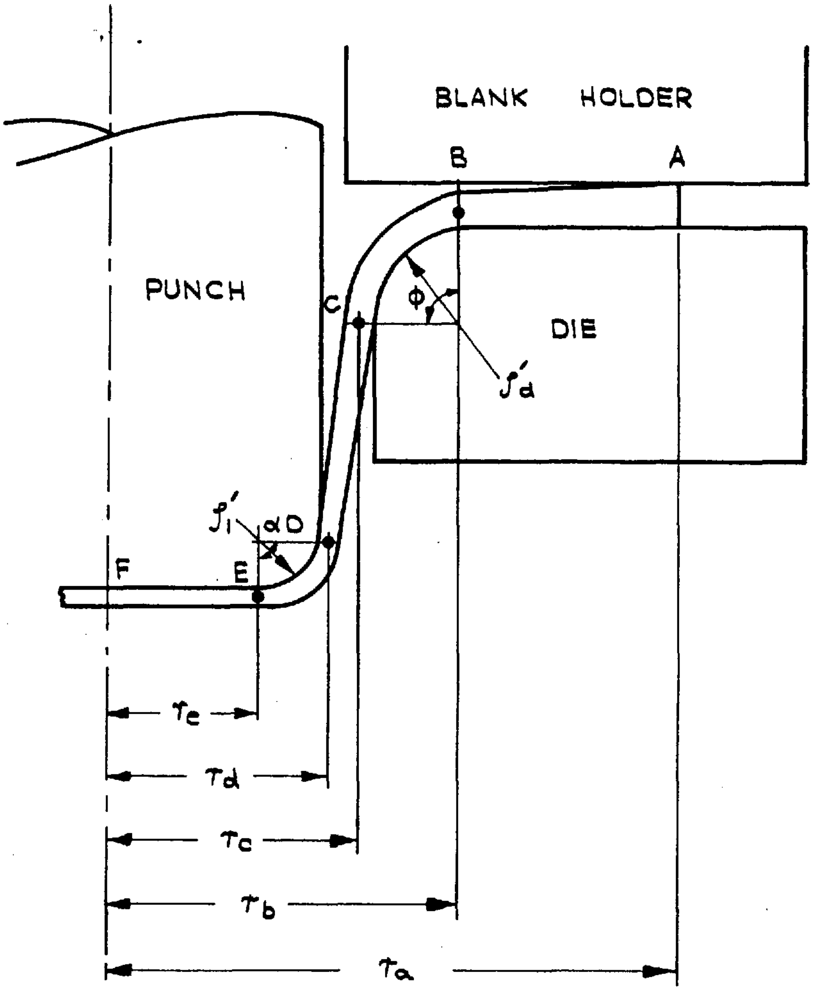

FIG. 1. NOTATION IN DEEP-DRAWING.

drawing of axisymmetrical shells, are discussed below.

1.1.1. Drawing over Die Surface

This region, sometimes referred to as the "radial drawing" region, although it may not be truly radial as in the case of the dies with curved or conical profile, is bound by the rim of the blank, point A, and the point of departure of sheet metal from the die, point C, in Fig.1.

One of the earliest researches was by Siebel and Pomp (75). In their theory, they used the Tresca criterion, the equilibrium equation to estimate the punch load and the stresses. They neglected the effects of strain-hardening, variations in thickness, friction, die profile, and blank-holding force. No attempt was made to predict the strain distribution. Sachs (72) improved this analysis by using the modified Tresca criterion, and an average value of the yield stress. Also an approximation was made to the die profile friction by using the belt formula, and he incorporated a term for the frictional force due to the blank-holder load. The calculated values of the punch loads were in fairly reasonable agreement with the experimental ones. Swift (80) proposed simplified solutions for flat and conical dies in drawing and redrawing covering non-strain-hardening and some special cases of strain-hardening materials by also including effects of variations in thickness. His results can be viewed as qualitative, and show the trends of the variables involved. Hill (38) analyzed the "pure" radial drawing process for a non-strain-hardening material and obtained an analytical formula for the thickness strain distribution under plane stress conditions, but this slightly underestimates the thickness strain near the die curvature partly owing to the bending under tension effect, as found by Loxley (59) in experiments made using 70/30 brass and aluminium.

A very comprehensive study of this problem was then undertaken by Chung and Swift (18) for isotropic materials, and it included theoretical and experimental investigations. They used the modified Tresca criterion, Levy-Mises stress-strain relationships, strain compatibility and equilibrium equations. Solutions were obtained by a step-by-step successive approximation method, for regions over flat, over curved parts of die, and between punch and die. The thickness variations in the equilibrium equations were neglected. A concentrated force due to the blank-holder was assumed to act on the rim of the blank, and the resulting frictional force was used in the calculations of the initial value of the radial stress. The circumferential strain was taken as an approximation to the equivalent strain within 3% as pointed out by Hill (38). The effect of friction on the die profile was allowed for approximately by integrating the friction term of the equilibrium equation separately. The authors included the effect of thinning and the consequent increase in the drawing stress at the die entry and exit due to plastic bending and unbending under tension. This was done by equating the back tension to the difference between the bending tension and compression, neglecting the comparatively small elastic strains. They postulated that if bending and unbending are instantaneous the metal elements would have no freedom to strain in the circumferential direction. Using the Levy-Mises stress strain relationship, it is possible to show that:

since $d\varepsilon_2 = d\lambda(\sigma_2 - \frac{1}{2}(\sigma_1 + \sigma_3) = 0$

where $\sigma_3 \approx 0$ and therefore $\sigma_2 = \frac{1}{2}\sigma_1$ which makes $\sigma_2 > 0$ since $\sigma_1 > 0$. Everywhere else in this region $\sigma_2 < 0$ and is the dominating stress. Although a discontinuity in σ_2 is expected, it seems reasonable even so to think that $\sigma_2 < 0$, which is also confirmed by the occurrence of wrinkles here without the use of a blankholder.

Also due to the constancy of volume in plastic flow, i.e. $d\varepsilon_1 + d\varepsilon_2 + d\varepsilon_3 = 0$, and since $d\varepsilon_2 = 0$ and $d\varepsilon_3 < 0$, therefore $d\varepsilon_1 > 0$. In Fig. 1, this would imply that while the material is thinning at point B, it moves the neighbouring elements on either side towards points

A and C respectively, where the former seems to be less likely. This reasoning indicates that bending under tension may not take place under exactly plane strain conditions. Although this anomaly may be resolved by considering the variations through the thickness, a better approximation may be obtained if an average stress ratio is used in the calculation as outlined in Appendix-G.

It is also found that the lower integration limit in the equation of equilibrium obtained by Chung and Swift (18) was not consistent with the sign convention adopted, and it is only valid for some values of the drawing stress. This is shown in Appendix - G and the supplementary equation is given. Since the maximum equivalent strain in bending and unbending was less than 0.11, the effects of these assumptions were not readily seen in their curves for total strains. The authors obtained satisfactory agreement between the experimental and theoretical strains, and punch loads, indicating that the assumptions made on the whole were reasonable.

More simplified versions of Chung and Swift's theory were developed by Barlow (5), and Wallace (87) which were used later by Warwick and Alexander (89) to find the wall stresses between a flat bottommed punch and die for calculations of L.D.R. Very useful apprai-sals of Chung and Swift's work and other related investigations were given by Alexander (2), and also by Johnson (43).

Fukui (28) et al and Yamada (97) studied this problem using the Hencky-Mises theory of plastic flow. This theory was shown to be incompatible for deformations involving non-linear strain-paths in the deviatoric plane by Hill (38), and Alexander (3), and therefore the authors' results should be regarded as being more approximate than those of Chung and Swift's (18). A limited number of comparisons were made by Fukui for materials obeying the Ludwik power law (i.e. $\bar{\sigma} = A(\bar{\varepsilon})^n$), which showed agreement within 10% with the experimental strains. Yamada compared the theoretical results obtained by the incremental and the total strain theories for a non-strain-hardening material and found negligible differences in the computed strains, but since the effect of strain-hardening is important for most materials, his comparisons are of limited value. Furthermore, he made no comparisons with any experimental findings.

Some of the assumptions (i.e. (i) $\frac{dt}{dr} = 0$ in the equilibrium equation, (ii) blank-holding force acting only on the rim, and (iii) $\bar{\varepsilon} = |\bar{\varepsilon}_2|$) made by Chung and Swift (18) were recently examined by Woo (95). He considered a finite area on which the blank-holder load acted with non-uniform pressure, and included the effect of variations in thickness across the flange by integrating the equilibrium equation using the trapezoidal rule. He also used the equivalent strain-increment compatible with the Levy-Mises theory, instead of the above approximation. The effects of plastic bending and unbending under tension were neglected. He found that (ii) had negligible effect, and (iii) showed differences of the order of 0.05 in equivalent strain over the die profile. Assumptions (i) and (iii) should not be made, if accuracy in calculating the strains is required. Generally, the agreement with the experimental results did not seem to have a marked improvement over that of Chung and Swift's (18) partly due to anisotropy developed in Woo's tests which was not allowed for in his theory.

Wood said, "The main object of this investigation is to find how closely the maximum punch load can be predicted using the present method of analysis", and used the following vertical equilibrium equation:

$P = 2\pi r\,(\sigma_1 t)\sin\varphi$, where φ is the angle of contact along the die profile, but he did not explain how $\varphi < \frac{\pi}{2}$ was calculated. His analysis will be insufficient to find this φ without introducing a method of matching the boundary conditions of radial drawing and stretching regions including the moving contacts on punch and die as shown in section 5.3. of the present thesis. Alternatively, the approximate analysis adopted by Chung and Swift can be used, which assumes no stretching in regions over punch head and between punch and die, the second region being approximated to a truncated cone. The assumption of $\varphi = \pi/2$, which was apparently used (46), will only apply for limiting blank diameters at final stages with no clearance between the cup and die. For all the other cases $\varphi < \pi/2$. Wood said, in reply to Kaftanoğlu (46) that in fact for the earlier stages of deformation, φ was determined from experiments, which of course limits the usefulness of his theory.

1.1.2. Related Investigations

There are also other types of possible deformations quite different in character which may be eliminated, or combined with the type discussed above. The main related researches are briefly discussed below.

1.1.2.1. Flange Wrinkling

This is a mode of buckling initiated by the compressive circumferential stresses which are induced by the tensile radial stresses during radial drawing. If they are above a critical value which depends on the geometry of the flange, blank-holding conditions, and material properties, waves or folds would be formed in the flange.

The first theoretical investigation of this phenomenon was due to Geckler (29). Senior (74) later extended this work to cover the cases of wrinkling without a blank-holder, and also with constant load and spring loaded blank-holders. He has used an energy method in which the flange was assumed to be fixed between the die and the punch. This could be approximated to having a uniform lateral pressure distribution over the flange surface proportional to its deflection at the mean surface. The flange was assumed to consist of initially straight, free-ended struts of a half wave-length long, later having a sinusoidal deflected shape. The energy supplied by the circumferential stresses was equated to the total of the energy dissipated in (i) bending, (ii) against the assumed pressure distribution, and (iii) pressure distribution due to the blank-holder. To eliminate the unknown in this expression, the circumferential stress was minimised with respect to the number of waves. Although the analysis was basically elastic, the concept of the "plastic buckling modulus" was used, and upper and lower bounds were obtained for the number of wrinkles, and the circumferential stress. The corresponding blank-holder loads could be computed. The theory is not exact, but the results agree with experiments fairly well, and therefore the mechanism of flange wrinkling could be considered as sufficiently well understood.

1.1.2.2. Ironing of Cup Wall

When a cup is deep-drawn from a blank with a uniform thickness, the thickness of the material near the rim may increase by 30 - 40%. This is even higher in the case of re-drawing. If the radial clearance between the punch and the die throat is not sufficient, the thicker and the wrinkled parts of the cup will be ironed. It is desirable to have some ironing in practice because it produces a more uniform wall thickness, improves the surface finish, removes small wrinkles, bell-mouth, and the associated residual stresses. This can be achieved either by combining it with the deep-drawing operation by having one or more ironing dies placed concentricly along the axis of punch, or separately on its own (5). Since the maximum in the ironing load occurs after the maximum of the drawing load, it does not seriously influence the stability of the cup (18) during deep-drawing.

The most advanced theoretical study of this problem is due to Briggs and Swift (13). They have considered the equilibrium of an element in the wall of a thick-walled cup in ironing. They neglected the effect of the surface shear stresses on the directions of the principal stresses, assumed plane strain conditions, Tresca criterion for yield, quasi-linear strain-hardening, and a special relation between the two operative coefficients of friction on either side of the cup wall. They were able to get an analytical expression for the wall stress under the die. Total punch load for ironing could be found by the summation of (i) the load transmitted to the head of the punch through the walls, (ii) the frictional force between the cup wall and the punch, and (iii) the load for the assumed mode of the redundant deformation caused by the shear distortion at entry and exit of the die, which could be calculated by finding the work done per unit volume of the material.

Their theoretical prediction of the ironing loads were satisfactory for thickness ratios less than 0.25. For thicker cups, the loads were overestimated particularly due to the "ironing wave" which forms just at the entry of the die, similar to the one in the case of an indentation process. The experimental investigation of Freeman and Leeming (25) was in qualitative agreement with the theoretical results of Swift and his co-workers.

Barlow (5) modified the above analysis by using a von Mises yield criterion and mean yield stresses obtained from the effective regions of the true-stress true-strain curve of the material undergoing ironing. A "slip-line field" solution of this problem was given by Hill (38). This allows for variation of stresses through the thickness, but is limited to non-strain-hardening materials.

Although the above analyses could be improved by eliminating some of the assumptions, they are adequate for the calculations of ironing loads related to deep-drawing for moderate reductions.

1.1.2.3. Plastic Bending under Tension

When an element of sheet metal, while under a dominating tensile stress system, is forced to change its radius of curvature, further plastic flow will take place at this point causing further thinning of the material. The extent of this thinning would be a function of the applied stress, material properties, thickness, and the radius of curvature in the plane of bending.

Swift investigated this phenomenon theoretically and experimentally (78), for a linear strain-hardening strip, under essentially plane strain conditions, i.e. width strain being negligible. Assuming that plane sections remained plane, it was possible to derive an expression for the stress of each fiber across the thickness. He equated the applied tension to the integral of the bending stresses, to find the displacement of the neutral axis from the central axis. It seems that his lower integration limit in equation (1) of his paper and in the related equations is not compatible with the sign convention adopted, and also the discontinuity of the bending stress at the neutral axis must be allowed for. A similar incompatibility was also previously pointed out for his other publication (18). However, these two errors were self-cancelling when the neutral axis remained within the thickness of the material. A different equation results as shown in the Appendix-G of this report, when the neutral axis moves outside the thickness of the material due to higher tensile forces. Swift obtained experimental results for thinning strains due to bending and unbending under various levels of applied tension, which agreed with theory closely for the smaller strains.

Using the analysis presented in Appendix-G, the limiting values of the applied tensile stresses to bring the neutral axis onto the inner surface of the strip were calculated for the materials and conditions given in Table-I and Figs. 15-17 of Swift's paper. It was found that only in the case of brass (Fig.16), beyond 15.4 tons/sq.in. applied stress, was the neutral axis outside the strip. In this case Swift got the largest differences between his theory and experiment. For the purpose of comparison, in this case the present equation G.13 at 16 T/sq.in. gave 0.08% thinning strain if bending and unbending strains were equal, where Swift's upper and lower bounds covering the possibilities of pre-straining in tension were 0.12% and 0.085% for an $\sim$0.083% experimental strain.

Analyses of plastic bending under tension similar to Swift's work, are given by Alexander and Brewer (4), and also by Ford and Alexander (24).

1.1.3. Stretching over Punch Head and between Punch and Die

This region is bound by point C, (i.e. the point of departure of sheet metal from the die), and by point F which is coincident with the axis of symmetry, sometimes referred to as the "pole" (see Fig. 1). From F to D, sheet metal is in contact with the punch and conforms to its shape. Between D to C its both surfaces are free, and they are concave looking from outside in the plane of the paper in Fig.1. At later stages of the deformation, the material between C - D, could originally be in B-A or B-C or C-D. Similarly, for D-F it could be in C-D or D-F which makes the strain history of each element quite complicated.

In deep-drawing, the main functions of this region are (i) to contribute to the depth of the shell by deforming plastically, and (ii) to support the load induced by the radial drawing region. Therefore it governs the limiting deformation attainable.

Swift (80), and later Chung and Swift (18) obtained experimental results for strains in this region for flat punches with different profile radii, and a hemispherical punch for various ferrous and non-ferrous materials under graphite and tallow lubrication. The strains plotted for different parameters showed that, the region near the departure of sheet metal from the punch deformed most, later leading to fracture. They assumed plane strain conditions and zero curvature for the region between die and punch in their simplified analysis of stresses, which is an approximation.

Swift (77)(79), in a theoretical investigation hinted that stress-strain distribution over the punch head could be obtained by the consideration of equilibrium, and the laws of plastic flow, but he did not give a method of solution. His suggestion for descriptive purposes, that the stress ratio x may vary as a cosine function over the punch head will be seen to be quite unrealistic (see Chapter 13).

Yamada (97) presented an investigation for a stress-strain analysis over flat and hemispherical punches for isotropic materials obeying the Ludwik strain-hardening law, based on the Hencky-Mises theory, which was previously shown to be incompatible for non-proportional plastic straining. He further simplified the problem by assuming that the sheet metal completely covered the punch from the beginning of the deformation, i.e. $\alpha = \frac{\pi}{2}$, and therefore the complicated strain history was not taken into account. Plane stress conditions were assumed, and bending was neglected. He has obtained power series expansions of the variables and solved the differential equations of equilibrium, compatibility and his "similarity" equation on a differential analyzer and on a computer, but did not clarify how the variables in the product terms $(\sigma_1 t)$ were separated. Since these variables are multi-valued, it is important that the correct σ_1 and t should be chosen. It is also difficult to see how the four unknowns in three equations can be found. Reference to equation (65) of his paper, which is derived from the power series expansion of the thickness strain gives:

$$- \left(\frac{d\varepsilon_t}{d\theta}\right)_{\theta=0} = \frac{12\mu\,\varepsilon_o}{1+3n-6\varepsilon_o} \qquad (65 - \text{Yamada})$$

where ε_o is the polar circumferential strain. This is incorrect, because the present author proved exactly for all values of μ, ε_o and n, that $\left(\frac{d\varepsilon_t}{d\theta}\right)_{\theta=0} = 0$ (see section 3.2.3.1. of the present thesis). Therefore the two methods of determining μ, depending on this and subsequent related equations proposed by Yamada, seems to be in error. His second method utilizes the slope constructed to the ε_t versus r_o curve at $\theta = 0$. Reference to Figs. 65-66 in his paper shows that the experimental points were joined by broken lines instead of smooth curves, and the tangents constructed seem to be valid for 30^o and not for 0^o. Since the same expansions are used in the theoretical analysis, the effect of this error might be self-cancelling. The only comparisons made were between his theoretical results and Coupland and Wilson's (19) experimental results for a hemispherical punch, for partly strained specimens having maximum thickness strains of about 40% of that at plastic instability. The agreement between experiment and theory was within about 20% for strains up to $\theta = 55^{\circ}$ but got worse beyond. No results of strain distributions and their comparisons with experiments were given at or near plastic instability or fracture, which would have been very valuable.

Recently Woo (95) attempted to analyze the problem of stretching over flat and hemispherical punches for isotropic materials under plane stress conditions. He made the assumption that the sheet metal was completely stretch formed over the entire punch surface (i.e. $\alpha = \frac{\pi}{2}$) for a polar thickness strain of -0.01 (-1%). This is quite unrealistic as was found by the large disagreement between his theoretically predicted thickness strains and the experimental ones for partly deformed specimens with flat and hemispherical punches. In these comparisons, the thickness strains were less than $|-0.14|$ whereas those at plastic instability as estimated in relation to the present author's results would be about -1.0, if $\mu \approx 0.13$ for the material (brass with $n \approx 0.5$). Also the results from the present investigation, as discussed in Chapters

11 and 13, show that his assumption will lead to serious error. He also gives a comparison between incremental strain theory, (i.e. Levy-Mises), total strain theory (i.e. Hencky-Mises), and the experimental results. The stresses calculated from the two theories differ appreciably, and the difference between the experimental and theoretical strains get larger in the case of the total strain theory. Although this is influenced by the assumption that $\alpha = \frac{\pi}{2}$, which was also made by Yamada, it is interesting that Yamada seems to have obtained a slightly better correlation on a percentage basis between experimental results and those obtained using the Hencky-Mises theory.

Woo did not attempt to predict the plastic instability, or the strains at large deformations. He used a method of successive approximations involving the trapezoidal rule for integration of the equilibrium equation. As in the case of Yamada's theory, in the integration of the equilibrium equation, the terms in $(\sigma_1 t)$ are multi-valued, and a criterion for the choice of the correct values of σ_1 and t was not given. The necessary criterion is given in section 5.1. of the present thesis. Woo's suggestion for extending the solution into the region between the punch and die, (i.e. D-C in Fig.1) in order to find the strain history of elements before they come over the punch head seems to be in error. Using his figure and equations:

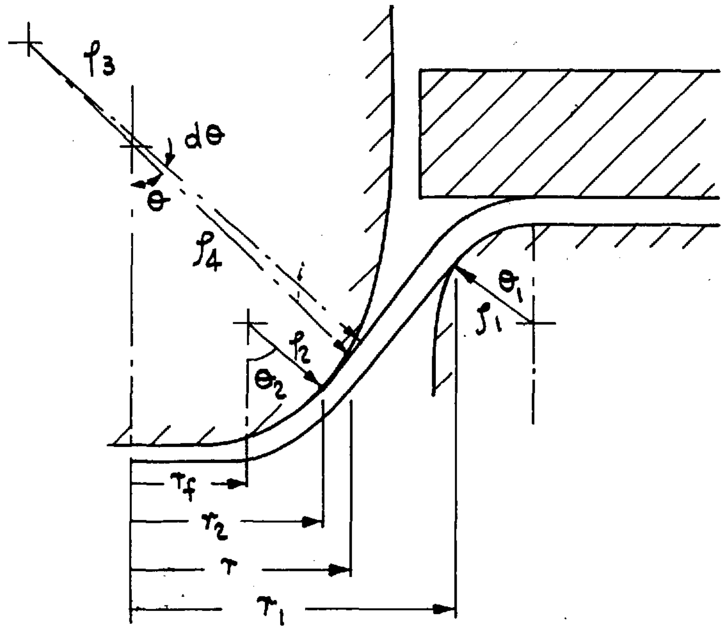

FIG.4. STRETCH-FORMING OVER A PUNCH HEAD. (Woo).

$$d\bar{\varepsilon} = \left[\frac{4}{3} \left\{ (d\,\varepsilon_\theta + d\varepsilon_t)^2 - d\,\varepsilon_\theta\, d\,\varepsilon_t \right\} \right]^{\frac{1}{2}} \qquad (3)\ (\text{Woo})$$

$$\left. \begin{aligned} \sigma_\theta - \sigma_r &= \frac{2}{3}\,\frac{\bar{\sigma}}{d\,\bar{\varepsilon}}\,(2d\varepsilon_\theta + d\varepsilon_t) \\ \sigma_t - \sigma_r &= \frac{2}{3}\,\frac{\bar{\sigma}}{d\,\bar{\varepsilon}}\,(2d\varepsilon_t + d\,\varepsilon_\theta) \end{aligned} \right\} \qquad (4)\ (\text{Woo})$$

$$\bar{\sigma} = \sigma_o + A\bar{\varepsilon}^n \qquad (5)\ (\text{Woo})$$

$$(\sigma_r t)_{i+1} = (\sigma_r t)_i + \int_{r_i}^{r_{i+1}} \frac{(\sigma_\theta - \sigma_r)t}{r}\,dr \qquad (8)\ (\text{Woo})$$

$$\Delta\,\dot{\varepsilon}_{t,i+1} = -\frac{1}{2}\left[\frac{3}{2}\left(\frac{\Delta\bar{\varepsilon}}{\bar{\sigma}}\right)_{i+1} \frac{(\sigma_r t)'_{i+1}}{t_{i+1}} + \Delta\varepsilon_{\theta,i+1}\right] \qquad (10)\ (\text{Woo})$$

$$(R_{i+1}{}^2 - R_i{}^2)t_o = 2\left(\frac{\rho_{3,i} + \rho_{3,i+1}}{2}\right)\left(\frac{\rho_{4,i} + \rho_{4,i+1}}{2}\right)$$

$$x\ (\cos\theta_i - \cos\theta_{i+1})\ \frac{t_i + t_{i+1}}{2} \qquad (16)\ (\text{Woo})$$

$$\rho_4 = \frac{(\sigma_r t)_2\ r_2 \sin\theta_2}{(\sigma_r t)\sin^2\theta} \qquad (17)\ (\text{Woo})$$

$$\rho_3 = -\frac{\sigma_r}{\sigma_\theta}\ \rho_4 \qquad (18)\ (\text{Woo})$$

where R is the initial radius of any element, and suffix i shows the location of an element in space. Subscripts r, θ, and t correspond to radial, circumferential and thickness directions. The rest of the notation is as shown in Fig.4. Woo said, "The method of successive approximations is used for the solution. Computation starts at the point of r_2 at which the stresses and strains have been determined previously. For the next point of r_{i+1}, corresponding to an initial radius R_{i+1}, the values of t_{i+1} (hence $\varepsilon_{t,i+1}$), $\rho_{3,i+1}$ and $\rho_{4,i+1}$ are assumed in the first approximation to be the same as those at r_2." In section 3.2.3.2. of the present thesis, it is shown that for both biaxial ($\sigma_t = 0$) and triaxial stress conditions over the punch head, the strains and the meridional stress are continuous at r_2, but in neither case is ρ_3 continuous. In fact it is discontinuous, negative, and even has a different absolute value. Woo does not seem to have considered this discontinuity as seen from the outline of the method and Fig.4 of his paper, which would give a completely erroneous result or no result. However, he has accepted and corrected this error in his reply to Kaftanoğlu (46).

He then says that θ_{i+1} can be determined from eqn. (16), hence r_{i+1}, $\varepsilon_{\theta,i+1}$, $d\bar{\varepsilon}$ from eqn. (3), $\bar{\sigma}$ from eqn. (5), σ_r and σ_θ from eqns. (4). $(\sigma_r t)'_{i+1}$ is found from eqn. (8) by integration. For the next approximation, new values of t_{i+1}, $\rho_{4,i+1}$ and $\rho_{3,i+1}$ are obtained from eqns. (10), (17) and (18) using the value $(\sigma_r t)'_{i+1}$ found from eqn. (8). It must be pointed out that in the eqns. (8), (17) and (18) (i.e. equations of equilibrium), only two are independent. Eqn. (17) is merely another integral form of eqn. (8). There can be only two independent equations of equilibrium in a three dimensional system where one equation is already satisfied by the axial symmetry in the θ direction. Woo had not provided an answer on the above question in his reply to Kaftanoğlu (46).

1.2. Stretch Forming

In this process, the material is securely clamped by a set of serrated dies, or drawing-in is prevented by the restraint of the large undeformed material in the region of the die, as in the Erichsen test. Hence there are two regions as shown in Fig.2. As the deformation progresses, the amount of material in contact with the punch (region F-D), increases, but at all times F-D $<$ F-C and $\alpha < 90^{\circ}$.

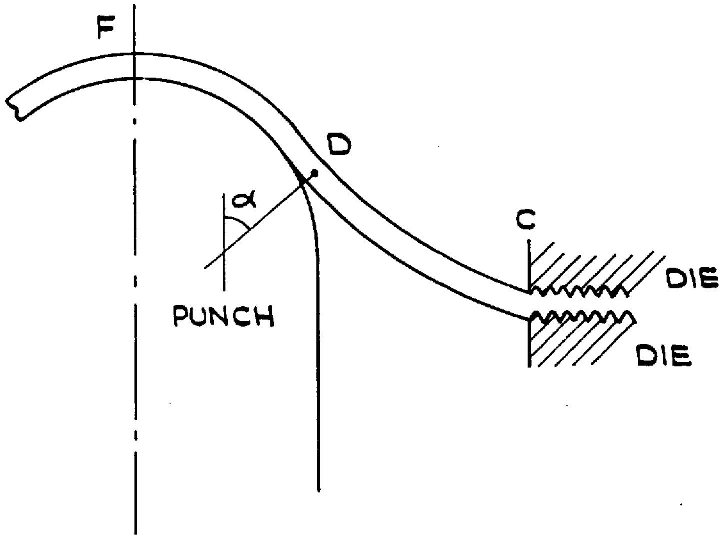

FIG.2. MAIN FEATURES OF STRETCH FORMING

The circumferential strain at point C is zero or very small, and therefore the deformation of material within the die region does not influence the deformation in region F-C.

Previous experimental and theoretical investigations conducted for the stretching of metal over the punch head in deep-drawing would apply qualitatively to stretch forming of metal, due to there being a similar state of stress but different boundary conditions. These prior investigations (mainly by Yamada and Woo) in any case were, as discussed before, neither complete nor adequate. Also this problem on its own, seems to have received practically no theoretical attention for the prediction of stresses, strains, plastic instability, or fracture.

Recently a systematic experimental investigation was reported by Keeler and Backofen (50) in stretch forming by hemispherical, hemispherical-conical, and elliptical-in-plan punches with aluminium, brass, copper and steel. The authors obtained distributions of three principal strains for various stages of deformation up to fracture for Teflon lubricated, and unlubricated specimens. They showed the effect of friction on strain distribution, and their experimental results are in general agreement with those of the present author's. This research was aimed at the explanation of plastic instability and fracture which will be discussed in section 1.5.2.

Distribution of strains obtained experimentally were also given for the same materials as above, by Kaftanoğlu and Alexander (45), in the Erichsen Test which is basically a stretch forming operation, and they showed the same trends as those by Keeler and Backofen.

1.3. Hydraulic Bulging

Considerable research has been done in the deformation of thin sheet metal under lateral pressure. Due to the nature and the application of pressure this subject can be conveniently discussed in the following sections.

1.3.1. Static Bulging

The pressure is applied generally on one side of a clamped diaphragm by an incompressible fluid such as water or oil, where $\frac{dP}{dT} \approx 0$, and therefore the strain rate and inertia effects are negligible. Almost all the investigations so far recorded are for circularly clamped specimens.

Brown and Sachs (14) and later Brown and Thompson (15) carried out extensive experimental investigation of the circular bulging of metal membranes. They obtained strain distributions, radii of curvature at the pole as functions of the applied pressure up to fracture, which in all cases took place in the vicinity of the pole, at a decreasing pressure for annealed materials and an increasing pressure for strain-hardened materials.

Gleyzal (31) investigated the plastic deformation of a circular diaphragm under pressure theoretically and experimentally for small strains. He used engineering strains with the Hencky-Mises theory which led to larger differences between theory and experiment for higher strains. The method consisted of the numerical solution of equations derived from equilibrium and plasticity laws.

Hill (34), for a Levy-Mises material obtained a special solution assuming that the particles in the membrane describe circular paths which are orthogonal to the momentary bulge profile. With this assumption, relationships between polar strain, curvature and bulge depth were obtained. Although this analysis was valid for a material of $\bar{\sigma} = Y e^{\bar{\varepsilon}}$, due to the insensitivity of the above relationships, other strain-hardening laws could be used. He derived the instability strain for maximum pressure in hydraulic bulging. He also gave a general solution for linear strain-hardening materials which justified the assumptions made in the simplified theory. Mellor's (42) experiments with copper, brass, aluminium and steel gave good agreement with Hill's theory for polar strains at maximum pressure. The present author discusses an alternative criterion of plastic instability in section 4.3. which explains why fracture can take place after the applied pressure has reached a maximum with annealed materials, but before with strain-hardened materials, as evidenced by Mellor and Brown et al.

An extension of Gleyzal's analysis was presented by Weil and Newmark (92), where the authors used logarithmic strains instead of the engineering strains of Gleyzal, with the Hencky-Mises theory. A numerical method of solution of the necessary equations was outlined, but this led to divergence of the solution near the maximum hydrostatic pressure, which was used as the instability criterion. Comparisons were made between the theoretical and experimental results obtained for annealed copper. They showed good agreement at maximum pressure for strains, stresses and deflections at the pole, where the Hencky-Mises and Levy-Mises theories give identical predictions. No results for strains were given for elsewhere in the bulge, which would be expected to show more differences because of the effect of neglecting the strain history of the elements due to varying stress ratios, as found experimentally by Mellor (42).

Munday and Newitt (69) presented a trial and error solution for this problem again based on the Hencky-Mises theory. They effectively used a different criterion of instability from those of previous authors and quoted results for polar thickness strain and pressure at instability which will be discussed in section 1.5.1.

Recently Woo (96) obtained a numerical solution for hydrostatic bulging for a Hencky-Mises material by a similar method to that discussed in 1.1.3. for stretching over the punch head. He seems to have used three equilibrium equations (i.e. tangential, vertical, and normal to the shell wall, eqns. (6), (8) and (9)), two of which can be independent since the third equation in the direction of σ_2 is identically satisfied with the symmetry of the problem. Woo did not provide a satisfactory answer on the above question in his reply to Kaftanoğlu (47). Eqn. (10) in his paper was obtained from eqns. (8) and (9), and not from eqns. (7) and (8) as said in the paper. Also for the terms in ($\sigma_1 t$), in the equation of equilibrium, a discrimination between the several possible combinations of σ_1 and t was not made. The necessary criterion is given in section 5.3. of the present thesis. The author seems to have found satisfactory agreement with Mellor's experimental results.

1.3.2. Dynamic Bulging

When the lateral pressure applied to the clamped sheet metal varies rapidly with time, then the inertia, strain-rate, and strain propagation effects are no longer negligible. This could be achieved by a rapid pressure built up from an accumulator source, or shock waves produced by explosives, electrical discharges of condensers, or similar methods. The common energy transfer media are, air, water, plasticine, rubber, and P.V.C. (32). The liquids are more efficient in terms of energy transfer, whereas the strain-rate sensitive, and easily deformable media are well suited for obtaining local deformations.

Munday and Newitt (69) in experiments with shock loaded copper discs, and from a qualitative analysis of the process observed that, due to the interaction of the inertia wave starting from the rim, and the strain propagation wave starting from the pole, a discontinuity existed in the bulge. This separated the central flat initially less strained section from the sloping sides of the remaining section which grew larger as the deformation progressed. In the light of this work, they suggestted that the bursting pressure in dynamic loading might be smaller than that in the static case, although this lacked full experimental verification.

Travis and Johnson (83), in explosive forming, investigated the effects of size of charge, thickness of sheet metal, stand-off distance, strain in deformed specimens, and the tensile stress-strain characteristics of various metals. Both the circumferential, and the thickness strains decreased as functions of distance measured from the pole at different stages of deformation. The highest strained point was the pole, and subsequent necking and fracture took place there. Their results for strains at or near rupture were within 10-15% of those obtained by Mellor (42) in hydrostatic bulging which suggests that there is no marked improvement in the ductility of the materials formed at high rates of strain as also found by Finnie (22). These authors' results do not support the findings of Munday and Newitt (69) for the moving discontinuity, and the mode of deformation as described by them. On the contrary, the bulge profile is very similar to that obtained in hydrostatic bulging, but with a slightly steeper slope.

A comprehensive review of the theory and experiment and of the industrial applications of explosive forming is given by Baron and Castello (6). Johnson et al (44) experimentally investigated the parameters involved in free forming and deep-drawing by explosives, and also by using a water hammer technique. It was found that the overall efficiency of the latter process was an order of magnitude greater than the former. Comparisons of the behaviour of different materials formed by the underwater spark discharge method were made, and a good correlation was obtained between the electrical energy discharged and the central deflection of the diaphragms, using an exponential relationship.

The strain rate involved in high rate forming is generally between 10^2 to 10^6 sec^{-1}. It depends on the process, and the energy source used, and the higher rates can only be obtained by the high power explosives, such as TNT.

1.4. On Factors Influencing Sheet Metal Deformation

1.4.1. Stress-Strain Characteristics

Many researchers have tried to correlate the performance of sheet metal in presswork with its basic stress-strain properties. These, so far, should be regarded as only capable of predicting the trends qualitatively, and by no means without fail. The significant properties are pre-strain, strain-hardening rate, and the anisotropy parameter "R", all of which also affect the yield stress, U.T.S., total and uniform elongations in the tensile test.

An anomaly was observed by Loxley (58) in the deep-drawing of aluminium and 70/30 brass. With a flat punch harder tempers gave deeper draws, whereas with a hemispherical punch softer tempers gave deeper draws. Moreover softer tempers drew better with a hemispherical punch than with a flat punch, while the opposite effect was observed for the harder tempers. Loxley's (58) experiments to correlate the sheet metal performance with tensile tests were not successful in the explanation of this anomaly, and required an analysis of plastic instability as presented later in this thesis.

Pearce (70) observed that, materials having high uniform and total elongations in the tensile test, gave higher Olsen values than the others, indicating their better "stretchability". Lilet and Wybo's (55) results also confirmed this finding. For materials, whose stress-strain curves in tension could be expressed by the Ludwik power law (i.e. $\bar{\sigma} = A\bar{\varepsilon}^n$), they found that the Erichsen value, and the bulge depth in hydrostatic bulge tests increased with the strain-hardening exponent "n". Poor correlation was obtained between n and the Swift and Fukui deep-drawing tests.

Wallace (87), based on a theoretical analysis to determine the wall stress in deep-drawing, gives the following performance factor for comparison between similar materials:

$$\pi = \frac{\text{U.T.S.}}{\text{Yield Stress times strain hardening rate}}$$

Although he only tested this for mild steel, it seems reasonable to use it for other materials as well.

1.4.2. Strain-Rate Effects

Wallace (88) investigated the effects of strain-rate in deep-drawing for flat and hemispherical bottommed cups in mild steel for the drawing speed range of 1-30 ft/min. He has used the criterion of L.D.R., but observed no significant strain-rate effects. This was also true when the blanks were lubricated by graphite in tallow - a boundary lubricant - which is insensitive to changes in speed. Coupland and Wilson's (19) results also confirm this trend for brass, but for mild steel lubricated with graphite under increasing speed, there was a reduction in the L.D.R. when using a hemispherical punch, but a small increase was observed when deep-drawing by a flat punch. Both these changes were attributed to the effects of strain-rate on the plastic behaviour of the metal. This could not be very significant, because, Baron (7), from his uni-axial tension tests on various materials and treatments, did not find any significant change in ductility or the instability strain, for a strain-rate range of from 10^{-3} to 100 sec^{-1}, although the stresses corresponding to the same strains for the higher strain-rates were about 15% higher. Similar findings for hydraulic bulging were discussed in section 1.3.2. of this thesis.

1.4.3. Plastic Anisotropy

Variation of material properties as a function of direction in the plastic range - plastic anisotropy - has important effects on the deformation of materials. Hill (38) gives a self-consistent set of equations governing such deformations.

Sheet metals can be anisotropic in their plane, or/and in the thickness direction. The former generally results in "earing" of deep-drawn cups which have wavy rims, ears and troughs being symmetrically distributed and are usually four or six in number. The researches (82)(38)(45) showed that this depends on the previous mechanical and heat treatment, which governs the crystal orientation and macroscopic structure of materials, and cannot be predicted from the geometry of the observed fracture in a stretch forming test, e.g. Erichsen test. Plastic anisotropy in the thickness direction has been investigated by Lankford et al. (54), Whiteley et al. (93), Pearce (70), and Lilet and Wybo (55) using the parameter $R = \frac{\varepsilon_w}{\varepsilon_t}$ (R-value) in a uniaxial tension test. They found that in Swift type cupping tests, L.D.R. increased approximately linearly with the average R. For the tests where stretching is more dominant, as in the Erichsen and the bulge tests, the correlation with the R-value was less significant and discrimination of the materials by means of this criterion was less satisfactory.

1.4.4. Lubrication and Heat-Treatment

Lubrication plays an important role in sheet metal deformation by tools. In deep-drawing or stretch forming, over the punch head, it influences the distribution of stresses, strains and the location and magnitude of the instability, and fracture strains. Over the die in deep-drawing, it mainly affects the punch load, and therefore the L.D.R.

Loxley and Freeman (60) and Freeman (26) obtained strain distributions in stretch forming and deep-drawing for steel and brass with and without a lubricant (graphite in tallow). They showed that the fracture point moved away from the pole for the unlubricated specimens, and there was less overall straining. For both the flat and the hemispherical punches, only die side lubrication gave higher L.D.R.'s, and the reverse was true for the punch side lubrication. Later Wallace (86) obtained a remarkably high L.D.R. by using a knurled flat punch, where the fracture point was furthermost from the pole.

The effects of drawing speed on lubrication were studied by Wallace (88) and Coupland and Wilson (19). It was shown that for boundary lubricants such as graphite in tallow, there was no lubrication effect on deep-drawing. However, for liquid lubricants with increased speed, a higher L.D.R. was obtained with flat punches, and a lower one with the hemispherical punch. This was due to the stability and effectiveness of the hydrodynamic film at higher speeds. Increase in lubricant viscosity had a similar influence.

Recently, plastic films such as P.T.F.E. and polythene have been used as lubricants to reduce friction between tools and metals, and have proved to be better than many of the conventional boundary lubricants, which get squeezed out. Lloyd (57) shows the large difference in Olsen values obtained by an etched ball, and one lubricated by polythene. Mear et al. (64) have found that the use of firmly adherent films of methacrylate copolymers applied from trichloroethylene solution as dry-film lubricants, were more convenient to apply and effective for complicated pressings.

Maeder (62) has shown that for a differentially annealed blank where the flange is induction-heated and therefore softened, one can obtain a much higher L.D.R. This is analogous to differential lubrication where the force to deform the flange can be reduced by applying good lubrication there.

1.5. Plastic Instability

The common types of plastic instability which occur in sheet metal deformation are wrinkling under a dominant compressive stress, and necking leading to fracture under a dominant tensile stress system. The former was discussed in section 1.1.2.1., In the case of the latter, with continued plastic deformation the material thins and also strain hardens. However, the process can continue until the net load through a section can be transmitted to the neighbouring element. This generally has an upper limit beyond which strain-hardening cannot compensate the decrease in load due to thinning and tensile plastic instability sets in. This term (plastic instability) is also used in cases when an independent loading function reaches a maximum, e.g. maximum pressure in hydraulic bulging and maximum load in uniaxial tension, which is not synonymous with the previous definition as shown in Chapter 4.

1.5.1. Uniaxial and Biaxial Stress Systems and Hydraulic Bulging

Swift (77, 79) examined the plastic instability under plane stress for a Hencky-Mises material. His analysis is effectively based on the maximum load criterion across the load transmitting area in uniaxial and biaxial tension under constant stress ratio. For shells deforming under fluid pressure, i.e. cylinder, sphere and hydrostatic bulge, he used the maximum pressure as the criterion of plastic instability. The corresponding instability strains for such processes could be found from a given equivalent stress-strain curve by constructing a tangent such that $\frac{d\bar{\sigma}}{d\bar{\varepsilon}} = \frac{\bar{\sigma}}{z}$ where z is the subtangent found according to the existing stress system.

Hill (35) investigated the conditions for localized necking in thin sheets. He obtained the same instability criterion as Swift's for biaxial tension and diffused necking. His results indicate that localized necking cannot take place in the stretch forming process, where $0.5 < x < 1$ for an isotropic material.

Hill (37) has also studied the relation of the uniqueness condition to the stability criterion for a rigid-plastic solid, and gave particular solutions for uniaxial tension, compression of a strut, torsion, and hydraulic bulging. He showed that all-round hydrostatic pressure has no effect on the point of occurrence of tensile plastic instability.

Johnson and Mellor (42) using the same criteria of instability as Swift, derived formulae expressing the strains and stresses at instability in terms of the constants A, B and n of the empirical strain hardening formula, for uniaxial tension, and plastic deformations of sphere, cylinder and a membrane under hydrostatic pressure for a Mises material. Hillier (39) deduced the criterion of instability from the principle of plastic work for a Mises material for uniformly distributed stress systems. He obtained the same formula for the instability strain under a biaxial stress system as Swift. Although his analysis incorporates the effects of external loading characteristics, it would not be easily applicable to non-uniform stress states as in stretch-forming, where the load rates cannot be computed.

Previous investigators (14, 15, 34, 42, 92, 96) used the maximum pressure criterion in hydrostatic bulging, except for Munday and Newitt (69), who calculated the instability condition by the maximum in the load, in the plane of the sheet at the pole. It is shown in section 4.3. of this thesis that these two criteria will lead to different results. They can only give the same result for certain values of n and B, which presumably was the case when the authors compared their instability strains with those of other workers and reported good agreement.

1.5.2. Stretching over Punch Head

Yamada (97) used the Swift and Hill instability criterion for biaxial stress and the Hencky-Mises material, and obtained curves for the instability stress (σ_1) as functions of n and strain ratio. From his analysis applied over the punch head, he suggested that when $(\sigma_1)_{max}$ reaches the value of $(\sigma_1)_{inst.}$ instability takes place. He did not give any stress or strain distributions, or any comparisons with experiments at instability. Although he said that the fracture load can be calculated by this method, it is shown in Chapter 13 of this thesis for stretch forming that strains beyond those predicted by the Swift-Hill criterion are achievable up to the onset of fracture.

Keeler and Backofen (50) from an experimentally obtained strain history, calculated the stress-ratio x, and used it in the instability criterion of Swift-Hill and found the strains at the diffused necking. However, the experiments carried out to fracture showed that for aluminium with Teflon lubrication $\Delta\bar{\varepsilon} = 0.20$ was obtained beyond diffused necking. Similar trends were observed with the other materials to a lesser extent, but brass fractured at a strain slightly less than that associated with diffused necking; however, this could be within the error of constructing a tangent to the stress-strain curve. The present author's results follow the same trend.

Recently Moore and Wallace (67) showed the effect of the R-value on the L.D.R. for flat punches using Hill's theory (38) for anisotropic materials and total strains. They assumed that fracture occurred under plane strain conditions at the junction of the cup wall with the punch profile. The plastic instability criterion was effectively that of Swift's and predicted the stress and strain when the maximum load in the plane of the sheet was reached. The drawing ratio could be calculated by a simplified theory giving the maximum radial stress in the drawing region, and the ratio which gave the same load as that predicted by the instability criterion was considered to be the L.D.R. Their results are in good agreement with Whiteley's experiments (93). This approach would be valid for a small punch profile radius, to justify plane strain conditions, and as shown in 4.3.of this thesis, strains beyond those predicted by this criterion may exist up to fracture.

1.6. Formability Tests

The common tests assessing the formability of sheet metals can be categorized into two groups:

i) Fundamental tests - Measure the fundamental properties of the materials, e.g. a) Tests giving the basic stress-strain relationships of the materials such as the tensile, and the bulge tests. b) Hardness tests. c) Metallurgical tests. d) Chemical analysis. e) X-ray diffraction.

ii) Simulative tests - Try to assess the performance of materials in industrial processes, under simulated laboratory conditions by also bringing in the geometrical and operational variables. They are summarized in Table 1.1.

TABLE 1.1. - Simulative formability tests

Tests	Name	Criterion of Performance
Stretch Forming	Erichsen	Depth of penetration up to fracture
	Olsen	" "
	Hole Expanding	Increase in the diameter of the hole.
Deep-Drawing	Swift (F.P.)	L.D.R.
	Fukui (F.P.)	"
Bend Test		Deflection at fracture
Combined Formability	Modified Swift (H.P., ellipsoidal and parabolic punches.)	L.D.R.
	Fukui (H.P.)	L.D.R.
	Fukui conical cup	Depth of Pentration up to fracture.

The most important earlier researches seem to have been those by Fukui et al. (27), Krüger (53) and Kokkonen and Nygren (52). Fukui attempted to correlate various formability tests, and found some degree of correlation between the L.D.R. for hemispherical-ended cups, and both general elongation in tension and the "standard Erichsen value", although this could not be expressed quantitatively. Krüger reported that the Erichsen test gave a better indication of the suitability of a given sheet of metal for deep-drawing than did cup-drawing tests, and also it was more sensitive to any changes in the properties of the sheet. Kokkonen and Nygren investigated the scatter of results caused by variations in the surface finish of the tools, and differences in the materials. They gave the limits of uncertainty in determining the Erichsen number for a single machine, and also the uncertainty between different machines. The most recent official statement about the Erichsen test is contained in a draft German specification (30). In addition, Jevons (41) and Yoshida (98) discuss the application of these and other tests, and Kemmis (51) gives a useful account of the Swift test with experimental findings. The contents of the paper by Kaftanoğlu and Alexander (45) are contained in this thesis.

Wallace (85) said that some simulative tests may broadly classify the materials. The interaction of geometry and material properties is of such importance that any detailed correlation is probably either fortuitous or due to some overriding factor, which blankets the influence of geometrical scale and other factors. Little is to be gained by refining the existing tests, but a fundamental understanding of the process of the relevant material behaviour is necessary. This is a view to which the present author also subscribes.

1.7. Coefficient of Friction under Conditions of Plastic Flow

It is generally known from practice and also from detailed investigations (8,17), that the mechanism of friction under bulk plastic deformation, where the die remains elastic in bulk is substantially different from the cases where both contacting bodies remain elastic in bulk.
A summary of coefficients of friction found by workers in this field under different modes of deformation and lubrication, is given in Table -1.2. As indicated in this Table, some of the coefficients are found by effectively comparing theories with experiments, and solving for the unknown coefficients of friction, and the rest by independent assessment of the surface shear and normal stresses. These latter are more reliable, since they do not incorporate errors due to simplifications in the theories. Although there is considerable scatter and uncertainty, it is possible to say that coefficients of friction decrease

Table-1.2. - Coefficients of friction found by previous workers mainly under conditions of bulk plastic deformation unless otherwise indicated.

No.	Source	Type of Test	Lubricant	Material	Coefficient of friction	Comments
1	Swift (78)	Bending under tension (Steel pulley)	Dry Graphite in tallow	M.S.Brass, Al. " "	0.08 -0.13 0.022-0.078	Calculated by a modified belt friction formula
2	Littlewood (56)	Belt friction (steel quadrant die)	SAE -5 SAE -40 SAE -140	M.S. " "	0.22 -0.25 0.18 -0.23 0.15 -0.18	Calculated by the belt friction formula
3	Bowden and Tabor (8)	Slider	Dry " Mineral Oils "	Pure Metals Alloys on Steel Steel on Steel Metals on Steel	0.4 -1.5 0.22 -0.8 0.08 -0.48 0.1 -0.6	Values are mainly for elastic deformation but they appear to be insensitive to applied load and hence could be effective for small plastic deformation too.
4	Abdel Aziz (68)	"	Various oils and greases	Aluminium on Steel	0.03 -0.19	"

Table-1.2. (Cont..)

No.	Source	Type of Test	Lubricant	Material	Coefficient of friction	Comments
5	Takahashi and Alexander (81)	Plane-Strain Compression (Steel dies)	Dry, paraffin, SAE10 " " Dry and paraffin SAE10, paraffin+5% lead oleate Dry and paraffin SAE10, paraffin +5% lead oleate	Brass Copper Aluminium " Mild Steel "	~0.067 ~0.1 ~0.19 ~0.06 ~0.2 ~0.07	Accumulated débris reduces μ. Pressure welding increases μ.
6	Watts and Ford (90)	"Cigar test" (Steel platens)	Graphite and Polished surfaces	High Conductivity copper	0.015-0.02	With incremental loading and lubrication. Approximate plane-strain conditions.
7	Hill (36)	" "	Calcium oleate Vacuum solvac	Copper "	0.015 0.045	" "
8	Whitton and Ford (94)	Cold rolling (Steel rolls) Smooth <9 μ-inch. Rough ~20 μ-inch " "	Dry Common oils Dry Common oils	M.S., brass, high conductivity Copper, aluminium High conductivity Copper "	0.085-0.101 0.026-0.08 0.0113-0.124 0.046-0.061	Calculated μ is independent of the rolling theory used. Only assumptions are 1) μ is constant along the arc of contact. 2) Deformation takes place under plane-strain conditions.

Table-1.2. (Cont..)

No.	Source	Type of Test	Lubricant	Material	Coefficient of friction	Comments
9.	Schroeder and Webster (73)	Uniaxial compression of thin cylinders.	Dry MoS_2 and silicone greases Silicone grease + flake graphite	Aluminium Alloys "	$\geqslant$ 0.577 0.05 -0.15 0.02	Calculation of μ may be slightly affected by the approximations in the theory.
10.	Male and Cockcroft (63)	Uniaxial compression on a flat ring shaped specimen	Dry	Aluminium M.S. α Brass Copper	0.18 0.17 -0.31 0.10 -0.15 0.17 -0.30 Smooth Rough Dies	Calculation of μ does not involve the yield stress but a calibration curve valid for geometrically similar specimens must be obtained using also Schroeder and Webster's analysis.
11.	Rooyen and Backofen (84)	Uniaxial compression of cylinders (Platens : 12 - 13 μ-inches)	MoS_2 Dry Soap Teflon Liquid lubricants " "	Aluminium " " " " Iron Copper	0.05 -0.15 0.2 -0.57 0.03 0.01 0.08 -0.44 0.11 -0.28 0.2 -0.36	Normal and shear stresses were measured by the pins in the plates and calculated accordingly. μ increased with reduction and radius from centre. Only with MoS_2 and dry, it decreased with reduction. Most values are valid for $\frac{3}{4}$th of outer radius.

in the following order. When:

(i) two contacting bodies remain elastic in bulk, (e.g. slider tests).

(ii) the bulk plastic deformation is caused in one of the bodies by stresses which are not normal to the surface. (e.g. Stretch forming, and bending of sheet metal.)

(iii) the bulk plastic deformation in one of the contacting bodies is caused by stresses normal to its surface. (e.g. rolling and compression.)

The coefficient of friction can also vary with the amount of deformation, and also instantaneously across the interface depending on the following factors:

(i) Change of surface finish or generation of a new surface.

(ii) Accumulated debris.

(iii) Pressure welding.

(iv) Deterioration of the lubrication and breakdown of the lubricant film.

(v) Relative speed between the two bodies. If a hydrodynamic film is present or if there is a change-over to boundary or mixed lubrication, this has a pronounced effect.

Such variations in the coefficient of friction can be as much as 400% - 500% of the initial value as seen from the detailed results of Rooyen and Backofen (84).

Another important aspect of friction under bulk plastic deformation is that the material cannot carry a surface frictional stress greater than its current yield stress in shear.

CHAPTER - 2 - OBJECT OF PRESENT INVESTIGATION

Researches previously conducted have helped to explain some of the controversial points encountered in sheet metal deformation processes as discussed in the previous Chapter.

The aim of any research of significance in this field should be the prediction of material behaviour from given data about is basic stress-strain characteristics, geometry, friction and other operational variables. Desirable as this state of affairs would be, even for an axi-symmetrical shell this has not previously been achieved due to complications in the theory.

The present work is directed towards trying to elucidate some of the unresolved problems related to sheet metal deformation for which urgent solutions are required. These problems which will be discussed in the remainder of this thesis, and for which solutions have been attempted can be grouped as follows.

2.1. Theoretical

Since previously there was no satisfactory theory for the stretch forming process, this has now been attempted for a material which is isotropic in its plane but anisotropic in the thickness direction, with a non-linear strain-hardening characteristic, and pre-strain. The undeformed shell can be of any axi-symmetrical shape and can have any variation in thickness, initial strain etc., along the radius, but the final shape is also restricted to being a shell of revolution. The coefficient of friction can vary instantaneously along the contacting zone, and also with plastic deformation (in time). The complete strain history of each element is taken into account using the incremental theory of plasticity for anisotropic materials, and considering moving contact between sheet metal and punch during continued deformation. Various instability criteria are studied and conditions at the onset of fracture are predicted by a new method. The analysis does not include the effect of bending, but takes into account the thickness stress approximately, over the punch. The assumption of neglecting bending was later shown to be justified by comparison between theoretical and experimental results. The analysis was programmed for the Atlas computer.

The experience gained from the analysis of stretch forming helped in formulating more refined theories and methods of solution for drawing over the die in deep-drawing, and plastic deformation and instability in the hydraulic bulging of diaphragms including the effects of the same factors as in the stretch forming analysis. No numerical results were obtained for these latter problems due to limitations in the computer time available, but the analytical formulae obtained for different instability criteria are discussed for hydraulic bulging.

Two theories for estimating the coefficient of friction, and its variation with plastic deformation are presented for stretch forming, and drawing over die regions. These methods provide data for the stretch forming theory, and also to study the associated lubrication problem, since such analyses were not available from the previous investigations.

An extension of the work of Chung and Swift (18) in plastic bending under tension, to cover anisotropic linear strain-hardening materials is presented showing the limitations of the previous investigation.

2.2. Empirical

In view of the laborious work in the determination of L.D.R. in deep-drawing experimentally, a method is proposed to predict it sufficiently accurately from only three tests conducted up to fracture with oversize blanks in deep-drawing. This idea can also find application in the determination of critical size blanks for non-symmetrical pressings in industry.

In order to express the basic stress-strain characteristics of materials by analytical formulae, computer programs were written to fit the experimental data to the chosen formula by determining its constants on the basis of least squares, and least moduli error. The constants and the formula were used in the stretch forming theory, and also in the equations predicting plastic instability.

2.3. Experimental

The first part of the experimental research was initiated by the need to know the influence of variables in the Erichsen test. This would be needed in particular for drawing up a universally accepted specification for the test. A survey of previous literature (see section 1.6.) indicated that no systematic study of variables such as strains and the amount of drawing-in, and stretching that occur in the test has been made. It is clear that the sheet metal must deform over the punch head mainly by stretching, but there must also be some drawing-in of the sheet over the die profile radius. Since rupture always occurs at some location over the punch head, the stretching component is the more important. The Erichsen test assesses the ability of a sheet of metal to withstand failure from quasi-biaxial tensile instability when being stretched over a spherical surface under given frictional conditions. Because of the drawing-in that takes place, however, the Erichsen number may not correctly evaluate this property; if much drawing-in occurs a higher Erichsen number will result for the same amount of stretching. Since this test should be regarded as a stretching test, any drawing-in is undesirable and will inevitably lead to undue scatter in results.

The following are the important factors that affect the test:

1. Specimen shape and plan dimensions.
2. Specimen thickness.
3. Specimen flatness.
4. Surface finish of specimens and tools.
5. Play and misalignment of tools; rigidity of machine.
6. Zero-point and fracture-point determination.
7. Blank holder load.
8. Lubrication.
9. Speed and temperature of testing.

The first five all relate to the geometry of the specimen and tools; the last four relate to the conduct of the test. In considering these variables in the present work, the temperature was kept substantially constant (between 20 and 23°C). Previous researches had indicated that speed of testing had litte influence, so this was kept constant and at a minimum, thereby easing the problem of detecting the initiation of fracture and ensuring reliability of the readings from the hydraulic gauges of the testing machine used, which could not be depended upon at high speeds. Alignment of the tools and the rigidity of the machine were checked and found to be satisfactory. The specimens were sufficiently flat, having been cut from 6 x 3 ft sheets. The zero point was always checked and corrected, if necessary, as described in section 10.2.1. For the end point determination, an electronic cut-out mechanism had been incorporated in the machine by the makers, and this was generally found to be adequate. The surface of the tools was highly polished (approximately 8 μ-in. c.l.a. for the die and 6 for the punch), and did not vary during the tests. The lubrication conditions were kept constant by applying the H.T.G. graphite grease supplied by the Shell Oil Company as recommended in the D.I.N. specification (30). In this way also the surface finish of the tools was protected and the sensitivity of the material to the test increased, since friction was reasonably low.

The remaining factors (items 1, 2, 7, 8) were varied in a systematic way for each material to cover a wide range of test conditions and effects of altering them were studied to indicate the requirements which might have to be met in any specification.

Stretch forming tests were conducted up to the onset of fracture by using serrated dies for positive clamping of the specimen. Tests were also carried out to observe the development of strains up to fracture. These covered various materials, frictional conditions, and hemispherical and ellipsoidal punch profile shapes. Strain distributions, punch load-punch penetration curves, etc. were obtained for comparisons with the theory. These were also obtained in the experiments on the Erichsen test.

A similar programme of experiments was completed for deep-drawing tests with dies of generous profile radii. Critical, under and oversize blanks were tested. Here the main emphasis was to test the method mentioned in section 2.2. for the prediction of L.D.R., and also compare strain distributions and other findings with those obtained in the stretch forming process.

Uniaxial tension and plane-strain tests were carried out on the materials used, to determine their basic stress-strain characteristics for use in the theory and in correlations.

Cross-correlations between different tests were attempted qualitatively.

CHAPTER - 3 - THEORY OF QUASISTATIC AXISYMMETRICAL DEFORMATION OF SHEET METAL

The term sheet metal implies that the thickness is small in comparison to the plan dimensions. A common range of thickness would be from 0.010 to 0.15 inch.

In the theory presented in the following sections, changes of variables through the thickness direction are not considered, except for an approximation for the thickness stress. A theory which included such considerations would solve the problem of indentation of a finite medium by a rigid body in the plastic range, as well as the axisymmetrical deformation of sheet metal. Although it is possible to formulate such a theory, however complicated it might be, it is not foreseen that a numerical solution can be obtained even by the high speed computers of the present day. This would require at least a ten to hundred fold multiplication of the "memory (or store)" and computer time required for the present theory, which would not be easily available in the foreseeable future.

It was therefore decided to make this theory as realistic as possible, introducing the effects of all the important variables (see section 2.1), nevertheless still solvable with present day facilities. Deformations in the elastic range are neglected, since they represent a very small fraction of the plastic strains involved.

This is equivalent to taking the Young's modulus as infinity as in the case of a plastic-rigid material.

The class of problems, including stretch forming, deep-drawing, and hydraulic bulging, are known as non-steady motion problems. The stress field, and geometry of the material change in time, and also from point to point, unlike those occurring in steady-state rolling of strip or sheet-drawing, where the material goes through the same stationary stress field. This makes the strain history very complicated, and generally non-uniform, which prevents obtaining a solution in closed form.

3.1. Basic Equations

The plastic deformation of an element of sheet metal must satisfy the laws of plastic flow, equilibrium of forces, and the imposed geometrical and boundary conditions. The necessary and sufficient equations governing such deformations are derived below. Since large plastic deformations are involved, elastic strains are neglected, and therefore the plastic strains are equal to the total strains (superscript "p" is omitted for plastic strains). Also time and temperature effects are not considered since they do not fall within the scope of the present investigation.

(i) Yield Criterion and Stress-Strain Relationships

To be able to determine the conditions of yield, and to obtain a universal definition of an "equivalent stress" independent of any stress system, the concept of a yield criterion is used. By such means, the fundamental mechanical properties of a material obtained in a simple test (e.g. tension test), can be used in a complex state of stress, such as the one which exists in stretch forming.

The state of stress at a point in a material is uniquely determined by the three principal stress components, which are the roots of the following cubic equation.

$$s^3 - J_1 s^2 - J_2 s - J_3 = 0 \qquad (3.1)$$

where

$$J_1 = \sigma_{ii}$$

$$J_2 = \tfrac{1}{2}\sigma_{ij}\sigma_{ij} - \tfrac{1}{2}(\sigma_{ii})^2$$

$$J_3 = \tfrac{1}{3}\sigma_{ij}\sigma_{jk}\sigma_{ki} - \tfrac{1}{2}\sigma_{ij}^{\ 2}\sigma_{kk} + \tfrac{1}{6}(\sigma_{ii})^3$$

which are the invariants of the stress tensor σ_{ij}.

A possible yield criterion should then be a symmetric function in stresses which satisfies

$$f(J_1, J_2, J_3) = 0 \qquad (3.2)$$

Bridgman (11) showed that moderate hydrostatic pressure or tension does not influence yielding to a first approximation when applied alone or superposed on a state of combined stress. Hence a possible yield criterion can be expressed in terms of the stress deviations, independent of the hydrostatic stress.

$$\sigma'_{ij} = \sigma_{ij} - \sigma\delta_{ij}$$

and eq. (3.2) becomes:

$$f\,(J_2', J_3') = 0 \tag{3.3}$$

where
$$J_2' = \tfrac{1}{2}\sigma_{ij}'\,\sigma_{ij}'$$
$$J_3' = \tfrac{1}{3}\sigma_{ij}'\,\sigma_{jk}'\,\sigma_{ki}'$$

which are the invariants of the deviatoric or the reduced stress tensor σ_{ij}', where $\sigma_{ii}' = 0$.

The work of Dorn (20), of Fisher (23), of Jackson et al. (40), of Hill (38) and Drucker (21) indicated that for a wide range of anisotropic materials, a yield function quadratic in stresses is satisfactory. Then for a material free from "Bauschinger effects", eqn.(3.3) reduces to:

$$f\,(J_2') = 0 \tag{3.4}$$

which is identical with the criterion of von Mises for a vanishingly small anisotropy. In the case of orthotropic symmetry of plastic anisotropy in a material where the principal axes of anisotropy coincide with the Cartesian axes of reference, the yield criterion becomes (38, 21):

$$2f(\sigma_{ij}) = F(\sigma_{22}-\sigma_{33})^2 + G(\sigma_{33}-\sigma_{11})^2 + H(\sigma_{11}-\sigma_{22})^2$$
$$+ 2L\tau_{23}^{\ 2} + 2M\tau_{31}^{\ 2} + 2N\tau_{12}^{\ 2} = 1 \qquad (3.5)$$

where the coefficients of the quadratic terms are parameters characteristic of the current state of anisotropy.

If X, Y, Z are the tensile yield stresses (directions 11, 22, and 33 respectively), and X_s, Y_s, Z_s are the yield stresses in shear (directions 31, 12, and 23 respectively) with respect to the principal directions of anisotropy (1, 2, 3 respectively), from eqn. (3.5):

$$\frac{1}{X^2} = G + H \qquad 2F = \frac{1}{Y^2} + \frac{1}{Z^2} - \frac{1}{X^2} \qquad 2L = \frac{1}{Z_s}$$
$$\frac{1}{Y^2} = F + H\ , \qquad 2G = \frac{1}{Z^2} + \frac{1}{X^2} - \frac{1}{Y^2} \quad \text{and} \quad 2M = \frac{1}{X_s} \qquad (3.6)$$
$$\frac{1}{Z^2} = F + G \qquad 2H = \frac{1}{X^2} + \frac{1}{Y^2} - \frac{1}{Z^2} \qquad 2N = \frac{1}{Y_s}$$

Since the task of relating the parameters of anisotropy to the strain history is very complicated, Hill (38) considered a material having an initial pronounced preferred orientation which remained the same throughout the deformation. This requires the yield stresses increase in a strict proportion as the material strain-hardens.

$$\text{i.e.} \quad X = h\,X_o \qquad Y = h\,Y_o \qquad Z = h\,Z_o \quad \text{etc.} \tag{3.7}$$

where h is a parameter monotonically increasing with respect to straining and therefore showing the amount of strain-hardening. From eqns. (3.6) using eqns. (3.7)

$$F = \frac{F_o}{h^2} \qquad G = \frac{G_o}{h^2} \qquad H = \frac{H_o}{h^2} \quad \text{etc.} \tag{3.8}$$

Substituting eqns. (3.8) in eqn. (3.5) and adjusting the numerical constant such that the equivalent stress will be equal to the uniaxial tensile stress for the isotropic case, Hill (38) obtained:

$$\bar{\sigma} = \left[\frac{3}{2}\left(\frac{F_o(\sigma_2-\sigma_3)^2+G_o(\sigma_3-\sigma_1)^2+H_o(\sigma_1-\sigma_2)^2+2L_o\tau_{23}^2+2M_o\tau_{31}^2+2N_o\tau_{12}^2}{F_o+G_o+H_o}\right)\right]^{\frac{1}{2}} \tag{3.9}$$

It is important to note that the experimental evidence (21) shows that the yield function usually depends explicitly on the strain. Also, the equivalent stress, in general, must include "stress history" or the path of loading rather than the final values only. Therefore the concepts of the above, and the following supplementary rules of plastic flow are limited although they have a very useful range of validity.

To obtain the stress-strain relationships in the plastic range for strain-hardening materials the three fundamental laws of plasticity must be satisfied.
i.e. the requirements of positive plastic work:

$$\sigma_{ij} \; d\varepsilon_{ij}^{*p} > 0 \quad ,$$

positive plastic work by the stress increments:

$$d\sigma_{ij}^{*} \; d\varepsilon_{ij}^{*p} > 0 \quad ,$$

and the existence of a loading surface at each stage of plastic deformation. However, as shown by Drucker (21), these are insufficient, and the indeterminacy can be overcome by the assumption of a linear relation between $d\varepsilon_{ij}^{*p}$ and $d\sigma_{ij}^{*}$ such as:

$$d\varepsilon_{ij}^{*p} = H_{ijkl} \; d\sigma_{kl}^{*}$$

where H_{ijkl} are functions of stress, strain and the history of loading. The assumption of linearity is associated with taking H_{ijkl} as independent of the $d\sigma_{kl}^{*}$.

The above conditions, and the assumption ofequality of the plastic potential to the yield function lead to the following general definition of the plastic strain increments (21):

$$d\varepsilon^{*p}_{ij} = g \frac{\partial f}{\partial \sigma^{*}_{ij}} \frac{\partial f}{\partial \sigma^{*}_{kl}} d\sigma^{*}_{kl} \tag{3.10}$$

where g is a scalar. If $f = F^{*}(\sigma_{ij})$ only, as is the case in eqn. (3.5), then eqn. (3.10) becomes:

$$d\varepsilon^{*p}_{ij} = g \frac{\partial f}{\partial \sigma^{*}_{ij}} df \tag{3.11}$$

Now the explicit stress-strain relationships can be obtained by applying eqn. (3.11) to the yield function, eqn. (3.5). Therefore the principal plastic strain-increments referred to the principal axes of anisotropy are (38, and 21):

$$\begin{aligned} d\varepsilon^{*}_{1} &= d\lambda \left[H(\sigma_1-\sigma_2) + G(\sigma_1-\sigma_3) \right] \\ d\varepsilon^{*}_{2} &= d\lambda \left[F(\sigma_2-\sigma_3) + H(\sigma_2-\sigma_1) \right] \\ d\varepsilon^{*}_{3} &= d\lambda \left[G(\sigma_3-\sigma_1) + F(\sigma_3-\sigma_2) \right] \end{aligned} \tag{3.12}$$

or alternatively substituting eqns. (3.8) in eqns. (3.12):

$$\begin{aligned} d\varepsilon^{*}_{1} &= d\lambda' \left[H_o(\sigma_1-\sigma_2) + G_o(\sigma_1-\sigma_3) \right] \\ d\varepsilon^{*}_{2} &= d\lambda' \left[F_o(\sigma_2-\sigma_3) + H_o(\sigma_2 \ \sigma_1) \right] \\ d\varepsilon^{*}_{3} &= d\lambda' \left[G_o(\sigma_3-\sigma_1) + F_o(\sigma_3-\sigma_2) \right] \end{aligned} \tag{3.13}$$

where $d\lambda = gdf$ and $d\lambda' = gdf/h^2$ are scalar parameters of proportionality. The relations between the strain-increment ratios and the stress ratios are independent of the value of h.

It must also be observed that only two of the three equations of each set are independent since:

$$d\varepsilon_1^* + d\varepsilon_2^* + d\varepsilon_3^* = 0$$

and hence

$$\varepsilon_1 + \varepsilon_2 + \varepsilon_3 = 0 \tag{3.14}$$

which is the constancy of volume in plastic flow.

Considering a sheet of metal which is isotropic in its plane, and anisotropic in the thickness direction, the strain ratio R can be determined in an uniaxial tension test.

$$\text{Where } R = \frac{\varepsilon_w}{\varepsilon_t} = \frac{d\varepsilon_w^*}{d\varepsilon_t^*} = \text{constant} \tag{3.15}$$

R is expected to be unity for isotropic materials if the results are not influenced by the "size effect" which might be present in short tensile specimens.

It is possible to show from eqns. (3.6), (3.8), and (3.13) for the above state of plastic anisotropy that:

$$F_o = G_o$$

$$\text{and} \quad H_o = R\,G_o \tag{3.16}$$

For a three dimensional stress system, the yield criterion and the stress-strain relationship can be written in terms of the stress ratios which would be more convenient for computational purposes.

If $\sigma_2 = x\sigma_1$ and $\sigma_3 = k\sigma_1$ (3.17)

then substituting eqns. (3.16), (3.17) into eqns. (3.9), and (3.13) we find:

$$\bar{\sigma} = \left\{ \frac{3\left[x^2+1+2k(k-1-x) + R(1-2x+x^2)\right]}{2(2+R)} \right\}^{\frac{1}{2}} \sigma_1$$

(yield criterion) (3.18)

$$d\varepsilon_1^{*} = d\lambda'' \left[R(1-x) + (1-k) \right]$$

$$d\varepsilon_2^{*} = d\lambda'' \left[(x-k) + R(x-1) \right]$$

$$d\varepsilon_3^{*} = d\lambda'' \left[2k - 1 - x \right]$$

(stress-strain relations) (3.19)

where $d\lambda''$ is another scalar parameter.

(ii) Equivalent Anisotropic Plastic Strain-Increment

It is advantageous to be able to define a scalar measure, which would be equivalent to the effects of the incremental plastic strains ($d\varepsilon_{ij}^{*p}$) as far as strain-hardening is concerned. This can be done by assuming that strain hardening is a function of the plastic work and independent of path of straining. However, this is not strictly true and Drucker (21) shows the path and strain dependence of plastic work. The error is increased by the amount that the path of loading deviates from a radial one, but this assumption seems to be reasonable for a strain history such as occurs in stretch forming where the stress ratios do not usually change by more than about 100%.

Hence $dW^{p} = \sigma_{ij} d\varepsilon^{*}_{ij} = \bar{\sigma}\, d\bar{\varepsilon}^{*}$ (3.20)

where $d\bar{\varepsilon}^{*}$ is the equivalent anisotropic plastic strain increment, and is expressed only in terms of $d\varepsilon^{*}_{ij}$, because:

$$dW^{p} = \sigma_{ij} d\varepsilon^{*p}_{ij} = \sigma_{ij}\, g \frac{\partial f}{\partial \sigma^{*}_{ij}} df = g\, 2f df$$

$$= \frac{2}{c}\, g\, c\sqrt{f}\sqrt{f}\ df = \left(g \frac{2}{c} \sqrt{f}\ df\right) \bar{\sigma}$$

$$\text{where } d\bar{\varepsilon}^{*} = g \frac{2}{c} \sqrt{f}\ df \qquad (3.21)$$

To find f as a function of the strain increments, eqns. (3.13) are used. The stress differences in terms of strain increments are then substituted in eqn. (3.5). Hence from eqn. (3.21), using this f, and adjusting the numerical constant such that for isotropic materials $d\bar{\varepsilon}^{*} = d\varepsilon^{*}_{\ell}$ in uniaxial tension, the following expression for $d\bar{\varepsilon}^{*}$ in terms of the principal incremental plastic strains is obtained (38, 21):

$$d\bar{\varepsilon}^{*} = \frac{\left[\frac{2}{3}\ (F_o+G_o+H_o)\right]^{\frac{1}{2}}}{F_oG_o+G_oH_o+H_oF_o} \Big[F_o\ (G_o\ d\varepsilon^{*}_2 - H_o\ d\varepsilon^{*}_3)^2$$

$$+ G_o(H_o d\varepsilon^{*}_3 - F_o d\varepsilon^{*}_1)^2 + H_o(F_o d\varepsilon^{*}_1 - G_o d\varepsilon^{*}_2)^2\Big]^{\frac{1}{2}} \qquad (3.22)$$

For a sheet metal which is isotropic in its plane and anisotropic in the thickness direction, $d\bar{\varepsilon}^*$ can be written in terms of R, by using eqn. (3.16).

$$d\bar{\varepsilon}^* = \frac{\left[\frac{2}{3}\ (2+R)\right]^{\frac{1}{2}}}{1+2R}\left[\ (1+2R)(d\varepsilon_1^{*2} + d\varepsilon_2^{*2})+(2R^2+R)\ d\varepsilon_3^{*2}\ \right]^{\frac{1}{2}}$$

or also using the constancy of volume (eq. 3.14);

$$d\bar{\varepsilon}^* = \frac{\left[\frac{2}{3}\ (2+R)\right]^{\frac{1}{2}}}{1+2R}\left[\ (2R^2+3R+1)(d\varepsilon_1^{*2}+d\varepsilon_2^{*2})+2(R+2R^2)d\varepsilon_1^* d\varepsilon_2^*\right]^{\frac{1}{2}} \tag{3.23}$$

or

$$d\bar{\varepsilon}^* = \frac{\left[\frac{2}{3}\ (2+R)\ \right]^{\frac{1}{2}}}{1+2R}\left[(1+3R+2R^2)d\varepsilon_3^{*2}\ +2(2R+1)(d\varepsilon_2^{*2}+d\varepsilon_2^* d\varepsilon_3^*)\right]^{\frac{1}{2}}$$

(iii) <u>Strain-Hardening Law</u>

The derivation of $d\bar{\varepsilon}^*$ was based on the hypothesis that plastic work was independent of strain history.

i.e. $W^p = \int \sigma_{ij} d\varepsilon_{ij}^* = \int \bar{\sigma}\, d\bar{\varepsilon}^*$

Here $\bar{\sigma} = F^* \left(\int \bar{\sigma}\, d\bar{\varepsilon}^*\right)$, and

therefore $\bar{\sigma} = \bar{F}^* \int d\bar{\varepsilon}^*$ (3.24)

where $\int d\bar{\varepsilon}^*$ is evaluated over the strain path. Eqn. (3.24) can now be regarded as unique, and giving the functional relationship between $\bar{\sigma}$ and $\bar{\varepsilon}$.

It would be convenient to represent this function ($\bar{F}^*$) in a mathematical form for possible uses in numerical computation, and also to judge the material characteristics from the magnitudes of the constants involved in a suitable formula. Such a formula should include the effects of strain-hardening rate and its variation, and pre-strain, which are essential, at any rate for the present work. Swift (79) proposed the following formula fulfilling these requirements. However, in the present work, for anisotropic materials, this formula is used to express the relationship between the true stresses and true strains in the directions of the tests. e.g. in direction 1:

$$X = A(B + \varepsilon_{\ell})^{n} \qquad (3.25)$$

This can easily be converted to $\overline{F}^{*}$ ($\bar{\sigma}$ vs. $\bar{\varepsilon}$) by means of constants involving R, as shown in section 3.2. In eqn. (3.25), n indicates the rate of strain-hardening and its variation with strain, and B shows the amount of pre-strain which are both dimensionless. "A" is in the dimensions of stress. The exponent n does not depend on pre-strain B which is an advantage. The special case of this equation in which B = 0 is generally known as the Ludwik power law (61), and it gives a more approximate representation of strain-hardening for many materials. The constant n depends on pre-strain, but the process of curve fitting to experimental data is much simpler. The technique used to find the constants in eqn. (3.25) for a given material is described in section 8.1.5.

For investigations related to plastic instability, such formulae should give a "smooth" curve free from oscillations, as might be obtained by using high degree polynomials for an attempt to obtain a better fit to the experimental data. Such an effect might lead to a result giving apparent multiple plastic instability points which would be unacceptable if such an oscillation is not present in the real experimental data. The above formula is smooth and satisfies this requirement.

(iv) Equilibrium of Forces

In the derivation of the equations of equilibrium of quasistatic forces, variations of stresses through the shell wall are neglected. This is a very realistic assumption where $\rho_1 > 6\ t_o$ as indicated by Wallace (85), in sheet metal deformation. Hence the effects of bending and the transverse shear stresses are also not considered. Inclusion of these factors would have complicated the problem without a marked improvement in the results, and would have demanded large amounts of computer time which was not available.

In Fig. 3, the membrane stresses acting on an element of the shell wall are shown. This is a general element and applies to the region over the punch head and between the die and the punch in stretch forming, and is also valid in hydraulic bulging. The stresses

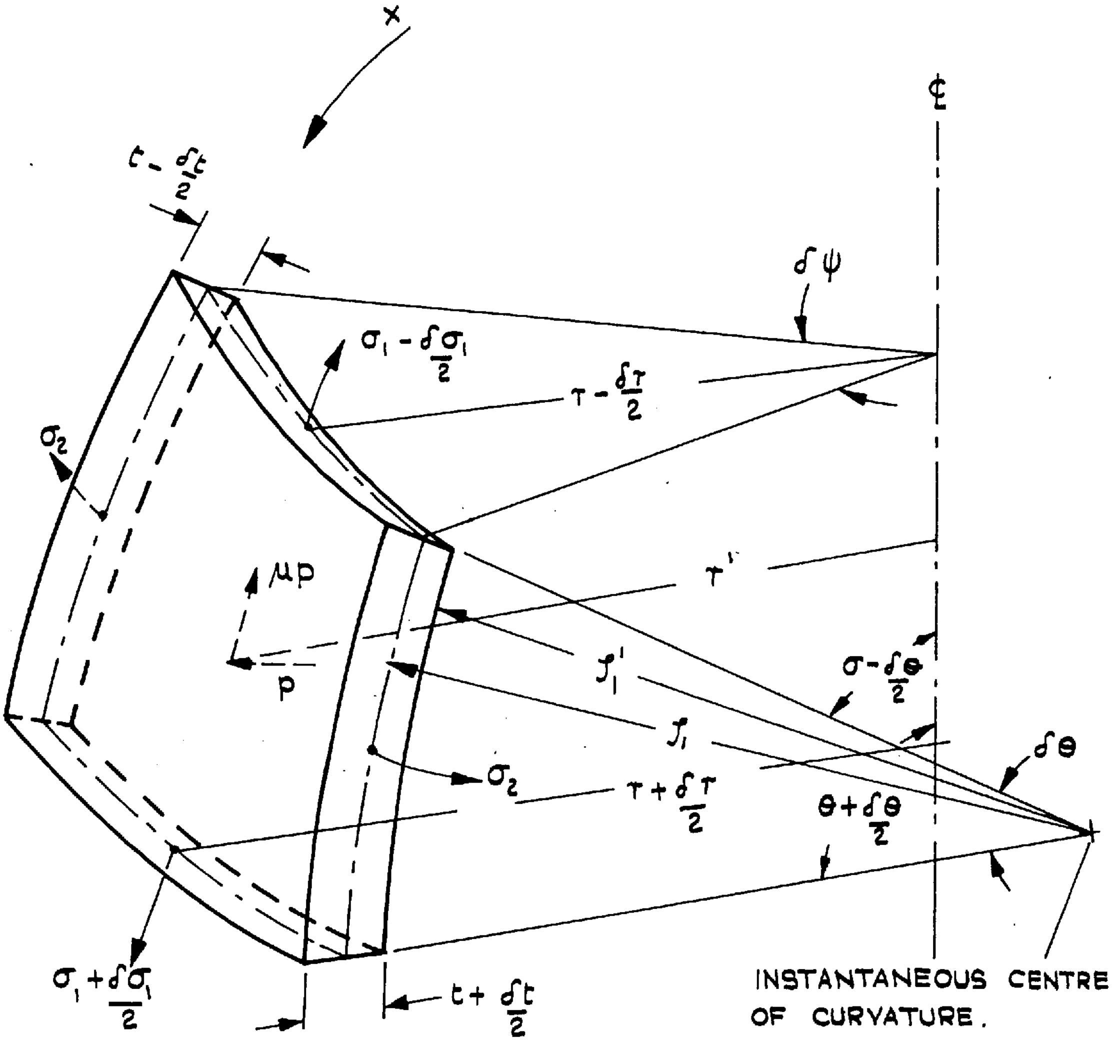

FIG. 3. - STRESSES ON ELEMENT OF SHELL WALL.

σ_1 and σ_2 (meridional and circumferential) would be the principal stresses in the absence of boundary friction. However when there is friction the direction of σ_1 is influenced, but the magnitude of the surface shear stress does not exceed 6% of σ_1 when $\mu \leqslant 1$, and therefore σ_1 tangent to the mean shell wall can be taken as a principal stress.

The rate of change of the variables with respect to ϕ is zero because of the axial symmetry and also the consideration of plastic isotropy in the plane of the sheet metal. These conditions are satisfied by the equiation of equilibrium in the direction of σ_2. The two other independent equations are for the radial and the vertical directions.

In the radial direction:

$$
\begin{aligned}
&- (\sigma_1 - \frac{\delta\sigma_1}{2})(r - \frac{\delta r}{2})\ \delta\phi(t - \frac{\delta t}{2}) \cos\left(\theta - \frac{\delta\theta}{2}\right) + \\
&+ (\sigma_1 + \frac{\delta\sigma_1}{2})(r + \frac{\delta r}{2})\ \delta\phi(t + \frac{\delta t}{2}) \cos\left(\theta + \frac{\delta\theta}{2}\right) + \\
&+ pr'\ \delta\phi\,\rho_1'\,\delta\theta \sin\theta - \mu pr'\delta\phi\,\rho_1'\,\delta\theta\cos\theta - \\
&- 2\sigma_2\ \rho_1\,\delta\theta\, t \sin\frac{\delta\phi}{2} = 0
\end{aligned}
\qquad (3.26)
$$

if $\sin\frac{\delta\phi}{2} \cong \frac{\delta\phi}{2}$, $\sin\frac{\delta\theta}{2} \cong \frac{\delta\theta}{2}$, $\cos\frac{\delta\theta}{2} \cong 1$,

$$\cos\left(\theta - \frac{\delta\theta}{2}\right) = \cos\theta + \sin\theta\frac{\delta\theta}{2}$$

and, (3.27)

$$\cos\left(\theta + \frac{\delta\theta}{2}\right) = \cos\theta - \sin\theta\frac{\delta\theta}{2}$$

Eqns. (3.27) are substituted in eqn. (3.26). After expanding and collecting terms, and neglecting one term involving third order differences, in the limit ($dr \rightarrow o$) the following equation is obtained:

$$\frac{1}{r}\frac{d}{dr}(\sigma_1 tr) + \left[p\rho_1'\frac{r'}{r}(\tan\theta - \mu) - \sigma_1 t\tan\theta - \sigma_2\frac{\rho_1 t}{r\cos\theta}\right]\frac{d\theta}{dr} = 0 \tag{3.28}$$

Similarly, in the vertical direction the equation of equilibrium is:

$$\frac{1}{r}\frac{d}{dr}(\sigma_1 tr) + \left[\sigma_1 t\cot\theta - p\rho_1'\frac{r'}{r}(\cot\theta + \mu)\right]\frac{d\theta}{dr} = 0 \tag{3.29}$$

Substracting eqn. (3.29) from eqn. (3.28) and after some manipulation:

$$p = \frac{t}{\rho_1' r'}(\sigma_1 r + \sigma_2\rho_1\sin\theta) \tag{3.30}$$

where $\rho_1 = \rho_1' + \frac{t}{2}$

and $r = r' + \sin\theta\frac{t}{2}$ (3.31)

Since for an axisymmetrical shell, from eqn. (B.1):

$$\frac{d\theta}{dr} = \frac{1}{\rho_1 \cos\theta} \tag{3.32}$$

and if $\sigma_2 = x\sigma_1$, and also from eqns. (3.29) and (3.30):

$$\frac{d}{dr}(\sigma_1 t) = \sigma_1 t\left[\frac{x-1}{r} + \mu\left(\frac{1}{\rho_1 \cos\theta} + \frac{x\tan\theta}{r}\right)\right] \tag{3.33}$$

which is in a form convenient for numerical computation.

(v) Strain Compatibility

The strains in a deforming shell cannot be independent of each other, and they must satisfy a relationship demanded by the initial and current geometry of the shell. Here again the variations of the strains through the shell wall are neglected consistent with the similar assumption with the stresses in the equilibrium equations. Since the elastic strains are neglected, this relationship is in terms of plastic or total strains. Moreover, logarithmic (or true) strains are used since the plastic deformations encountered are very large.

The principal strains are in meridional, circumferential and thickness directions, and they are given by the following equations:

$$\varepsilon_1 = \int_0^{\varepsilon_1} d\varepsilon_1^* = \ln\left(\frac{\cos\theta_o}{\cos\theta}\,\frac{dr}{dr_o}\right)$$

$$\varepsilon_2 = \int_0^{\varepsilon_2} d\varepsilon_2^* = \int_{r_o}^{r} \frac{dr^*}{r} = \ln\frac{r}{r_o} \tag{3.34}$$

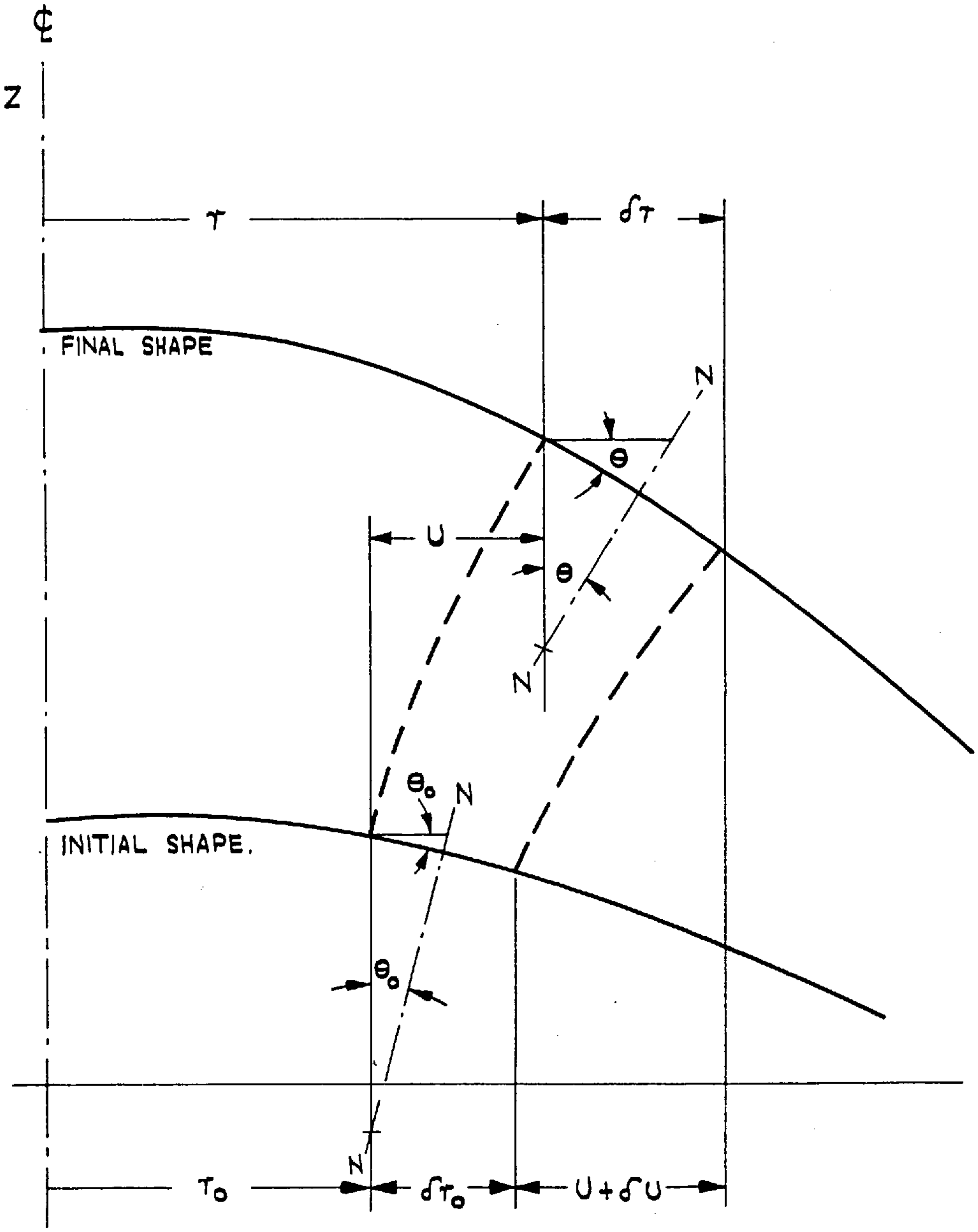

FIG. 4. DEFORMATION OF THE MIDDLE SURFACE OF THE SHELL.

$$\varepsilon_3 = \int_0^{\varepsilon_3} d\varepsilon_3^* = \int_{t_o}^{t} \frac{dt^*}{t} = \ln\left(\frac{t}{t_o}\right)$$

Fig.4 shows the deformation of the middle surface of the shell. If u is the radial displacement from an initial position:

$$r = r_o + u \quad , \quad \text{and} \quad dr = dr_o + du \,. \tag{3.35}$$

From the first of eqns. (3.34) and the second of eqns. (3.35):

$$e^{\varepsilon_1} = \frac{\cos\theta_o \; dr}{\cos\theta \; dr_o} = \frac{\cos\theta_o \; dr}{\cos\theta(dr - du)}$$

After rearranging:

$$\frac{du}{dr} = 1 - e^{-\varepsilon_1} \frac{\cos\theta_o}{\cos\theta} \,. \tag{3.36}$$

From the second of eqns. (3.34):

$$e^{\varepsilon_2} = \frac{r}{r_o} = \frac{r}{r-u} \,, \text{ and}$$

after differentiating with respect to r and rearranging:

$$\frac{du}{dr} = 1 - e^{-\varepsilon_2}\left[1 - r\frac{d\varepsilon_2}{dr}\right] \tag{3.37}$$

Equating the eqns. (3.36) and (3.37), and rearranging:

$$\frac{d\varepsilon_2}{dr} = \frac{1}{r}\left(1 - e^{-\varepsilon_1+\varepsilon_2} \frac{\cos\theta_o}{\cos\theta}\right) \tag{3.38}$$

A more useful form of this equation can be obtained using eqn. (3.14):

$-\varepsilon_1 = \varepsilon_2 + \varepsilon_3$ and substituting this in eqn.(3.38):

$$\frac{d\varepsilon_2}{dr} = \frac{1}{r}\left(1 - e^{2\varepsilon_2+\varepsilon_3} \frac{\cos\theta_o}{\cos\theta}\right) \qquad (3.39)$$

The equations (3.38) and (3.39) although they involve the total strains ε_2 and ε_3, can be used in the incremental theory of plasticity, as long as:

$$\varepsilon_2 = \int_0^{\varepsilon_2} d\varepsilon_2^{*}, \quad \text{and } \varepsilon_3 = \int_0^{\varepsilon_3} d\varepsilon_3^{*}$$ are taken along the strain paths. It must also be emphasized that the L.H.S. of eqns. (3.38) and (3.39) give the instantaneous rate of change of the true circumferential strain across a bulge unlike the equations (3.12) and (3.13), which give the increments of strain along the corresponding strain paths in time. The relationship between the two types of increments are given in the following section.

(ii) Compatibility of the Increments of the Variables in Time and Space

The increments of the variables between two neighbouring points on the bulge at an instant, and the increments between the two values of the same point at different instants are dependent on each other. It is possible to find one in terms of the other.

Fig.5 shows the increments of the variables in time and space co-ordinates including a discontinuity. Since in general the following argument applies to all variables (e.g. stress, strain, radius, angle, etc.), such a variable is designated by "V". If currently one is dealing with point T at time "n", and location "m" in space, then the useful neighbouring points will have the values and the increments as shown in Fig.5. Generally points E and S are known either from the boundary conditions or from the previously calculated points. A moving discontinuity is shown in the figure which can be the moving contact of sheet metal with the punch or die, and it separates the two regions where the stress systems are different, e.g. over the punch head, and between punch and die.

The types of discontinuities at points P and Q (or G) are different. At point Q the equilibrium equations, and the strain compatibility equations are discontinuous due to the changes in frictional conditions and geometry, which results in a different method of solution in the second region. Generally the solution of the first region is extended to the next point beyond Q, and Q is treated as an interior point and the corresponding values of the variables are determined by Lagrangian interpolation, as described in Chapter 5. Solution of the second region is obtained starting from

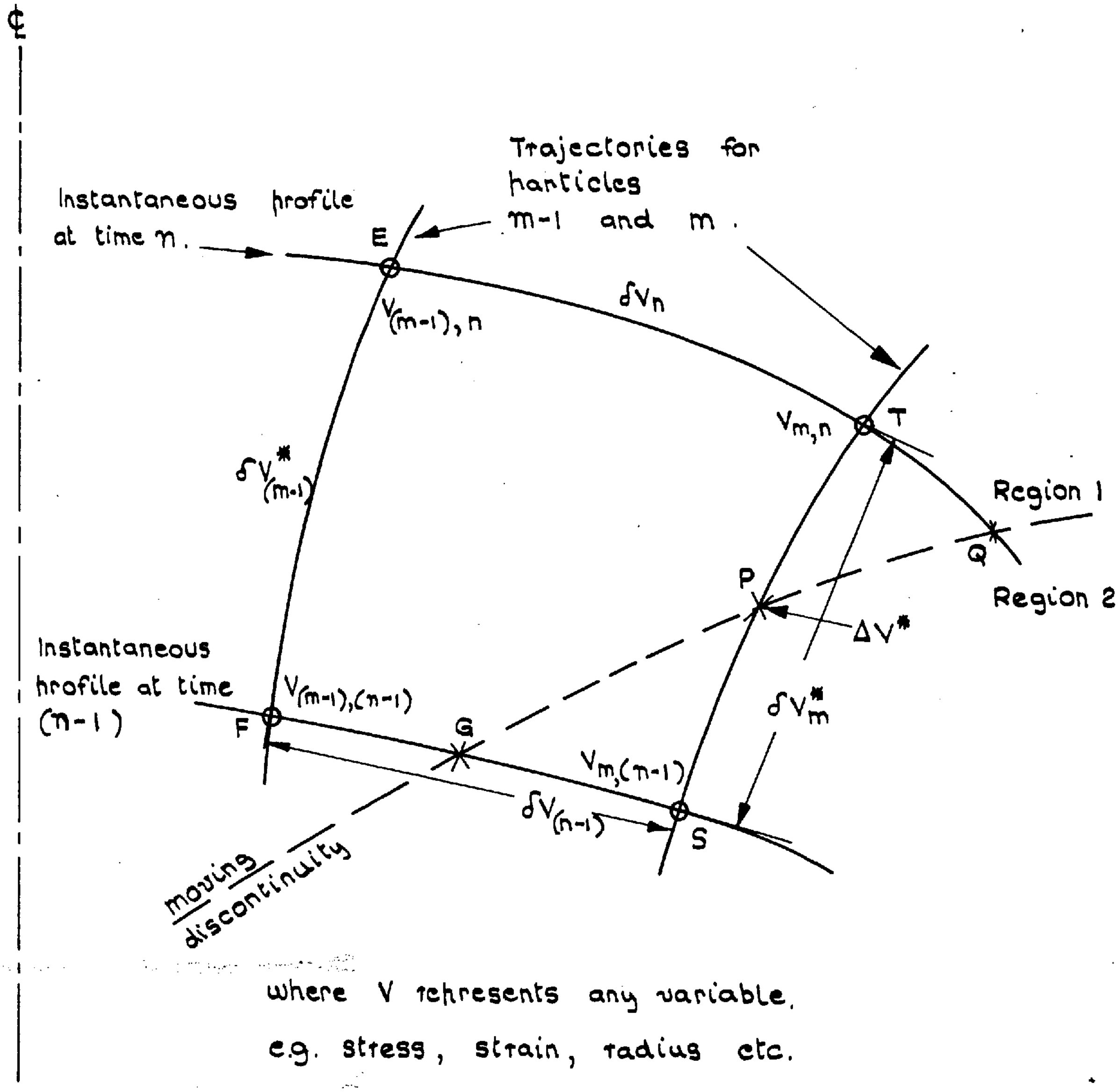

FIG. 5. INCREMENTS OF VARIABLES IN TIME AND SPACE - ALSO SHOWING A DISCONTINUITY.

Q with new boundary conditions.

However at point P, the stress-strain relations, and the incremental equivalent plastic strain equations are affected due to the change from a biaxial to a triaxial stress system or vice versa, if the effect of the thickness stress is considered. At both points the yield criterion is influenced. Also at P, if this is a singular point where there might be additional straining, e.g. due to bending under tension, discontinuities (ΔV^*) in the variables might occur.

Hence allowing for the above effects, and considering the fact that point T can be reached either from point E or from point S with the corresponding increments:

$$V_{m,n} = V_{(m-1),n} + \delta V_n$$

and $$V_{m,n} = V_{m,(n-1)} + \delta V_m^*$$

therefore $$V_{(m-1),n} + \delta V_n = V_{m,(n-1)} + \delta V_m^* \qquad (3.40)$$

is obtained where,

$$\delta V_m^* = \delta V_{m,(S-P)}^* + \Delta V^* + \delta V_{m,(P-T)}^* \qquad (3.41)$$

Eqn. (3.40) is used particularly for the variables ϵ_2, ϵ_3, x and θ in the present work, since the remaining ones are dependent on these.

(vii) <u>Geometrical Relationships and the Boundary Conditions</u>

The geometrical relationships related to the hemispherical and ellipsoidal punches, and bulge depth calculations are given in Appendix-B.

There are two types of boundary conditions:

a) Initial conditions at a point - Analytical formulae can be derived to find all or some of the variables involved only at some special points (e.g. pole, contact of sheet metal with punch or die, and clamped edge), at a fixed time or stage during the deformation. The derivation of the necessary initial and boundary conditions are presented in the remainder of this Chapter.

b) Initial conditions as functions of radius before the occurrence of any plastic deformation - These initial conditions take into account the previous history of the deformation of sheet metal prior to the current deformation process. By such means it is possible to take into account the variations of ε_1, ε_2, ε_3, $\bar{\varepsilon}$, and θ on the original undeformed blank.

i.e. if subscript n = 0 for the original blank

$V_{m,o}$ must be known for the whole blank for the above variables. In the present work flat blanks of uniform thickness, and prestrain were used, so all strains, and slope were zero except for, $\bar{\varepsilon}_{m,o}$ = B. Theoretically there is no difficulty involved in introducing such variations but such cases are not encountered very often in practice.

3.2. Equations for Stretch Forming

The necessary and the sufficient equations for solving the stretch forming problem can be obtained, some directly, and others with some manipulation, from the equations given in section 3.1., and Appendix-B. Due to the existence of the two regions, corresponding to two different states of stress, the respective equations, some of which are different, are given separately.

3.2.1. Region over Punch Head

This region where the sheet metal is in contact with the punch is called region one*. The required basic equations, which are effective in this region are:

Equilibrium: Eqn. (3.33) can directly be used without further modification. Since r is chosen as the independent variable as opposed to θ in the numerical analysis, it is advantageous to compute ρ_1, $\cos\theta$, and $\tan\theta$ from eqns. (B.14), (B.12), (B.11), (B.17), and (B.18) for the ellipsoidal, and the hemispherical punches. For use in the above equations r' is computed from eqn. (3.31) from a given r value, because the inside of the shell is truly ellipsoidal or hemispherical, and not the mean surface.

---

* 'One' will be used as a subscript to the brackets containing terms belonging to this region. This convention will be similarly applied to the other regions, and will be used when terms related to different regions are discussed together.

The interfacial pressure is found from the second equation of equilibrium, eqn. (3.30).

<u>Strain Compatibility</u>: Since all of the calculations were made for the initially flat blanks, $\cos\theta_o = 1$ and equation (3.39) can be reduced to:

$$\frac{d\varepsilon_2}{dr} = \frac{1}{r}\left(1 - \frac{e^{2\varepsilon_2+\varepsilon_3}}{\cos\theta}\right) \tag{3.42}$$

Here, as with the equation of equilibrium, $\cos\theta$ is calculated from eqns. (B.12) or (B.17) using r'.

<u>Stress-Strain Relationships</u>: Since only two out of the three equations are independent as shown before, the second and the third of eqns. (3.19) are used to eliminate the unknown scalar parameter $d\lambda''$ between them. Dividing them side by side and simplifying:

$$d\varepsilon_3^{*} \cong \frac{2k - 1 - x}{(R+1)x-R-k}\, d\varepsilon_2^{*} \tag{3.43}$$

where $k = \frac{\sigma_3}{\sigma_1}$, and the thickness stress is equal to the interfacial pressure on the inner surface of the shell, and is zero on the outer surface. The thickness stress at the mean surface is approximated by the half of the interfacial pressure, hence $\sigma_3 \cong -\frac{p}{2} = -\frac{\sigma_1 t}{2\rho_1' r'}(r+x\rho_1\sin\theta)$

therefore
$$k = -\frac{t}{2\rho_1' r'}(r+x\rho_1\sin\theta) \tag{3.44}$$

which should be used in eqn. (3.43).

<u>Yield Criterion</u>: The yield criterion is given by eqn. (3.18) which can be used as it is, where k is substituted from eqn. (3.44).

<u>Equivalent Strain-Increment</u>: Since $d\varepsilon_2^*$ and $d\varepsilon_3^*$ are used in the numerical analysis, and $d\varepsilon_1^*$ is derived from the constancy of volume (eqn. 3.14), the third of eqn. (3.23), which involves the above increments is used to calculate $d\bar{\varepsilon}^*$.

<u>Strain-Hardening Law</u>: This is used in order to find $\bar{\sigma}$ from a given $\bar{\varepsilon}$. Eqn. (3.25) gives the relationship between ε_ℓ and X in simple tension, and for a complex state of stress the following analysis is adopted.

To obtain the relationship between the uniaxial stress (σ_1) (or the yield stress (X) in the same direction) and the equivalent stress ($\bar{\sigma}$) in uniaxial tension:

x = k = 0 is substituted in eqn.(3.18), and after simplifying,

$$\bar{\sigma} = \left[\frac{3(R + 1)}{2(R + 2)}\right]^{\frac{1}{2}} X \qquad (3.45)$$

To obtain the relationship between the longitudinal strain-increment and the equivalent strain-increment x = k = 0 is substituted in eqns. (3.19) and dividing them side by side the following ratios are obtained:

$$\frac{d\varepsilon_2}{d\varepsilon_1} = \frac{-R}{R+1} \quad \text{and} \quad \frac{d\varepsilon_3}{d\varepsilon_1} = \frac{-1}{R+1} \tag{3.46}$$

Eqns. (3.46) are then substituted in the last of eqns. (3.23), and after simplifying:

$$d\bar{\varepsilon} = \left[\frac{2(R+2)}{3(R+1)}\right]^{\frac{1}{2}} d\varepsilon_\ell \qquad \text{since } d\varepsilon_\ell = d\varepsilon_1$$

and (3.47)

$$\bar{\varepsilon} = \left[\frac{2(R+2)}{3(R+1)}\right]^{\frac{1}{2}} \varepsilon_\ell \qquad \text{are obtained}$$

considering that, in uniaxial tension the strain ratios remain constant throughout the deformation.

Hence substituting eqns. (3.45) and (3.47) in eqn. (3.25),

$$\bar{\sigma} = \left[\frac{3(R+1)}{2(R+2)}\right]^{\frac{1}{2}} A\left(B + \left[\frac{3(R+1)}{2(R+2)}\right]^{\frac{1}{2}} \bar{\varepsilon}\right)^n \tag{3.48}$$

the desired relationship between $\bar{\sigma}$ and $\bar{\varepsilon}$ is obtained for the state of plastic anisotropy considered, in terms of known constants.

<u>Compatibility of the Increments of the Variables in Time and Space</u>:

Eqn. (3.40) is used to find the relationship between the two types (see 3.1-vi) of increments of the variables ε_2, ε_3, and x. $\Delta V^* = 0$ for points in region one at the (n-1) th and nth stages of deformation, and also for points in region two at (n-1)th and in region one at nth stages except for x. The discontinuity in x will be discussed in 5.1.

3.2.2. Region between Die and Punch

This region where the sheet metal is in between die and punch, and not in contact with any rigid body is called region two. The relevant basic equations, governing the plastic deformation are given below:

Equilibrium: Eqn. (3.33) can be used by substituting $\mu = 0$. However, it is more advantageous to derive another equation for vertical equilibrium considering the large element shown in Fig.6.

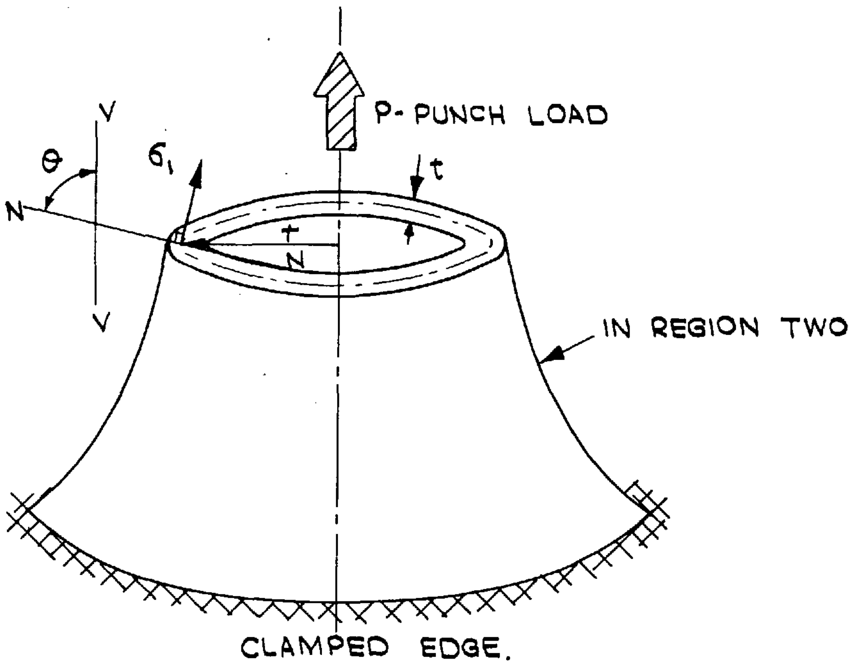

FIG.6 - LARGE ELEMENT OF SHEET METAL IN REGION TWO.

which yields:

$$P = 2\pi r \sigma_1 t \sin\theta \tag{3.49}$$

Here P is the total vertical load transmitted by every section in region two which is equal to the punch load.

It is possible to show that eqn. (3.49) reduces to eqn. (3.33) with $\mu = 0$, but this form is more convenient since it eliminates one integration.

If p = 0 is substituted in the second equation of equilibrium (eqn. (3.30)), after rearranging:

$$\frac{\sigma_1}{\rho_1} = -\frac{\sigma_2}{r}\sin\theta \qquad \text{or with} \qquad \frac{\sigma_2}{\sigma_1} = x$$

$$\frac{1}{\rho_1} = -\frac{x}{r}\sin\theta \tag{3.50}$$

From eqn. (B.1):

$$\cos\theta\frac{d\theta}{dr} = \frac{1}{\rho_1} \tag{3.51}$$

and combining eqns. (3.50), and (3.51):

$$x = -r\cot\theta\frac{d\theta}{dr} \tag{3.52}$$

Equations (3.49) and (3.52) can alternatively be expressed in terms of radii of curvatures as follows:

From eqn. (B.4):

$$\sin\theta = \frac{r}{\rho_2} \tag{3.53}$$

substituting eqn. (3.53) in eqn. (3.49):

$$P = \frac{2\pi r^2\sigma_1 t}{\rho_2} \qquad \text{(equivalent to eqn. 3.49)} \tag{3.54}$$

and substituting eqn. (3.53) in eqn. (3.50):

$$x = -\frac{\rho_2}{\rho_1} \quad \text{(equivalent to eqn. 3.52)} \tag{3.52-a}$$

Strain Compatibility: Eqn. (3.42) as in region one is used for region two. However, in this region the relationship between r and θ is unknown, and is obtained from the numerical solution as explained in 5.1.2. by using a Lagrangian formula.

Stress-Strain Relationships: Since in this region $p = \sigma_3 = k = 0$, eqn. (3.43) will reduce to:

$$d\varepsilon_3^* = -\frac{1+x}{(R+1)x - R}\, d\varepsilon_2^* \tag{3.55}$$

which is the only independent one obtained from the initial three equations (3.19).

Yield Criterion: By substituting k = 0 in eqn. (3.18) the yield criterion effective in this region is obtained:

$$\bar{\sigma} = \left\{ \frac{3\left[x^2+R(x^2-2x+1)+1\right]}{2(2+R)} \right\}^{\frac{1}{2}} \sigma_1 \tag{3.56}$$

The Other Equations, i.e. for the equivalent strain-increment (eqn. 3.23), strain-hardening law (3.48) remain the same and they are used as in region one. Since all variables remain in region two in (n-1)th and nth stages, eqn. (3.40) can be used with $\Delta V^* = 0$ as there is no discontinuity, and this is applied in particular to ε_2, ε_3 and θ.

3.2.3. Boundary Conditions

In stretch forming there are three boundaries, i.e. pole, moving contact of sheet metal with punch with continued deformation, and the clamped edge, which bound the two regions. For the numerical solution it is necessary that the relationships between the different variables, and their derivatives are established by analytical formulae at these boundaries as shown below.

3.2.3.1. At the Pole

Functional Relationships:

At the pole $r = \theta = 0$, and from eqn. (3.33), rewriting for x:

$$x = \frac{\frac{r}{\sigma_1 t}\,\frac{d}{dr}(\sigma_1 t) - \frac{\mu r}{\rho_1 \cos\theta} + 1}{1 + \mu \tan\theta} \qquad (3.57)$$

Substituting $r = \tan\theta = 0$ and $\cos\theta = 1$ in eqn. (3.57):

$$x = 1 \quad \text{or} \quad \sigma_1 = \sigma_2 \qquad (3.58)$$

Using eqns. (3.31), (3.58), (B.4) and B.1), from eqn. (3.30):

$$p = \frac{2\sigma_1 t\,(\rho_1' + 0.5t)}{\rho_1'^2} \qquad (3.59)$$

hence $$\sigma_3 \cong -\frac{p}{2} = -\frac{\sigma_1 t(\rho_1' + 0.5t)}{\rho_1'^2} \tag{3.60}$$

and $$k = \frac{\sigma_3}{\sigma_1} = -\frac{t(\rho_1' + 0.5t)}{\rho_1'^2} \tag{3.61}$$

Substituting eqns. (3.61) and (3.58) in eqn. (3.18) results in:

$$\sigma_1 = \frac{\left(\frac{2 + R}{3}\right)^{\frac{1}{2}} \bar{\sigma}}{\frac{t(\rho_1' + 0.5t)}{\rho_1'^2} + 1} \tag{3.62}$$

From eqns. (3.58) and (3.19):

$$d\varepsilon_1 = d\varepsilon_2 \quad \text{and} \quad d\varepsilon_2 = -\frac{d\varepsilon_3}{2}$$

$$\text{hence} \quad \varepsilon_1 = \varepsilon_2 \quad \text{and} \quad \varepsilon_2 = -\frac{\varepsilon_3}{2} \tag{3.63}$$

Substituting eqns. (3.63) in eqn. (3.23) and integrating yields:

$$\bar{\varepsilon} = \frac{2\left[\frac{1}{3}(4R^3 + 12R^2 + 9R + 2)\right]^{\frac{1}{2}}}{(1 + 2R)} \varepsilon_2 \tag{3.64}$$

Also, eqn. (3.48) is valid at the pole to find $\bar{\sigma}$ from the calculated $\bar{\varepsilon}$.

<u>Derivatives of the Variables</u>:

To find $\frac{d\varepsilon_2}{dr}$, the strain compatibility eqn. (3.42) is used. It is seen that at r = 0, and considering eqns. (3.63), and (3.42) one obtains an indeterminate form ($^0/0$).

Applying the L'Hospitals rule (76) to these equations, does not provide further information, because it either gives further indeterminate forms, or terms involving some unknown derivatives. Studying eqn. (3.42) qualitatively, it is

$$\frac{d\varepsilon_2}{dr} = \frac{1}{r}\left(1 - \frac{e^{2\varepsilon_2+\varepsilon_3}}{\cos\theta}\right)$$ (Repeated, see section 3.2.1. eqn. (3.42))

seen that for a punch with large ρ_1, $\cos\theta \cong e^{2\varepsilon_2+\varepsilon_3} = 1$ a little distance away from the pole. This is strictly true for a flat punch where $\rho_1 \rightarrow \infty$. Therefore the term in the brackets is zero whereas $^1/r$ is finite. Hence in the limit, when $r \rightarrow 0$:

$$\frac{d\varepsilon_2}{dr} = 0 \quad \text{at the pole .} \tag{3.65}$$

To find $\frac{d\varepsilon_3}{dr}$ eqn. (3.42) is rewritten and is differentiated giving:

$$\frac{d\varepsilon_3}{dr} = e^{-(2\varepsilon_2+\varepsilon_3)}\left[\sin\theta\left(r\frac{d\varepsilon_2}{dr} - 1\right)\frac{d\theta}{dr} - \left(\frac{d\varepsilon_2}{dr} + r\frac{d^2\varepsilon_2}{dr^2}\right)\cos\theta\right] - 2\frac{d\varepsilon_2}{dr} \tag{3.66}$$

Substituting the values hitherto found in this section (3.2.3.1.) in eqn. (3.66) gives:

$$\frac{d\varepsilon_3}{dr} = 0 \tag{3.67}$$

Differentiating eqn. (3.14) w.r.t. r results in:

$$\frac{d\varepsilon_1}{dr} + \frac{d\varepsilon_2}{dr} + \frac{d\varepsilon_3}{dr} = 0 \tag{3.68}$$

Substituting eqns. (3.65) and (3.67) in eqn. (3.68):

$$\frac{d\varepsilon_1}{dr} = 0 \tag{3.69}$$

The incremental strains in eqn. (3.23) can be replaced by total strains at the pole, because x=1 (see eqns. (3.58) and (3.63)). Then differentiating $\bar{\varepsilon}$ w.r.t. r and using eqns. (3.65), (3.67), and (3.68) gives:

$$\frac{d\bar{\varepsilon}}{dr} = 0 \tag{3.70}$$

Differentiating $\bar{\sigma}$ in eqn. (3.48) w.r.t. r:

$$\frac{d\bar{\sigma}}{dr} = \frac{n\,\bar{\sigma}}{B + \dfrac{\bar{\varepsilon}}{\sqrt{\dfrac{2}{3}\dfrac{(2+R)}{(R+1)}}}} \quad \frac{1}{\sqrt{\dfrac{2\ (2+R)}{3(R+1)}}} \quad \frac{d\bar{\varepsilon}}{dr} \tag{3.71}$$

and using eqn. (3.70) it is seen that:

$$\frac{d\bar{\sigma}}{dr} = 0 \tag{3.72}$$

The variables in the yield criterion (eqn. 3.18) are differentiated w.r.t. r, and $\frac{d\bar{\sigma}}{dr} = 0$ and $x = 1$ are substituted. After simplifying and rearranging:

$$\frac{1}{\sigma_1}\ \frac{d\sigma_1}{dr} = \frac{1}{2(k-1)} \left[\frac{dx}{dr} - 2\,\frac{dk}{dr} \right] \tag{3.73}$$

In this equation there are three unknowns, namely $\frac{d\sigma_1}{dr}$,

$\frac{dx}{dr}$, and $\frac{dk}{dr}$. The two other relationships which are necessary to determine the unknowns are supplied by the two equilibrium equations. Differentiating eqn. (3.57) w.r.t. r, substituting r = θ = 0, and simplifying:

$$\frac{dx}{dr} = \frac{1}{\sigma_1}\frac{d\sigma_1}{dr} - \frac{2\mu}{\rho' + 0.5t} \tag{3.74}$$

Since $k = \frac{\sigma_3}{\sigma_1} \cong -\frac{p}{2\sigma_1}$ and substituting for p from eqn. (3.30):

$$k = -\frac{t}{2\rho' r'}(r + x\rho\sin\theta) \tag{3.75}$$

Differentiating eqn. (3.75) w.r.t. r and using the derivatives hitherto found, the equation reduces to:

$$\frac{dk}{dr} = -\frac{t(\rho' + 0.5t)}{2\rho'^2}\frac{dx}{dr} \tag{3.76}$$

Hence from eqns. (3.73), (3.74), and (3.76):

$$\frac{dx}{dr} = -\frac{4}{3}\frac{\mu}{\rho' + 0.5t} \tag{3.77}$$

$$\frac{dk}{dr} = \frac{2}{3}\frac{\mu t}{\rho'^2} \tag{3.78}$$

$$\frac{1}{\sigma_1}\frac{d\sigma_1}{dr} = \frac{2}{3}\frac{\mu}{\rho' + 0.5t} \tag{3.79}$$

and $$\frac{d}{dr}(\sigma_1 t) = \frac{2}{3}\frac{\mu\sigma_1 t}{\rho' + 0.5t}$$

To find $\frac{dp}{dr}$, eqn. (3.30) is differentiated w.r.t. r, and using eqns. (3.77) and (3.79):

$$\frac{dp}{dr} = 0 \tag{3.80}$$

Since $\sigma_2 = x\sigma_1$:

$$\frac{d\sigma_2}{dr} = \sigma_1 \frac{dx}{dr} + x \frac{d\sigma_1}{dr}$$

Also using eqns. (3.77) and (3.79):

$$\frac{d\sigma_2}{dr} = -\frac{2}{3} \frac{\mu\sigma_1}{\rho' + 0.5t} \tag{3.81}$$

3.2.3.2. At the Point of Contact with Punch

In this section the continuity of the variables, and their necessary derivatives at the moving contact are studied. A split point at the boundary is considered which is in both regions, and the variables belonging to the two regions at this point are shown in brackets with the corresponding suffices (1 or 2).

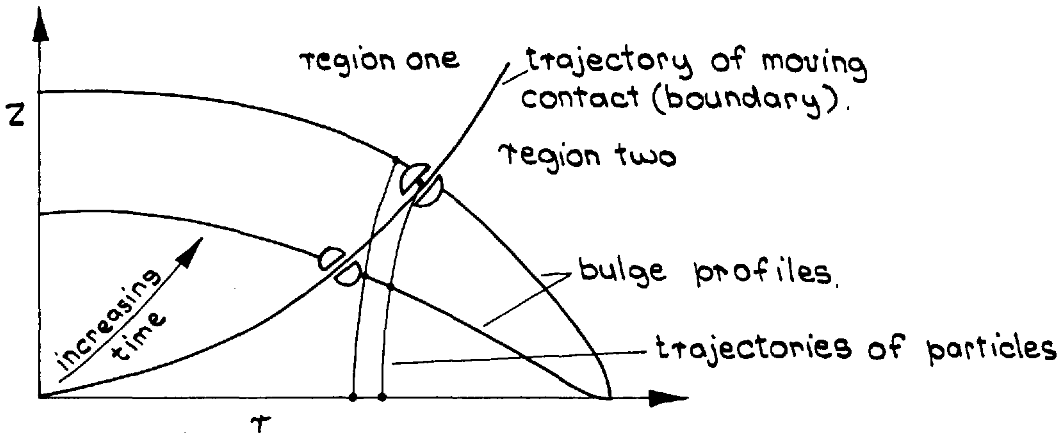

FIG.7 - TRAJECTORY OF THE MOVING CONTACT (BOUNDARY) OF SHEET METAL WITH PUNCH

Functions:

From eqn. (3.34), since $(r)_1 = (r)_2$ and $(r_o)_1 = (r_o)_2$

$$(\varepsilon_2)_1 = \ln \frac{(r)_1}{(r_o)_1} = (\varepsilon_2)_2 = \ln \frac{(r)_2}{(r_o)_2}$$

and hence $\Delta(d\varepsilon_2^*) = 0$ (3.82)

Eqn. (3.43) which has $k = 0$ in region two and $k \neq 0$ in region one, shows that except in the case of plane strain (i.e. $d\varepsilon_2^* = 0$ and $x = \frac{R+k}{R+1}$), the increments $d\varepsilon_2^*$ and $d\varepsilon_3^*$ are related by a finite and non-singular function, even at the moving boundary. Hence since $\Delta(d\varepsilon_2^*) = 0$ from eqn. (3.82), $\Delta(d\varepsilon_3^*) = 0$ and consequently $(\varepsilon_3)_1 = (\varepsilon_3)_2$

(3.83)

From the constancy of volume (eqn. 3.14) and from eqns. (3.82) and (3.83):

$$(\varepsilon_1 + \varepsilon_2 + \varepsilon_3)_1 = (\varepsilon_1 + \varepsilon_2 + \varepsilon_3)_2$$

$$\therefore \quad (\varepsilon_1)_1 = (\varepsilon_1)_2 \text{ and } \Delta(d\varepsilon_1^*) = 0 \qquad (3.84)$$

Substituting $\Delta(d\varepsilon_2^*) = 0$ and $\Delta(d\varepsilon_3^*) = 0$ from eqns. (3.82) and (3.83) in eqn. (3.23):

$$\Delta(d\bar{\varepsilon}^*) = 0 \quad \text{and} \quad (\bar{\varepsilon})_1 = (\bar{\varepsilon})_2 \qquad (3.85)$$

Since $\bar{\sigma} = \bar{F}^*(\bar{\varepsilon})$, as given by eqn. (3.48), and also using eqn. (3.85), it can be shown that:

$$(\bar{\sigma})_1 = (\bar{\sigma})_2 \qquad (3.86)$$

Considering the vertical force transmitted at the moving boundary:

$$(2\pi r\sigma_1 t \sin\theta)_1 = (2\pi r\sigma_1 t \sin\theta)_2 \qquad (3.87)$$

It has not been possible to prove the continuity of θ at the moving boundary, but it seems very reasonable to assume that it is, since bending is also neglected in the analysis. Using eqns. (3.83) and (3.82), from eqn. (3.87) it can be shown that:

$$(\sigma_1)_1 = (\sigma_1)_2 \qquad (3.88)$$

It is obvious that p is discontinuous and so is σ_3, since they vanish in the second region.

The approximation to the thickness stress in region one leads to a discontinuity in x and σ_2. The new value of x or σ_2 can be found as follows: Since the ratio $\bar{\sigma}/\sigma_1$ is continuous (see eqns. (3.86), (3.88)) and it can be obtained from the two forms of the yield criterion for regions one and two (see eqns. (3.18) and (3.56)), these two ratios $(\bar{\sigma}/\sigma_1)$ can be equated to give the relationship between $(x)_1$ and $(x)_2$.

Hence $$(x)_2 = \frac{1}{R+1}\left[R + \left(R^2-(R+1)\left[R-(x^2)_1 -2k(k-1-(x)_1)- - R\,(1-(2x)_1 + (x^2)_1)\right]\right)^{\frac{1}{2}}\right] \qquad (3.89)$$

and also $$(\sigma_2)_2 = (\sigma_1)_1\,(x)_2$$

Derivatives:

In region two as well as in region one since the material stretches and consequently thins, then $d\varepsilon_2^* \geqslant 0$ and $d\varepsilon_3^* \leqslant 0$. Examining eqn. (3.55) shows that

$x \geqslant \frac{R}{R+1}$, and since $R > 0$, then $x > 0$.

Rewriting eqn. (3.52):

$$\frac{d\theta}{dr} = -\frac{x}{r}\tan\theta \quad \text{and since } x,\ r,\ \tan\theta > 0$$

then $\frac{d\theta}{dr} < 0$ throughout region two.

For all the common punch profiles, the shell geometry in region one dictates that $\frac{d\theta}{dr} > 0$ in that region. Hence there is a discontinuity of $\frac{d\theta}{dr}$ at the moving boundary, and the new value for region two can be computed by the following eqn.:

$$\frac{d\theta}{dr} = -\frac{(x)_2}{(r)_{1or2}}(\tan\theta)_{1or2} \tag{3.90}$$

It can also be seen from eqn. (B.4) that ρ_2 is continuous, but considering eqn. (B.1) ρ_1 is discontinuous, since it is related to $\frac{d\theta}{dr}$ whereas the former is only a function of $\sin\theta$. This was not considered by Woo (95) as mentioned in section 1.1.3.

From eqn. (3.42) since r, θ, ε_2, and ε_3 are all continuous, it can be shown that:

$$\left(\frac{d\varepsilon_2}{dr}\right)_1 = \left(\frac{d\varepsilon_2}{dr}\right)_2 \tag{3.91}$$

Rearranging eqn. (3.42) for ε_3 and differentiating w.r.t. r gives:

$$\frac{d\varepsilon_3}{dr} = e^{-(2\varepsilon_2+\varepsilon_3)}\left[\left(r\frac{d\varepsilon_2}{dr}-1\right)\sin\theta\frac{d\theta}{dr} - \cos\theta\left(r\frac{d^2\varepsilon_2}{dr^2}+\frac{d\varepsilon_2}{dr}\right)\right] - 2\frac{d\varepsilon_2}{dr} \qquad (3.92)$$

As seen the R.H.S. of eqn. (3.92) contains all known terms except one ($\frac{d^2\varepsilon_2}{dr^2}$) when evaluated at the moving boundary. It seems reasonable to assume that $\frac{d^2\varepsilon_2}{dr^2}$ is continuous without a formal mathematical proof, and it can be evaluated numerically using eqn. (A.10). Eqn. (3.92) shows that $\frac{d\varepsilon_3}{dr}$ is discontinuous at the moving boundary since it involves $\frac{d\theta}{dr}$ which is discontinuous, hence $(\frac{d\theta}{dr})_2$ is used for the evaluation of $(\frac{d\varepsilon_3}{dr})_2$ from eqn. (3.92).

3.2.3.3. At the Clamped Edge

The boundary conditions at the clamped edge which terminates region two, involving the functions and the derivatives of the variables can be found in a similar way as for the cases of the other boundaries previously considered. However this is not necessary, since the numerical solution does not require explicit analytical formulae, because it involves forward integration and differentiation and interpolation from the moving boundary towards the clamped edge. Hence the only required boundary condition is:

$$\varepsilon_2 = 0 \qquad (3.93)$$

at the mean surface corresponding to the radius of the clamped periphery, which characterizes a pure stretch forming operation without any drawing-in.

3.3. Equations for Drawing over Die

As in stretch forming, most of the equations effective in the following regions can be obtained from the basic equations given in section 3.1. As shown in Fig.1, in practice the sheet metal between the points A and B in contact with the die, is normally flat, but it can in general assume the shape of a surface of revolution. The region between the points B and C is generally a toroidal surface, but the present analysis does not restrict it to be so, and it can also be of any axisymmetrical shape. In the following sections the relevant equations and the boundary conditions will be discussed.

3.3.1. Radial Drawing Region

This region is called region four (between points A and B in Fig.1).

Equilibrium: From the work of Chung and Swift (18), and also Woo (95) it can be concluded that the assumption of the blank-holding force being concentrated on the rim is very satisfactory. This means that the frictional stresses between the tools and the sheet metal will be operative at the rim of the blank. However, if the die surface is curved then there will be interfacial pressure and frictional stresses between the die and sheet metal.

Hence for a flat die from eqn. (3.33):

$$\frac{d}{dr}(\sigma_1 t) = \frac{\sigma_1 t}{r}(x - 1), \text{ and } p = \sigma_3 = 0 \qquad (3.94)$$

For a curved die eqns. (3.33) and (3.30) can be used with a given relationship between r and θ.

The remaining equations are the same as in region one, i.e. strain compatibility (eqn. 3.42), stress-strain relationships (eqns. 3.43 and 3.44), yield criterion (eqn. 3.18), equivalent strain-increment (eqn. 3.23), strain-hardening law (eqn. 3.48), and compatibility of increments in time and space (3.40), where $\Delta V^* = 0$ for all the points.

3.3.2. Over the Die Profile

This region is called region three, (between the points B and C in Fig.1). The effective eqns. are the same as the ones in region one (see section 3.2.1). However, some differences in the numerical solution will be pointed out in section 5.2.

The major difference compared to region one is found to be in the relationship between r and θ, and if the die profile is toroidal then:

$$r' = r_b - \rho_d' \sin\theta \qquad (3.95)$$

and $$\frac{dr'}{d\theta} = - \rho_d' \cos \theta \qquad (3.95)$$

Substitution of the above eqns. in those given in section 3.2.1. will give the equations effective in this region.

3.3.3. Boundary Conditions

The drawing of sheet metal over the die surface is governed by the above eqns. and the boundary conditions, (i) at the rim of the blank, (ii) at the start of the die curvature and (iii) at the point of departure of sheet metal from the die. Boundaries (i) and (iii) move in space as functions of deformation in time, but (ii) remains fixed. The necessary analytical relationships of the variables at these boundaries are given below.

3.3.3.1. Rim of Blank

Functions: In deep-drawing, the rim of the blank moves inwards, with continued deformation. In the numerical solution to be presented in section 5.2.1, the displacement of the rim between two consecutive stages is arbitrary, but it governs the accuracy of the solution.

Hence at the rim:

$$(\varepsilon_2)_{m,n} = \ln \frac{r_{m,n}}{r_{m,o}}$$ where $r_{m,n}$ is the current radius of rim. (repeated eqn.) (3.34)

From eqn. (3.40):

$$(d\varepsilon_2^*)_m = (\varepsilon_2)_{m,n} - (\varepsilon_2)_{m,n-1} \tag{3.96}$$

Then a value of x is assumed such that:

$$x = 0.5x_{m,n} + 0.5x_{m,n-1} \tag{3.97}$$

where $x_{m,n-1}$ is known from the previous stage. Using this x and eqns. (3.43) and (3.44) (effectively considering any curvature on the die, i.e. non-flat die), $(d\varepsilon_3^*)_m$ can be calculated, and hence from eqn. (3.23) $d\bar{\varepsilon}_m^*$ is known.

Since $\bar{\varepsilon}_{m,n} = \bar{\varepsilon}_{m,n-1} + d\bar{\varepsilon}_m^*$, where $\bar{\varepsilon}_{m,n-1}$ is known from the previous stage, $\bar{\sigma}_{m,n}$ can be calculated from eqn. (3.48). Assuming that all the blank-holding force acts on the rim, from the horizontal equilibrium of forces:

$$(\sigma_1)_{m,n} = \left.\frac{\mu H \cos\theta}{\pi r t}\right._{m,n} \tag{3.98}$$

Hence from the known $\bar{\sigma}$, σ_1 and k (at m,n) $x_{m,n}$ can be found from eqn. (3.18), which is used in eqn. (3.97) to find x. Now this value of x is checked against the assumed one, and the initial x is varied, and the above steps are repeated until the difference between the two x's is negligible. However the equations involved are non-linear and may give two values of x satisfying all the equations. Then the one which gives the smaller $|d\varepsilon_3^*|$ is to be taken since it satisfies the condition of minimum plastic work, because $d\varepsilon_2^*$ remains constant in this iteration. σ_2 at the rim can be found from eqn. (3.17), and hence all the variables are then known.

Derivatives: The derivatives $\frac{d}{dr}(\sigma_1 t)$ and $\frac{d\varepsilon_2}{dr}$ can be computed from eqns. (3.94) and (3.42) respectively with given function values. Although it would have been desirable to obtain analytical formulae for $\frac{dx}{dr}$ and $\frac{d\varepsilon_3}{dr}$ at the rim as well, this has not been possible. As a first approximation it can be assumed that these derivatives vanish, and the numerical solution can advance to the third nodal point as explained in section 5.2.1. Then the above two derivatives can be computed using the Lagrangian formula (A.8). If they are different from zero, the new values can be used and the solution re-started. The iteration can go on until satisfactory agreement is reached with the previous values.

3.3.3.2. At the Start of the Die Curvature

This is point B as shown in Fig. 1.

Functions: Following the same procedure as in section 3.2.3.2. it is possible to prove that ε_2, ε_3, ε_1, $\bar{\varepsilon}$, $\bar{\sigma}$, and σ_1 are continuous except in cases where instantaneous plane straining occurs. At this point p, k, σ_2 and x can be discontinuous depending on the meridional radius of curvature. New values can be calculated as follows: From eqn. (3.18), since $\bar{\sigma}/\sigma_1$ is continuous:

$$\left[x^2+2k(k-1-x)+R(x^2-2x)\right]_4 = \left[x^2+2k(k-1-x)+R(x^2-2x)\right]_3 \qquad (3.99)$$

and $$(\sigma_2)_3 = (x)_3 \, (\sigma_1)_3$$

also from eqn. (3.30):

$$(p)_3 = \left[\frac{t}{\rho_1' r'} \, (\sigma_1 r + \sigma_2 \rho_1 \sin\theta)\right]_3 \qquad (3.100)$$

and $$(k)_3 = -\left(\frac{p}{2\sigma_1}\right)_3$$

The L.H.S. of eqn. (3.99) is known from the results in region four. To find $(x)_3$, a first approximation to $(k)_3 = 0$ is used, and $(x)_3$ can then be calculated. Then $(\sigma_2)_3$, $(p)_3$ and $(k)_3$ can be found using the above equations. The new value of $(k)_3$ can now be substituted back in eqn. (3.99) and the iteration can continue until the required accuracy is obtained, which would be very rapid. Hence all functions are known.

<u>Derivatives</u>: Using eqn. (3.42), it is possible to prove the continuity of $\frac{d\varepsilon_2}{dr}$. $(\frac{d\theta}{dr})_3$ will depend on the geometry of the die and it can be computed. Hence from eqn. (3.92), using the same outlined procedure, $(\frac{d\varepsilon_3}{dr})_3$ which is discontinuous can be found.

It would have been desirable to have had an analytical formula to calculate $(\frac{dx}{dr})_3$, but this has not been possible to obtain. However, in the numerical solution outlined in 5.2.2. it is possible to use initially a linear approximation to this derivative at the boundary, but when the third nodal point is computed in this region, using eqn. (A.8) a more accurate derivative can be calculated. This process can be repeated until the desired accuracy is obtained.

3.3.3.3. At Point of Departure of Sheet Metal from Die

This boundary separates regions two and three and is shown as point C in Fig.1. It is seen that this point is very similar to that which exists at the junction of regions one and two. The boundary conditions can be found following the same procedure as was given in section 3.2.3.2. which will result in the same formulae, except that the suffices outside the brackets referring to region one should be changed to region three.

It should be recalled that this boundary moves with continued deformation in time, and the solution of the deep-drawing problem will demand the matching of the boundary conditions here, as explained in section 5.3.

3.4. Equations for Hydraulic Bulging

Unlike stretch forming by a rigid punch, the deformation of sheet metal under hydrostatic pressure is governed from the pole to the clamped periphery by one set of equations, i.e. there is effectively one region (see Fig.8). It is assumed that the pressure is generated at a slow rate and there are therefore no speed effects.

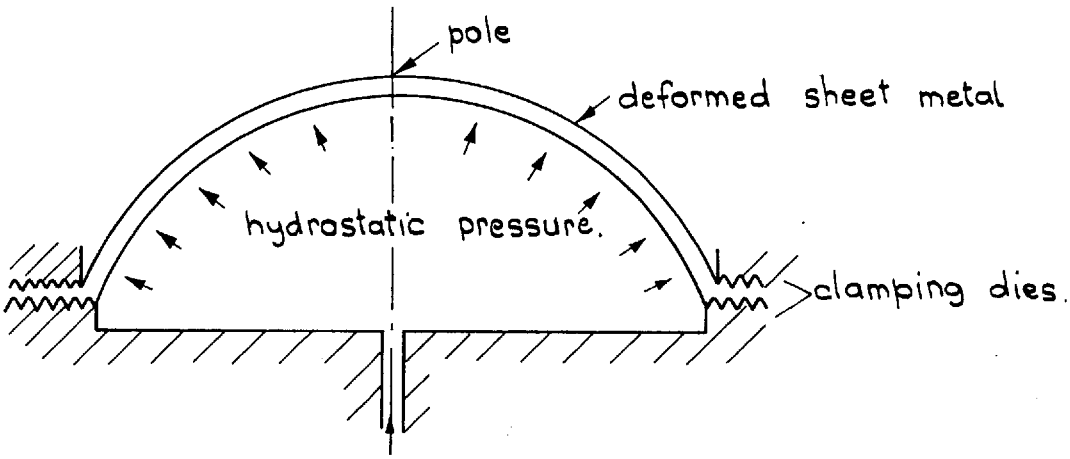

FIG.8. MAIN FEATURES OF HYDRAULIC BULGING.

3.4.1. Governing Equations

Equilibrium: For use in the numerical analysis it is more convenient to rewrite eqn. (3.30) using eqns. (3.31), and (3.32) as follows:

$$x = \left[\frac{p}{\sigma_1 t}\left(\frac{1}{\cos\theta}\ \frac{dr}{d\theta} - \frac{t}{2}\right)\left(r - \sin\theta\ \frac{t}{2}\right) - r\right]\cot\theta\ \frac{d\theta}{dr} \tag{3.101}$$

and from eqn. (3.33) with $\mu = 0$:

$$\frac{d}{dr}(\sigma_1 t) = \sigma_1 t\left(\frac{x-1}{r}\right) \qquad (3.102)$$

These are the two eqns. of equilibrium.

Strain Compatibility is as given by eqn. (3.42), but the relationship between r and θ is numerical and is obtained from eqn. (A.15).

Stress-Strain Relationship is expressed by eqn. (3.43). In hydrostatic bulging $p \neq f(r)$ and is constant along the bulge profile, hence

$$k = -\frac{(p)_p}{2\sigma_1} \qquad (3.103)$$

Yield Criterion: Eqn. (3.18) is to be used with eqn. (3.103).

Equivalent Strain-Increment is as given by eqn. (3.23).

Strain-Hardening Law is expressed by eqn. (3.48).

Compatibility of Increments of Variables in Time and and Space: In hydraulic bulging, since there is no moving boundary as in stretch forming, in which there can be a possibility of having discontinuities of functions and derivatives, $\Delta V^{*} = 0$ and accordingly eqn. (3.40) can be used.

Other Geometrical Relationships are as given by eqns.

(B.1), (B.4), and (B.5).

3.4.2. Boundary Conditions

In hydraulic bulging there are two boundaries, i.e. (i) pole and (ii) clamped periphery.

At the pole the values of the functions can be computed as in stretch forming, as outlined in section 3.2.3.1. Referring to the same section for the evaluation of the derivatives, it is seen that:

$$\frac{d\varepsilon_2}{dr} = \frac{d\varepsilon_3}{dr} = \frac{d\varepsilon_1}{dr} = \frac{d\bar{\varepsilon}}{dr} = \frac{d\bar{\sigma}}{dr} = \frac{dp}{dr} = 0$$

as in stretch forming, furthermore

$$\frac{dx}{dr} = \frac{dk}{dr} = \frac{d\sigma_1}{dr} = \frac{d\sigma_2}{dr} = 0$$

since $\mu = 0$ in hydraulic bulging.

At the clamped periphery, the discussion given in section 3.2.3.3. applies, and the only useful boundary condition is $\varepsilon_2 = 0$ as in stretch forming.

CHAPTER 4 - PLASTIC INSTABILITY

The subject of this Chapter is concerned with plastic instability under a predominantly tensile stress system, and not under a compressive stress system which could result in plastic buckling or a wrinkling type of instability.

The phrase "plastic instability" has been used by various authors to embrace the different criteria expressing the onset of unstable plastic flow (see 1.5). This generally happens after a certain variable (e.g. load, or pressure) reaches a maximum beyond which unstable flow is followed by fracture. However, sometimes fracture can take place before reaching a maximum in one or more of such variables (14, 15), or on the contrary an appreciable amount of straining can occur between such a maximum and fracture. Although such simpler concepts are easier to work with, they by no means supply the complete answer, and are not generally valid for a wide range of cases.

In the following sections various conventional, and a more sophisticated ~~criterion~~ criteria are discussed, and their interrelations are shown, relevant to plastic instability in stretch forming and hydraulic bulging.

4.1. Criteria of Plastic Instability

It is of interest to be able to predict the state of stress and strain at plastic instability as well as its location, which can be anywhere along the bulge in the case of stretch forming. ♠ The following criteria are studied with this in mind.

(i)* Maximum Load Criterion (ML)

This corresponds to the state of stress and strain when the net load across any section reaches a maximum in time, taking into account the variation of the dimensions.

In stretch forming, considering a large element as shown below, the load supported by any segment of angle

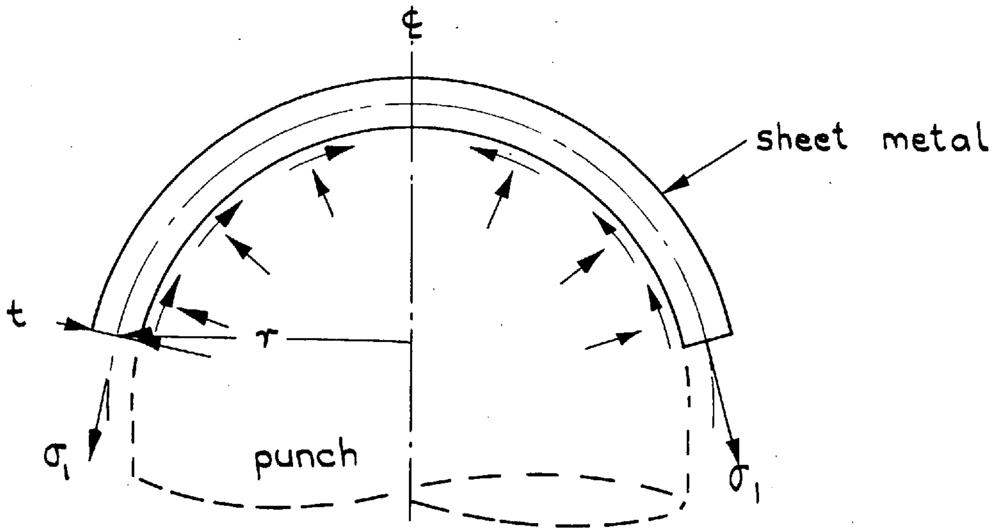

FIG.9 - A LARGE ELEMENT OF SHEET METAL IN STRETCH FORMING

$\delta\phi$ in the direction of the tangent to its mean surface is:

$$Q = 2\pi r\sigma_1 t \cdot \frac{\delta\phi}{2\pi} = r\sigma_1 t\, \delta\phi \quad . \tag{4.1}$$

To find the maximum load in time, the logarithms of both sides are taken and the resulting equation is differentiated:

Hence $$\frac{dQ^*}{Q} = \frac{dr^*}{r} + \frac{d\sigma_1^*}{\sigma_1} + \frac{dt^*}{t} = 0 \qquad (4.2)$$

Substituting eqns. (3.14) and(3.34) in eqn. (4.2):

$$\frac{d\sigma_1^*}{\sigma_1} = d\varepsilon_1^* \qquad (4.3)$$

It can be shown that eqn. (4.3) applies to other triaxial, biaxial, and uniaxial stress systems. It coincides with the Swift-Hill criterion (79, 35) for proportional straining. However eqn. (4.3) can be used for non-proportional straining as well, but in such cases explicit formulae for stress and strain at instability in terms of $\bar{\sigma}$ and $\bar{\varepsilon}$ cannot be obtained as in the case of the former.

It should be noted that such a maximum load may not be reached before the occurrence of fracture as will be discussed later in this Chapter.

(ii) Maximum Pressure Criterion (MP)

This type of instability takes place when the internal pressure in a shell reaches a maximum in time. However, as mentioned before fracture may take place before such a maximum is reached. Nevertheless, in many applications especially with ductile materials this is not expected, and it is useful to find the stability of such a structure from the point of view of the internal pressure.

It is not possible to derive a single formula that will express the MP instability for a variety of systems. This requires a knowledge of the state of stress and strain for the particular structure under consideration. Analytical formulae can be derived for simple states such as a sphere, and a cylinder under internal pressure, but resort to numerical methods must be made when the stress state varies in time and space as in hydraulic bulging, if a general solution is desired.

Application of this criterion to a few systems is shown in sections 4.2. and 4.3.

(iii) Strain Propagation Criterion (SP)

At a point in a plastically deforming body, the state of strain and stress depends also on those at the neighbouring points through the governing equations. If the material remains stable and does not fracture at such points, an increase in strains of one of the points will cause increases in the strains of the others, no matter how small or large they may be. However, there will be a limiting set of strains for each point which is generally different for each, beyond which a further increase in strains of one will cause no increases in the strains of the others. Effectively the strain propagation will cease, and at one point the rate of strain development will tend to infinity and it will soon fracture there.

This can in general happen anywhere along the bulge in stretch forming with a rigid punch, and is affected by friction and previous strain history. In hydraulic bulging of diaphragms with uniform strain history it is expected to take place at the pole, except possibly for a material which is anisotropic in the plane of the sheet.

It is not possible to express this criterion in simple mathematical formulae. As shown in section 5.1 a solution can be achieved by numerical analysis in the case of stretch forming. It corresponds to the state when the equilibrium conditions related to the point under consideration can no longer be satisfied, hence no solution to the problem exists after reaching such a state.

As explained in Chapter 13, SP instability can take place when Q or p for any point may be increasing, decreasing or is at a maximum. This theoretical concept, and the comparison of the calculated SP instability strains with the experimental strains suggest that this predicted state of strain corresponds to that of at the onset of fracture.

In the author's opinion this is the most general and powerful criterion to predict the onset of local unstable plastic flow, and there appears to be no previous results published using this concept. On the other hand it requires a very large amount of computing which can only be done by the high speed computers of the present day.

4.2. Plastic Instability of Simple Systems

The criteria discussed in section 4.1 will now be applied to simple states of stress where the stress ratios remain constant, and the directions of the principal axes of stress remain fixed with respect to the element throughout the deformation. The material is assumed to obey the flow rules given in section 3.1.

(i) ML Instability of a Triaxial Stress System

From eqns. (3.23) and (3.19):

$$d\bar{\varepsilon}^{*} = \frac{\left[\frac{2}{3}(2+R)\right]^{\frac{1}{2}}}{1+2R}\left[(2R^2+3R+1)\left\{1+\left[\frac{(x-k)+R(x-1)}{R(1-x)+(1-k)}\right]^2\right\}\right.$$

$$\left.+\;2(R+2R^2)\left[\frac{(x-k)+R(x-1)}{R(1-x)+(1-k)}\right]\right]^{\frac{1}{2}} d\varepsilon_1^{*} \qquad (4.4)$$

or say $d\bar{\varepsilon}^{*} = K_1 d\varepsilon_1^{*}$, where K_1 is a constant.

Also from eqn. (3.18):

$$\frac{d\sigma_1^{*}}{\sigma_1} = \frac{d\bar{\sigma}^{*}}{\bar{\sigma}} \qquad (4.5)$$

Hence substituting eqns. (4.4) and (4.5) in eqn. (4.3):

$$\frac{d\bar{\sigma}^*}{d\bar{\varepsilon}^*} = \frac{\bar{\sigma}}{K_1} \tag{4.6}$$

Another $\frac{d\bar{\sigma}^*}{d\bar{\varepsilon}^*}$ can be obtained from eqn. (3.48):

$$\frac{d\bar{\sigma}^*}{d\bar{\varepsilon}^*} = \frac{n\bar{\sigma}}{B + \frac{\bar{\varepsilon}}{\left[\frac{2(2+R)}{3(R+1)}\right]^{\frac{1}{2}}}} \qquad \frac{1}{\left[\frac{2(2+R)}{3(R+1)}\right]^{\frac{1}{2}}} \tag{4.7}$$

Equating eqns. (4.6) and (4.7), and solving for the unknown $\bar{\varepsilon}$ at ML instability:

$$\bar{\varepsilon} = nK_1 - \left[\frac{2(2+R)}{3(R+1)}\right]^{\frac{1}{2}} B \tag{4.8}$$

or $\bar{\varepsilon} = nK_1 - BK_2$ where K_2 is another constant.

Using eqns. (3.19) this ML instability strain can be expressed in terms of the thickness strain:

$$\varepsilon_3 = \left[n - \frac{BK_2}{K_1}\right]\left[\frac{2k-1-x}{R(1-x)+(1-k)}\right] \tag{4.9}$$

or $\varepsilon_3 = nK_3 - BK_4$ where K_3 and K_4 are constants.

The variations of the constants (K_1, K_2, K_3 and K_4) are seen in Fig.10 for typical values of x, R and k. It is seen that increases in x will increase both the $|\varepsilon_3|$ and $\bar{\varepsilon}$ at ML instability. An increase in R will result in a decrease in $|\varepsilon_3|$, but an increase in $\bar{\varepsilon}$ for

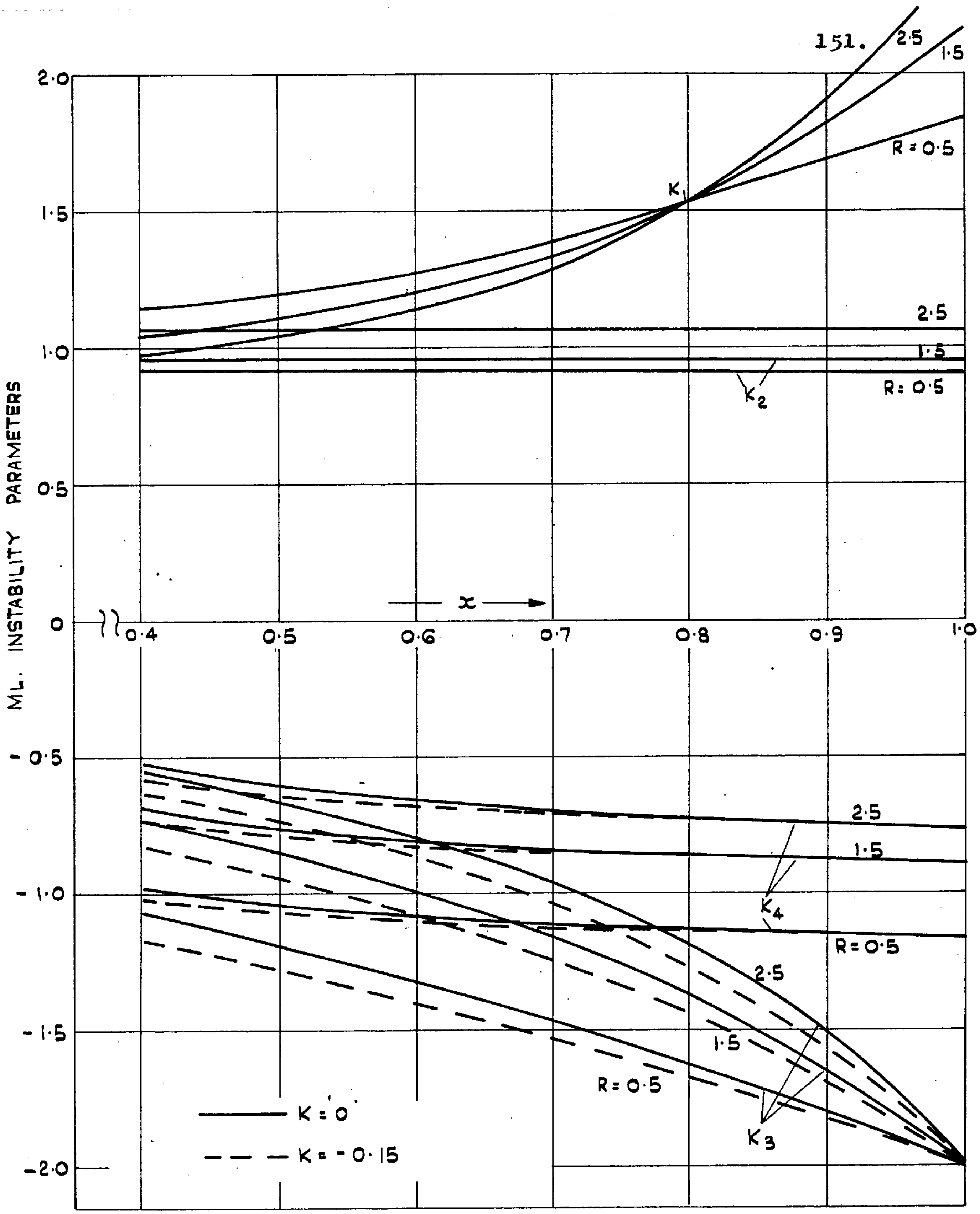

FIG. 10. ML INSTABILITY PARAMETERS.

$x > 0.8$ however $\bar{\varepsilon}$ will decrease for $x < 0.8$. For isotropic materials (R=1) eqn. (4.8) will reduce to:

a) $\bar{\varepsilon} = n-B$ for uniaxial tension (4.10)

b) $\bar{\varepsilon} = 2n-B$ for biaxial tension (4.11)

as found by Mellor (65).

Alternatively, the length of the subtangent to the $\bar{\sigma}$ versus $\bar{\varepsilon}$ curve can be found at the point of ML instability using eqn. (4.6) as shown graphically in Fig. 11.

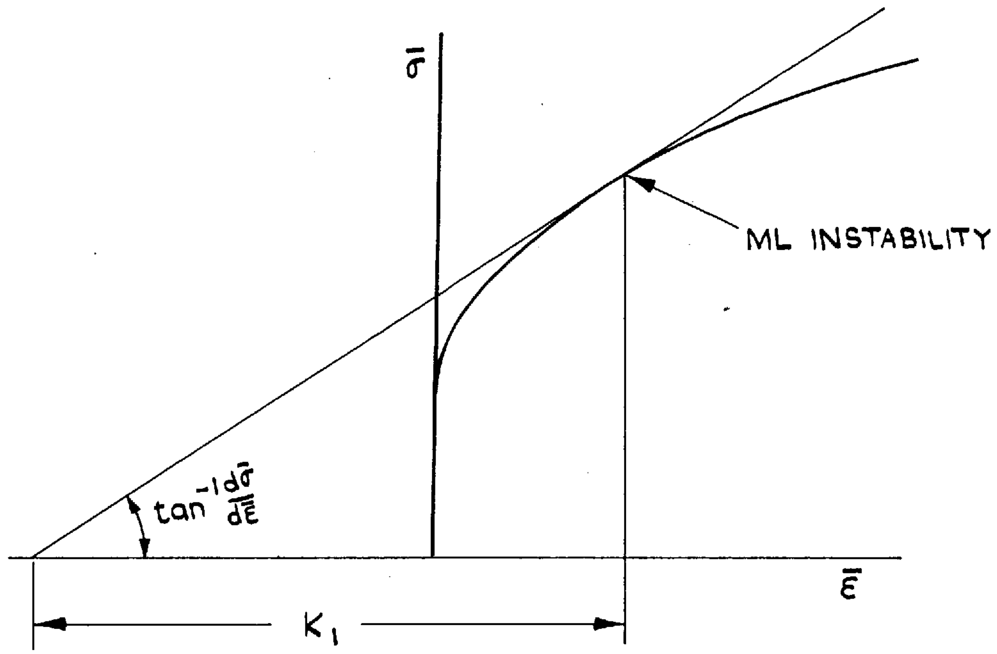

FIG.11 - SUBTANGENT AT ML INSTABILITY

This technique was originally suggested by Swift (79). If the material obeys the strain-hardening law given by eqn. (3.48), then the following relation between K_1 and $\bar{\varepsilon}$ at ML instability can be found from eqns. (4.6) and (4.7):

$$K_1 = \frac{B + \left(\frac{3R + 3}{4 + 2R}\right)^{\frac{1}{2}}}{n\left(\frac{3R + 3}{4 + 2R}\right)^{\frac{1}{2}}} \quad \bar{\varepsilon} \tag{4.12}$$

(ii) Thin Walled Sphere

The eqn. of equilibrium demands that:

$$\sigma_1 = \sigma_2 = \frac{p\rho_1}{2t} \tag{4.13}$$

Taking the logarithm of both sides and differentiating:

$$\frac{d\sigma_1^*}{\sigma_1} = \frac{dp^*}{p} + \frac{d\rho_1^*}{\rho_1} - \frac{dt^*}{t} \tag{4.14}$$

Substituting eqns. (3.34) in (4.14):

$$\frac{d\sigma_1^*}{1} = \frac{dp^*}{p} + d\varepsilon_2^* - d\varepsilon_3^* \tag{4.15}$$

From eqns. (4.3) (ML instability criterion), (3.14) and (4.15):

$$\frac{dp^*}{p} = d\varepsilon_3^* \tag{4.16}$$

Hence at ML instability the rate of decrease of pressure will be equal to the rate of thinning, when the section carries the maximum load. Mellor (65) used $\frac{dp^*}{p} = 0$ which obviously occurs before that predicted by eqn. (4.16), and at an increasing Q.

To find the strain at which ML instability occurs:

From eqns. (3.19), (3.23), and (3.18) respectively:

$$d\varepsilon_1^* = d\varepsilon_2^* = -\tfrac{1}{2}\, d\varepsilon_3^* \qquad (4.16)$$

$$d\bar{\varepsilon}^* = \frac{\left[\frac{2}{3}\,(2+R)(8R^2+8R+2)\right]^{\frac{1}{2}}}{1+2R}\, d\varepsilon_1^* = -\frac{\left[\frac{2}{3}(2+R)(8R^2+8R+2)\right]^{\frac{1}{2}}}{2\,(1+2R)}\, d\varepsilon_3^* \qquad (4.17)$$

or say $d\bar{\varepsilon}^* = d\varepsilon_3^* / K_5$

where K_5 is a constant.

$$\text{Also}\quad \bar{\sigma} = \left(\frac{3}{2+R}\right)^{\frac{1}{2}} (1-k)\,\sigma_1 = \left(\frac{3}{2+R}\right)^{\frac{1}{2}} \left(1 - \frac{t}{\rho_1}\right)\sigma_1 \qquad (4.18)$$

$$\text{and}\quad d\bar{\sigma}^* = \left(\frac{3}{2+R}\right)^{\frac{1}{2}} \left[-\frac{dt^*}{\rho_1}\,\sigma_1 + d\sigma_1^*\left(1 - \frac{t}{\rho_1}\right)\right]$$

with $t = t_o e^{\varepsilon_3}$ and $dt^* = t_o e^{K_5\bar{\varepsilon}} K_5 d\bar{\varepsilon}^*$ neglecting second order effects on k.

Substituting eqns. (4.16), (4.17), and (4.18) in eqn. (4.3), and simplifying:

$$\frac{d\bar{\sigma}^*}{d\bar{\varepsilon}^*} = \frac{K_5\left[-\tfrac{1}{2} - \dfrac{t_o e^{K_5\bar{\varepsilon}}}{2\rho_1}\right]}{1 - \dfrac{t_o e^{K_5\bar{\varepsilon}}}{\rho_1}}\;\bar{\sigma} \qquad (4.19)$$

Equating eqn. (4.7) to eqn. (4.19), and solving for the unknown strain $\bar{\varepsilon}$ at ML instability:

$$-\frac{2\varepsilon_1}{K_5} = \frac{1}{K_5}\varepsilon_3 = \bar{\varepsilon} = \frac{n}{K_5\left[\dfrac{-\frac{1}{2} - \dfrac{t_o e^{K_5\bar{\varepsilon}}}{2\rho_1}}{1 - \dfrac{t_o e^{K_5\bar{\varepsilon}}}{\rho_1}}\right]} - HK_2 \qquad (4.20)$$

To find the MP instability strain, from eqn. (4.14):

$$\frac{dp^*}{p} = \frac{d\sigma_1^*}{\sigma_1} - \frac{d\rho_1^*}{\rho_1} + \frac{dt^*}{t} = 0$$

Hence $$\frac{d\sigma_1^*}{\sigma_1} = d\varepsilon_2^* - d\varepsilon_3^* = -\frac{3}{2}\,d\varepsilon_3^* \qquad (4.21)$$

Following a similar procedure as for the ML instability strain using eqn. (4.21), the MP instability strain thus becomes:

$$-\frac{2\varepsilon_1}{K_5} = \frac{1}{K_5}\varepsilon_3 = \bar{\varepsilon} = \frac{n}{K_5\left[\dfrac{-\frac{3}{2} + \dfrac{t_o e^{K_5\bar{\varepsilon}}}{2\rho_1}}{1 - \dfrac{t_o e^{K_5\bar{\varepsilon}}}{\rho_1}}\right]} - BK_2 \qquad (4.22)$$

For a very thin and isotropic shell, i.e. $t_o = 0$ and $R = 1$, from eqns. (4.20) and (4.22):

for ML instability -

$$\bar{\varepsilon} = 2n - B \qquad (4.23)$$

and for MP instability -

$$\bar{\varepsilon} = \frac{2}{3} n - B \qquad \text{(same as Mellor's, see ref. 65)} \tag{4.24}$$

It is possible to derive the ML and MP instability strains for cylindrical shells, and others with internal pressure. It will be found that if geometrical similarity is maintained in the shape of the shell before and after deformation, then the ML instability point will always occur after the MP one.

There seems to be a lack of experimental evidence to test the truth of these criteria. Experiments must be performed carefully, on geometrically exact shells which are metallurgically homogeneous. However, the experimental evidence from hydraulic bulging of diaphragms suggests that fracture may take place <u>between</u> the strains predicted by MP and ML criteria, but in the case of the above examples with uniform stress fields, the local inhomogeneities will play a more important part.

The SP instability criterion cannot be applied satisfactorily to such idealized cases as those above with the assumptions of geometrical perfections and metallurgical homogeneity. For such cases the SP instability strain is expected to be infinite. The reasons will be more apparent in 5.1 when the numerical method for SP instability for stretch forming will be introduced.

4.3. Plastic Instability in Stretch Forming and Hydraulic Bulging

(i) In Stretch Forming

In the case of stretch forming by a rigid punch with frictional effects, the states of stress and strain are non-uniform. Hence it is not possible to obtain analytical formulae for the criteria of plastic instability. Furthermore in stretch forming fracture can take place anywhere along the bulge, but usually in region one for blanks with uniform initial conditions, and the location of this fracture is an additional unknown. Therefore results for the three criteria considered can only be obtained from the complete numerical analysis (see section 5.1), and are discussed in Chaper 13.

However a special case of stretch forming when $\mu = 0$ can be considered, assuming that the subsequent fracture takes place at the pole, which is later justified by experimental and theoretical results. Analytical formulae for ML and MP instability strains can be obtained as follows:

ML Instability:

Procedure is similar to that described in section 4.2. Eqns. (3.62) (with their differential forms), (3.63), and (3.64) are substituted in eqn. (4.3). Hence the derivative $\frac{d\bar{\sigma}^*}{d\bar{\varepsilon}^*}$ can be found which is then equated to that obtained from eqn. (4.7). The ML instability strain can be obtained by solving the resulting equation which gives:

$$-\frac{2\varepsilon_1}{K_5} = \frac{1}{K_5}\varepsilon_3 = \bar{\varepsilon} = \frac{n}{K_5\left\{-\frac{1}{2} + \left[\dfrac{\dfrac{t_o e^{K_5\bar{\varepsilon}}}{\rho'_1} + \dfrac{t_o^2 e^{2K_5\bar{\varepsilon}}}{\rho'^2_1}}{1 + \dfrac{t_o e^{K_5\bar{\varepsilon}}}{\rho_1'} + \dfrac{t_o^2 e^{2K_5\bar{\varepsilon}}}{2\rho_1'^2}}\right]\right\}} - BK_2 \tag{4.25}$$

MP Instability:

Using $\rho_1' \cong \rho_1$ in eqn. (3.59), taking the logarithms of both sides and differentiating gives:

$$\frac{dp^*}{p} = \frac{d\sigma_1^*}{\sigma_1} + \frac{dt^*}{t} = \frac{d\sigma_1^*}{\sigma_1} + d\varepsilon_3^* = 0 \tag{4.26}$$

$$\text{hence } \frac{d\sigma_1^*}{\sigma_1} = -d\varepsilon_3^* = -K_5 d\bar{\varepsilon}^* \tag{4.27}$$

Substituting the differential of eqn. (3.62) and itself in eqn. (4.27), and also using eqn. (4.7) gives the following MP instability strain:

$$-\frac{2\varepsilon_1}{K_5} = \frac{1}{K_5}\varepsilon_3 = \bar{\varepsilon} = \frac{n}{K_5\left\{-1+\left[\dfrac{\dfrac{t_o e^{K_5\bar{\varepsilon}}}{\rho_1'}+\dfrac{t_o^{2}\, e^{2K_5\bar{\varepsilon}}}{\rho_1'^{2}}}{1+\dfrac{t_o e^{K_5\bar{\varepsilon}}}{\rho_1'}+\dfrac{t_o^{2} e^{2K_5\bar{\varepsilon}}}{2\rho'^{2}}}\right]\right\}} - BK_2 \tag{4.28}$$

For $t_o = 0$ and $R = 1$:

ML instability:

$$\bar{\varepsilon} = 2n - B \tag{4.29}$$

MP instability:

$$\bar{\varepsilon} = n - B \tag{4.30}$$

Here it should be noted that ML instability strain of a thin isotropic spherical shell is the same as that in stretch forming (see eqns. (4.23) and (4.29)), but the MP instability strains are different due to constant radius of polar curvature in the case of stretch forming. MP instability in stretch forming has little significance as is also found from the experimental results, discussed in Chapter 13.

Eqn. (4.8) can be contrasted with eqns. (4.20) and (4.25). For $x = 1$, and $R = 1$ the former predicts a smaller ML instability strain compared to those obtained from the latter formulae. The difference is due to the fact that eqns. (4.20) and (4.25) take into account the variation (decrease) in k whereas eqn. (4.8) does not. Therefore the effect of decrease in lateral pressure is to increase ML instability strain.

(ii) In Hydraulic Bulging

Plastic instability and fracture in hydraulic bulging will always take place in the vicinity of the pole if a flat blank with uniform strain history is used. Otherwise it can occur anywhere along the bulge.

The general solution is outlined in section 5.4 incorporating the method of determination of the SP instability, but no numerical results have been obtained. It is envisaged that it can take place when Q or p is increasing, decreasing or at a maximum.

It is also of interest to study the predictions of the ML and MP instability criteria which throw some light on the occurrence of fracture (14, 15, 34) at pressures other than the maximum.

ML Instability:

This is the same as that in stretch forming with $\mu=0$ and neglecting the effect of the change in ρ_1 or k which is very small, and is given by eqn. (4.25), where eqn. (4.3) is used. It effectively corresponds to the Swift-Hill criterion.

MP Instability:

At the pole of the hydrostatic bulge assuming $t \approx 0$, eqn. (4.14) remains valid, hence by rearranging:

$$\frac{1}{\sigma_1}\,\frac{d\sigma_1^*}{d\varepsilon_3^*} = \frac{1}{\rho_1}\,\frac{d\rho_1^*}{d\varepsilon_3^*} - 1 \tag{4.31}$$

Assuming that the particles in the diaphragm describe circular paths which are orthogonal to the momentary profile, Hill (34) obtained the following relations in his special solution:

$$\varepsilon_3 = -2\ln\left(1 + \frac{4h^2}{D^2}\right) \tag{4.32}$$

$$\rho_1 = \frac{\frac{D^2}{4} + h^2}{2h} \tag{4.33}$$

From eqns. (4.31), (4.32), and (4.33), the MP instability occurs at:

$$\frac{1}{\sigma_1}\,\frac{d\sigma_1^*}{d\varepsilon_3^*} = -\frac{3}{2} + \frac{\rho}{2h}$$

On expanding in powers of ε_3 this becomes:

$$\frac{1}{\sigma_1}\,\frac{d\sigma_1^*}{d\varepsilon_3^*} = -\frac{11}{8} - \frac{1}{2\varepsilon_3} \tag{4.34}$$

If the material obeys the strain-hardening law given by eqn. (3.48), neglecting the secondary effect of σ_3, the polar thickness strain at MP instability can be found by the following equation:

$$11\varepsilon_3^{\,2} + \left[11\ K_5BK_2 + 8n + 4 \right] \varepsilon_3 + 4\ K_5BK_2 = 0 \qquad (4.35)$$

If for an annealed and isotropic material $B = 0$ and $R = 1$, then:

$$\varepsilon_3 = -\frac{4}{11}(2n + 1) \qquad (4.36)$$

as found by Hill (34). For the same conditions from eqn. (4.25) the ML instability becomes:

$$\varepsilon_3 = -2n \qquad (4.37)$$

It is seen that ML and MP instability strains do not coincide except for one value of n which can be found by equation eqns. (4.36) and (4.37).

Hence at $n = {}^2/7 = 0.285$

ML and MP criteria give identical results. For anisotropic materials with prestrain such critical values of the parameters can be found from eqns.(4.35) and (4.25) where n_{cr} would generally be different from 0.285. Since it involves trial and error calculation it is not attempted here. However, it may be seen that in cases where $n > 0.285$, ML instability will take place after MP instability at a decreasing pressure. If $n < 0.285$, MP instability will follow the ML instability which occurs at an increasing pressure.

For isotropic materials with prestrain, the critical values of n and B are given by the following equation.

$$B = 2n - {}^{4}/7 \qquad (4.38)$$

This equation when considered with eqns. (4.25) and (4.35) indicate the same trend as for the case where B = 0.

Although the predictions of the two criteria cannot be considered as conclusive, they throw some light on the fracture of strain-hardened materials before reaching the maximum pressure ($n < n_{cr}$), and the fracture of ductile materials ($n > n_{cr}$) under decreasing pressure in hydrostatic bulging.

As mentioned in section 1.5.1, Munday and Newitt (69) effectively used the ML criterion but claimed that their results compared well with others in which the MP criterion was used. This is not possible as shown by the present analysis. The authors must have used material parameters which may have been near the critical values, but these were not quoted in their paper.

CHAPTER 5 - METHOD OF SOLUTION AND NUMERICAL ANALYSIS

In this Chapter methods of solution are proposed for the formulae and ideas so far developed. Attention will mainly be focused on the stretch forming problem for which numerical results are obtained, but extensions of the solution to drawing over the die, and hydraulic bulging are presented.

From the stand-point of the theory of plasticity, the process of sheet metal deformation of this type is a non-steady state problem. The stress field changes from time to time and from point to point, and never reaches a steady state before the eventual occurrence of plastic instability and fracture.

From a mathematical stand-point, the process of stretch forming is a "moving boundary" problem with "two-point boundary conditions" due to the moving contact between punch and sheet metal, and the insufficient number of known boundary conditions at either the pole or the clamped edge. This results in the necessity of "matching" the boundary conditions if an "initial value" or a "marching" technique is used as was done with the proposed solution.

The problem of deep-drawing is even more complicated, since it is a "multiple moving boundary" problem with two sets of two-point boundary conditions. This results because of the moving contacts on punch and die, and the moving rim in the radial drawing region.

Hydraulic bulging is simpler due to the absence of a moving boundary, but still it is a boundary-value problem with two-point boundary conditions, since all the variables cannot be determined at one or the other of the boundaries (the pole, or the clamped edge).

The complications due to the boundary conditions, number and complexity of the differential and the algebraic equations, and the consideration of the strain-history eliminate the possibility of using any known mathematical methods resulting in a set of analytical formulae. Hence resort was made to numerical analysis and computer programming.

A further complication in problems of large plastic flow, as in stretch forming and deep-drawing, is the continuous change of geometry of the deforming medium. In numerical analysis, a "mesh" fixed in the material must be defined so that the required function values at these discrete points can be calculated. To start with, the mesh can be taken as uniformly spaced, but with continued deformation the distances between mesh points change as functions of local strains. Hence such spacings add to the unknowns and increase the complexity of the mathematical treatment. Realistic results would not be obtained if this factor is neglected.

Stability of the mathematical method is also important. Since any numerical solution is an approximation to an exact solution, the "tolerance" with a finite mesh size must be estimated by e.g. making the mesh finer and extrapolating the results to a zero mesh size. From trial solutions in stretch forming, it was found that dividing the radius of the clamped periphery of a round blank into sixty uniform steps gave not less than four significant figure accuracy in any result.

On the other hand, it is also of interest especially in stretch forming to find the conditions beyond which no solution to the problem exists, since this corresponds to the SP instability.

In the present work, the method used for the integration of the differential equations is a fourth order Runga-Kutta process. The details of the method are given in section A.1, and the reasons for its suitability to the present problem can be enumerated as follows:

(1) Self starting, no estimation of the first few values is required.

(2) Possibility of varying the steplength (ℓ) at every step.

(3) Less possibility of having an extraneous solution.

(4) Lightdemands on computer storage.

(5) Truncation error is proportional to ℓ^5, and hence convergence can be easily checked by successively halving the mesh size.

(6) Availability of only $\frac{dy_r}{dx} = \xi_r\ (x,\ y_q)$ and not any higher order derivatives.

Now the procedures followed in the numerical solution are presented for each region in stretch forming, deep-drawing, and hydraulic bulging.

In all the cases considered, the initial conditions on the blanks, i.e. $V_{m,o}$ are set before entering the respective procedures.

5.1. Stretch Forming

The network used in the numerical analysis for stretch forming is shown in Fig. 12 on a ε_2 versus r plane since $(\varepsilon_2)_p$ is used as a measure of time.

The general solutions with the view of determining all of the required variables for regions one and two are given below. The methods are generally the same for any nodal point in each region, but there are minor differences for those near initial, final and moving boundaries, and also for the first stage of deformation which will be indicated.

Although the numerical analysis requires a more detailed and precise specification of the procedure, and allowances to deal with ill-conditioned cases, and etc.,

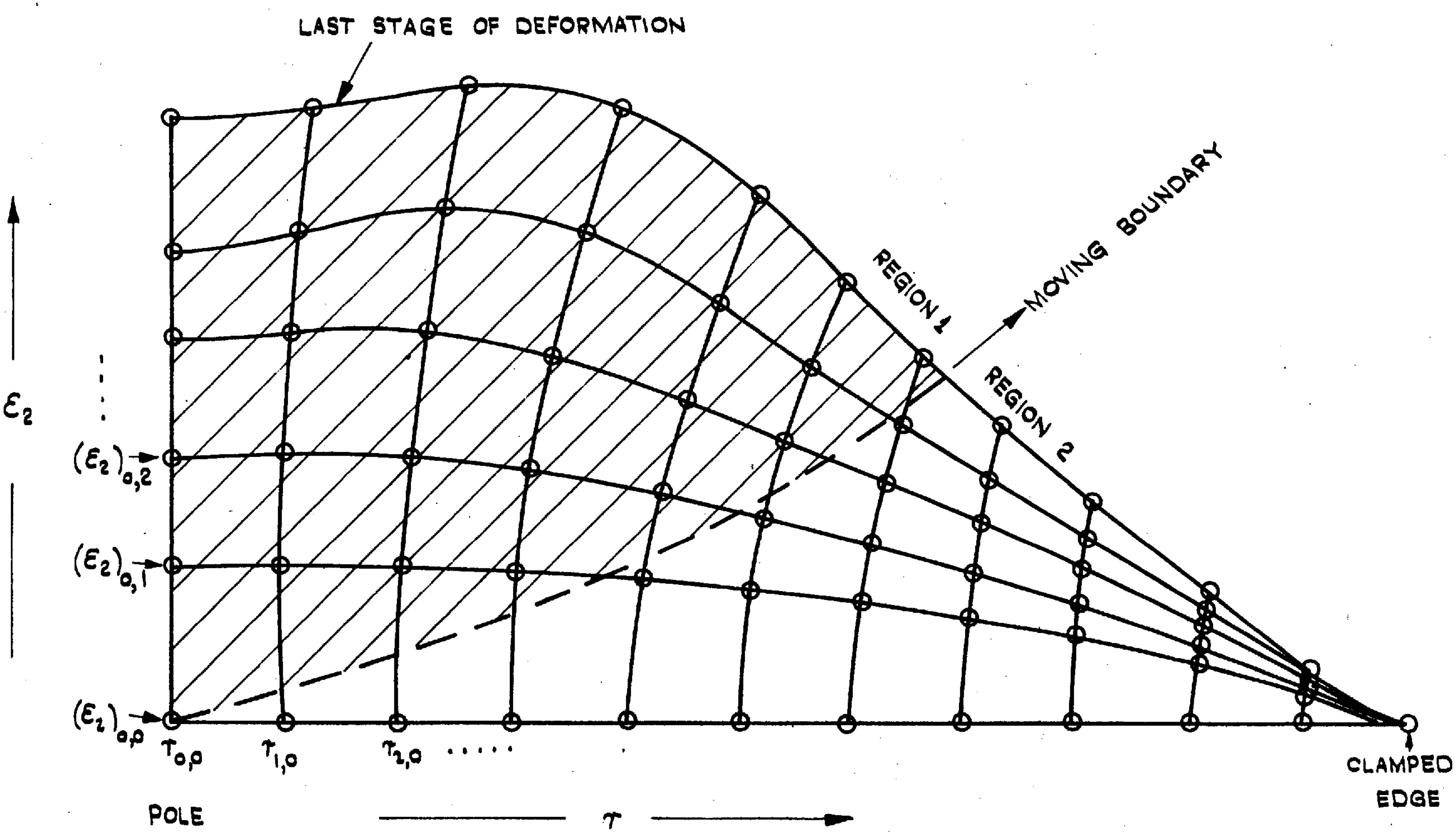

FIG. 12. NETWORK USED IN NUMERICAL ANALYSIS FOR STRETCH FORMING.

the following procedures give the essence of the applied analyses.

5.1.1. Over the Punch Head

The procedure of calculation is as follows:

(1) The functions and the derivatives at the pole are calculated by the formulae given in section 3.2.3.1. The only starting value needed is $(\varepsilon_2)_p$. For the first stage, to ensure that the equivalent strain at any point in the region is less than about 0.05 the following equation is used for $(\varepsilon_2)_p$:

$$(\varepsilon_2)_p = -0.024\,\mu + 0.03 \tag{5.1}$$

Hence, all of the required variables and derivatives then can be computed by the formulae given in section 3.2.3.1. and Appendix-B. (Suffix m = 0).

(2) The suffix m is then advanced by one. The numerical solution requires the convergence of two loops according to certain criteria which will be given later. For use in the outer and inner loops δx_n and $(\delta\varepsilon_2)_n$ are set as starting values such that:

if suffices m = n = 1 :

$$\left.\begin{aligned} \delta x_n &= -0.5\,\delta r_o \\ (\delta\varepsilon_2)_n &= 0.3\,\delta r_o \end{aligned}\right\} \tag{5.2}$$

if $m \neq 1$

$$\delta x_n = x_{(m-1),n} - x_{(m-2),n}$$

$$(\delta \varepsilon_2)_n = (\varepsilon_2)_{(m-1),n} - (\varepsilon_2)_{(m-2),n} \qquad (5.3)$$

if $m = 1$ and $n \neq 1$

$$\delta x_n = \delta x_{(n-1)}$$

$$(\delta \varepsilon_2)_n = (\delta \varepsilon_2)_{(n-1)} \qquad (5.4)$$

(3) In order to save computer time the following approximations were made:

For the hemispherical punch, the internal surface of the sheet metal is hemispherical and the current dimensions of the shell can be found using eqns. (3.31). However if $\rho_1 \sin\theta \cong r$, then eqn. (3.44) becomes;

$$k \cong - \frac{t}{2\rho_1'} (1+x) \left(1+ 0.5 \frac{t}{\rho_1'}\right) \qquad (5.5)$$

where only the middle term need to be modified during the outer loop, the remaining having been calculated before entering the loop. The error introduced is less than 0.1%.

With a similar magnitude of error for an ellipsoidal punch, it is assumed that the middle surface is ellipsoidal rather than the inner surface. The effective values of a, and b are calculated as follows:

a_e = a + mean thickness in region one in the previous stage

b_e = b + " " " " "

Also the value of k belonging to the previous point has been used. No successive approximation was required due to the close proximity of the two values and their weight in the results.

Beginning of the outer loop:

(4) From eqn. (3.40):

$$x_{m,n} = x_{(m-1),n} + \delta x_n \tag{5.6}$$

where δx_n is either the initially set value in step (2) or the modified one after the first cycle. Also the mean stress ratio following an element can be calculated as follows:

$$x^* = 0.5\, x_{m,n} + 0.5\, x_{m,(n-1)} \tag{5.7}$$

for points which were in region 1 at the (n-1)th stage.

For others such as point S in Fig.5, the mean stress ratio is taken as the same as $x_{m,n}$ with less than 1% error on the strains. This is to avoid the unnecessary complications in the numerical analysis, which would result, if the variations in x between points P and T in Fig.5 are considered.

<u>Beginning of the inner loop</u>:

(5) $(\varepsilon_2)_{m,n}$ can be computed from eqn. (3.40):

$$(\varepsilon_2)_{m,n} = (\varepsilon_2)_{(m-1),n} + (\delta\varepsilon_2)_n \qquad (5.8)$$

and hence:

$$\ell = r_{m,o} \exp(\ (\varepsilon_2)_{m,n}) - r_{(m-1),o} \exp(\ (\varepsilon_2)_{(m-1),n}) \qquad (5.9)$$

It should be noted that $(\delta\varepsilon_2)_n$ is either the initially set value or the modified one which is forced to satisfy the convergence of the inner loop. All the others in this equation are known from the boundary conditions or the previously calculated points.

(6) From eqn. (3.40)

$$(\delta\varepsilon_2)_m^* = (\varepsilon_2)_{(m-1),n} + (\delta\varepsilon_2)_n - (\varepsilon_2)_{m,(n-1)} \qquad (5.10)$$

(7) Now using $(\delta\varepsilon_2)_m^*$ from eqn. (5.10) and the value of x^* from eqn. (5.7), $(\delta\varepsilon_3)_m^*$ can be calculated from eqn. (3.43).

(8) Eqn. (3.42) can now be integrated. $\cos\theta = \zeta(r)$, can be found from eqns. (B.12) or (B.17). From eqn. (3.40):

$$(\varepsilon_3)_{m,n} = (\varepsilon_3)_{m,(n-1)} + (\delta\varepsilon_3)_m^* \qquad (5.11)$$

If m = 1, eqns. (3.67), (3.63), and (5.11) can be used with eqn. (A.13) to express ε_3 as a continuous function of r within the steplength, otherwise values of ε_3 at $(m-2),n$; $(m-1),n$; and m,n are used with eqn. (A.15). Hence in eqn. (3.42), $\frac{d\varepsilon_2}{dr} = \zeta(\varepsilon_2, r)$. Using the method of Runga-Kutta integration, from eqns. (A.2) and (A.3), $(\varepsilon_2)_{m,n}$ is calculated. Then:

$$(\delta\varepsilon_2)_n = (\varepsilon_2)_{m,n} - (\varepsilon_2)_{(m-1),n} \qquad (5.12)$$

(9) From the $(\delta\varepsilon_2)_n$ obtained from eqn. (5.12), the initially assumed (see step 2) or the previously modified $(\delta\varepsilon_2)_n$ is subtracted. If the modulus of the difference "Δ" is less than 0.005% of $(\delta\varepsilon_2)_n$, the inner loop is considered as satisfied, i.e. the strain compatibility equation solved. If the error is greater than the specified value, the $(\delta\varepsilon_2)_n$ is modified as follows:

If in <u>1st loop</u>:

$(\delta\varepsilon_2)^*_m > 0$ $(\delta\varepsilon_2)_n$ + positive increment

" < 0 " + negative "

If in <u>2nd loop</u>:

Inverse linear interpolation for $\Delta = 0$

If in <u>3rd or a higher loop</u>:

Inverse Lagrangian interpolation for $\Delta = 0$ using eqn. (A.15), and the previous points with minimum error.

A typical characteristic of convergence for the inner loop is shown in Fig. 13a. It was confirmed by trial

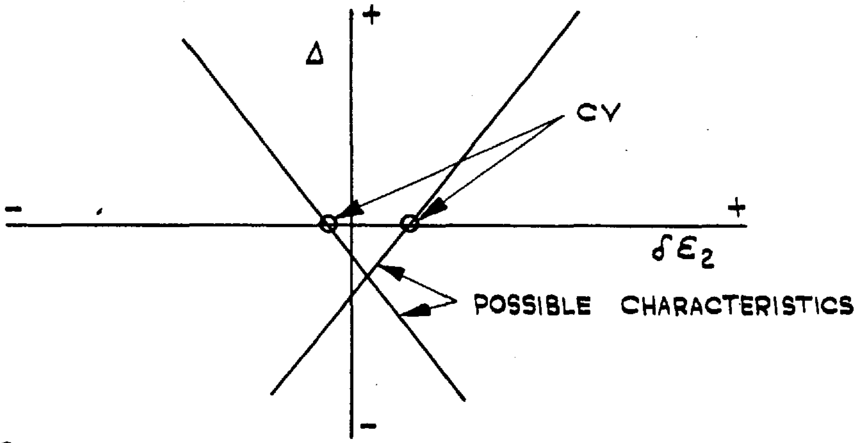

$\Delta = \delta\varepsilon_2$ (assumed) $- \; \delta\varepsilon_2$ (from strain compatability)

a) INNER LOOP IN REGION ONE OR TWO

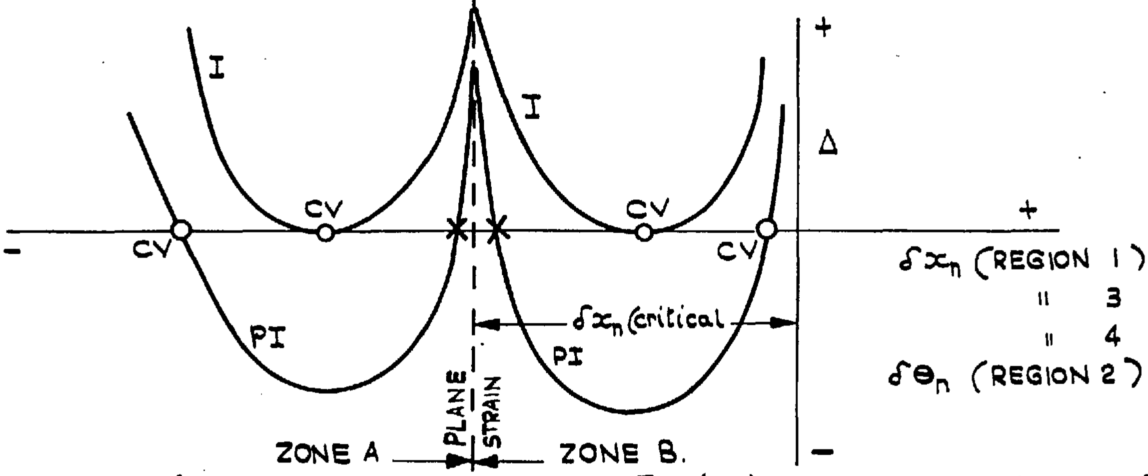

$\Delta = (\sigma_1 t)_{m,n}$ [from equilibrium eqn.] $-(\sigma_1 t)_{m,n}$ [from plasticity laws]

b) OUTER LOOP IN REGION ONE OR TWO

where

CV - CONVERGED VALUES
PI - PRE-INSTABILITY CHARACTERISTICS
I - SP INSTABILITY CHARACTERISTICS

FIG. 13. TYPICAL CHARACTERISTICS OF CONVERGENCE FOR INNER AND OUTER LOOPS IN STRETCH FORMING ANALYSIS.

calculations that it always remained linear which helped to get a rapid convergence.

Hence the new value of $(\delta\varepsilon_2)_n$ is fed again into the inner loop at step (5) until the required accuracy is obtained.

<u>End of the inner loop</u>:

(10) Using $(\delta\varepsilon_2)^*_m$ and $(\delta\varepsilon_3)^*_m$ obtained in steps (6) and (7), $(\delta\bar{\varepsilon}^*)_m$ is evaluated from eqn. (3. 23 .), and therefore $\bar{\varepsilon}_{m,n} = \sum_{o}^{n} (\delta\bar{\varepsilon}^*)_m$.

(11) With $\bar{\varepsilon}_{m,n}$ from step (10), $\bar{\sigma}_{m,n}$ can be calculated from eqn. (3.48).

(12) Using $x_{m,n}$ from eqn. (5.6) in eqns. (5.5) and (3.18), $(\sigma_1)_{m,n}$ is obtained.

(13) It is now possible to compute $(\sigma_1 t)_{m,n}$ from step (12) and eqn. (5.11).

(14) The equation of equilibrium (eqn. 3.33) can now be integrated. ρ_1, $\cos\theta$, and $\tan\theta$ can be computed as functions of r from eqns. (B.14), (B.12), (B.11), (B.17) and (B.18) with also using eqns. (3.31). To express $x = \xi(r)$: if m = 1, eqns. (3.58), (3.77), with $x_{m,n}$ from eqn. (5.6) are used in eqn. (A.13).
If $m > 1$, values of x at (m-2),n; (m-1),n; and m,n are used in eqn. (A.15).
Hence eqn. (3.33) is now $(\sigma_1 t) = \zeta\left[(\sigma_1 t), r\right]$, and it

can be integrated by the Runga Kutta method given by eqns. (A.2), and (A.3), resulting in $(\sigma_1 t)_{m,n}$.

(15) If the assumed or the later modified value of δx_n used in eqn. (5.6) was right, then the $(\sigma_1 t)_{m,n}$ obtained in steps (14) and (13) would be equal. However, initially this can only occur by chance and the modification of δx_n is necessary so that it can be fed back to step (4) for another attempt to get the two $(\sigma_1 t)_{m,n}$ equal.

If $\Delta = (\sigma_1 t)_{m,n}$ [step 14] $-$ $(\sigma_1 t)_{m,n}$ [step 13] , then the trial calculations indicate that the characteristics shown in Fig.13.b are obtained on a Δ versus δx_n plane. As seen, there are four possible points where the related equations can be satisfied, but the following restrictions exist:

(i) It can be shown that the parameters $d\lambda$, $d\lambda'$, and $d\lambda''$ in stress-strain relationships given by eqns. (3.12), (3.13) and (3.19) are positive, compatible with the positive strain-hardening hypothesis. To find the $x_{m,n}$ when $d\varepsilon^*_2 = 0$, eqn. (3.19) is used, which results in:

$$(x_{m,n})_{cr} = \frac{R+k}{R+1} \tag{5.13}$$

and $$(\delta x_n)_{cr} = (x_{m,n})_{cr} - x_{(m-1),n} \tag{5.14}$$

Studying eqn. (3.19) under the above restrictions show that:

$$(\delta \overset{*}{\varepsilon}_2)_m \gtrless 0 \qquad \text{then} \qquad \delta x_n \lessgtr (\delta x_n)_{cr}$$

Hence zone A or B in Fig. 13.b can be determined.

(ii) Since in either of the above zones there are two possible solutions, the one requiring the minimum plastic work should be considered. This can easily be determined by studying the denominator of eqn. (3.43). In step (6) of this numerical procedure $(d\overset{*}{\varepsilon}_2)_m$ was found. In step (7), $(d\overset{*}{\varepsilon}_3)_m$ was computed using eqn. (3.43). It is seen that the values of x nearer to that of obtained from eqn. (5.13) will decrease the numerical value of the denominator in eqn. (3.43), and hence produce a greater $\left|(d\overset{*}{\varepsilon}_3)_m\right|$ resulting in a greater $d\bar{\varepsilon}^*$. Therefore $x_{m,n}$ and $\delta x_{m,n}$ away from the critical value in either zone should be chosen to produce the points shown by circles in Fig. 13-b, which satisfy the minimum plastic work principle. The unacceptable solutions are shown by crosses.

Therefore with the above restrictions in mind, the correct branch of the characteristics is selected.. δx_n is varied in the successive cycles to get a change in sign of Δ, and then a mean value (binary chopped) in between the two is tried. From the three available points, by inverse interpolation using eqn. (A15) with $\Delta = 0$ in successive loops, the correct solution is determined.

<u>End of the outer loop</u>.

Now all the equations are satisfied after the convergence of the two loops. Hence the values produced are the correct ones for that particular point. The solution can now be advanced to the next point merely by changing the suffix m and repeating the steps (2) on, until an assumed location for the moving boundary is reached. In section 5.1.3, the procedure for finding the correct position of the moving boundary is presented.

Using the above procedure, the solution may tend to converge to a case where $(\delta\varepsilon_2)_m^* \approx 0$. This will cause a singularity in eqn. (3.43). If such a case occurs, then the inner cycle can be considered as satisfied, and a value of x can be computed from eqn. (5.13) corresponding to the instantaneous plane strain conditions. Instead of δx_n, $(\delta\varepsilon_3)_n$ can be used as an independent variable to control convergence, and a very similar procedure can be followed from step (10) on.

However, in the above described cases, it may not be possible to obtain a solution if the characteristic does not intersect the δx_n axis in Fig. 13.b. The limiting case is shown in the figure which corresponds to the SP instability. This occurs when the $(\sigma_1 t)_{m,n}$ obtained in step (13) is never greater than the one obtained in step (14) for any value of δx_n, hence the local equilibrium can never be satisfied no matter how the material there tries to deform. Therefore after such a state, the local rate of thinning becomes infinite and the fracture occurs almost instantaneously. Also beyond the limiting stage, from such a point the strains cannot propagate to the neighbouring points, since the equilibrium conditions would not be satisfied, and the necessary force to deform the neighbouring elements further, cannot be produced. When this occurs, the $(\varepsilon_2)_p$ is decreased and the solution for the whole stage is started from the beginning, and this is repeated until the limiting case is found, when the characteristic at the critical point becomes tangent to the axis. The procedure outlined in section A.4 is used to find the minimum Δ as shown in Fig.13.b within a given tolerance, in the case of the SP instability.

This stage corresponding to SP instability can take place at an increasing or decreasing Q or p. In some cases it is necessary to approach the unstable point from two directions, i.e. increasing and decreasing m. These are discussed in Chapter 13.

5.1.2. Between Die and Punch

The procedure of calculation is as follows:

(1) Calculation of the variables and the derivatives at the moving boundary for region two can be effected by

using the already known values for region one at the moving boundary, and the formulae given in 3.2.3.2.

The punch load can be computed by using the values of the variables at the moving boundary in eqn. (3.49):

$$P = 2\pi(r\,\sigma_1 t\,\sin\theta)_{1 \text{ or } 2} \tag{5.15}$$

(2) The numerical solution requires the convergence of two loops in a similar way as for the region one. However, a study of the effects of the variables on the equations showed that this had to be done in a different order also using a different variable in one of the loops compared with that in region one. Hence the starting values of the variables to be converged, for use in:

the outer loop:

$$(\delta\varepsilon_2)_n = \left(\frac{d\varepsilon_2}{dr}\right)_2 \delta r_n \,, \tag{5.16}$$

and the inner loop:

$$\delta\theta_n = \left(\frac{d\theta}{dr}\right)_2 \delta r_n \,, \tag{5.17}$$

where the derivatives were calculated in step (1). For points not next to the moving boundary, the previously converged values of $(\delta\varepsilon_2)_n$ and $\delta\theta_n$ for the (m-1)th points are to be used. The suffix m is then advanced by one.

<u>Beginning of the outer loop</u>:

(3) Steplength (ℓ), and $r_{m,n}$ can be computed using the

initially set, or the modified $(\delta\varepsilon_2)_n$ and eqns. (5.8) and (5.9).

(4) From eqn. (3.40), and using $(\delta\varepsilon_2)_n$ from step (2):

$$(\delta\varepsilon_2)^{*}_{m} = (\varepsilon_2)_{(m-1),n} + (\delta\varepsilon_2)_n - (\varepsilon_2)_{m,(n-1)} \qquad (5.18)$$

<u>Beginning of the inner loop</u>:

(5) The trial calculations showed that Δ for the inner loop is most sensitive to changes in $\delta\theta_n$. Hence the system of equations is ill-conditioned. It is then necessary first to determine the critical value of $\delta\theta_n$ which would correspond to instantaneous plane strain conditions. From eqn. (3.55), this would be when:

$$x = x_{cr} = \frac{R}{R+1} \qquad (5.19)$$

Eqn. (3.52) can be transformed to find $\delta\theta_n$ corresponding to x_{cr} as follows:

$$- r_{m,n} \cot\left(\theta_{(m-1)n} + \delta\theta_n\right) \frac{d\theta}{dr}_{m,n} - x_{cr} = \Delta \qquad (5.20)$$

In eqn. (5.20), $r_{m,n}$ is known from step (3), and $\left(\frac{d\theta}{dr}\right)_{m,n}$ can be determined from either of the eqns. (A.14) or (A.9) depending on whether the point is next to the moving boundary in which case the derivative found in step (1) will be used, or away from the moving boundary when the previous function values would be sufficient.

Since $\delta\theta_n$ appears in two terms in eqn. (5.20), a systematic trial and error method also incorporating the inverse interpolation (eqn. A.15) is used to get $\Delta \approx 0$, which would then give $(\delta\theta_n)_{cr}$.

(6) Using the same principle as in step (15) in section 5.1.1. when:

$$(\delta\varepsilon_2^*)_m \gtrless 0 \quad \text{then} \quad \delta\theta_n \gtrless (\delta\theta_n)_{cr}$$

$\delta\theta_n$ is first set to this critical value, and then it is given a small increment in the appropriate direction (see Fig. 13.b).

(7) Using the $\delta\theta_n$ from step (6) in eqn. (3.52), where r is known from step (3), $x_{m,n}$ can be found. Here $(\frac{d\theta}{dr})_{m,n}$ is computed either by using eqn. (A.14) with the boundary conditions obtained in step (1), or by eqn. (A.9) with the previously determined function values.

(8) The stress ratio at m,n was found in step (7), and the mean stress ratio following an element is given by eqn. (5.7). Hence using the latter in eqn. (3.55) with $(\delta\varepsilon_2^*)_m$ from step (4), $(\delta\varepsilon_3^*)_m$ can be determined.

(9) The equivalent strain-increment can now be calculated since all the terms in eqn. (3.23) are known from the previous steps.

$$\text{Also} \quad \bar{\varepsilon}_{m,n} = \sum_{o}^{n} (d\bar{\varepsilon}^*)_m$$

(10) With $\bar{\varepsilon}_{m,n}$ from step (9) $\bar{\sigma}_{m,n}$ can be determined from eqn. (3.48).

(11) Substituting $x_{m,n}$ from step (8) in eqn. (3.56) with $\bar{\sigma}_{m,n}$ from step (10), $(\sigma_1)_{m,n}$ is calculated.

(12) It is now possible to calculate $(\sigma_1 t)_{m,n}$ from steps (8) and (11).

(13) Using eqn. (3.49) (eqn. of equilibrium), where P is obtained from step (1), $r_{m,n}$ from step (3) and $\theta_{m,n}$ from step (6), $(\sigma_1 t)_{m,n}$ can be calculated.

(14) If the $\delta\theta_n$ used in step (6) was correct, $(\sigma_1 t)_{m,n}$ in steps (12) and (13) would be equal, but in general the error is given by:

$$\Delta = (\sigma_1 t)_{m,n}\left[\text{step 13}\right] - (\sigma_1 t)_{m,n}\left[\text{step 12}\right] \qquad (5.21)$$

The characteristic Δ versus $\delta\theta_n$ is shown in Fig. 13.b.

For the same reasons as given in step (15-ii) of section 5.1.1., the solutions furthest away from the $(d\theta_n)_{cr}$ should be chosen. The solution is started off at a point near the critical one, and $\delta\theta_n$ is increased or decreased with increasing steps so that the correct crossing is obtained on the Δ versus $\delta\theta_n$ characteristic. Then four successive $\delta\theta_n$ values are binary chopped. This is followed by successive inverse interpolation for $\Delta = 0$ using eqn. (A.15) until the required accuracy of 0.001% is obtained. The binary chopping is required for the mathematical stability of the inverse interpolation. At the end of each loop step (6) is entered with a new value of $\delta\theta_n$.

It may not be possible to obtain a solution in some cases. However this may not be due to a genuine SP instability, but it may be due to the initially incorrect $(\delta\varepsilon_2)_n$ which is yet to be satisfied in the outer loop. Hence one has to return to step (2) and choose a value of $(\delta\varepsilon_2)_n$ which will give a solution for the inner loop. This is done in a herauistic manner by a systematical trial and error method. However, such a later modified value of $(\delta\varepsilon_2)_n$ may not satisfy the outer loop, in which case one has genuine SP instability.

<u>End of the inner loop</u>.

(15) It is now possible to integrate the strain compatibility equation (eqn. (3.42)) by the Runga-Kutta method. For points next to the moving boundary $\varepsilon_3 = f(r)$ is expressed by eqn. (A.13) using the derivative found in step (1), and the current function value. For the other points eqn. (A.15) can be used with the previously determined and the current function values. $\theta = f(r)$ is also determined in a similar way, since it is an unknown in this region unlike to that in region one, where it is given by the punch geometry. Hence eqn. (3.42) becomes $\frac{d\varepsilon_2}{dr} = f(\varepsilon_2, r)$ which can be integrated to give $(\varepsilon_2)_{m,n}$, and $(\delta\varepsilon_2)_n$ can be found from eqn. (3.40).

(16) If the initially set $(\delta\varepsilon_2)_n$ in step (2) is not

correct, then it would not be equal to the one obtained in step (15). In general the error is given by:

$$\Delta = (\delta\varepsilon_2)_n \left[\text{from step 2}\right] - (\delta\varepsilon_2)_n \left[\text{from step 15}\right] \quad (5.22)$$

The trial calculations showed that $(\delta\varepsilon_2)_n$ versus Δ is a linear relationship as shown in Fig.13.a. The modification to $(\delta\varepsilon_2)_n$, to get $\Delta = 0$ is the same as the procedure described in step (9) of section 5.1.1.

<u>End of the outer loop</u>.

Hence all of the equations are now satisfied, and the suffix m can be advanced, and the procedure can be re-started at step (2). The process of computation is repeated until the final boundary, clamped edge is reached.

5.1.3. <u>Matching of the Boundary Conditions</u>

In section 5.1.1., the procedure for the numerical solution for region one was presented which started with a value of $(\varepsilon_2)_p$ at the pole and ended at an assumed location of the moving boundary, at first, at a nodal point. Since this location of the moving boundary may not necessarily be correct, with the procedure given in section 5.1.2. it may result with $\varepsilon_2 \neq 0$ at the clamped edge.

Fig. 14 shows a typical characteristic obtained by plotting the assumed locations of the moving boundary, against ε_2 at the clamped edge or the final boundary at any stage of the deformation.

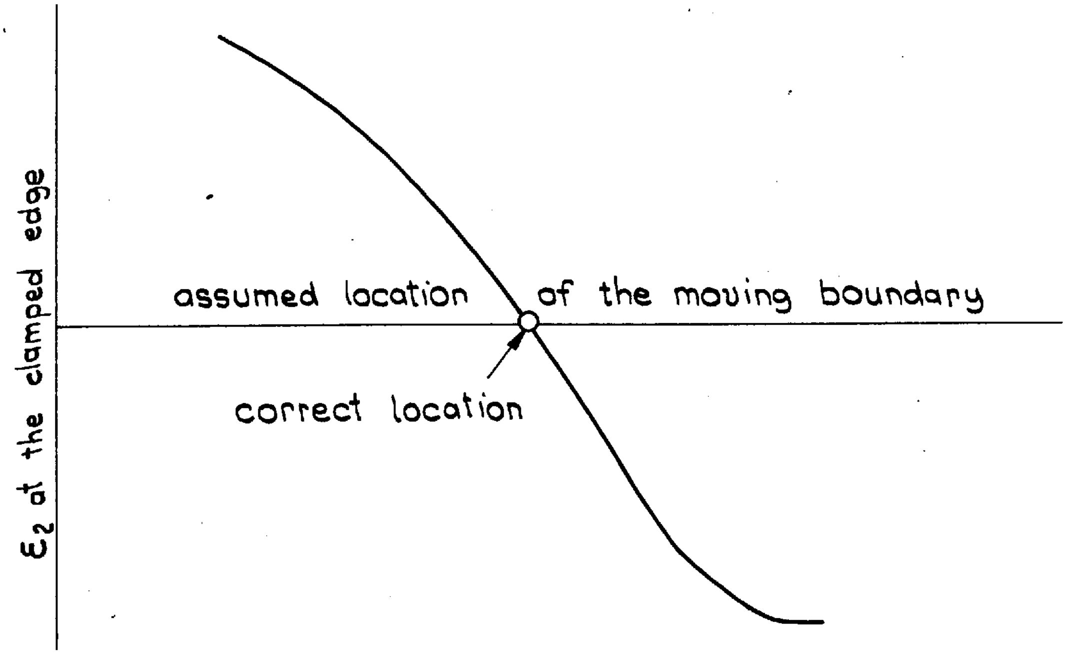

FIG.14 - CHARACTERISTIC FOR MATCHING THE BOUNDARY CONDITIONS IN STRETCH FORMING

The procedure to find the correct location is as follows:

(1) In the first stage and the first cycle in boundary matching, the moving boundary is assumed to be at the nodal point whose m = integral part (0.2 x no. of divisions on the blank).

In the first cycle of the other stages ($n > 1$), since the rate of movement of the moving boundary can be computed from the previous stages, a better prediction is made.

(2) In the second and the following cycles for the matching of the boundary conditions, the location of the moving boundary is changed per point at a time until a change in the sign of ε_2 at the clamped edge is obtained.

(3) The characteristic is then binary chopped once to obtain stability in the following step. Effectively the boundary is forced in between the two nodal points.

(4) Successive inverse Lagrangian interpolation is carried out with $\varepsilon_2 = 0$ using eqn. (A.15) until the required accuracy of $|\varepsilon_2| < 0.000008$ is obtained.

Hence all of the equations and the boundary conditions are satisfied for one stage. It should be noted that in step (2) and the following, the solution goes back to the assumed or the modified location of the moving boundary, and it is only necessary to recompute region two and not region one.

For the other stages, the same procedure of the boundary matching is used. The solution at the end may reach a stage when the equations in region one or region two cannot all be satisfied corresponding to, in effect, a post SP instability. In such cases, the calculation returns to the pole, binary chops the last increment on $(\varepsilon_2)_p$, and recomputes regions one and two until convergence is obtained for all of the points. At this time the boundary matching is initiated and the same procedure given above is used. Hence the last stage corresponds to a limiting state to the SP instability conditions with satisfied boundary conditions as before.

At the end of each stage the bulge depth is computed using the exact method given in section B.4.

At each stage the variation of μ is also considered. The effective value is found by interpolation of the given polar strain versus μ curve by eqn. (A.15).

5.2. Drawing over the Die Surface

The numerical procedures to be presented here are very similar to those given earlier in sections 5.1.1. and 5.1.2. for stretch forming. They will be briefly outlined as follows:

5.2.1. Radial Drawing Region
(Region four)

(1) The boundary conditions at the rim are computed from the formulae and procedure given in section 3.3.3.1. This only requires an arbitrary starting value for ε_2 at the rim. If a deep-drawing problem is to be solved, then the ε_2 at the rim and the ε_2 at the pole in region one should be compatible, and the matching of these boundary conditions is givenin section 5.3. Otherwise $\delta\varepsilon_2^*$ at the rim merely governs the time increment between two successive stages, and the larger values make the solution more approximate. All the required derivatives

except $\frac{dx}{dr}$ and $\frac{d\varepsilon_3}{dr}$ can be computed. These can initially be assumed to be zero. After the computation of the third nodal point in this region, the values can be checked back using eqn. (A.8). If appreciably different from zero, the solution using the new values can be restarted from the rim.

(2) The value of suffix m is decreased by one. There are again two loops in the same order as in stretch forming. The starting values for δx_n, and $(\delta\varepsilon_2)_n$ are set as follows:

if the point whose solution is considered is at the first stage and next to the rim:

$$\begin{aligned} \delta x_n &= 0.5\,\delta r_o \\ (\delta\varepsilon_2)_n &= -\,0.3\delta r_o \end{aligned} \qquad (5.23)$$

if different than the point next to the rim:

$$\begin{aligned} \delta x_n &= x_{(m+1),n} - x_{(m+2),n} \\ (\delta\varepsilon_2)_n &= (\delta\varepsilon_2)_{(m+1),n} - (\delta\varepsilon_2)_{(m+2),n} \end{aligned} \qquad (5.24)$$

if next to the rim but not in first stage:

$$\begin{aligned} \delta x_n &= \delta x_{(n-1)} \\ (\delta\varepsilon_2)_n &= (\delta\varepsilon_2)_{(n-1)} \end{aligned} \qquad (5.25)$$

(3) Here the general case of a curved die is considered. The same valid approximation for k is made as given by

eqn. (5.5).

All the remaining steps of this procedure, with the exception of the following, are the same as in section 5.1.1. if the suffices (m-1) and (m-2) are replaced by (m+1), and (m+2) respectively.

(8) Eqn. (3.42) can now be integrated. $\cos\theta = \xi(r)$ can be obtained from equations giving this relationship for a particular die. If the die is flat, then $\cos\theta = 1$.

Eqn. (5.11) is also valid. If the point is next to the rim, then $\frac{d\varepsilon_3}{dr} = 0$, and with (ε_3) from step (1), and eqns. (5.11) and (A.13), $\varepsilon_3 = \xi(r)\cdot \frac{d\varepsilon_3}{dr}$ can later be modified as mentioned in step (1) if it is different from zero. If the point is not next to the rim, the values of ε_3 at (m+2),n; (m+1),n; and m,n are used with eqn. (A.15). The remaining part of this step is the same as that of step (8) in section 5.1.1.

(14) The equation of equilibrium can now be integrated. ρ_1, $\cos\theta$, and $\tan\theta$ can be computed for a given die geometry by also using the eqns. (3.31). To express $x = \xi(r)$: if the point considered is next to the rim, then x for the rim (see step 1), $\frac{dx}{dr} = 0$ at the rim, and eqn. (5.6) are used in eqn. (A.13). If the point is not next to the rim, then the values of x at (m+2), n; (m+1),n; and m,n are used in eqn. (A.15).

Hence eqn. (3.33), or eqn. (3.94) if the die is flat, now becomes: $(\sigma_1 t) = \xi\left[(\sigma_1 t), r\right]$, and it is integrated by the Runga-Kutta method given by eqns. (A.2) and (A.3), resulting in $(\sigma_1 t)_{m,n}$.

Fig.13 applies to this region as well, and the criteria for choosing the correct solution, and the necessary procedure as given in step (15) in section 5.1.1. remains also valid for this region.

When the solution for one point is completed, the suffix m is decreased by one and the steps (2) on are repeated until the start of the die curvature is met. However, if the die profile is a tractrix, then there is no geometrical discontinuity, and the solution can be advanced to the point of departure of the sheet metal from the die. This is an assumed location and the method for finding the correct one is given in section 5.3. In the case of geometrical continuity over the die, the region three disappears.

Although the possibility of having SP instability with blanks having non-uniform initial conditions exist, in the majority of the cases with uniform initial properties $(\delta\varepsilon_3^*)_m > 0$, and the SP instability is not expected.

5.2.2. Over the Die Profile
(Region three)

(1) Computation of the boundary conditions at the start of the die curvature is given in section 3.3.3.2, where the equations require the values at this point belonging

to region four. Initially a linear approximation is required for $\frac{dx}{dr}$ at this boundary such that:

$$\frac{dx}{dr} \approx \frac{\delta x_n}{\delta r_n} \tag{5.26}$$

This approximation can be checked back by eqn. (A.8) after the computation of the third nodal point in this region. If appreciably different, then using the new value, the solution can be restarted.

The remainder of the numerical procedure is the same as that for region four given in section 5.2.1, from step (2) on. The minor differences in steps (8) and (14) are indicated below.

(8) Eqn. (3.42) can now be integrated. $\cos\theta = \xi(r)$ can be obtained from the equations giving this relationship for the particular die under consideration. If the shape is toroidal then eqns. (3.95) can be used.

If the point considered is next to the start of the die curvature, then using $\frac{d\varepsilon_3}{dr}$ from step (1), eqns. (5.11) and (A.13) with the other boundary conditions from step (1), $\varepsilon_3 = \xi(r)$. If it is not next to the start of the die curvature, the values of ε_3 at $(m+2),n$; $(m+1),n$; and m,n are used with eqn. (A.15). The remaining part of this step is the same as that of step (8) in section 5.1.1.

(14) The equation of equilibrium (eqn. (3.33)) can now be

integrated. ρ_1, $\cos\theta$, and $\tan\theta$ can be computed from the given die geometry, or from eqns. (3.95) if it is toroidal. To express $x = \xi(r)$:

If the point considered is next to the start of the die curvature, then x from step (1), and $\frac{dx}{dr}$ from eqn. (5.26), with eqn. (5.6) are used in eqn. (A.13). If the point is not next to the rim, then the values of x at (m+2),n; (m+1),n; and m,n are used in eqn. (A.15).

The remaining part of this step is the same as that of step (14) in section 5.2.1.

The solution to the other points in this region can be extended by decreasing m by one at a time until an assumed or modified location of the departure of sheet metal from the die is reached. The matching of the boundary conditions is explained in section 5.3.

As in region four, the SP instability is not expected with blanks of uniform initial conditions.

5.3. Deep-Drawing

In a deep-drawing problem there are essentially four regions with different states of stress. The methods of numerical solutions for these regions (regions one to four inclusive) were presented previously in this Chapter. What remains to be done is the matching of the boundary conditions, between these regions. This was done for the stretch forming problem in section 5.1.3.

In drawing over the die surface, if only the radial drawing problem is to be considered, the only starting value needed is the ε_2 at the rim.

In any stage in deep-drawing, the following boundary conditions are not known, and a method of matching of the boundary conditions would be necessary.

(i) ε_2 at the pole in region one. This can be regarded as a measure of time, and its increase governs the finite increments of the variables between any two successive stages. Hence it is not an unknown, but an arbitrarily assigned parameter which also influences the accuracy of the numerical solution.

(ii) Location of the moving boundary between the regions one and two. This is an unknown.

(iii) Location of the moving boundary between the regions two and three. This is an unknown.

(iv) ε_2 at the rim in region four. This is an unknown.

To find the above three unknown boundary conditions the following procedure which includes the two loops can be used.

(1) The boundary conditions at the pole for an arbitrary value of ε_2 can be calculated and the solution can be advanced point by point as described in section 5.1.1.

Beginning of the outer loop.

(2) The solution in region one terminates at an initially assumed or later modified location of the moving boundary between regions one and two. The boundary conditions here are calculated and the solution in region two proceeds as described in section 5.1.2.

* (3) The solution of region two terminates at a point such that the slope of the bulge is tangent to that of the die at the same point.

Beginning of the inner loop.

(4) The solution of region four is started by an initially assumed or a later modified value of ε_2 at the rim, and continues into region three as explained in sections 5.2.1. and 5.2.2.

(5) The solution of region three terminates at the point where the solution of region two terminated as mentioned in step (3). However, it should be noted that the suffix m for the end points of the two solutions may not be the same, although the current radii for both are the same.

(6) The values of $Q = 2\pi r\sigma_1 t \sin\theta$ calculated from the results of steps (3) and (5) are compared. They must be equal to satisfy the conditions of vertical equilibrium of forces at the boundary. If they are different more than an allowed inaccuracy, then ε_2 at the rim in region four is changed in a way as to reduce this difference in

the following cycles. This can be achieved by a method similar to that described in stretch-forming in section 5.1.3., using binary chopping and successive inverse interpolations. After a few cycles the two values can be made equal, meaning that the correct ε_2 at the rim in region four is found for an assumed location of the moving boundary between region one and two.

<u>End of the inner loop</u>.

(7) At this stage the two values of the suffix m at the boundary between regions two and three obtained from the solution in steps (3) and (5) are compared. They must be the same if the assumed location of the boundary between regions one and two was correct.

(8) When $(m)_2 \neq (m)_3$ then the location of the moving boundary between regions one and two is varied such that $(m)_2 = (m)_3$ is obtained. Hence with a modified location of the moving boundary between regions one and two solution returns to step (2), and after a few cycles using a method similar to that described in section 5.1.3. for stretch forming, with binary chopping and successive inverse interpolation, the correct location of the boundary can be found.

<u>End of the outer loop</u>.

Hence all of the boundary conditions and the equations at every point in each region are satisfied, and the solution can proceed to the next stage, until the SP instability in one of the regions is obtained. Then $(\varepsilon_2)_p$ in step one is reduced such that a solution can be obtained, which would be the limiting one to the SP instability.

This procedure is very general and no assumptions or approximations are made except for the ones within the framework of the basic theory presented in Chapter 3.

This approach has not been used or recommended by any of the previous researchers. The approximations, and the assumptions involved in the other simplified methods were mentioned in sections 1.1.1. and 1.1.3.

5.4. Hydraulic Bulging

As mentioned in section 3.4., there is only one effective region in hydraulic bulging. It is not a moving boundary problem, but is a two-point boundary problem since all of the variables at the pole, or at the clamped edge cannot be determined, and it requires the matching of the boundary conditions.

The procedure of the numerical solution is as follows:

(1) The boundary conditions can be calculated by the formulae referred to in section 3.4.2. However, this would require the values of $(\varepsilon_2)_p$ and $(\rho_1)_p$ at the pole to start the computation. $(\varepsilon_2)_p$ as in stretch forming,

can be regarded as a variable that defines the time increments, and hence it can be chosen arbitrarily, but with small enough increments to make the solution sufficiently accurate.

$(\rho_1)_p$ is initially an unknown, and the correct value can only be found at the end of the boundary matching. Initially a starting value can be estimated from eqn. (4.33) based on Hill's (34) approximate solution. It would then be possible to find all of the variables at the pole.

(2) The suffix m is then advanced by one. The numerical solution requires the convergence of the two loops as in the stretch forming problem. For use in the outer and inner loops, $\delta\theta_n$ and $(\delta\epsilon_2)_n$ are set as starting values such that:

If suffices $m = 1$, and $n = 1$

$$\begin{aligned} \delta\theta_n &= \delta r_n/(\rho_1)_p \\ (\delta\epsilon_2)_n &= 0.3\,\delta r_o \end{aligned} \tag{5.27}$$

if $m \neq 1$

$$\begin{aligned} \delta\theta_n &= \theta_{(m-1),n} - \theta_{(m-2),n} \\ (\delta\epsilon_2)_n &= (\epsilon_2)_{(m-1),n} - (\epsilon_2)_{(m-2),n} \end{aligned} \tag{5.28}$$

if $m = 1$ and $n \neq 1$

$$\delta\theta_n = \delta\theta_{(n-1)} \qquad (5.29)$$

$$(\delta\varepsilon_2)_n = (\delta\varepsilon_2)_{(n-1)}$$

Beginning of the outer loop:

Beginning of the inner loop:

(3) Using either the initially set or the later modified value of $(\delta\varepsilon_2)_n$, from eqns. (5.8) and (5.9), $(\varepsilon_2)_{m,n}$, $r_{m,n}$ and ℓ are calculated. $(\delta\varepsilon_2^*)_m$ is calculated from eqn. (5.10).

(4) From eqn. (3.101), $x_{m,n}$ can be calculated. In the first cycle t, and σ_1 can be taken as those corresponding to (m-1)st point, to be replaced in the following cycles by the ones calculated in the following steps. Also $\theta_{m,n} = \theta_{(m-1),n} + \delta\theta_n$ (5.30)

To find $(\frac{d\theta}{dr})_{m,n}$:

if $m = 1$, $(\frac{d\theta}{dr})_p$ from step (1), and eqn. (5.30) are used in eqn. (A.14).

if $m \neq 1$ then θ at $(m-2),n$; $(m-1),n$; and m,n are used in eqn. (A.9).

Since p has the same value as that of at the pole throughout the regiun, $x_{m,n}$ can be computed from eqn. (3.101).

(5) Then the mean stress ratio following an element can

be calculated from eqn. (5.7).

(6) Using the $(\delta\varepsilon_2^*)_m$ from step (3), x from step (5), and k from eqn. (3.103) where the same value of σ_1 is used as in step (4), $(\delta\varepsilon_3^*)_m$ can be calculated from eqn. (3.43). $(\varepsilon_3)_{m,n}$ can be caloulated from eqn. (5.11).

(7) Eqn. (3.42) can now be integrated. To express θ and ε_3 as continuous functions of r within the step-length: if m = 1, then θ_p, $(\frac{d\theta}{dr})_p$ and $(\varepsilon_3)_p$, $(\frac{d\varepsilon_3}{dr})$ as found in step (1), with $\theta_{m,n}$ from eqn. (5.30) and $(\varepsilon_3)_{m,n}$ from step (6) are substituted in eqn. (A.13).

If $m \neq 1$, then the values of ε_3 and θ at (m-2),n; (m-1),n; m,n are used in eqn. (A.15).

Hence eqn. (3.42) becomes $\frac{d\varepsilon_2}{dr} = \zeta(\varepsilon_2, r)$, and using the Runge-Kutta method given by eqns. (A.2), and (A.3) it can be integrated to give $(\varepsilon_2)_{m,n}$.

Hence $(\delta\varepsilon_2)_n = (\varepsilon_2)_{m,n} - (\varepsilon_2)_{(m-1),n}$ (5.31)

and this is compared with the one assumed in step (2), or the modified one in the previous cycle. If the difference exceeds a specified accuracy, then $(\delta\varepsilon_2)_n$ is modified in a manner shown in step (8) of section 5.1.1. and a new value is fed into step (3) until the convergence is obtained.

<u>End of the inner loop.</u>

(8) Using $(\delta\varepsilon_2^*)_m$ and $(\delta\varepsilon_3)_m^*$ obtained in steps (3) and (6), $(\delta\bar{\varepsilon}^*)_m$ is evaluated from eqn. (3.23), and hence $\bar{\varepsilon}_{m,n}$

$$= \sum_{o}^{n} (\delta\bar{\varepsilon}^{*})_m.$$

(9) With $\bar{\varepsilon}_{m,n}$ from step (8) $\bar{\sigma}_{m,n}$ can be obtained from eqn. (3.48).

(10) Using $x_{m,n}$ from step (4) with k from eqn. (3.103) in eqn. (3.18), $(\sigma_1)_{m,n}$ can be calculated.

(11) It is now possible to compute $(\sigma_1 t)_{m,n}$ from steps (10) and (6).

(12) The second of the equations of equilibrium (eqn. (3.102)) can now be integrated. In order to include its variation within the steplength, x must be calculated from eqn. (3.101) at the points demanded by the Runga-Kutta integration (see eqns. (A.2) and (A.3)), i.e. at the beginning, middle and at the end of any step. Since the value at the beginning of a step is known from the previous point, and the one at the end was found in step (4), the only additional value of x in the middle can be calculated from eqn. (3.101) by the method given in step (4) with the values of the variables corresponding to the mid-step.

Hence $(\sigma_1 t)_{m,n}$ is obtained.

(13) If the assumed or the later modified value of $\delta\theta_n$ in step (2) was right, then the $(\sigma_1 t)_{m,n}$ obtained in steps (11) and (12) would be equal. Otherwise the error Δ is:

$$\Delta = (\sigma_1 t)_{m,n} \left[\text{step } 12\right] - (\sigma_1 t)_{m,n} \left[\text{step } 11\right]$$

The characteristic $\delta\theta_n$ versus Δ can then be obtained by trial calculations, but the corresponding δx_n versus Δ curve should be the same as that of region one in stretch forming as shown in Fig.13.b.

As in stretch forming four possible solutions exist and the correct one should be chosen using the same criteria. The procedure, along with the method of reducing Δ within an acceptable value, and hence finding the correct solution is the same as that given in step (15) of section 5.1.1. The modified value of $\delta\theta_n$ in this step is then fed back into step (3) until the accuracy limit is satisfied.

End of the outer loop.

This completes the solution of one point. To advance the solution to the others, the suffix m is increased by one until the final boundary is met. At this point ε_2 is checked. From section 3.4.2. the requirement is, $\varepsilon_2 = 0$. If $\varepsilon_2 \neq 0$, then the initially assumed, or the modified value of $(\rho_1)_p$ in the successive cycles was not right. Hence each time $\varepsilon_2 \neq 0$ at the clamped edge, the calculation returns to step (1) with a modified value of $(\rho_1)_p$ to reduce the $|\varepsilon_2|$ at the clamped edge. This procedure for matching the boundary conditions is very similar to that of given for the determination of the location of the moving boundary in stretch forming (see section 5.1.3.), and reduces to the problem of finding the crossing point of the $(\rho_1)_p$ versus ε_2 (at the clamped edge) curve (characteristic) with the $(\rho_1)_p$ axis.

This then gives the complete solution for one stage satisfying all the equations and the boundary conditions. To obtain the solution for the following stages $(\varepsilon_2)_p$ is increased and the whole procedure is repeated.

The computation can go on until the SP instability is reached. This would take place at the pole with blanks of uniform initial conditions, but it can occur anywhere on the bulge if blanks with non-uniform initial conditions (thickness, etc.) are used.

The numerical results for stretch forming with $\mu \approx 0$, which is analogous to hydraulic bulging suggests that it may not be possible to find the SP instability by only advancing the calculation from the pole to the clamped edge. It seems that after the completion of the computation for each stage, advancing from the pole to the clamped edge, it is also necessary to check back for the SP instability by starting at the clamped edge and finishing at the pole. This check back will not need boundary matching since it can use the correct boundary conditions as found in the forward calculations.

When the SP instability is reached in any of the above directions of the calculation at any stage, $(\varepsilon_2)_p$ can be reduced and the calculation can be restarted. This would go on until a stable stage is obtained within a specified proximity to the unstable one.

It should be mentioned that this solution is very general. Although no numerical solution is obtained for hydraulic bulging, from similar results in stretch forming, it can be deduced that the SP instability can take place at an increasing, or decreasing Q or p.

CHAPTER 6 - COMPUTER PROGRAM FOR STRETCH FORMING

In the previous chapters, the basic equations and the numerical procedures for the solutions of stretch forming, radial drawing, deep-drawing, and hydraulic bulging problems were developed. Since the equations involved are complicated to evaluate and the numerical processes are highly iterative, no computation could be attempted by manual means. Due to the complexity of the analyses, logical branchings in the computations, and the high accuracy required for their mathematical stability, the electronic digital computers had to be used.

Two computer programs were written for the solution of the stretch forming problem, one for a hemispherical punch, the other for an ellipsoidal punch. No programs were written, and no numerical results were obtained for the other processes, for which the numerical procedures were presented in Chapter 5.

In this Chapter, only the program written for a hemispherical punch in stretch forming will be discussed, without going into much detail due to the space limitations. The one written for an ellipsoidal punch is very similar to this.

6.1. General Features

The computer program was written such that it would be compatible with $CHLF_3$ (University of London Autocode) and EMA (Extended Mercury Autocode) programming languages, and with the Mercury and Atlas computers. This was necessary, because the initial short development was done on the Mercury computer, and for the long development and the production runs, the Atlas computer was used, since the Mercury computer could not provide the required facilities, and the speed.

The general requirements of the program is given below:

Main Store (Memory):

For the program - 13360 48 bit Atlas words or 26 Atlas blocks.

For the intermediate and final results - 2000 48 bit Atlas words or 4 Atlas blocks.

Time requirements for the solution of a case:

Compiling* of the program - about 5000 instruction interrupts+ or $\sim 1 \times 10^7$ elementary operations.

---

* Compiling is the process by which a program written in a high level language like EMA is translated into the basic machine codes by a built in compiler program.

\+ Instruction interrupts in the Atlas computer are obeyed at every 0.004 sec. Within each interrupt 2048 elementary instructions are obeyed.

Execution of the program - This changes according to the specified parameters, e.g. μ, A, B, and n, etc., but the effective range is given below.

Maximum: 300000 instruction interrupts or 6.15×10^8 elementary operations or 25 minutes or approximately 850 man-years.*

Minimum: 120000 instruction interrupts or 2.45×10^8 elementary operations or 10 minutes or approximately 340 man-years.

Average: 200000 instruction interrupts or 4.1×10^8 elementary operations or 17 minutes or approximately 570 man-years.

Since Atlas is a time-sharing computer, depending on the load on the computing system, the time between the input of the program and the output of the results may run into hours. Due to the probability of computer faults and breakdowns within this time, unless a "rescue" procedure is incorporated in the program, the results might be lost. Therefore the intermediate results at the completion of every stage in stretch forming are stored on a private magnetic tape. The computation could then be restarted in case of a fault, wasting not more than a minute of the computer time.

---

* Equivalent of the computing effort in man-years is assessed by taking 4 operations/minute, 10 hrs/day, and 300 days/year.

Storage on the private magnetic tape: 12 Atlas blocks (10-21 inc.) or 6144 48 bit Atlas words.

This rescue procedure required a small program to set the magnetic tape to known values which could be tested in the main program. This was necessary for an initial start but not for a restart.

The input of the program is separate from that of the data, and both are on five-track paper tape. The output is designed for a 120-character wide Analex line-printer.

6.2. Variable Allocation and Layout

In the EMA and $CHLF_3$ languages on the Atlas computer, the following types of variables with the corresponding properties are available:

(i) Main variables are identified by the suffixed letters of the alphabet from A-H and U-Z. They are floating point numbers.*

(ii) Special variables use the same letters as the main variables. They have no suffices but can be primed. They are floating point numbers.

(iii) Auxiliary variables were not used in this program, since the total of main and the special variables was sufficient for the requirements.

---

* Floating point representation of a number requires the specification of its argument and exponent to attain the highest accuracy in calculations using a finite length of a register.

(iv) Indices range from I-T. Their number can be increased by priming this range of letters. They represent integers.

According to the above properties of the variables the following have been chosen to represent the corresponding physical quantities. Some of the important variables are:

Special Variables	Physical Quantity	Indices	Physical Quantity
A	A	I	No. of cases to be computed
B	B		
C	n	J	No. of steps for numerical integration
D	ρ_1		
E	b (for ellipsoidal punch)	M	printing interval
F	D	N	No. of differential equations
G	t_o		
H	ℓ	P	No. of stages in the computation
U	μ		
		T	the value of the nodal point beyond the location of the moving boundary

Main variables

$A_o, A_2, \ldots\ldots, A_{120}$	-	$r_{m,n}$
$A_1, A_3, \ldots\ldots, A_{121}$	-	$r_{m,(n-1)}$
$B_o, B_2, \ldots\ldots, B_{120}$	-	$(\varepsilon_2)_{m,n}$
$B_1, B_3, \ldots\ldots, B_{121}$	-	$(\varepsilon_2)_{m,(n-1)}$
$C_o, C_2, \ldots\ldots, C_{120}$	-	$(\varepsilon_3)_{m,n}$
$C_1, C_3, \ldots\ldots, C_{121}$	-	$(\varepsilon_3)_{m,(n-1)}$
$D_o, D_2, \ldots\ldots, D_{120}$	-	$(\bar{\varepsilon})_{m,n}$
$D_1, D_3, \ldots\ldots, D_{121}$	-	$(\bar{\varepsilon})_{m,(n-1)}$
$E_o, E_2, \ldots\ldots, E_{120}$	-	$(\sigma_1)_{m,n}$
$E_1, E_3, \ldots\ldots, E_{121}$	-	$(\sigma_1)_{m,(n-1)}$
F_o, F_1	-	$\frac{dy_r}{dx}$ of differential equations
G_o, G_1	-	working store for numerical integration
H_o, H_1	-	" " "
$U_o, U_2, \ldots\ldots, U_{120}$	-	$x_{m,n}$
$U_1, U_3, \ldots\ldots, U_{121}$	-	$x_{m,(n-1)}$
$V_o, V_2, \ldots\ldots, V_{120}$	-	$\theta_{m,n}$
$V_1, V_3, \ldots\ldots, V_{121}$	-	$\theta_{m,(n-1)}$

The above layout for the storage of the variables and indices had been designed to minimize the storage requirements in the computer by only storing the essential variables needed for the calculations taking into account the strain history. Some (e.g. σ_1) not required for this purpose were stored to avoid recomputation, and hence to minimize the computation time.

The other variables and indices not included in the above lists, but included in the computer program (see Appendix-C) are either used as temporary working space to store the intermediate values of the variables, or can be deduced from the knowledge of the above. Some of the important ones of such variables are given below, since the whole list would be prohibitively long:

$(\delta\varepsilon_2^*)_m$ - X_7		$(\delta\bar{\varepsilon}^*)_m$	- X_{19}	
$(\delta\varepsilon_2)_n$ - X_5		δx_n	- X_{10}	(Region 1)
	and	$\delta\theta_n$	- X_{10}	(Region 2)
$(\delta\varepsilon^*)_m$ - X_9		π_{88}	$\gtrless 0$	Unstable stage Stable stage

Δ - X_{13} (Regions 1 & 2, inner cycle)

" - π_{16} (" " ", outer cycle)

6.3. Layout of Input and Output

Since the computer program is very general, it would produce results with any given combination of the parameters within reasonable numerical ranges.

Except for the trivial changes in the "Job Description" (See Appendix-C) related to the "red tape" of running a program on the Atlas computer, which also depends on the storage, time, and output requirements for a particular run, the program itself does not need to be changed. The same physical paper tape (5-track) can be input as a separate document to the computer for every run.

However, the program requires a separate data tape containing the parameters for which the solution is sought for. The numbers on this tape must be punched according to the strict format given below:

1.	Number of cases to be computed - integer.				
2.	A -	decimal	or floating	point.	(p.s.i.)
3.	B -	"	"	"	(dimensionless)
4.	n -	"	"	"	(")
5.	ρ_1 -	"	"	"	(inch)
6.	D -	"	"	"	(")
7.	t_o -	"	"	"	(")

8. Print interval - integer. e.g. if 1, prints for all m.
if 2, prints for every even m.

9. Number of integration steps - integer.
(It is useful to have this as part of data since by decreasing it, the convergence of the numerical solution can be checked.)

10. R value - decimal or floating point.

11. Variation of μ by $(\varepsilon_2)_p$.

$$\begin{tikzcd}
(\varepsilon_2)_{p,1} \arrow[r] & \mu_1 \arrow[dl] \\
(\varepsilon_2)_{p,2} \arrow[r] & \mu_2 \arrow[dl] \\
(\varepsilon_2)_{p,3} \arrow[r] & \mu_3
\end{tikzcd}$$

(If item (1) has a value greater than 1, then steps 2-11 must be repeated the same number of times as its value.)

12. ***Z - An Atlas input terminator indicating the physical end of the input document.

The three physical tapes involved should be read by the computer in the following order:

(i) Auxiliary program - "Magnetic tape initialization".

(ii) Main program - "Theoretical Analysis of Stretch Forming for Anisotropic Materials - Hemispherical Punch".

(iii) The above described data tape.

After a machine breakdown or fault whilst computation, (i) should <u>not</u> be reread. The automatic rescue procedure of the program restarts the computation at a point corresponding to the previous stage after a computer operator's restart procedure is obeyed or by repeating (ii) and (iii).

After the input, the program gets compiled and enters the execution phase. At the end of the computation of every twelfth stage, the "break output" facility is used, and the results so far available are printed on a line-printer.

The first page of the output contains the monitoring information showing the structure of the program, i.e. the beginnings of the routines and chapters in the program. After the "Program Entered" statement, the input parameters given earlier are printed with their appropriate captions (See Fig.15.a).

The explanations of the columns are given in Fig. 15.a. with the units of the variables calculated. Columns 3 and 4 are computed realizing that the normal to an element of sheet metal before deformation, remains normal to the mean surface of the shell during the course of the deformation. The validity of this argument is shown in section 11.3.1. The variables in columns 1-14 are obtained from the numerical solution given in the previous chapter. K_1 is computed using eqn. (4.12). ML instability in column 16 is found by computing Q from eqn. (4.1) for the current stage, and comparing it with the one in the previous stage. If

$Q_n > Q_{n-1}$ the location in the column is left blank. If:

$Q_n < Q_{n-1}$ letter "D" - meaning decrease in Q - is printed. Hence it indicates that

00.00.31 / 01.01.65 13.02.29 — -DATE AND TIME OF THE COMPUTATION
OUTPUT 0
LSC44EC1, KAFTANOGLU HEMISPHERICAL RUN 29 1964 — -JOB NUMBER AND TITLE OF THE PROGRAM

EMA 9 NOV 1964 — -VERSION OF THE COMPILER

5: HEADING FOR ROUTINE 2
6: HEADING FOR ROUTINE 4 — -LISTING OF THE ROUTINES
7: HEADING FOR ROUTINE 6
B.KAFTANOGLU ICST MECH.ENG. JOB.NO.LSC44EC1.1964

THEORETICAL ANALYSIS OF STRETCH-FORMING FOR ANISOTROPIC MATERIALS — -TITLE OF THE INVESTIGATION

-HEMISPHERICAL PUNCH-

14: START OF CHAPTER 1
258: START OF ROUTINE 2
267: START OF CHAPTER 2
529: START OF ROUTINE 2 — -LISTING OF CHAPTERS AND ROUTINES ACCORDING TO THE ORDER OF COMPILATION
538: START OF CHAPTER 3
720: START OF ROUTINE 2
729: START OF CHAPTER 4
952: START OF ROUTINE 2
961: START OF CHAPTER 5
1130: START OF ROUTINE 4
1149: START OF ROUTINE 6
1160: START OF ROUTINE 2
1169: START OF CHAPTER 6
1549: START OF ROUTINE 2
1558: START OF CHAPTER 0
2050: START OF ROUTINE 2 — -END OF COMPILING
PROGRAMME ENTERED — -BEGINNING OF EXECUTION

PARAMETERS USED IN THE THEORETICAL COMPUTATION- — MATERIAL- SOFT COPPER

AF 68394psi R= 0.0122 N= 0.370 — LUBRICANT- H.T.G. GREASE
PUNCH PROFILE RADIUS= 0.650 in.
DIAMETER OF THE CLAMPED EDGE= 1.320 in.
INITIAL THICKNESS= 0.0486 in. — -INPUT PARAMETERS
NUMBER OF INTEGRATION STEPS= 60
STRAIN RATIO IN TENSION= 0.80
GIVEN VARIATION OF COEFFICIENT OF FRICTION WITH POLAR STRAIN-

POLAR CIRCUMFERENTIAL STRAIN	COEFF. OF FRICTION
0.045	0.470
0.100	0.320
0.135	0.260

COLUMN:

1	2	3	4	5	6	7	8	9	10	11	12	13	14	15	16
r_0 in.	r in.	ε_2 OUTER SURFACE	ε_2 INNER SURFACE	ε_2 MEAN	ε_3	ε_1	$\bar{\varepsilon}$	$\bar{\sigma}$ psi	σ_1 psi	σ_2 psi	x	θ degree	p psi	κ_1 (z)	ML Instability

REGION 2 IS NOT FULLY PLASTICALLY DEFORMED AT STAGE 1 — In Region 1 ....

REGION 1

0.000	0.000			0.019	-0.037	0.019	0.036	21789	19588	19588	1.000	0.0	2923	0.131
0.022	0.022	0.053	-0.016	0.019	-0.039	0.020	0.037	21992	19923	19619	0.985	1.9	2947	0.135
0.044	0.045	0.053	-0.016	0.019	-0.040	0.021	0.038	22127	20236	19540	0.966	3.8	2961	0.137
0.066	0.067	0.053	-0.017	0.018	-0.040	0.021	0.038	22159	20494	19315	0.942	5.7	2963	0.137
0.088	0.090	0.052	-0.018	0.017	-0.039	0.022	0.038	22083	20692	18933	0.915	7.6	2951	0.136
0.110	0.112	0.050	-0.019	0.016	-0.038	0.022	0.037	21892	20622	18372	0.882	9.6	2923	0.133
0.132	0.134	0.046	-0.021	0.014	-0.036	0.022	0.035	21573	20675	17598	0.843	11.5	2876	0.128
0.154	0.156	0.046	-0.024	0.012	-0.033	0.021	0.032	21106	20239	16552	0.794	13.4	2803	0.121

STAGE- 2 PUNCH LOAD- 0.220 Te, BULGE DEPTH- 3.258 mm, MOVING BOUNDARY IS AT- 0.2136 in 18.51° INITIAL RADIUS, 0.2099 in.

CURRENT EFFECTIVE COEFFICIENT OF FRICTION- 0.470

REGION 1

0.000	0.000			0.028	-0.056	0.028	0.054	24495	22051	22051	1.000	0.0	3228	0.180
0.022	0.023	0.062	-0.006	0.029	-0.058	0.030	0.056	24786	22472	22153	0.986	1.9	3258	0.185
0.044	0.045	0.062	-0.006	0.029	-0.060	0.031	0.058	25050	22896	22232	0.970	3.9	3286	0.191
0.066	0.068	0.062	-0.006	0.029	-0.062	0.033	0.060	25262	23293	22175	0.952	5.8	3307	0.195
0.088	0.091	0.062	-0.006	0.028	-0.063	0.035	0.061	25431	23665	22081	0.933	7.7	3323	0.199
0.110	0.113	0.061	-0.007	0.028	-0.064	0.037	0.062	25566	24014	21935	0.913	9.7	3334	0.202
0.132	0.136	0.060	-0.008	0.026	-0.065	0.039	0.063	25667	24347	21766	0.894	11.6	3343	0.205
0.154	0.158	0.058	-0.010	0.025	-0.066	0.041	0.065	25827	24677	21627	0.876	13.6	3354	0.208
0.176	0.180	0.056	-0.012	0.023	-0.061	0.038	0.059	25156	24736	20014	0.809	15.5	3260	0.194
0.198	0.202	0.053	-0.015	0.020	-0.057	0.038	0.055	24794	24767	19046	0.769	17.5	3202	0.185

REGION 2 (Moving Boundary is here) — In Region 2 .... p_1 in. p_2 in. ML Instability

0.220	0.224	0.047	-0.016	0.016	-0.045	0.029	0.044	23076	24347	19569	0.804	17.8	-0.91	0.73

FIG. 15. a) COMPUTER OUTPUT SHOWING THE MONITORING INFORMATION, INPUT PARAMETERS, STAGE ONE, AND REGION ONE OF STAGE TWO.

REGION 2 (Moving Boundary is here)

											In Region 2		ρ_1 in.	ρ_2 in. ML Instability
0.220	0.224	0.047	-0.016	0.016	-0.045	0.029	0.044	23076	24347	19569	0.804	17.8	-0.91	0.73
0.242	0.245	0.040	-0.014	0.013	-0.040	0.026	0.039	22264	23777	18339	0.771	16.5	-1.12	0.87
0.264	0.267	0.034	-0.013	0.011	-0.035	0.024	0.035	21547	23201	17347	0.748	15.4	-1.34	1.00
0.286	0.289	0.029	-0.011	0.009	-0.031	0.022	0.031	20935	22648	16515	0.729	14.5	-1.58	1.15
0.308	0.310	0.026	-0.010	0.008	-0.028	0.020	0.028	20325	22125	15800	0.714	13.8	-1.83	1.31
0.330	0.332	0.023	-0.010	0.007	-0.025	0.018	0.025	19796	21631	15173	0.701	13.1	-2.09	1.47
0.352	0.354	0.020	-0.009	0.006	-0.022	0.017	0.023	19308	21166	14614	0.690	12.5	-2.37	1.63
0.374	0.376	0.018	-0.008	0.005	-0.020	0.015	0.020	18855	20727	14105	0.681	12.0	-2.66	1.81
0.396	0.398	0.016	-0.008	0.004	-0.018	0.014	0.018	18431	20311	13636	0.671	11.5	-2.96	1.99
0.418	0.420	0.015	-0.007	0.004	-0.016	0.013	0.017	18033	19918	13195	0.662	11.1	-3.28	2.17
0.440	0.441	0.013	-0.007	0.003	-0.015	0.011	0.015	17655	19544	12775	0.654	10.8	-3.62	2.36
0.462	0.463	0.012	-0.007	0.003	-0.013	0.010	0.014	17294	19187	12368	0.645	10.4	-3.97	2.56
0.484	0.485	0.011	-0.006	0.002	-0.012	0.009	0.012	16949	18845	11967	0.635	10.1	-4.35	2.76
0.506	0.507	0.010	-0.005	0.002	-0.011	0.008	0.011	16615	18517	11565	0.625	9.8	-4.75	2.97
0.528	0.529	0.010	-0.006	0.002	-0.009	0.008	0.010	16296	18200	11153	0.613	9.6	-5.18	3.19
0.550	0.551	0.009	-0.005	0.001	-0.008	0.007	0.009	15972	17891	10722	0.599	9.4	-5.66	3.39
0.572	0.573	0.008	-0.006	0.001	-0.007	0.006	0.007	15657	17590	10256	0.583	9.1	-6.18	3.61
0.594	0.594	0.007	-0.006	0.001	-0.006	0.005	0.006	15345	17293	9736	0.563	8.9	-6.79	3.82
0.616	0.616	0.007	-0.005	0.001	-0.005	0.004	0.005	15031	16997	9125	0.537	8.8	-7.53	4.05
0.638	0.638	0.006	-0.005	0.000	-0.004	0.004	0.004	14714	16694	8356	0.506	8.6	-8.52	4.26
0.660	0.660	0.005	-0.005	0.000	-0.003	0.003	0.003	14418	[illegible]	7302	0.445	8.5	-10.06	4.48

(Clamped Edge)

STAGE= 3 PUNCH LOAD= 0.3702 Te, BULGE DEPTH= 4.50 mm, MOVING BOUNDARY IS AT= 0.2621 in 22.93° INITIAL RADIUS, 0.2557 in

CURRENT EFFECTIVE COEFFICIENT OF FRICTION= 0.473

REGION 1

0.000	0.002			0.037	-0.075	0.037	0.072	26764	24136	24136	1.000	0.0	3464	0.229
0.022	0.023	0.072	[illegible]	0.038	-0.078	[illegible]	0.073	27121	24623	24274	0.985	1.9	3498	0.237
0.044	0.046	0.072	[illegible]	0.039	[illegible]	0.082	0.074	27468	25130	24344	0.971	3.9	3532	0.246
0.066	0.069	[illegible]	[illegible]	0.039	-0.144	[illegible]	0.081	27765	25525	24462	0.955	5.9	3561	0.253
0.088	0.092	0.072	[illegible]	0.139	-0.147	0.044	0.094	[illegible]	[illegible]	24489	0.938	7.9	3588	0.261
0.110	0.114	0.071	[illegible]	0.139	-0.149	[illegible]	0.087	[illegible]	26547	24469	0.921	9.8	3612	0.268
0.132	0.137	[illegible]	[illegible]	0.138	[illegible]	[illegible]	[illegible]	28883	[illegible]	24485	0.906	11.8	3635	0.275
0.154	0.160	0.069	[illegible]	0.137	[illegible]	[illegible]	0.092	28969	[illegible]	24573	0.889	13.8	3661	0.283
0.176	0.182	0.068	[illegible]	0.135	[illegible]	[illegible]	[illegible]	[illegible]	[illegible]	23846	0.865	15.7	3642	0.281
0.198	0.205	0.066	[illegible]	0.133	[illegible]	[illegible]	0.193	[illegible]	[illegible]	23645	0.837	17.7	3651	0.285
0.220	0.227	0.063	[illegible]	0.131	[illegible]	[illegible]	[illegible]	[illegible]	[illegible]	21766	0.767	19.7	3552	0.267
0.242	0.249	[illegible]	[illegible]	0.027	[illegible]	[illegible]	[illegible]	[illegible]	24415	21778	0.731	21.7	3498	0.259

REGION 2

0.264	0.270	0.054	[illegible]	0.023	[illegible]	[illegible]	0.071	[illegible]	[illegible]	22631	0.801	22.3	-0.69	0.71
0.286	0.292	0.047	[illegible]	0.019	[illegible]	[illegible]	0.062	[illegible]	27353	20993	0.768	21.9	-1.06	0.82
0.308	0.313	0.041	-0.009	0.016	[illegible]	[illegible]	0.055	24727	[illegible]	19771	0.741	19.8	-1.25	0.92
0.330	0.335	0.036	[illegible]	0.014	[illegible]	[illegible]	[illegible]	[illegible]	[illegible]	18692	0.717	18.8	-1.45	1.04
0.352	0.356	0.032	[illegible]	0.012	[illegible]	0.038	0.045	[illegible]	[illegible]	17722	0.696	18.0	-1.66	1.15
0.374	0.378	0.028	-0.008	0.010	-0.041	0.031	0.041	24517	[illegible]	16837	0.676	17.2	-1.89	1.28
0.396	0.400	0.024	-0.008	0.009	-0.037	0.028	0.034	[illegible]	26349	16016	0.656	16.6	-2.13	1.40
0.418	0.421	0.023	-0.008	0.008	-0.033	0.026	0.034	[illegible]	[illegible]	15242	0.640	16.0	-2.39	1.53
0.440	0.443	0.021	-0.008	0.007	-0.030	0.024	0.031	[illegible]	23259	14522	0.622	15.5	-2.66	1.66
0.462	0.465	0.019	-0.008	0.006	-0.027	0.022	0.025	[illegible]	[illegible]	13783	0.604	15.0	-2.96	1.79
0.484	0.486	0.017	[illegible]	0.005	-0.025	[illegible]	0.026	[illegible]	22511	13175	0.586	14.6	-3.29	1.93
0.506	0.508	0.016	-0.007	0.004	-0.022	[illegible]	0.023	19412	[illegible]	12369	0.566	14.3	-3.65	2.06
0.528	0.530	0.014	-0.007	0.003	-0.021	0.017	0.021	[illegible]	[illegible]	11657	0.544	13.9	-4.05	2.20
0.550	0.552	0.013	-0.006	0.003	-0.018	0.015	0.019	[illegible]	[illegible]	10937	0.521	13.6	-4.49	2.34
0.572	0.573	0.012	-0.006	0.002	-0.016	0.015	0.017	[illegible]	[illegible]	10215	0.497	13.3	-4.99	2.48
0.594	0.595	0.010	[illegible]	0.002	-0.014	0.013	0.015	[illegible]	21114	9516	0.473	13.1	-5.55	2.62
0.616	0.617	[illegible]	[illegible]	0.001	-0.013	[illegible]	0.014	17352	[illegible]	[illegible]	0.451	12.9	-6.13	2.77
0.638	0.638	[illegible]	[illegible]	[illegible]	[illegible]	[illegible]	0.012	[illegible]	19498	8456	0.436	12.7	-6.63	2.91
0.660	0.660	[illegible]	[illegible]	[illegible]	[illegible]	[illegible]	[illegible]	[illegible]	19414	8369	0.442	12.5	-6.89	3.05

STAGE= 4 PUNCH LOAD= 0.4440 Te, BULGE DEPTH= 4.83 mm, MOVING BOUNDARY IS AT= 0.2867 in 25.25° INITIAL RADIUS, 0.2787 in

CURRENT EFFECTIVE COEFFICIENT OF FRICTION= 0.471

REGION 1

0.000	0.000			0.042	[illegible]	[illegible]	[illegible]	27441	25112	25112	1.000	0.0	3569	0.255
0.022	0.023	0.076	[illegible]	0.043	-0.088	[illegible]	[illegible]	[illegible]	25537	25274	0.986	2.0	3604	0.264
0.044	0.046	0.077	[illegible]	0.044	-0.092	[illegible]	[illegible]	[illegible]	26165	25420	0.971	3.9	3639	0.274
0.066	0.069	0.077	[illegible]	0.045	-0.096	[illegible]	0.092	[illegible]	26726	25522	0.955	5.9	3671	0.283
0.088	0.092	0.077	[illegible]	0.045	-0.099	[illegible]	[illegible]	[illegible]	27260	25590	0.939	7.9	3700	0.293
0.110	0.115	0.077	[illegible]	0.045	-0.102	[illegible]	0.099	[illegible]	27793	25636	0.922	9.9	3728	0.302
0.132	0.138	0.076	[illegible]	0.045	-0.106	0.062	0.103	[illegible]	[illegible]	25679	0.906	11.9	3755	0.311
0.154	0.161	0.076	[illegible]	0.043	-0.109	[illegible]	0.107	[illegible]	[illegible]	25743	0.891	13.9	3784	0.321
0.176	0.184	0.074	[illegible]	0.042	-0.110	[illegible]	0.107	[illegible]	[illegible]	25284	0.863	15.9	3780	0.323
0.198	0.206	0.072	[illegible]	0.040	-0.112	[illegible]	[illegible]	[illegible]	[illegible]	25190	0.846	17.9	3797	0.331
0.220	0.228	[illegible]	[illegible]	0.038	[illegible]	[illegible]	0.106	[illegible]	[illegible]	24014	0.799	19.9	3750	0.321
0.242	0.251	0.067	[illegible]	0.035	[illegible]	[illegible]	0.107	[illegible]	30344	23557	0.776	21.9	3739	0.322
0.264	0.272	[illegible]	[illegible]	0.031	-0.110	[illegible]	0.099	[illegible]	[illegible]	21369	0.754	23.9	3619	0.300

REGION 2

0.280	0.294	0.058	[illegible]	0.027	[illegible]	[illegible]	0.084	[illegible]	29657	23480	0.786	24.7	-0.69	0.70
0.308	0.315	0.050	[illegible]	0.022	[illegible]	0.053	0.075	27127	29129	22016	0.756	23.3	-1.05	0.80
0.330	0.334	0.044	-0.007	0.019	[illegible]	[illegible]	0.064	[illegible]	28423	20747	0.730	22.2	-1.22	0.89
0.352	0.354	0.039	-0.007	0.016	-0.061	0.045	0.061	25431	27747	19603	0.706	21.1	-1.40	0.99
0.374	0.379	0.035	-0.007	0.014	-0.055	0.041	0.055	24662	27100	18556	0.685	20.3	-1.60	1.10
0.396	0.401	0.031	-0.008	0.012	-0.050	0.035	0.051	23984	26480	17587	0.664	19.5	-1.81	1.20
0.418	0.422	0.028	-0.008	0.010	-0.045	0.035	0.046	23336	25986	16679	0.644	18.8	-2.03	1.31
0.440	0.444	0.025	-0.008	0.009	-0.041	0.032	0.042	22715	25314	15821	0.625	18.2	-2.27	1.42
0.462	0.465	0.023	-0.008	0.007	-0.037	0.030	0.038	22135	24763	15006	0.606	17.7	-2.53	1.53
0.484	0.487	0.020	-0.008	0.006	-0.034	0.027	0.035	21585	24232	14231	0.587	17.2	-2.81	1.65
0.506	0.509	0.019	-0.008	0.005	-0.031	0.025	0.032	21066	23719	13499	0.569	16.7	-3.11	1.77
0.528	0.530	0.017	-0.008	0.004	-0.028	0.023	0.029	20576	23224	12819	0.552	16.3	-3.42	1.89
0.550	0.552	0.015	-0.008	0.003	-0.025	0.022	0.027	20116	22747	12206	0.537	16.0	-3.74	2.01
0.572	0.574	0.014	-0.009	0.003	-0.023	0.020	0.024	19683	22288	11669	0.524	15.6	-4.06	2.13
0.594	0.595	0.012	-0.009	0.002	-0.021	0.019	0.022	19274	21848	11197	0.512	15.3	-4.39	2.25
0.616	0.617	0.011	-0.009	0.001	-0.019	0.018	0.021	18884	21424	10730	0.501	15.1	-4.74	2.37
0.638	0.638	0.010	-0.009	0.001	-0.017	0.016	0.019	18511	21013	10139	0.483	14.8	-5.18	2.50
0.660	0.660	0.009	-0.009	0.000	-0.015	0.015	0.017	18126	20605	9192	0.446	14.6	-5.68	2.63

STAGE= 5 PUNCH LOAD= 1.5711 Te, BULGE DEPTH= 5.35 mm, MOVING BOUNDARY IS AT= 0.3105 in 27.53° INITIAL RADIUS, 0.3008 in

CURRENT EFFECTIVE COEFFICIENT OF FRICTION= 0.463

REGION 1

FIG.15.b) COMPUTER OUTPUT SHOWING REGION TWO OF STAGE TWO, AND ALSO STAGES THREE AND FOUR.

0.374	0.437	0.176	0.134	0.155	-0.544	0.389	0.545	53721	56235	39872	0.709	41.1	4260	1.505	
0.396	0.461	0.173	0.131	0.152	-0.564	0.412	0.567	54507	57639	39157	0.679	44.0	4205	1.565	
0.418	0.485	0.169	0.128	0.148	-0.591	0.433	0.587	55194	58906	38286	0.650	46.9	4150	1.619	
0.440	0.508	0.163	0.123	0.143	-0.593	0.450	0.602	55709	59897	37393	0.624	49.9	4103	1.661	
0.462	0.530	0.157	0.116	0.137	-0.596	0.460	0.608	55914	60360	36840	0.610	53.0	4086	1.677	D
0.484	0.550	0.147	0.107	0.127	-0.591	0.464	0.606	55836	60485	35393	0.585	55.9	4053	1.671	D
0.506	0.568	0.137	0.093	0.115	-0.511	0.395	0.521	52888	56339	36708	0.652	58.7	4269	1.443	D
0.528	0.584	0.124	0.077	0.100	-0.439	0.338	0.448	50067	53030	35081	0.662	61.3	4350	1.244	D
0.550	0.598	0.108	0.058	0.083	-0.369	0.286	0.378	47065	50025	32133	0.642	63.7	4356	1.054	D

REGION 2

0.572	0.610	0.091	0.037	0.064	-0.297	0.233	0.305	43634	46810	35505	0.758	64.7	-0.89	0.67
0.594	0.622	0.073	0.019	0.046	-0.249	0.203	0.259	41199	44419	33044	0.744	63.0	-0.94	0.70
0.616	0.634	0.056	0.002	0.030	-0.207	0.177	0.219	38822	42341	29970	0.708	61.4	-1.02	0.72
0.638	0.647	0.041	-0.014	0.014	-0.168	0.153	0.182	36417	40452	25863	0.639	60.1	-1.17	0.75
0.660	0.660	0.027	-0.028	0.000	-0.132	0.132	0.150	34046	38698	17766	0.459	59.0	-1.68	0.77

PLASTIC INSTABILITY AT- 0.4510 in. —Y **(Occurance of SP Instability)**

STAGE- 22 PUNCH LOAD- 2.6826Te, BULGE DEPTH- 13.103mm, MOVING BOUNDARY IS AT- 0.6094in 65.88° INITIAL RADIUS, 0.5684 in

CURRENT EFFECTIVE COEFFICIENT OF FRICTION- 0.260

REGION 1

0.000	0.000			0.136	-0.272	0.136	0.263	41390	37773	37773	1.000	0.0	4426	0.744	
0.022	0.025	0.166	0.112	0.139	-0.283	0.144	0.274	41988	38533	38126	0.989	2.2	4439	0.773	
0.044	0.051	0.170	0.116	0.143	-0.296	0.153	0.286	42629	39362	38512	0.978	4.4	4453	0.806	
0.066	0.076	0.173	0.119	0.146	-0.308	0.162	0.298	43278	40218	38882	0.967	6.6	4464	0.839	
0.088	0.102	0.175	0.122	0.149	-0.322	0.172	0.311	43940	41105	39239	0.955	8.8	4473	0.874	
0.110	0.128	0.178	0.126	0.152	-0.336	0.184	0.325	44619	42028	39583	0.942	11.1	4479	0.911	
0.132	0.154	0.180	0.128	0.154	-0.350	0.196	0.339	45322	42995	39918	0.928	13.4	4483	0.951	
0.154	0.180	0.182	0.131	0.157	-0.366	0.209	0.355	46055	44016	40244	0.914	15.7	4483	0.993	
0.176	0.206	0.183	0.133	0.159	-0.381	0.222	0.370	46743	45024	40477	0.899	18.0	4480	1.033	
0.198	0.232	0.184	0.135	0.160	-0.398	0.238	0.387	47514	46135	40744	0.883	20.4	4474	1.080	
0.220	0.259	0.185	0.137	0.161	-0.413	0.252	0.403	48208	47204	40889	0.866	22.8	4464	1.123	
0.242	0.285	0.185	0.138	0.162	-0.432	0.270	0.423	49032	48433	41065	0.848	25.3	4450	1.176	
0.264	0.311	0.186	0.139	0.163	-0.450	0.288	0.442	49809	49649	41139	0.829	27.8	4431	1.227	
0.286	0.336	0.185	0.139	0.163	-0.469	0.306	0.462	50611	50927	41134	0.808	30.4	4407	1.281	
0.308	0.362	0.184	0.139	0.162	-0.489	0.327	0.483	51427	52258	41032	0.785	33.0	4377	1.338	
0.330	0.388	0.183	0.139	0.161	-0.509	0.348	0.505	52260	53646	40810	0.761	35.7	4341	1.397	
0.352	0.413	0.181	0.138	0.159	-0.530	0.370	0.527	53101	55080	40439	0.734	38.4	4298	1.459	
0.374	0.438	0.178	0.136	0.157	-0.551	0.393	0.551	53940	56542	39887	0.705	41.2	4247	1.522	
0.396	0.462	0.175	0.133	0.154	-0.571	0.417	0.574	54754	57995	39129	0.675	44.1	4189	1.585	
0.418	0.486	0.170	0.130	0.150	-0.589	0.439	0.595	55482	59328	38196	0.644	47.1	4129	1.642	
0.440	0.509	0.165	0.125	0.145	-0.633	0.458	0.612	56552	60400	37256	0.616	50.1	4076	1.688	
0.462	0.531	0.159	0.119	0.139	-0.608	0.469	0.620	56322	60930	36766	0.603	53.2	4057	1.710	D
0.484	0.551	0.149	0.109	0.130	-0.605	0.475	0.621	56329	61190	35056	0.573	56.2	4010	1.711	D
0.506	0.569	0.139	0.096	0.118	-0.521	0.403	0.532	53263	56760	36988	0.652	59.0	4257	1.471	D
0.528	0.585	0.126	0.079	0.103	-0.448	0.345	0.457	50444	53598	35512	0.665	61.5	4348	1.270	D
0.550	0.599	0.110	0.060	0.086	-0.379	0.293	0.347	47512	51396	32755	0.650	64.0	4366	1.080	

REGION 2

0.572	0.611	0.094	0.039	0.060	-0.303	0.237	0.311	43944	47120	35804	0.760	65.6	-0.88	0.67
0.594	0.623	0.074	0.020	0.048	-0.254	0.206	0.264	41454	44650	33346	0.747	63.8	-0.93	0.69
0.616	0.635	0.058	0.003	0.035	-0.210	0.180	0.222	39025	42514	30252	0.712	62.3	-1.01	0.72
0.638	0.647	0.042	-0.013	0.015	-0.170	0.155	0.184	34562	40577	26100	0.643	60.9	-1.15	0.74
0.660	0.660	0.027	-0.025	-0.000	-0.133	0.133	0.151	34118	38766	16524	0.426	59.8	-1.79	0.76

END OF COMPUTATION

INSTRUCTION	274841	4792	-NUMBER OF INSTRUCTION INTERRUPTS
STORE 30	/ 26		-NUMBER OF BLOCKS OF STORE USED
INPUT 0	15	BLOCKS	-INPUT CHANNEL AND BLOCKS OF INPUT
OUTPUT 0	PRINT 2302	RECORDS	-OUTPUT CHANNEL AND LINES OF OUTPUT
END OUTPUT	13 BLOCKS		-EQUIVALENT NUMBER OF BLOCKS OF OUTPUT

FIG.15.c) COMPUTER OUTPUT SHOWING THE SP INSTABILITY STAGE AND THE LOGGING INFORMATION.

a particular point reached its ML instability between the two stages.

However, in region two since p = 0, and K_1 is not very important since the instability is not expected, columns 14, and 15 (see Fig.15.a) contain ρ_1, and ρ_2 calculated from eqns. (3.52.a) and (3.53).

As seen in Fig.15.a, in the first stage the material is not fully plastically deformed in region two whose results are not printed. This happens generally in stage one when the strains near the clamped edge are very small. In the numerical analysis such small strains cause a discontinuity in x at points where $(\delta\varepsilon_2^*)_{(m-1),n} > 0$, and $(\delta\varepsilon_2^*)_{m,n} < 0$ during the boundary matching. The study of the equations for region two showed that this was due to the fact that the material did not want to deform plastically, and hence the strains were very small. Then the computation for the second stage is started where only the strain history of region one in stage one is considered.

For each stage the values of the punch load, bulge depth, and the radial and angular locations of the moving boundary are printed (See Figs. 15.a, b, c).

In Fig.15.c. corresponding to the SP instability stage, the statement "PLASTIC INSTABILITY" is printed with a figure giving the radial location of the instability.

The computer output ends with the "logging information" giving the time taken to complete the computation, amount of the store used and the input and output volume.

6.4. General Flow Diagram

To explain the flow of control, and the procedure of the calculations in the program with the appropriate logical branchings, a general flow diagram is presented. This avoids the detailed flow of control, but merely concentrates on the main blocks of the computation, tests, transfers, input and output (see Fig.16). The cross-references to the different steps in the numerical procedure are included.

6.5. Discussion of Chapters and Routines

A print out of the computer program for stretch forming of anisotropic materials with a hemispherical punch is presented in Appendix-C.

It consists of three "routines" and seven "chapters". The frequently used blocks of instructions are written as routines which are referred to from various points in various chapters. Each chapter approximately corresponds to a section in the numerical procedure, e.g. Chapter two contains the inner loop of region one etc.

The program contains comments which start by "≫", and which are ignored by the computer. These statements

FIG.16. GENERAL FLOW DIAGRAM OF THE COMPUTER PROGRAM FOR STRETCH FORMING BY A HEMISPHERICAL PUNCH.

briefly explain what the following instructions or the blocks of instructions do. Cross-references to the numerical procedure in section 5.1 are provided as far as possible. Also a great similarity exists between these comments, and the statements in the flow diagram (Fig.16), for ease of determining the flow of control in the program.

CHAPTER 7 - THEORIES FOR ESTIMATING THE COEFFICIENT OF FRICTION

In section 1.7, a discussion of the previous work related to the estimation of coefficient of friction under conditions of bulk plastic deformation is presented. The results of Table-1.2 show that there is appreciable scatter and uncertainty in μ determined for similar conditions by different methods. Furthermore, within the author's frame of knowledge no systematic investigation exists where μ determined by a method was used in an independent theory to check back other experimental results.

No method for the estimation of μ in stretch forming or radial drawing has been previously reported except by Yamada (97) for which the author's disagreement over the proposed method was expressed in section 1.1.3. Swift (78) implied that μ estimated in bending under tension of a strip over a pulley is analogous to drawing over a deep-drawing die. Although the present investigation supports this argument, it is found that μ in stretch forming is quite different than in drawing over a deep-drawing die.

Hence to study the associated lubrication problem in stretch forming and in drawing over a die, and also to be able to use more realistic coefficients of friction in the theoretical analyses presented in the previous chapters, the following investigations were carried out.

7.1. μ in Drawing over Die Surface

To determine the effective μ operative on both surfaces of sheet metal in drawing over a die, the following method is adopted.

From the vertical equilibrium of the forces on the segment shown in Fig.17:

$$\frac{\phi_1}{2\pi}\int_{r_b}^{r_a} 2\pi p_2 r\,dr - \frac{\phi_1}{2\pi}\int_{r_{c'}}^{r_a} 2\pi p_1 r\,dr - \frac{\phi_1}{2\pi}\int_{r_{c'}}^{r_a} \mu\, 2\pi p_1 \tan\theta\, r\,dr + \frac{P\phi_1}{2\pi} = 0 \qquad (7.1)$$

where:

$$\int_{r_b}^{r_a} 2\pi p_2 r\,dr = H, \quad \int_{r_{c'}}^{r_a} 2\pi p_1 r\,dr + \int_{r_{c'}}^{r_a} \mu 2\pi p_1 \tan\theta\, r\,dr = H + P \qquad (7.2)$$

therefore,

$$\int_{r_{c'}}^{r_a} 2\pi p_1 r\,dr = H + P - \mu \int_{r_{c'}}^{r_a} 2\pi p_1 \tan\theta\, r\,dr = H + P - S_1 \qquad (7.3)$$

In this way the integrals can be related to the experimentally measured forces P and H.

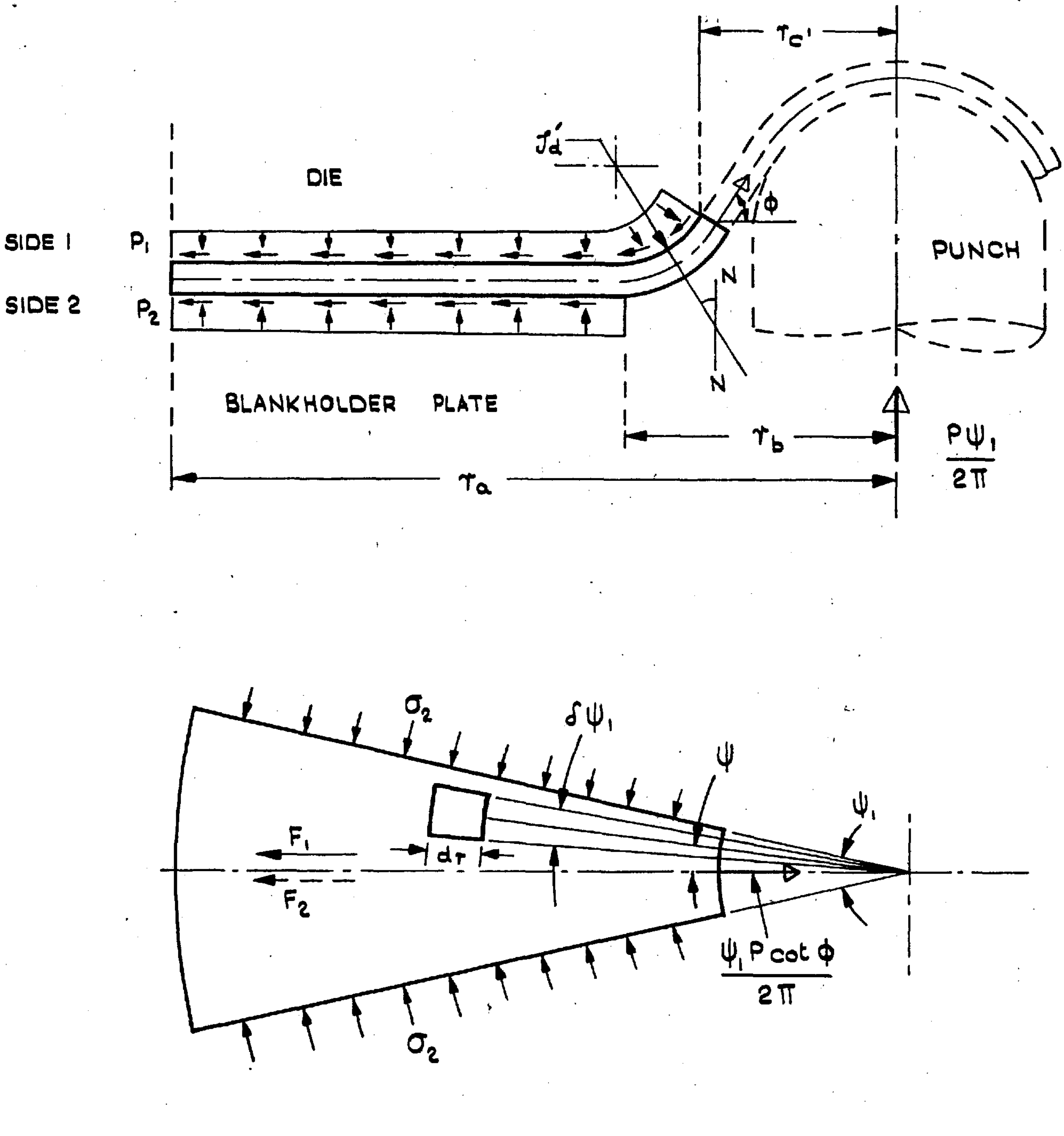

FIG. 17. A LARGE SEGMENT OF SHEET METAL IN CONTACT WITH THE DIE AND BLANK-HOLDER PLATE.

From the horizontal equilibrium of the forces:

$$2\mu\sin\frac{\phi_1}{2}\overbrace{\int_{r_b}^{r_a} p_2\, rdr}^{H/2\pi} + 2\mu\sin\frac{\phi_1}{2}\overbrace{\int_{r_{c'}}^{r_a} p_1\, rdr}^{\frac{1}{2\pi}(H+P-S_1)}$$

$$- 2\sin\frac{\phi_1}{2}\int_{r_{c'}}^{r_a} p_1 \tan\theta\, rdr - \frac{\phi_1 P\cot\varphi}{2\pi} + 2\sin\frac{\phi_1}{2}\int_{r_{c'}}^{r_a}\sigma_2 t\, dr = 0 \tag{7.4}$$

Hence

$$S_1 = \mu\int_{r_{c'}}^{r_a} 2\pi p_1 \tan\theta\, r\, dr \tag{7.5}$$

and if $S_2 = \displaystyle\int_{r_{c'}}^{r_a} p_1 \tan\theta\, r\, dr$, $\quad S_3 = \displaystyle\int_{r_{c'}}^{r_a}\sigma_2 t dr$ (7.6)

when $\phi_1 \rightarrow 0$, substituting eqns. (7.5) and (7.6) in eqn. (7.4):

$$\mu H + \mu(H+P-S_1) - 2\pi S_2 - P\cot\varphi + 2\pi S_3 = 0 \tag{7.7}$$

Differentiating eqn. (7.7) totally keeping φ constant:

$$\mu\delta H + \mu(\delta H + \delta P - \delta S_1) - 2\pi\delta S_2 - \delta P \cot\varphi + 2\pi\delta S_3 \tag{7.8}$$

hence

$$\mu = \frac{\delta P \cot\varphi + 2\pi(\delta S_2 - \delta S_3)}{2\delta H + \delta P - \delta S_1} \tag{7.9}$$

However, eqn. (7.9) can be reduced to a more practical one by eliminating some of the variables with negligible effect. It was discussed in section 1.1.1. that the assumption of H acting on the rim as a concentrated force is a very good one. Therefore an increase in H would not alter the pressure distribution around the die curvature significantly, especially when $r_a - r_b \gg r_b - r_{c'}$.

Hence $$\delta S_1 \approx \delta S_2 \approx 0 \tag{7.10}$$

Also an increase in H would similarly not alter the σ_2 distribution in the plane of the sheet to a first order approximation. This is because the two are related by the frictional stresses which are a very small fraction (e.g. 0.1%) of σ_2.

Then $$\delta S_3 \approx 0 \tag{7.11}$$

With the conditions of (7.10) and (7.11) eqn. (7.9) becomes:

$$\mu = \frac{\delta P \cot\varphi}{2\delta H + \delta P} \tag{7.12}$$

To find μ using eqn. (7.12), it is necessary to carry out two deep-drawing tests under identical conditions with the exception that H is altered by an amount δH, which will lead to a change in P of δP. From the punch load versus punch penetration curves obtained experimentally, a range of δP's can be obtained corresponding to various h's or φ's results of which will show any variation of μ in the drawing process. Although it is possible to find φ experimentally, it is more convenient to calculate it from h as shown in Appendix-B.4.ii. For this purpose, for the bulge it can be assumed that $t = t_o$, and $\varphi \approx \alpha$ neglecting the curvature of the shell in region two. For a hemispherical punch, which was used in the present investigation:

$$h = (D/_2 + \rho_d') \tan\alpha - (\rho_1' + \rho_d' + t_o)(\sec\alpha - 1)$$

(Eqn. B.29 - repeated)

where $\varphi = \alpha$

The main disadvantage of this method is that the result is dependent on taking the difference between large, nearly equal quantities and is therefore subject to some error. However this error can be reduced if three to five tests are carried out with uniform increases in δH. Then μ found for the same h or φ can be plotted as a function of δH and when the curve is extrapolated to zero δH, not only the errors due to individual points can be reduced, but also the assumptions (7.10) and (7.11) can be eliminated. Nevertheless, accurate load measuring devices should be used as will be discussed in section 9.1.

The values of μ found by this method are presented in Chapter 11 along with the other experimental results.

7.2. μ in Stretch Forming

To find the effective and operative μ between the inner shell surface and the punch the following method is used. It gives an average μ for each stage, but any variation of μ as a function of the radial coordinate, cannot be obtained.

For a hemispherical punch:

$$r = \rho_1 \sin\theta \quad \text{and} \quad dr = \rho_1 \cos\theta \, d\theta ,$$

with $r \approx r'$ and $\rho_1 \approx \rho_1'$ are substituted in eqn. (3.29) (eqn. of equilibrium in vertical direction) which results in:

$$\frac{d(\sigma_1 t)}{d\theta} + 2\,(\sigma_1 t)\cot\theta = p\rho_1(\cot\theta + \mu) \qquad (7.13)$$

It is assumed that the interfacial pressure $p \neq f(\theta)$. Although this is not strictly true for the whole of region one, it is valid at the pole where $\frac{dp}{d\theta} = 0$ (see eqn. 3.80). The extrapolation procedure given later would eliminate the effect of this assumption.

It is then possible to integrate the linear first order differential equation (7.13) by multiplying each term by $e^{\int 2\cot\theta d\theta}$ and then integrating the resulting exact differential equation which leads to:

$$\sigma_1 t \sin^2\theta = \frac{1}{2} p\rho_1(\sin^2\theta + \mu\theta - \mu\sin\theta\cos\theta) + C_1 \quad (7.14)$$

at $\theta = 0$ the constant of integration $C_1 = 0$

Eqn. (7.14) can then be written as:

$$\sigma_1 = \frac{p\rho_1}{2t}\left[1 + \frac{\mu}{\sin\theta}\left(\frac{\theta}{\sin\theta} - \cos\theta\right)\right] \quad (7.15)$$

For a hemispherical punch eqn. (3.30) (second equation of equilibrium) reduces to:

$$\sigma_2 = \frac{p\rho_1}{t} - \sigma_1 \quad (7.16)$$

substituting for σ_1 in eqn. (7.16) from eqn. (7.15) and then dividing σ_2 by σ_1 side by side and simplifying:

$$x = \frac{\sigma_2}{\sigma_1} = 1 - \frac{2\mu(\theta - \sin\theta\cos\theta)}{\sin^2\theta + \mu(\theta - \sin\theta\cos\theta)} \quad (7.17)$$

Rewriting eqn. (7.17) for μ :

$$\mu = \frac{(1-x)\sin^2\theta}{(1+x)(\theta - \sin\theta\cos\theta)} = \frac{(1-x)\sin^2\theta}{(1+x)(\theta - \frac{1}{2}\sin 2\theta)}$$

(7.18)

Eqn. (7.18) is the main eqn. from which μ is computed. It only requires the experimentally obtained $x = f(\theta)$ curve for the stage of deformation for which the effective μ is to be computed. Hence it is possible to find out the variation of μ with different stages in the deformation.

The determination of the $x = f(\theta)$ curve and the values of μ under different lubrication conditions are presented in Chapter 11.

Since the assumption of $p \neq f(\theta)$ is made in the derivation of eqn. (7.18), then the results obtained from it contain some error which would increase with the increase of the distance from the pole. At the pole it holds true, since $\frac{dp}{dr} = 0$. Hence, to obtain the true coefficient of friction, values of μ obtained from eqn. (7.18) at various radii should be plotted against θ, and this curve can then be extrapolated back to $\theta = 0$. This procedure also enables one to use the total strain theory in the determination of the $x = f(\theta)$ curve. The values of x away from the pole would contain some error, but this error gets less when moving towards the pole, and at the pole, since $x = 1$ throughout the deformation, total strain theory gives identical results with the incremental strain theory. Hence the plot of μ versus θ would contain the errors of both approximations away from the pole but for the reasons mentioned above, it is expected to converge to the correct value of μ at the pole.

No further information regarding the slope of this curve at the pole could be obtained, but it is believed that in general $\frac{d\mu}{d\theta} \neq 0$. The study of eqn. (7.18) shows that, near the pole, the accuracy of the values also decrease since the equation becomes indeterminate at the pole. Therefore it is desirable to have more than about five points in the construction of the μ versus θ curve.

The values of μ in stretch forming came out somewhat higher than those for radial drawing. The relevant discussion will be presented with the calculated values of the coefficient of friction in Chapter 11.

CHAPTER 8 - DETERMINATION OF THE MECHANICAL PROPERTIES OF THE MATERIALS USED AND CURVE-FITTING BY USING THE COMPUTER

In this chapter the methods employed for the determination of the equivalent stress-equivalent strain relationships for the materials used in the experiments are presented with the results obtained. The effect of plastic anisotropy in the thickness direction is considered consistent with the analysis of Chapter 3. By means of a computer program, the empirical relationship given by eqn. (3.48) is curve-fitted to the experimentally obtained true stress-true strain relationships.

The results of the hardness tests are reported for possible use in the correlation of the experimental results.

8.1. Equivalent Stress-Equivalent Strain Relationships

8.1.1. Theory

The concept and expressions for the equivalent stress and strain are developed in section 3.1 for plastically anisotropic materials.

From the study of the eqns. (3.9) to (3.25), and, for the kind of the anisotropy considered, i.e. sheet metal being isotropic in its plane but anisotropic in the thickness direction, the following two alternative methods exist for the determination, of the equivalent stress-equivalent strain curve.

(i) Determination of the yield stress (X versus ε_ℓ, and Z versus ε_t) curves in the plane of the sheet, and also in the thickness direction.

(ii) Determination of the yield stress curve either in the plane of the sheet, or in the thickness direction with an independent assessment of strain ratios between any two strains.

It may be noted that the common biaxial tests (e.g. plane strain, or bulge test) without the use of grid techniques, are insufficient for the determination of the equivalent stress-equivalent strain characteristics of anisotropic materials, since either a stress or a strain ratio cannot be determined independently.

However, in a uniaxial test since two of the stresses are zero, this eliminates some of the anisotropy parameters. The strain ratio can be easily computed from independent measurements of the lateral dimensions of the specimen, and the equivalent stress-equivalent strain curve can be found. Uniaxial compression test is unsuitable in the caseof sheet metals. If the stress is applied normal to its plane, frictional effects would influence the results, if the stress is applied in its plane, then buckling would result.

Hence the uniaxial tension test can be used since it satisfies the above requirements. However, with this test the range of strain is limited due to the occurrence of the tensile instability if only the uniform elongation is measured. After the maximum load, generally a visible neck develops, and further straining occurs here with little or no plastic deformation in the rest of the specimen, but it is possible to measure the current dimensions of the neck and compute the strain there. Bridgman (12) showed that the strain across the neck is quite uniform but a correction factor must be applied to the average stress to obtain the true flow stress independent of the hydrostatic tension. This is required due to the triaxiality of the stress system at the neck, and the correction depends on the radii of curvature of the neck. However, the present experiments on the ferrous and non-ferrous sheet metal specimens showed that even at fracture, the ratios of the halves of the neck dimensions to the radii of curvature in the respective planes were less than 0.1. For this range, the Bridgman's correction factor ranges from 1.0 to 0.965. Hence, load over current area is a very good approximation to the true stress. This approximation was used, and the error then would be generally within 3%, which is generally recognized as the experimental accuracy in the determination of the yield stress curves.

In the uniaxial tensile test with some materials, e.g. brass, very little further deformation can be obtained beyond the maximum load. In the present experiments, to obtain the yield stress curves for brass and copper for the required strain range, the plane strain compression test was used in addition to the tensile test. In order to convert the yield stress curve in the thickness direction to the equivalent stress-equivalent strain relationship, the average R-ratio obtained in the tension test was used. This method was preferred to pre-straining the tension specimens in cold rolling and then obtaining the yield stress curves in tension, where the envelope of such curves of the pre-strained specimens would give the yield stress curve over a larger range of strain. The reason for this preference is that, cold rolling introduces considerable plastic anisotropy in the specimens. Hence the R-ratio between the various pre-strained specimens would vary due to added anisotropy. Then the genuine anisotropic properties of the original material would be lost, resulting in some error in the determination of the equivalent stress-equivalent strain curve.

Based on the above discussion, the equivalent stress-equivalent strain curves for the materials used were determined as follows:

(i) For all of the materials tested, the uniaxial tension test was used until just before fracture. From the measurements of load, extension and lateral dimensions, the following could be computed:

$$X = \frac{P}{wt} \tag{8.1}$$

where w and t are the measured current lateral dimensions of the narrowest section of the specimen. During the uniform elongation, from constancy of volume:

$$wt = \frac{w_o t_o \ell_o}{\ell} \quad \text{which could be used instead.} \tag{8.2}$$

$$\varepsilon_\ell = \int_{\ell_o}^{\ell} \frac{d\ell}{\ell} = \ln\left(\frac{\ell}{\ell_o}\right) \quad \text{during uniform elongation.} \tag{8.3}$$

After the initiation of necking, from eqn. (8.2):

$$\varepsilon_\ell = \ln\left(\frac{w_o t_o}{wt}\right) \quad \text{can be used.} \tag{8.4}$$

Also

$$\varepsilon_w = \ln\left(\frac{w}{w_o}\right) \tag{8.5}$$

$$\varepsilon_t = \ln\left(\frac{t}{t_o}\right) \tag{8.6}$$

and from eqn. (3.15):

$$R = \frac{\varepsilon_w}{\varepsilon_t} \quad \text{(repeated, eqn. 3.15)}$$

From the above equations true stress and true strain can be found. To find the equivalent stress and the equivalent strain:

$$\bar{\sigma} = \left[\frac{3(R+1)}{2(R+2)}\right]^{\frac{1}{2}} X \quad \text{(repeated, eqn. 3.45)}$$

$$\bar{\varepsilon} = \left[\frac{2(R+2)}{3(R+1)}\right]^{\frac{1}{2}} \varepsilon_{\ell} \quad \text{(repeated, eqn. 3.47)}$$

(ii) In cases when sufficient range of strain could not be obtained in the uniaxial tension test, it was complemented by the plane strain test. The R-value obtained in the tensile test was used in the following equations to convert the yield stress curve obtained in the plane strain test, to the equivalent stress-equivalent strain curve.

If 1, 2, 3 directions correspond with ℓ, w, t and X, Y, Z then:

since $d\varepsilon_2^* = 0$ from eqn. (3.19):

$$\sigma_2 = \frac{\sigma_3}{1+R} \tag{8.7}$$

From eqn. (3.9) after substituting eqns. (8.7) and (3.15):

$$\bar{\sigma} = \sqrt{\frac{3\left[2 - \frac{1}{1+R}\right]}{2(2+R)}} \; \sigma_3 \tag{8.8}$$

Substituting $d\varepsilon_2^* = 0$, and eqn. (3.15) in eqn. (3.23), and integrating:

$$\bar{\varepsilon} = \frac{1}{1+2R} \sqrt{\frac{2(2+R)(1+3R+2R^2)}{3}} \; \varepsilon_3 \qquad (8.9)$$

As seen eqns. (8.8) and (8.9) require the R-value to be obtained from the tension test results. σ_3 and ε_3 can be calculated as follows:

$$\sigma_3 = -p = \frac{P}{w \times \text{breadth of plane strain die}} \qquad (8.10)$$

$$\varepsilon_3 = \int_{to}^{t} \frac{dt}{t} = \ln\left(\frac{t}{t_o}\right) \qquad (8.11)$$

The above analysis assumes that the yield stress curves in different directions in the plane of the sheet are the same, i.e. X = Y for the same strain. However, in general this is not the case and some variation as a function of direction is expected. In such cases, consistent with the framework of the theory, it is only possible to use an average of several tests performed in different directions, and regard this average as independent of direction. Several methods of averaging are discussed in sections 8.1.5. and 8.3.

8.1.2. Specimens

The specimens used for the two types of tests are described below.

8.1.2.1. Tensile

The tensile specimen should provide a uniform field of uniaxial stress, and triaxial strain. The specimens specified by BS-485 and ASTM-E8-57-T have 2 in. gauge length, 2.25 in. length of the parallel portion and 0.5 in. width. Since these specimens have enlarged portions (2 x 1 in.) at each end for the grips of the testing machines, it was felt that the results obtained by using them would be influenced by the "end effects".

Three exploratory tests were conducted using specimens with parallel portions of 3 in., 6 in., and 8 in. long and with a width of 0.5 in. as in the standard specimen. Only the middle 2 inches were used as gauge length. The results for the Extra Deep Drawing quality (E.D.D.S.) mild steel showed that at $\varepsilon_\ell = 0.40$, the true stress for the 8 in. specimen was about 4% lower than that of the 3 in. one. It was then decided to use a specimen with 5.5 in. long parallel portion for which any influence of the end effect would be within the experimental error.

Rectangular (1.25 x 11 in.) pieces were sheared from the 6 x 3 ft. sheets in which materials were supplied. These were cut in 0°, 45° and 90° to the rolling direction, in each thickness. They were then milled by a 1 in. diameter cutter to their exact shapes in batches of ten, with a plentiful supply of coolant. The edges were emery papered such that the specimens were not out of parallelism more than 0.001 in. in 0.5 in. width. 0.25 in. diameter holes were drilled at each end for the pins of the grips of the testing machine to go through (see Fig.18).

8.1.2.2. Plane Strain

The dimensions of the specimens for the plane strain test were chosen with reference to the results of Watts and Ford (91). The different thicknesses of sheet metal required different widths of the plane strain dies and also different widths of specimens under the following limits:

$$2t < \text{width of die} < 4t$$

and

$$\frac{\text{width of specimen}}{\text{width of die}} \gg 6$$

For the thickest specimens (0.80 in.) a width of 1.8 in. was thus sufficient, and for all the other thinner specimens this width was also used. The specimens were milled to this dimension with plentiful supply of coolant.

The plane strain specimens were only prepared for brass and copper, because they were needed to extend the range of the equivalent stress-equivalent strain curves. Since the tension results showed that these materials were sufficiently isotropic in the plane of the sheet, only one plane strain test for each thickness was sufficient.

8.1.3. Apparatus

The apparatus used in the determination of the equivalent stress-equivalent strain curves by the two methods is described below.

8.1.3.1. Tensile Testing

8.1.3.1.1. Tensile Testing Machine

The 15000 lb Denison testing machine was used for the tensile tests (Fig.18).

The specimen is mounted by the special jaws having pins which go through the holes drilled in the ends of the specimen. The load to the specimen is applied by the lower movable jaw which is driven by a screw. The screw can either be turned by means of a hand-wheel or through an electric motor drive. The slow power straining was preferred to obtain a uniform rate of extension which corresponds to a strain rate of about 0.001 sec^{-1} for the specimens used.

The load measuring mechanism of the machine consists of a mechanical leverage system, which is balanced by a spring to which an indicator is attached. The range and accuracy of the loading is as follows:

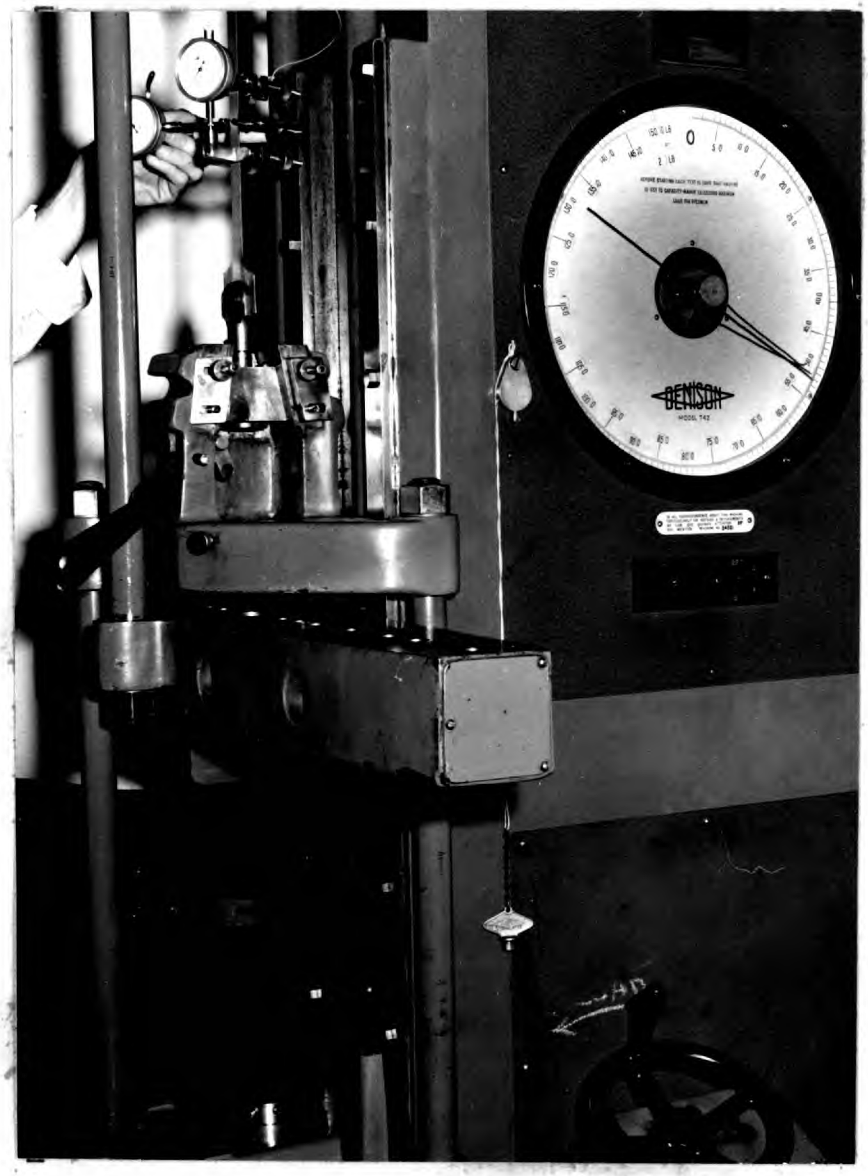

FIG.18 - TENSILE TESTING MACHINE

Range (lbs.)	Accuracy (lbs.)
1500	2
3000	4
7500	10
15000	20

The calibration of the testing machine is checked regularly by proving rings.

Since, by such a power-screw drive, the independent variable is the elongation and not the load, it enables a better control to be kept over the strain rate for the whole range of strain. This feature is particularly important after reaching the maximum load in uniaxial tension, when less reliable results would be obtained by the use of machines with hydraulic pressure actuated rams, where the load is the independent variable.

8.1.3.1.2. Extensometer and Lateral Contraction Transducer

To measure the elongation over the 2 in. gauge length accurately for the complete range of strain up to fracture, the extensometer shown in Fig.18 was designed and made. This also eliminated the need for changing from one extensometer for small strains to another for large strains during the test as would have been required if standard mechanical extensometers were used.

The extensometer is fixed on the specimen by two spring loaded knife edges resting on one side of the specimen which in turn rests on the flat surfaces of the clamps. A dial gauge with 0.5 in. travel and 0.0001 in. accuracy is attached to the upper clamp. Its spindle rests on the protrusion on the lower clamp. The gauge length is set by a gauge block put between the two clamps. The loads on the knife edges are varied by turning the nuts in or out. When 0.5 in. extension is reached, a 0.5 in. gauge block can be put under the spindle of the dial gauge to measure further elongations. Movable parts of the extensometer and the knife edges are kept lubricated to reduce the friction.

To measure the lateral dimensions of the specimen for use in the R-value calculations and also in finding the true strain and true stress beyond necking, a special transducer was designed and made. This is shown in Fig.19 with other anvils fitted for the measurement of thickness of shells. It can be fitted with the special anvils also shown in Fig.19 behind the micrometer, and used as demonstrated in Fig.18. The dial gauge used with this transducer has 0.5 in. travel and 0.0001 in. accuracy. Its spindle can be moved by the lever attached to it on one side. During the test, the transducer is held by hand, and while measuring the

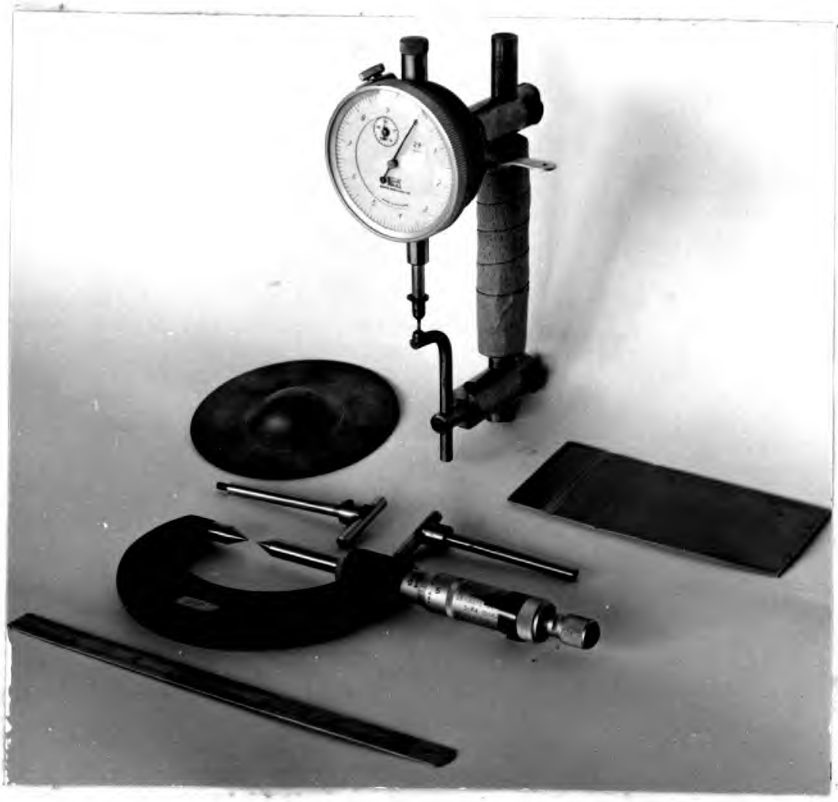

FIG.19 - THICKNESS MEASURING RIG, STRETCH FORMING AND PLANE STRAIN SPECIMENS, SPECIAL ANVILS FOR TENSILE SPECIMEN, MICROMETER AND RULER

FIG.20 - COMPRESSION TESTING MACHINE AND SUBPRESS

lateral dimensions of the specimen, it is slightly rotated in the two orthogonal planes and the minimum reading registered is taken as the true reading.

8.1.3.2. Plane Strain Compression Testing Machine, Subpress and Thickness Measuring Device

The 50 ton Denison testing machine (Fig.20) was used to provide the compressive load. The pressurized hydraulic fluid from the pump generates the load on the ram during its downward motion when also it compresses the helical springs. The return motion of the ram is provided by releasing the pressure and by the expansion of the springs. There are coarse and fine adjustments of loading. The load on the ram is balanced by a spring through a leverage system. An indicator is attached to this spring to read the load on the dial. The ranges of loading with the corresponding accuracies are given below:

Range (Tons)	Accuracy (Tons)
5	0.005
10	0.01
25	0.025
50	0.050

The calibration of the testing machine is regularly checked by proving rings or the dead weight testers.

The subpress used with this testing machine was the one described by Watts and Ford (90). This was specially made for plane strain testing ensuring the alignment of the dies and the axiality of the load. The dies used with the subpress conformed to the dimensional specifications given in section 8.1.2.2. Their surfaces were ground and polished, and the edges were slightly rounded.

The thickness measuring rig with its special anvils is shown in Fig.19. The anvils are suitable for the local measurement of thickness since they are spherical. The accuracy of the dial gauge used is 0.0001 in.

8.1.4. Experimental Procedure

8.1.4.1. Tensile Tests

The initial lateral dimensions of the specimen are measured by the lateral contraction transducer. The extensometer is then clamped on the specimen and its two pieces are spaced by a 1.5 in. gauge block to give a 2.0 in. gauge length. The whole assembly is then mounted on the testing machine whose dial is zeroed. The slow power straining is switched on and an estimated load of about half of that at the initial yield is applied and the dial gauge of the extensometer is zeroed. This is to eliminate the small deflections due to elastic bending of the specimen.

The load is then applied by the power straining mechanism to give increments of elongation which are initially about 0.020 in. and later 0.050 in. The lateral dimensions are measured at every increment with the transducer, and the instantaneous tensile load and the extension are also recorded. When 0.5 in. elongation is reached, a 0.5 in. block is placed under the spindle and hence larger extensions can be directly measured.

Beyond necking the minimum dimensions of the neck are recorded. In cases where multiple necking is obtained, the smaller one is considered. The test can be carried up to fracture without any danger to the extensometer. After the occurrence of fracture, the radii of curvature in the two planes at the neck are approximately measured by radius gauges.

8.1.4.2. Plane Strain Compression Tests

The initial thickness of the specimen is measured by the thickness measuring device. The width is measured by a vernier to within 0.001 in.

Plane strain dies are cleaned by acetone and slightly lubricated by the molybdenum disulfide grease. The specimen is also greased with the same lubricant. After choosing the most accurate scale and zeroing it, the load is applied gradually on the specimen between the two plane strain dies in the subpress. The increments of load are adjusted so that it would produce initially about 0.002 in., and later 0.004 in. thinning. After each "squeeze", when the load is applied for about 10 seconds, the specimen is taken out and degreased by acetone. The thickness across the width is measured at five points with the thickness measuring device, and the average is recorded.

Sides of the specimen where small extrusions of the metal have taken place, are filed off. The specimen is relubricated and the process is repeated until about $\varepsilon_3 = -0.70$.

8.1.5. Curve-Fitting of Stress-Strain Data

8.1.5.1. Method and Numerical Analysis

In section 3.1.(iii), the suitability of the empirical relationship,

$$X = A(B + \varepsilon_\ell)^n \quad \text{(repeated, 3.25)}$$

for use with the present theoretical analysis was discussed. Within the framework of the theory this is the yield stress curve of the material in the plane of the sheet. The yield stress curve in the thickness direction can be found from eqn. (3.25) by the use of eqns. (8.8 to 8.11) with the knowledge of the R-value.

In cases where the experiments showed that there was no significant variation of the yield stress curve with different directions in the plane of the sheet, then the method of curve-fitting of the experimental results to eqn. (3.25) was used, as described below.

Since in general the experimentally obtained relationship X versus ε_ℓ is not exact as given by eqn. (3.25), there will be some error in expressing the experimental results by this formula. The curve fitting cannot be directly achieved by plotting the experimental results on a logarithmic scale and finding the slopes and intercepts, due to the presence of B, when $B \neq 0$. Therefore a more general method was adopted which would not only work for this, but for any other empirical relationship no matter how complicated it may be. Two criteria were studied in the determination of the error involved in the curve fitting. They are given below:

If u refers to any of a set of v points:

Least Squares.

$$\Delta = \sum_{u=1}^{u=v} \left[X_u - \left((X)_{\varepsilon_\ell = (\varepsilon_\ell)_u} = A(B + (\varepsilon_\ell)_u)^n \right) \right]^2 \qquad (8.12)$$

Least Moduli.

$$\Delta = \sum_{u=1}^{u=v} \text{modulus} \left[X_u - \left((X)_{\varepsilon_\ell = (\varepsilon_\ell)_u} = A(B + (\varepsilon_\ell)_u)^n \right) \right] \qquad (8.13)$$

The problem of curve-fitting now reduces to a problem of optimization or minimization of error in a four dimensional "parameter space" where the parameters are Δ, A, B, and n. A certain combination of these parameters would give the least error with each of the two criteria and hence the best fit to the experimental results would be obtained.

At first the minimization of Δ was attempted by varying each parameter at a time to find the minimum Δ within its range. This was repeated for the other two parameters in sequence and the whole process was repeated until negligible change was obtained in Δ. Due to the high interaction between the parameters, this method was very slow even on the Mercury computer which was used at the time.

The method of "modified steepest descent" by Rosenbrock (71) was then adopted. This, at the end of each stage of computation, gives the values of A, B, and n which advance in the direction of the minimum of Δ in the parameter space. This method is rapidly convergent and very suitable for automatic computation. It requires the scaling of the parameters so that the same steplength can be used in all directions in the parameter space. This is achieved by using $10^6 \times A$ in place of A in eqn. (3.25), and hence all the parameters would then remain in the same order of magnitude.

Both of the above methods require the calculation of the initial values of the parameters to start the computations. This can be effected by taking only three points on the yield stress curve and evaluating A, B, and n exactly as follows:

Taking the logarithm of both sides of eqn. (3.25):

$$\ln X = \ln A + n \ln (B + \varepsilon_\ell) \tag{8.14}$$

Substituting the values of X and ε_ℓ for the three points arbitrarily selected:

$$\begin{aligned} \ln X_1 &= \ln A + n \ln (B + (\varepsilon_\ell)_1) \\ \ln X_2 &= \ln A + n \ln (B + (\varepsilon_\ell)_2) \\ \ln X_3 &= \ln A + n \ln (B + (\varepsilon_\ell)_3) \end{aligned} \tag{8.15}$$

By the method of elimination applied to the above eqns., the following relations are obtained:

$$\frac{\ln\left(\frac{X_3}{X_1}\right)}{\ln\left(\frac{X_3}{X_1}\right)} - \frac{\ln\left(\frac{B + (\varepsilon_\ell)_3}{B + (\varepsilon_\ell)_1}\right)}{\ln\left(\frac{B + (\varepsilon_\ell)_3}{B + (\varepsilon_\ell)_1}\right)} = 0 \tag{8.16}$$

By trial and error B can be determined from eqn. (8.16). n is determined from:

$$n = \frac{\ln\left(\frac{X_3}{X_1}\right)}{\ln\left(\frac{B + (\varepsilon_\ell)_3}{B + (\varepsilon_\ell)_1}\right)} \tag{8.17}$$

To find A any of eqns. (8.15) can be used with the calculated values of B, and n.

In cases when the yield stress curves show variations as a function of direction along which the specimens are cut, an effective or an average yield stress curve must be obtained to be consistent with the theory. Two methods were used for this purpose:

(i) The total set of points for the two (0^o, 45^o) or the three (0^o, 45^o, 90^o) directions were used in the curve fitting with the least squares, and the least moduli criteria.

(ii) Arithmetic means of the constants A, B, and n for the curves fitted separately in each direction were obtained.

In some cases the equivalent stress-equivalent strain curves obtained by the plane strain test were used to supplement those obtained in the tensile test. The yield stress curves in the thickness direction obtained by the plane strain test were first converted to the equivalent stress-equivalent strain data by eqns. (8.8) and (8.9). Then they were converted to the yield stress data in the plane of the sheet by eqns. (3.45) and (3.47). The process of curve fitting was then effected as if all of the points were obtained in the tensile test.

Hence for the materials used in the experiments, which are given in detail in section 8.2, the constants A, B, and n were determined. The results are presented in section 8.3.

The equivalent stress-equivalent strain relationship to be used in the theory can be obtained by using eqn. (3.25) with eqns. (3.45) and (3.47), which can be condensed to eqn. (3.48).

8.1.5.2. Computer Program

Two programs had been written for curve fitting using the least squares and the least moduli criteria. Only the least squares program will be discussed in this section since the two are very similar. These programs were specifically written for the Mercury computer, but they can be used on Atlas with slight modifications. Each program consists of three chapters and it takes 3 - 5 minutes of Mercury time to fit an approximately 25 point curve.

The layout of the input data is as follows:

(1) Accuracy limit. When the rate of change of the parameters A, B, and n remains within this limit, the curve-fitting is considered to be satisfactorily completed. It is found that 0.001 gives very satisfactory results.

(2) Number of sets of data to be processed (integer).

(3) The co-ordinates of any three arbitrary points on the curve to determine the starting values for A, B, and n arranged as:

log. strain	stress (psi)
$(\varepsilon_\ell)_1$	X_1
$(\varepsilon_\ell)_2$	X_2
$(\varepsilon_\ell)_3$	X_3

(4) Number of points on the yield stress curve to be used in curve fitting (integer).

(5) The co-ordinates of the points on the yield stress curve to be used in curve fitting are arranged as:

log. strain	yield stress (psi)
$(\varepsilon_\ell)_1$	X_1
$(\varepsilon_\ell)_2$	X_2
....	
$(\varepsilon_\ell)_u$	X_u
....	
$(\varepsilon_\ell)_v$	X_v

(6) If there is more than one set of data items 3 - 5 should be repeated.

The computer program (see Appendix-D) first reads the above data, and computes the starting values of A, B, and n from the information in item (3) of the above layout by using eqns. (8.16), (8.17), and (8.15), and prints these values. It then scales the initial values of the parameters to get them in the same order of magnitude, and sets the Minimization Routine* parameters. At this stage the routine is entered. The error is calculated from either eqn. (8.12) or eqn. (8.13) whichever the case may be, using also the scaled version of eqn. (3.25) as explained in section 8.1.5.1. The Minimization Routine calculates A, B, and n which are then subjected to the accuracy test. If the rate of improvement is greater than the number given in item (1) of the data layout, then the Routine is obeyed again with the last A, B, and n used as the starting values. When the rate of improvement is less than the prescribed value, three more iterations are carried out as a further check of the accuracy, and the main results are printed. However, if $0 > B$ is found as a result of curve-fitting this is not accepted since this implies a strain at zero stress. In such cases $B = 0$ is taken and the curve fitting is restarted.

The layout of the printed results is given below.

	psi			$(\text{psi})^2$
Starting values	A	B	n	
Penultimate "	"	"	"	Δ
Ultimate "	"	"	"	"

(1) log. strain	(2) exp. yield stress (psi)	(3) computed yield stress (psi)	(4) $\frac{(2)-(3)}{(\text{psi})}$	(5) $\frac{(4)}{(2)}$
$(\varepsilon_\ell)_u$	X_u	$(X)_{\varepsilon_\ell = (\varepsilon_\ell)_u}$	error	% error

* Minimization Routine is in the Program Library of the Institute of Computer Science, University of London.

After the print out of the above results, the program processes other sets of data if there is more than one, otherwise it ends.

8.2. Hardness Tests

Hardness tests were carried out according to B.S. 427, the mean of six indentations made at various points in each sheet being given in Table 8.1. Vickers pyramid tester was used with a pyramid indentor having a 136^{o} apex angle.

8.3. Discussion of Results

The ranges of strain obtained in the yield stress curves (Figs. 21-24) are quite sufficient for the present purposes. The plane strain results for brass and copper within the range of the tensile tests, are in very close agreement with them. This shows that the materials very closely followed the flow rules for anisotropic continua, used in this investigation.

Bramley and Mellor (9) recently conducted some experiments with extra deep-drawing quality steel to check the validity of Hill's theory of anisotropic plastic deformation. They obtained a rather poor correlation between experiment and theory on the variation of the R-value as a function of direction in the plane of the sheet. However the yield stress curve obtained in the bulge test compared very favourably, with that predicted using Hill's theory and the yield stress in the plane of the sheet obtained by the tensile test, using also the average R-value for the sheet.

Brass and copper conformed more closely to the type of anisotropy considered in the theory, since they showed negligible variations both in yield stress curves (Figs. 22 and 23), and R-value curves (Figs. 26 and 27) in the plane of the sheet. Hence better agreement between theory and experiment was obtained for them in stretch forming as expected.

Figs. 21, 24, and 25, 28 indicate that a high R-value is associated with a lower yield stress curve in the respective direction for the same material.

The numerical values of the constants A, B, and n given in Tables 8.2 and 8.3 are in close agreement with those published by Johnson and Mellor (42) for similar materials. The values of B for all of the materials used indicate that they were in soft condition as also specified by their manufacturers (see Table 8.1).

The two criteria, i.e. least squares, and least moduli, used in curve-fitting of the experimentally obtained yield stress curves to the empirical relationship (3.25) produced very similar results for most materials. In cases where there was appreciable scatter in the experimental results as with 20 S.W.G. soft aluminium, significant differences between the results of the two criteria were observed. This related to the contribution of the error of each point to the error function Δ. In such cases, if a better fit towards the end of the curve is required, then least squares approach should be used, otherwise least moduli criterion would be satisfactory.

Soft copper and soft brass showed negligible variation in their yield stress curves as a function of direction as seen in Figs. 22 and 23. Therefore all of the points for the three directions were used in curve-fitting which gave an average yield stress curve for the material.

In the case of mild steel, and soft aluminium which showed variations in their yield stress curves as a function of direction, each individual curve was curve-fitted. Average values of the constants A, B, and n were obtained by finding their arithmetic means. Also for a given material and thickness all of the points in different directions were used with the two criteria of curve-fitting. In the case of the least squares criterion, the differences in the numerical values of the constants were smaller than those of the least moduli criterion, as seen in Tables 8.2 and 8.3.

The accuracy of curve-fitting of the experimental results to the empirical relation is generally within

2% for most materials. This is quite satisfactory for the present purposes.

In view of the above discussion, for the theoretical solution of the stretch forming problem, least square results were used. For steel and aluminium the average curves obtained by the least squares method were preferred to the ones obtained by taking the arithmetic mean. These results are shown in Figs. 21 to 24 with the experimental points. However, due to the proximity of the least squares and least moduli results only one fitted curve was justified to be drawn for each material.

R-values obtained for the materials are plotted as functions of longitudinal strain in tension in Figs. 25-28. With brass and copper the variation as a function of direction is within 20%. This indicates a sufficiently high degree of isotropy in the plane of the sheet. The variations with strain are negligible except for the small strains when the grains of the materials are more randomly oriented.

Steel and aluminium show significant variations in R-value both as functions of direction of test, and straining. For steel, the R-values for 45^{o} direction are the minimum. Lilet and Wybo (55) obtained the same trends. They found that the results were also significantly influenced by the chemical composition of the steels. Their results ranged from 0.5 to 1.9 which covers the range obtained by the present author.

It is difficult to define an effective average R-value if it varies with strain and direction. In connection with the present work the arithmetic means of the values obtained as functions of strain and also of different directions were used. However, it was observed that with steel, better agreement between theory and experiment in stretch forming is obtained if the minimum R-value is used.

The results of the hardness tests are reported in Table 8.1. These confirm the softness of the materials.

CHAPTER 9 - APPARATUS

In this Chapter, the apparatus used in the experiments for the Erichsen, stretch forming and deep-drawing tests are described.

9.1. Sheet Metal Testing Machine and Blanking Press

These two machines are manufactured by Roell and Körthaus in West Germany.

The 35 Te (Te = Tonne) universal sheet metal testing machine is shown in Fig.29, with its controls and gauges appropriately labeled. The machine has a pump, driven by an electric motor. This provides the pressure for the motion of the double-acting piston on to whose push-rod, the punch assembly is connected. The up and down motion of the punch and its speed are controlled by valves shown in Fig.29.

Blank-holder load can be applied independently of the punch load by a separate valve. This controls the pressure on the symmetrically located pistons attached to the housing of the blank-holder plate. This load can remain constant during a test.

The machine incorporates an electronic cut-out mechanism which stops it, and releases the pressure on the main piston by means of a solenoid operated valve, when a certain decrement on the punch load is reached. The sensitivity knob, shown in Fig.30, when suitably

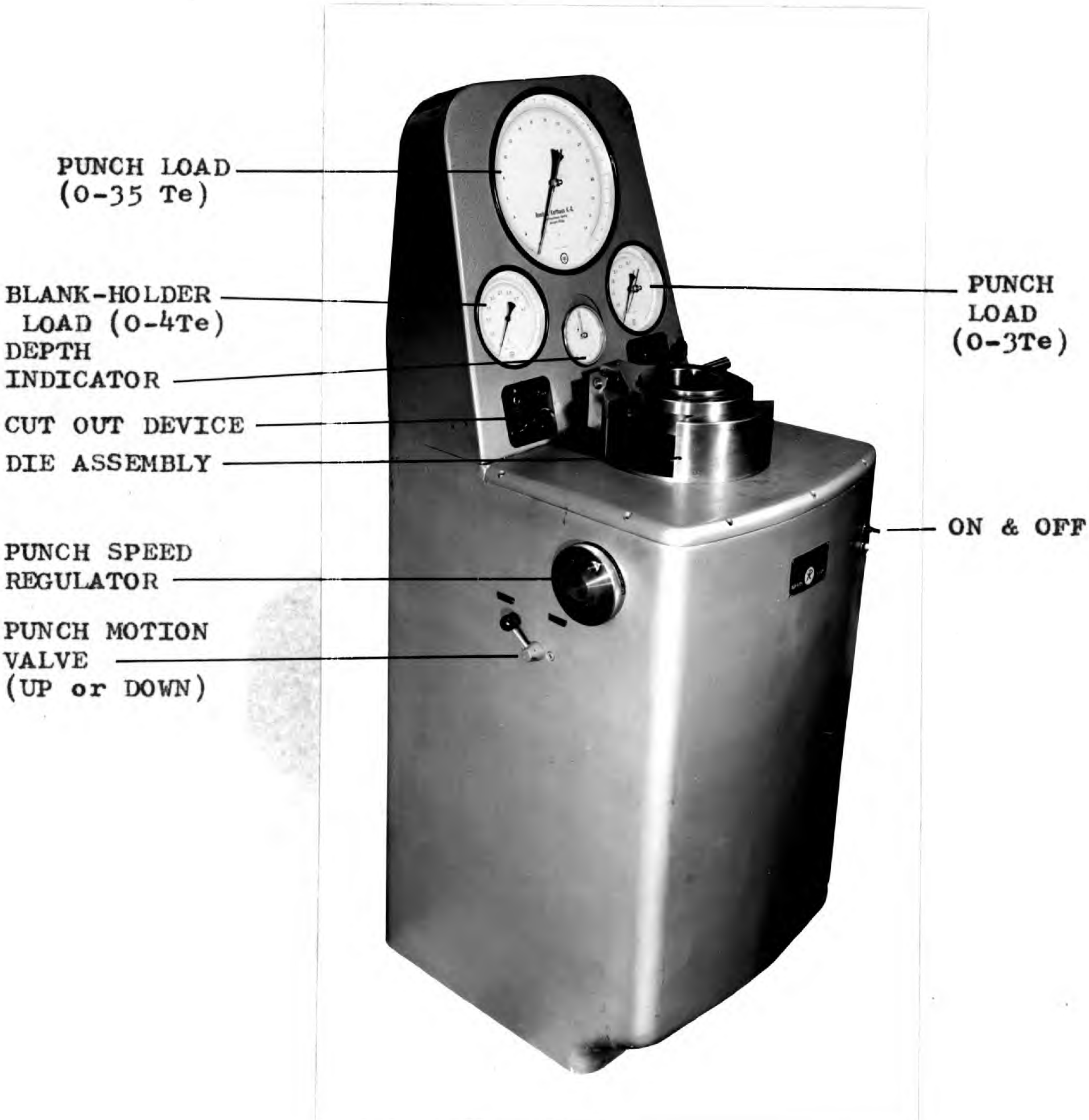

FIG.29 - UNIVERSAL SHEET METAL TESTING MACHINE.

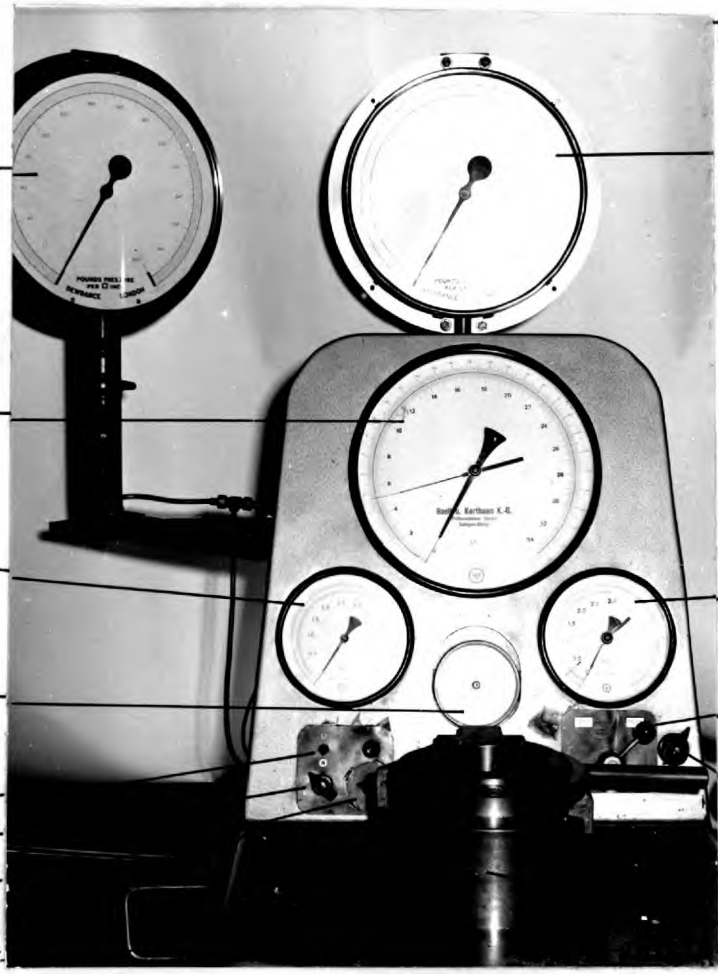

FIG.30 - INSTRUMENT PANEL OF THE UNIVERSAL SHEET METAL TESTING MACHINE

calibrated by trial tests, generally coincides with the initiation of fracture in stretch forming and deep-drawing tests; if it does not, pressing can be continued by switching the machine on again.

Two gauges are provided on which it is possible to reach punch load, one for the range 0-3 Te, the other 0-35 Te, while a third gauge records blank-holder load, range 0-4 Te. After the gauges had been recalibrated by means of a proving ring and special attachment shown in Fig.31, they were then accurate to within 0.05, 0.02, and 0.02 Te respectively. Two additional gauges were installed, and calibrated to obtain higher accuracy in the determination of punch loads for use in the calculation of the coefficient of friction by the method given in section 7.1. The one with the range 0-7 Te was accurate to within 0.01 Te and the other with the range 0-2 Te to within 0.003 Te.

To maintain a constant speed of penetration, it was necessary to open the speed-control valve slightly as punch load increased.

Also incorporated in the panel of the testing machine was an indicator that recorded the depth of penetration of the punch at any instant. The calibration of this gauge was also checked. The zero point of the punch was set to within 0.001 in. by means of a depth micrometer, alterations being made by putting shims under the punch.

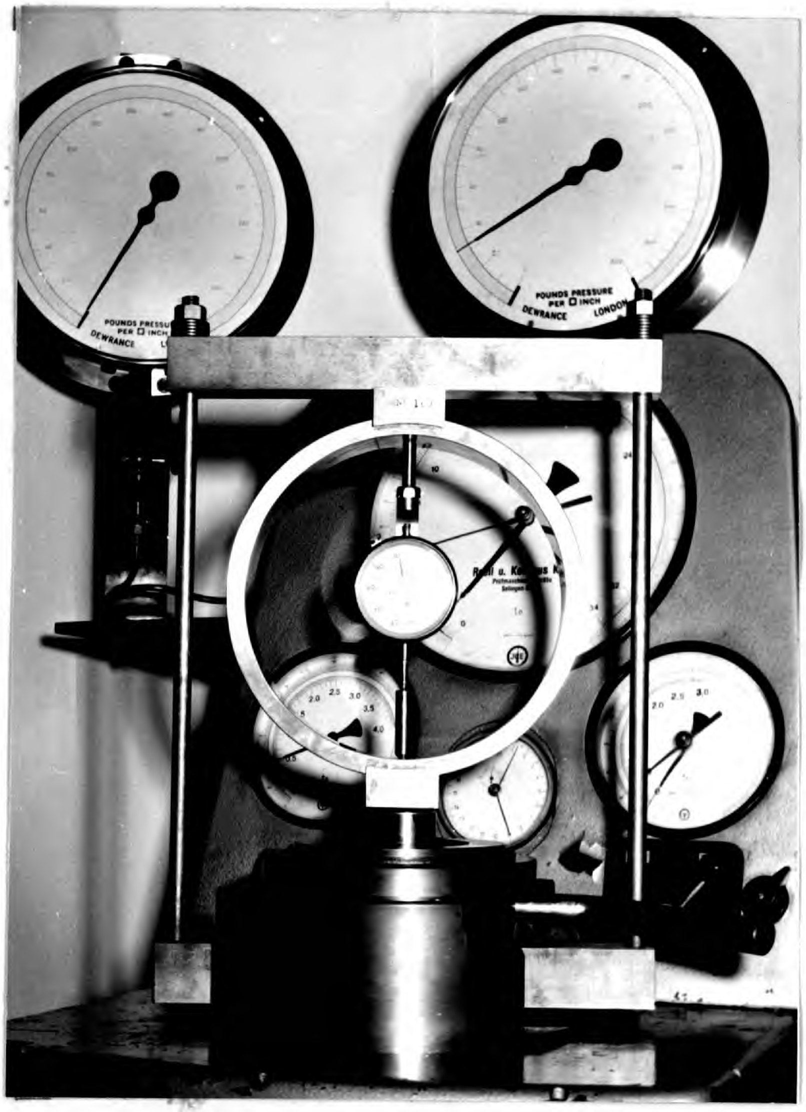

FIG.31 - CALIBRATION OF THE LOAD GAUGES OF THE UNIVERSAL SHEET METAL TESTING MACHINE BY PROVING RING.

A small 80 Te blanking press shown in Fig.32 was used to blank the circles of standard sizes required for the tests. The hydraulic pressure produced by the motor-pump unit is supplied to the double acting piston through a valve which controls the up and down motion of the ram attached to the piston arm.

FIG.32 - BLANKING PRESS

A number of dies are available to punch circles of standard sizes. These are placed underneath the ram and on a spacing ring which provides the correct clearance. The circles are punched out from strip metal by the downward motion of the ram and can be collected in the space underneath the die assembly.

The blanks with non-standard sizes were obtained by machining down the oversize standard ones in a lathe under plentiful coolant not to raise the metal temperature significantly.

9.2. Scribing Tool

Since the problem is predominantly an axially symmetrical one, and cylindrical co-ordinates are used in the calculations, it was necessary to scribe a grid of concentric circles on the round blanks. For this purpose an attachment was designed incorporating a hardened tool-steel scriber, the point of which had an included angle of 60° and a relief angle of 20°, suitable for fixing to the tool post of a toolroom lathe, as shown in Fig.33. The scriber was held in a carrier supported between pivot points, fitted with a movable weight that could be adjusted to vary the force on the scriber in a similar manner to that adopted for the tracelet mechanism described by Brewer and Alexander (10).

The round blanks were held by a special three jaw

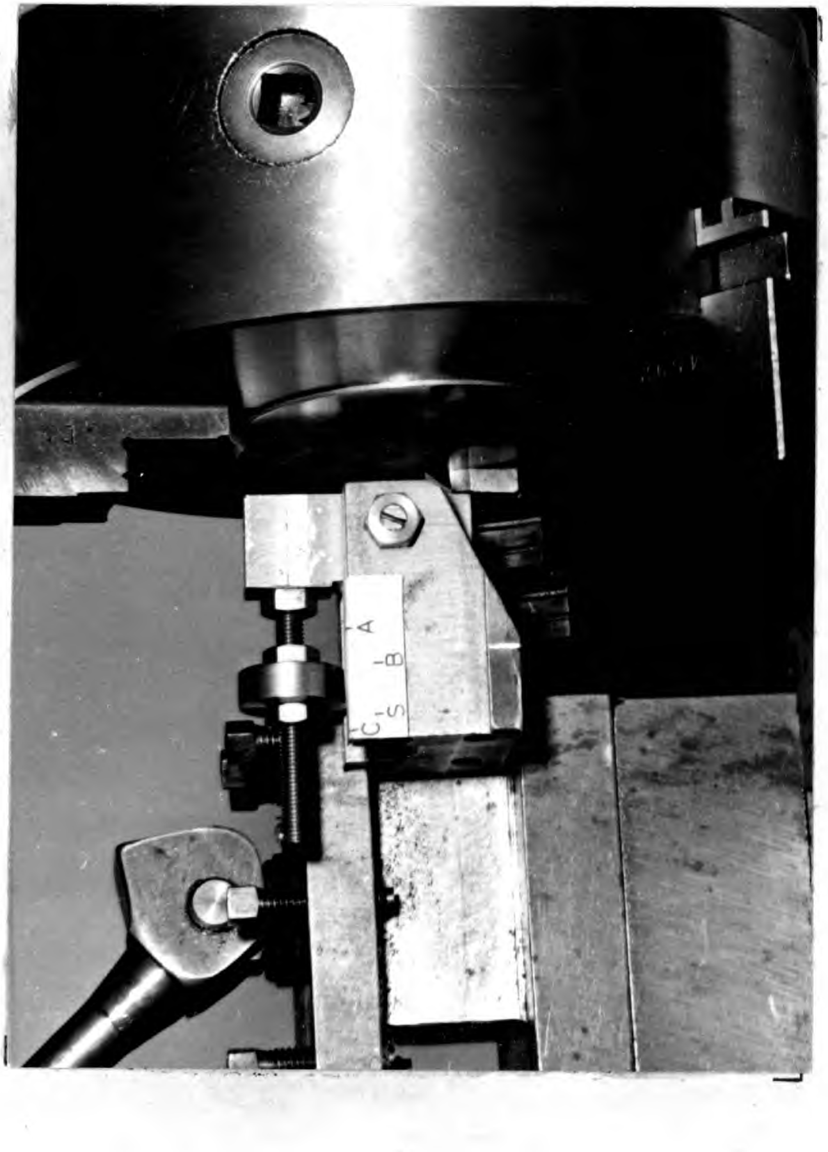

FIG.33 - SCRIBER ATTACHMENT

chuck whose eccentricity was checked and found to be within 0.001 in. When this was not available, a cylindrical groove was machined into a brass disc held by an ordinary three jaw chuck, with a diameter equal to that of the blank. This method of course induces no eccentricity.

Since most of the specimens used, received large plastic deformations, it was essential that the grid was still visible under microscope after the deformation. This could be ensured by scribing deep and therefore wide lines, but these themselves could initiate premature fractures. Hence to determine the optimum width or depth of scribed lines, number of trial tests were carried out using different loads on the scriber for each material. The corresponding locations of the movable weight on the scriber were marked as shown in Fig.33, for each material. The weight was kept at such settings in scribing the specimens proper.

It was found that on one hand to avoid premature fracture, and on the other, for the lines not to disappear, they generally had to be 0.0011 to 0.0015 in. wide.

The chuck was turned slowly by hand when scribing.

9.3. Measuring Instruments

The following measuring instruments were used to measure the scribed and distorted grid on the specimens, and also to check eccentricity and geometric accuracy of the tools used.

The first two are made by Societe d'Instruments Physiques, and the third by Hilger and Watts.

9.3.1. Co-ordinate Measuring Machine (U-10)

This instrument consists of a co-ordinate table movable in its plane by two orthogonally located micrometer screws, each accurate to within 0.00005 in., and a microscope whose axis is perpendicular to the table, as shown in Fig.34. A rotary table can be mounted on the co-ordinate table which makes it more convenient to take measurements on a circular grid in different radial directions.

The microscope is provided with several objective lenses, of which the one with 25 times magnification was found to be the most suitable for stretch formed and deep-drawn specimens.

The correct illumination of the specimens was very important in order to make accurate measurements. For this, two beams of light, one white the other green, at about 60^{o} to each other were used. By this method it was possible to see the centerline (the deepest part) of the scribed line as a boundary between green and white light.

The centring of the specimens with respect to their circular grids was achieved by aligning these with the

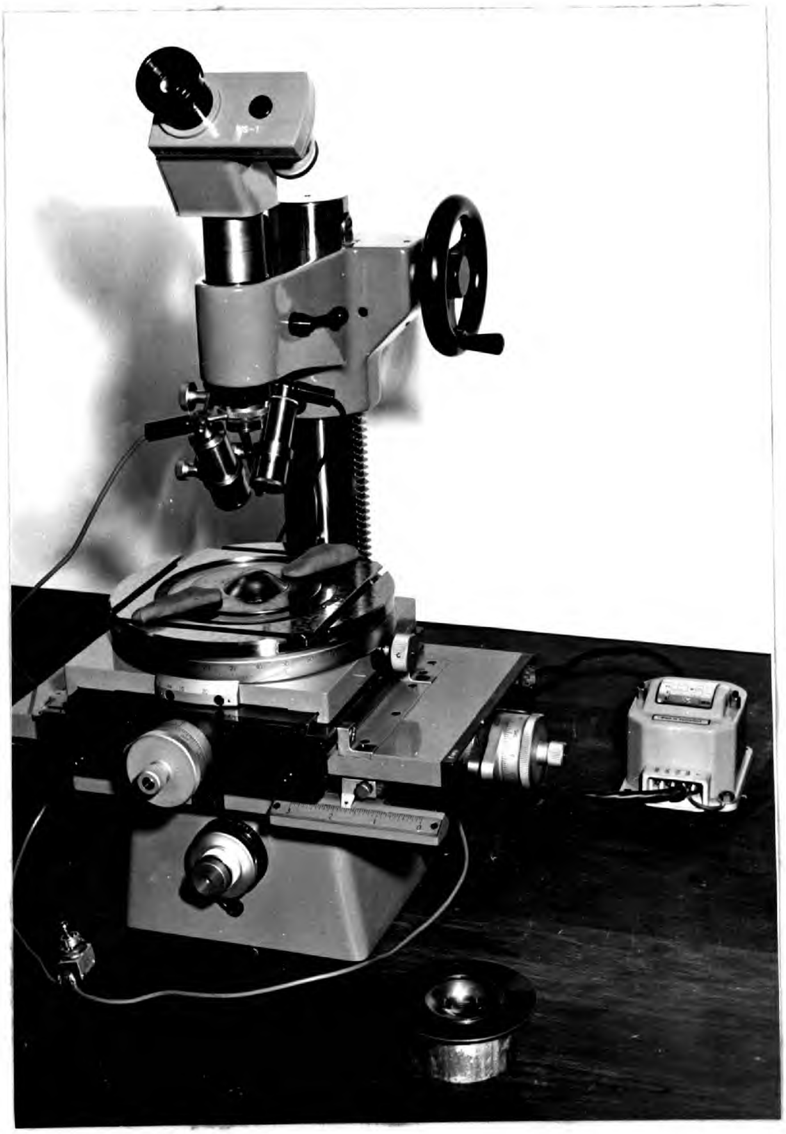

FIG.34 - CO-ORDINATE MEASURING MACHINE (U-10)

circles in the objective lens of the microscope.

9.3.2. Universal Measuring Machine (MU-214-B)

This instrument shown in Fig.35, enables measurements in three orthogonal directions to be taken. The horizontal motion of the table, and the vertical and transverse motions of the microscope are effected by rack and pinion and screw drives. The measuring system is entirely independent to this, and measurements are taken from the standard scales in the three orthogonal directions. The accuracy is to within 0.00001 in. However, since its microscope has a fixed magnification of 48 times, this was found to be too high for measuring the grids on the stretch formed and deep-drawn specimens, and hence it was not used for this purpose. Using this machine, the calibrations of the dial, and depth indicators, and checking the dimensional accuracy of the tools were satisfactorily carried out.

9.3.3. Optical Projector

The projector was used to check the geometric accuracy of the profiles of the hemispherical and ellipsoidal punches. The object is placed between the collimated light source and the lens system as shown in Fig.36. The magnified shadow then goes to a mirror which reflects it on the screen.

The reflected shadow can then be compared with the

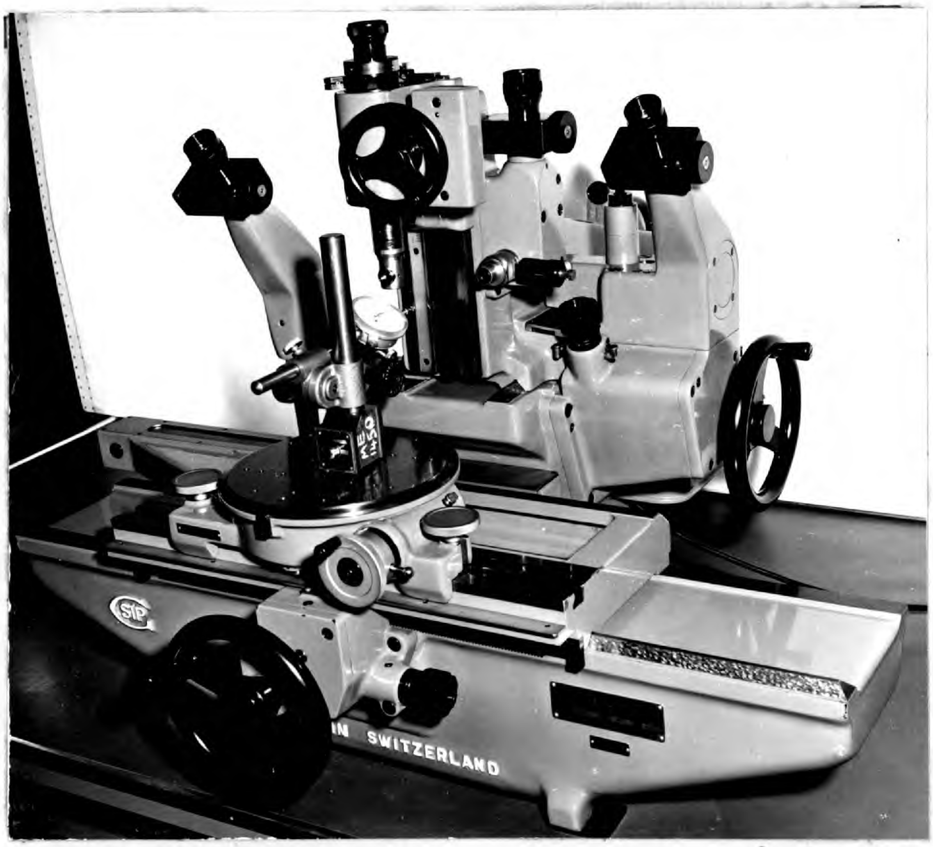

FIG.35 - UNIVERSAL MEASURING MACHINE (MU-214-B)

FIG.36 - OPTICAL PROJECTOR

required geometric shape drawn on a transparent paper and laid down on the screen, as was done for the punches. The accuracy is about 0.001 in. using 10 times magnification.

9.3.4. Thickness Measuring Devices

The thickness measuring rig, and the special micrometer with pointed anvils shown in Fig.19 were used to determine the local thicknesses, and thickness distributions on deformed specimens to calculate the plastic strains. Both the anvils of the rig and the micrometer had spherical tips with a radius of about $^{1}/64$ in. The accuracy of the dial indicator is 0.0001 in. and that of the micrometer is 0.001 in. In most measurements the rig was preferred to the micrometer because of its higher accuracy. It also provided a constant load on its anvils, which was important to get consistent results in the measurements of specimens made from softer materials, e.g. aluminium.

9.4. Punches, Dies, Blank-Holders and Centring Devices

With the sheet metal testing machine described in section 9.1, it is possible to use various kinds of punches, dies, and blank-holders to suit the application. These are described below.

In the Erichsen test the standard punch, die and blank-holder specified in DIN 50101 (30) were used, as shown in Fig.37. These were provided by the makers of the machine and the surfaces in contact with the sheet metal had approximately a C.L.A. figure of 6. An additional device was made to centralize round blanks and strip in the testing machine, to ensure that the centre of the scribed circles would coincide with the axis of symmetry of the punch. This was a "centring tool" which fitted over the blank-holder with no "play", and had four stops adjustable in the four perpendicular directions, moving in slots. These could be set to within 0.001 in. by using a micrometer or vernier in conjunction with a specially made measuring tool.

Also a blank-holder was made which was exactly the same as the standard blank-holder, except that the surface which contacted the sheet-metal was serrated. The serrations were produced in a lathe which gave a groove similar to that on a gramophone record; the depth of the groove being approximately 0.012 in. This blank-holder is referred to as the "rough" blank-holder.

For the stretch forming test all the required tools shown in Fig.38 were designed and made. Hemispherical, and ellipsoidal punches used in the tests had a diameter of 1.300 in. The major axis of the ellipsoidal punch was twice as long as the minor axis. They were ground to shape accurately, and this was checked by the optical projector, Fig.36, against a drawn template.

From DIN. 50101:

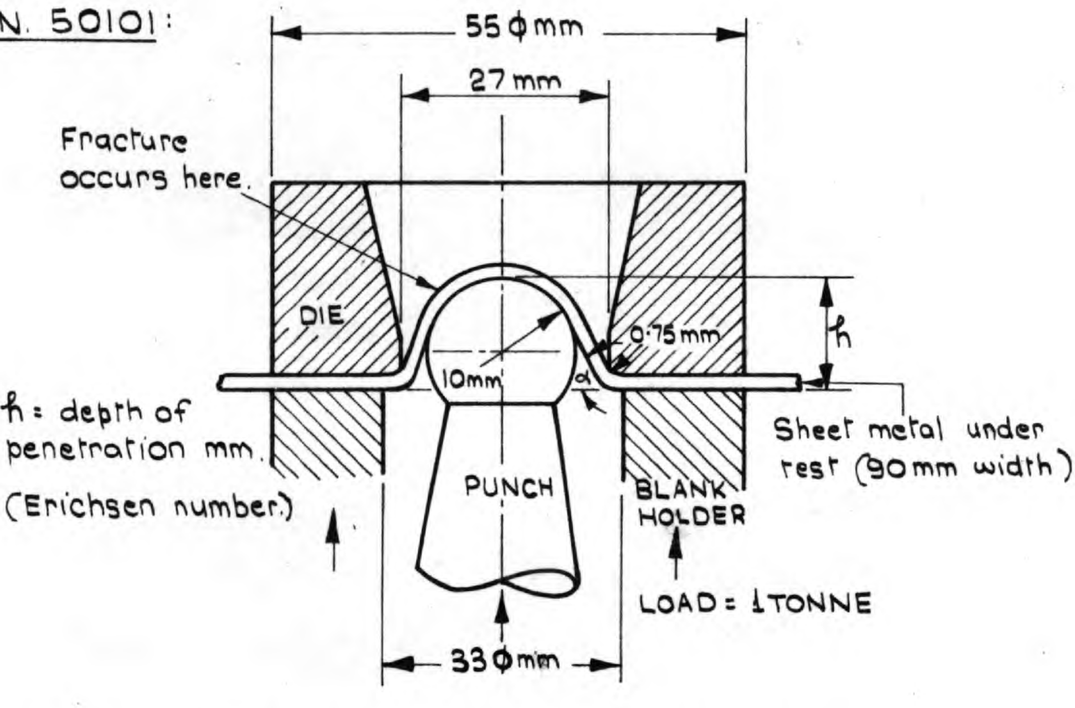

FIG. 3.7. TOOLS FOR THE ERICHSEN TEST.

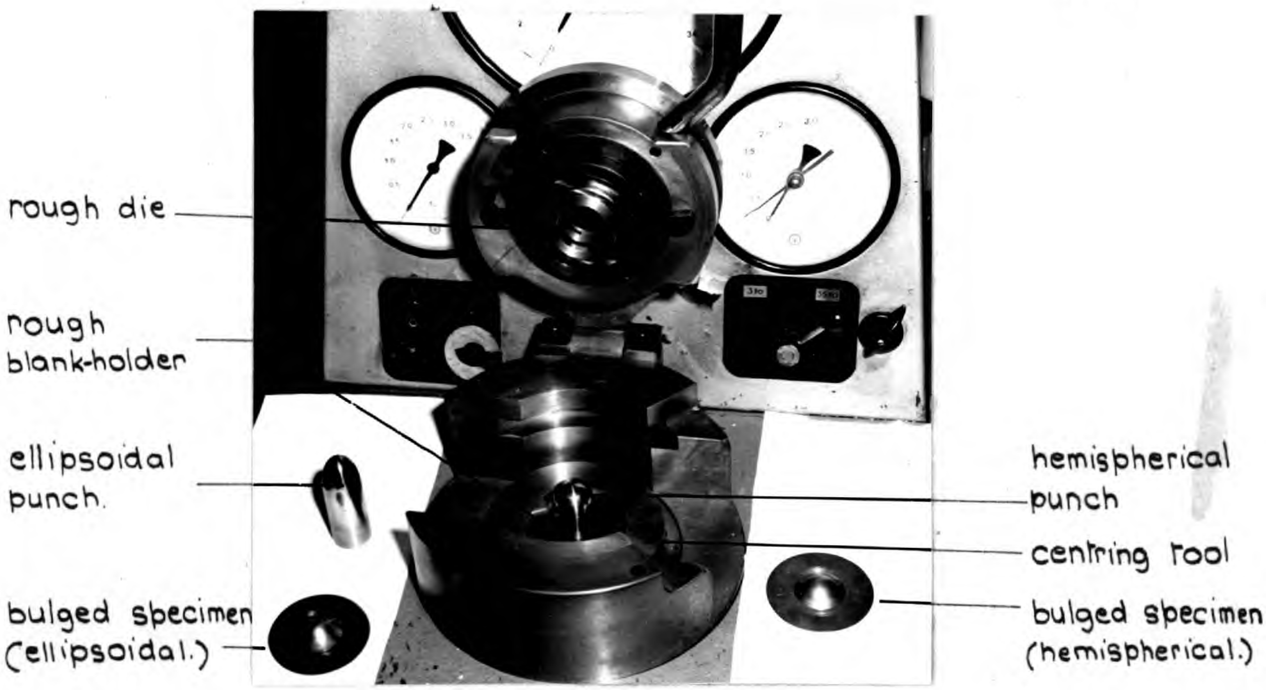

S.W.G.	14	16	18	20
D in.	1·524	1·481	1·434	1·400
A in.	2·075	2·045	2·015	1·990

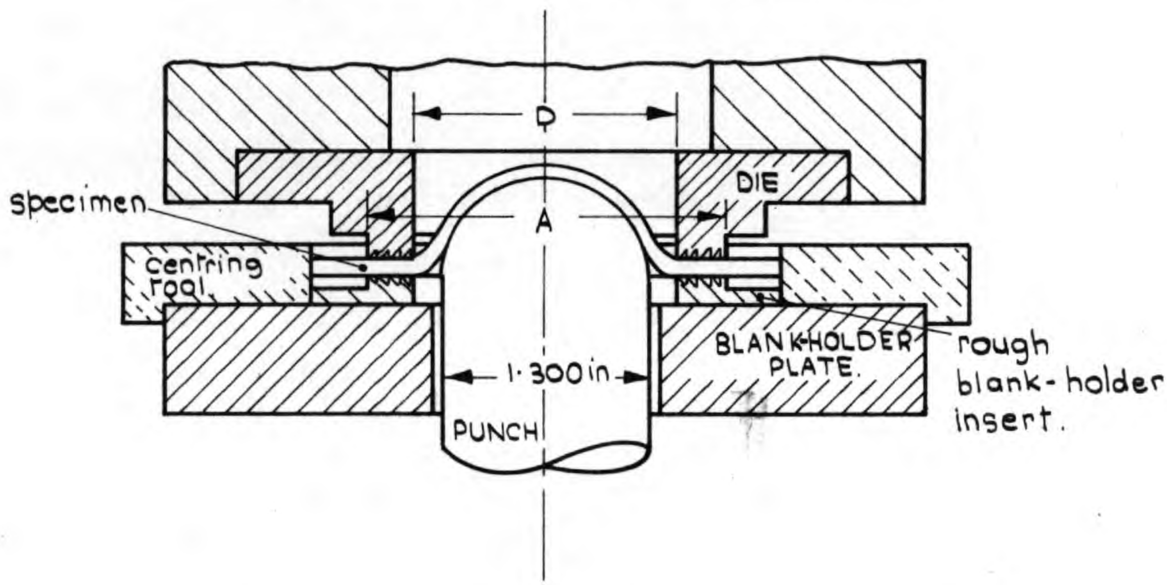

FIG. - 38. TOOLS FOR THE STRETCH FORMING TEST.

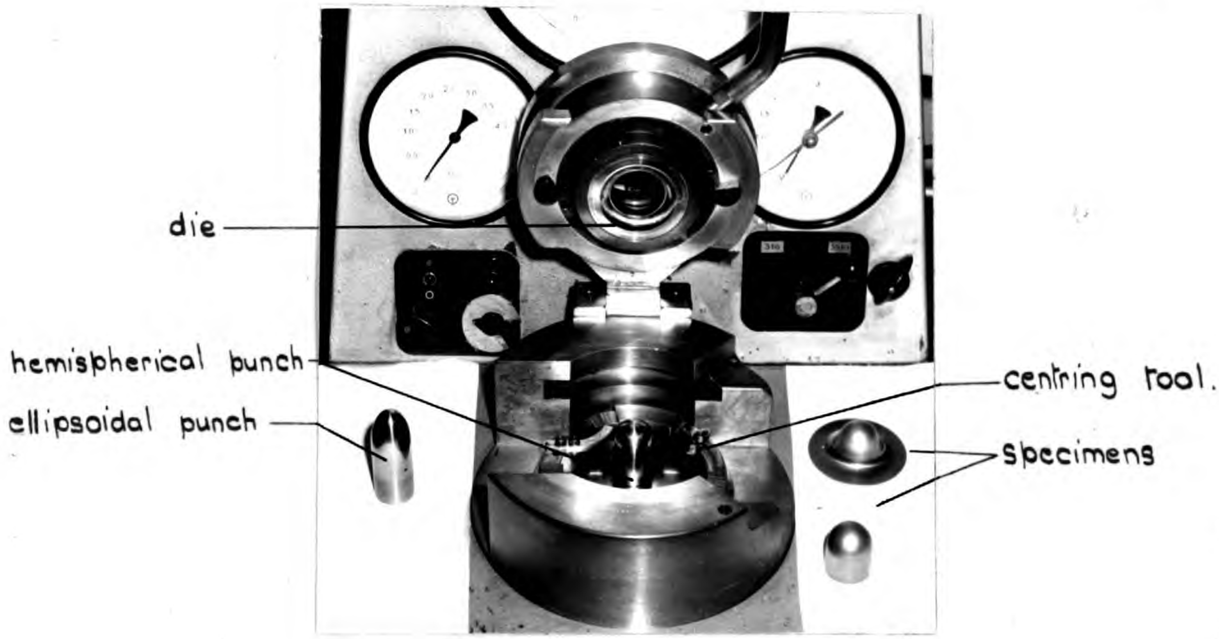

S.W.G.	14	16	18	20
D in	1·524	1·481	1·434	1·400
r_d' in	0·525	0·472	0·417	0·365

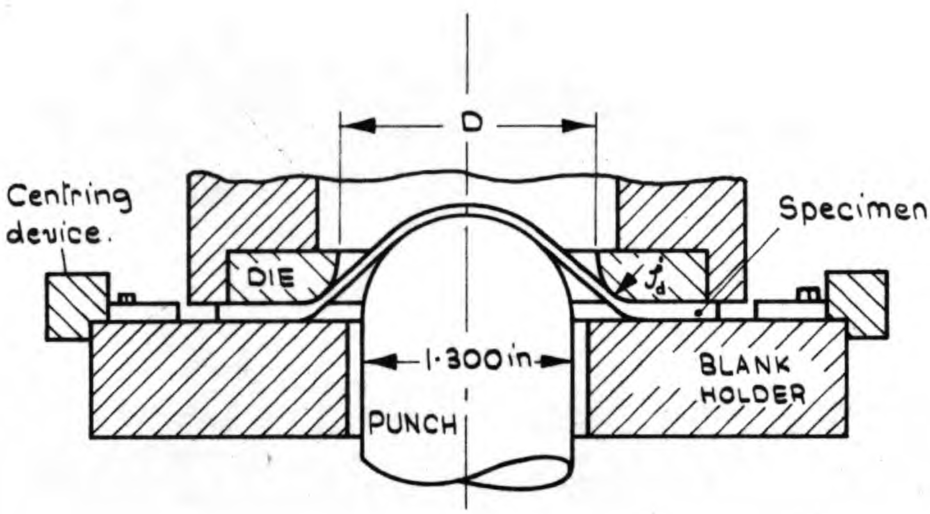

FIG. - 39. TOOLS FOR THE DEEP-DRAWING TEST.

They were polished to 6 C.L.A. figure smoothness. For tests with high coefficient of friction between sheet metal and punch, they were roughened by emergy paper to 45 C.L.A. figure.

Dies and blank-holder inserts of certain sizes, to give about 40% clearance between the sheet metal and the die for various thicknesses of sheet metal were made to the dimensions given in Fig.38. The serrations on them were produced in a similar way like the ones on the blank-holder in the Erichsen test.

In stretch forming, since circular specimens with 80 mm diameters were used, a centring tool with this internal diameter was made, which fitted on the round blank-holder without any play as shown in Fig.38. With this, the specimens with circular grids scribed on them, could be centered with an eccentricity less than 0.001 in.

In deep-drawing, the same punches were used as in stretch forming. A special blank-holder was designed and made which is shown in Fig.39. This has a movable ring at its rim which operates the three "fingers" which centre a round blank when put on the blank-holder plate, by a clockwise motion of the ring. The centring fingers retract, when the ring is turned in an anti-clockwise direction, leaving the centered blank in the middle, with less than

0.001 in eccentricity.

The deep-drawing dies were so designed that they left about 40% clearance on the original thickness of sheet metal in the die throat to prevent ironing. This, and the die profile radii for the dies were determined after a study of the results of Chung and Swift (18). The dies were draw polished to 6 C.L.A. figure to minimize metal pick-up.

CHAPTER 10 - EXPERIMENTAL PROCEDURE

In this Chapter, the experimental procedures along with the programme of experiments are presented for the Erichsen, stretch forming, and the deep-drawing tests.

10.1. Preparation of Specimens

The materials used in the experiments, with their specifications are presented in Table 8.1. These were provided in 6 ft. x 3 ft. sheets, and they were initially sheared into strips by a guillotine press. The small 80 Te blanking press was used to blank the circles required for the tests. Sizes which could not be obtained by using one of the available dies were obtained by turning down the oversize blanks in a lathe, with a plentiful supply of coolant to avoid raising the metal temperature. The edges of the blanks were smoothened by sand-paper.

For scribing, it was found sufficiently accurate to hold the specimens in the three-jaw chuck of a tool-room lathe, since on checking the scribed blanks in the MU-214-B, the Universal Measuring Machine, the scribed circles were found to be concentric with the outside edge of the blank to within 0.001 in. An alternative method which induces no eccentricity was given in section 9.2. Also as discussed in section 9.2, a width of between 0.0011 to 0.0015 in. was found to be satisfactory for the scribed lines, and this could be obtained by setting the movable weight of the scriber attachment to locations found by previous trial experiments for each material.

In the case of the steel blanks for the Erichsen test, which were tested first, the smallest circle scribed was 0.1 inch in diameter, each successive circle being increased by 0.2 inch in diameter. From the experience gained from carrying out the tests on steel, the non-ferrous metals were scribed with a finer mesh over the bulge where most of the stretching occurred, and with a coarser mesh over the flange as follows:

Diameter	0 to 0.8 inch,	0.1 inch	intervals in diameter.
"	0.8 " 2.0 " ,	0.2	" .
"	2.0 to Edge,	0.4	" .

For specimens used in stretch forming, the smallest circle was approximately 0.1 inch in diameter, and each successive circle was scribed with an 0.1 inch increment on its diameter. The deep-drawing specimens were scribed in a similar manner but for diameters greater than 1.4 inch, 0.2 inch increments were used for the successive circles.

For the deep-drawing specimens used in the determination of the coefficient of friction according to the method given in section 7.1, and other specimens used in trial tests, no scribing was necessary. The remainder were scribed on both sides.

Having scribed the grid, the radial distance between each circle being conditioned by the accuracy of the indexing mechanism of the lathe cross-slide, it was necessary to measure the grid accurately. This was done using the U-10, Co-ordinate Measuring Machine, a magnification of 25 times being found best for accuracy of measurement. Readings were taken to within 0.0001 inch up to a diameter of 0.4 inch, and to within 0.0005 inch for the larger diameters. In order to measure to within 0.0001 inch a scribed line of width 0.001 inch, special illumination was necessary, green and white light being used to illuminate each face of the groove and thus clearly defining its bottom and the edges.

To locate the centre of the scribed blank under the axis of the microscope, the circles in the objective lens of the microscope were aligned with those on the blank. To eliminate any possibility of error due to eccentricity, and also due to the limited travel of the co-ordinate table, the scribed circles were measured in one radial direction, and since they were mounted on the rotary table, this was turned 180^{o} and another set of measurements were taken. Hence diameters could be obtained very accurately.

The scribed specimens were then numbered, numbers being scribed in the rolling direction, and near the edge. They were cleaned and degreased using cotton wool soaked in acetone.

10.2. Testing

The programme of experiments and the testing procedures for the three tests are given below.

10.2.1. Erichsen Tests

Before beginning the programme proper, a number of tests were made with each material to determine realistic ranges for the various parameters, unscribed blanks being used. The blank-holder force, specimen thickness, size, and shape, selected lubrication, and cut-out sensitivity were determined for each thickness in each material to give minimum crack width (i.e. just letting light through).

To check the consistency of the lubrication, three identical blanks in each thickness and diameter were pressed. The results (Erichsen numbers) seldom differed by greater than 0.1 mm, and never by greater than 0.2 mm unless the cause was a material defect. This is generally within the accepted accuracy of the Erichsen number.

The electronic cut-out was sufficiently sensitive to detect the required craćk size in all materials and thicknesses except for the soft aluminium, S.W.G. 20. An incremental pressing procedure, in increments of 0.1 mm, had to be adopted for this material, until the desired crack was obtained. In the case of brass, it was difficult to obtain the required crack simply by relying on the electronic cut-out, because it happened too quickly for the machine to stop in time. However, a characteristic noise was heard and the depth indicator suddenly altered by approximately 0.2 mm after the crack had occurred, so that these signs could be used to establish the Erichsen number.

Exploratory tests with the rough blank-holder showed that the following loads could adequately indent the sheet: steel 3.8, brass 3.5, copper 3.5, aluminium 2 Te. Complete prevention of drawing-in was not obtained in the case of brass and copper at the loads shown above, as discussed in section 11.3.1.

On the basis of the results of the preliminary investigation with unscribed specimens, the following values of the variables were chosen, to be applied to each thickness:

Blank diameters (mm): 100, 75, 60, 41-43-45

Blank-holding loads:

Steel-0.4, 2.0 , 3.8, 3.8 with rough blank-holder.

Copper and brass - 0.4, 3.0, 3.5 with rough blank-holder.

Aluminium - 0.4, 2.0, 2.0 with rough blank-holder.

The specimens were prepared, scribed, measured, and cleaned as described previously. The graphite grease supplied by the Shell Oil Company and designated H.T.G.

grease, was applied uniformly over the specimen. The centring tool was set for the blank diameter being used and the sensitivity of the electronic cut-out set at the optimum point (as determined from the preliminary tests). The zero point of the punch was checked and the depth-indicator gauge set at zero. The specimen was then placed on the blank-holding plate between the stops of the centring tool and the die locked in position. Blank-holding load was applied gradually until the desired value was established. The speed control valve was set to give the minimum punch speed feasible ($\sim$0.05 mm/sec). The punch load was recorded at every 1 mm of penetration, since the speed was low enough for this to be done. The machine stopped automatically either at fracture or just before (at necking instability). If the machine stopped too soon it could be restarted to give a fracture of the desired appearance (light just passing).

Using the same procedure, unscribed specimens were tested to obtain punch load curves to be used in the calculation of the coefficient of friction operative over the flange of the specimen, in the Erichsen test.

10.2.2. Stretch Forming Tests

The stretch forming tests using the special rough die and blank-holder to reduce drawing-in to a minimum, were carried out to produce data to be directly compared with the theoretical results.

The experience from the Erichsen test was very useful in the determination of the ranges of the variables. However it was still necessary to find:

a) The blank-holder load for each material to obtain sufficient indentation of the sheet without causing premature fracture around the die throat.

b) To find the cut-out sensitivity to stop the machine just before fracture, for each material and thickness, which were slightly different from the ones for the Erichsen test.

c) To find a reasonably wide range of lubrication conditions over the punch head, to show its significant influence in stretch forming and to provide comparisons for the theoretical results.

Trial tests with unscribed and scribed specimens were carried out to determine the parameters required, which resulted in the following programme of the tests.

With the hemispherical and the ellipsoidal punches:
18 S.W.G. soft copper was tested under 3.5 Te blank-holder load, and the following lubrication conditions:

(i) 0.003 inch P.T.F.E. film used as lubricant between the sheet metal and punch head.

(ii) H.T.G. grease.

(iii) Dry punch surface roughened by sand paper.

With the hemispherical punch, using the H.T.G. grease as as the lubricant, the following materials were tested:

(i) 16 S.W.G. E.D.D.S. under 3.8 Te blank-holder load.

(ii) 18 S.W.G. soft brass under 3.5 Te blank-holder load.

(iii) 18 S.W.G. soft aluminium under 2.5 Te blank-holder load.

The tests under the above conditions were carried out till just before the onset of fracture (just before the occurrence of a hairline crack) over the bulge. Tests were also conducted exactly under the same conditions as above, except that these were stopped long before fracture occurred. This enabled to determine the strain development, and also to compare these with the corresponding theoretical results. These tests were stopped, such that the average strain over the bulge would be $\frac{1}{3}$ and $\frac{2}{3}$ of that at fracture, maintaining the same parameters and the conditions. Hence three tests, one up to just before fracture, the others to $\frac{2}{3}$ and $\frac{1}{3}$ of the average strain at fracture were carried out for each combination of parameters listed above. The data obtained from each test was also used in the determination of the coefficient of friction according to the method presented in section 7.2.

The specimens after having been scribed, measured, and cleaned, were then lubricated. H.T.G. grease was applied uniformly over the area of the specimen remaining inside the die bore. For P.T.F.E. lubrication, a round piece of P.T.F.E. film was cut out not exceeding the size of the die bore, and was placed at the top of the punch. For dry surfaces with no lubrication, punch and the specimen were cleaned with acetone.

The punch was set such that its top was about 0.002 in. lower than the peaks of the serrations on the blank-holder as was done in the Erichsen test with the rough blank-holder. This gap could be measured by a depth micrometer, and shims could be put under the punch to get the correct gap. Hence, when the sheet is indented by the blank-holder, it ~~will~~ would just touch the punch. The depth indicator was zeroed, and the electronic cut-out sensitivity was set to the optimum point as determined from the preliminary tests. The 80 mm diameter specimen (All had the same diameter.) was then placed inside the centring tool having the same bore (Fig.38), and the blank-holder load was gradually applied until the required value was established. The speed control valve was set to give the minimum punch speed feasible (~0.05 mm/sec). The punch load was recorded at intervals of 1 mm. The machine generally stopped just before the occurrence of fracture in the bulge. The tests, carried out to determine the development of the strains, were stopped long before nearing fracture, the depth of penetration of the punch having been determined by the preliminary trial tests.

10.2.3. Deep-Drawing Tests

The first series of the deep-drawing tests were carried out to find the Limiting Drawing Ratios (L.D.R.) for all the materials used. Hemispherical punch, and unscribed blanks lubricated with H.T.G. grease were used in the tests. Initially, for each material and thickness, one "increment" (0.025 of L.D.R.) oversize, and one increment undersize blanks, as predicted by the method presented in Chapter 12, were deep-drawn. In most cases the oversize blanks failed, and the undersize blanks drew. In others when this was not obtained, a new blank having a diameter half way in between was tried until L.D.R. could be established within one increment. This figure was found to lead to reproducible results by the previous researchers (86).

In deep-drawing, both sides of the blanks were lubricated by the H.T.G. grease. After checking that the top of the punch was level with the surface of the blank-holder plate, and zeroing the depth indicator, the speciment was put on the blank-holder plate (see Fig.39). It was centered by the three "fingers" actuated by a clockwise motion of the movable rim of the blank-holder. The fingers were then retracted. Using the manual controls of the testing machine, the specimen was deep-drawn at a punch speed of about 0.05 mm/sec. A blank-holding load of 0.2 Te was found to be sufficient to prevent wrinkling.

Having determined the L.D.R's for all the materials, second series of deep-drawing tests were started to determine the coefficient of friction operative in the flange according to the method outlined in section 7.1. For this, unscribed blanks having diameters smaller than the limiting ones were used. The blank-holder loads used with each material are given below:

Material	Blank-holder loads
E.D.D.S.	0.2 , 2.0 , 3.5
Soft Brass	0.2 , 2.0 , 3.5
Soft Copper	0.3 , 2.0 , 3.0
Soft Aluminium	0.3 , 1.5 , 2.5

The procedure in testing was the same as in the first series, except that three identical blanks under identical conditions were tested under the above blank-holder loads. Punch load versus punch penetration diagrams were obtained for each, at intervals of 1 mm punch penetration. Lubricants investigated were:

a) H.T.G. grease, and b) dry die, punch, and blank-holder surfaces with 45 C.L.A. figure roughness, with all the materials; c) P.T.F.E. lubrication was only applied to soft copper. For this circular pieces of a 0.003 inch thick P.T.F.E. film with the same diameter as the blank were put on either side of the blank.

The third series of deep-drawing tests were carried out with scribed specimens and H.T.G. grease lubrication. This was with the purpose of comparing the strain distributions just before the occurrence of fracture in deep-drawing with those in stretch forming. For these tests, blanks of one increment above the limiting blank sizes were used, so that fracture could be expected over the punch head. The scribed specimens were lubricated with the H.T.G. grease, and centred on the blank-holder plate as before. The electronic cut-off was set to the calibrated sensitivity to stop the machine just before fracture. Under a blank-holder load of 0.2 Te, blanks were drawn at a punch speed of 0.05 mm/sec. Since the drawing was stopped at the onset of fracture, a completely cylindrical cup was not obtained.

10.3. Measurements on Deformed Grid.

The plastically deformed, scribed specimens in the Erichsen, stretch forming, and deep-drawing tests were degreased and cleaned by acetone. It was found that U-10, Co-ordinate Measuring Machine (Fig.34) with 25 times magnification was again most satisfactory in measuring the distorted grid.

The specimen was put on the co-ordinate table such that the smallest circle of the scribed grid lined up with one of the circles in the objective lens of the microscope. The radii of the distorted circles were measured to 0.0001 inch. It was found that with materials that showed plastic anisotropy in the plane of the sheet, the initially scribed circles changed their shape during the deformation. Hence with E.D.D.S. and soft aluminium it was necessary to measure the grid in rolling, transverse and 45° directions. With copper and brass, since they were sufficiently isotropic, in the plane of the sheet, the grid was measured only in the rolling direction. Since the range of the measurement was limited by the travel of the micrometer screws, in each direction, two radial measurements starting from the centre were taken. The same procedure was applied in measuring the grid on the inner surface of the specimen. To illuminate the grid, white and green light beams at about 60° to each other, were used. It was found that at locations with steep slopes or heavy plastic deformation, only one beam could be used to identify the scribed line.

To determine the three plastic strains, it was also necessary to obtain the thickness distributions of the deformed specimens. This was effected by the rig described in section 9.3.4., and measurements to within 0.0001 inch could be made. Sometimes it was necessary to cut the specimen in a direction parallel to its meridional plane to reach some of the locations to be measured. The thickness measurements were taken in the same directions as the grid measurements.

CHAPTER 11 - EXPERIMENTAL DATA PROCESSING AND DISCUSSION OF RESULTS

This Chapter presents the derivation of the formulae, and the computer program used in the analysis of the experimental data. Experimental results obtained in the Erichsen, stretch forming, and deep-drawing tests, and also the coefficients of friction determined from the experimental data are discussed. The comparison of experiment with theory is presented in Chapter 13.

11.1. Derivation of Formulae

The derivation of the formulae is based on the basic plasticity theory, and the flow rules for anisotropic materials presented in Chapter 3.

The plastic strains were calculated using the data obtained from the measurements of initial and distorted grids, and the thickness distributions by the following formulae, whose derivations were given with eqns. (3.34):

Circumferential strain:

$$\varepsilon_2 = \ln \frac{r_m}{r_o} \tag{11.1}$$

Thickness strain:

$$\varepsilon_3 = \ln \frac{t_m}{t_o} \tag{11.2}$$

where the symbols have the previously assigned meansings.

Suffix "m" represents the arithmetic mean of the measurements taken in various directions as described before. Suffix "o" refers to the original dimensions.

Using equation (11.1), it is possible to find the circumferential strains on the outer, inner and mean surfaces of the specimens using the corresponding radii. ε_3 found from eqn. (11.2) is the average thickness strain through the thickness.

From the constancy of volume as expressed by eqn. (3.14), the meridional strain can be found.

$$\varepsilon_1 = -(\varepsilon_2 + \varepsilon_3) \tag{11.3}$$

From the knowledge of the development of plastic strain found by measurements taken at various stages of the deformation, it is possible to calculate the incremental, and hence the total equivalent plastic strain from one of the eqns. of (3.23). In cases where the straining takes place under stress ratios which do not vary significantly, the following equation for the equivalent plastic strain, found by replacing the incremental components of strain by total strain components can be used as an approximation:

$$\bar{\varepsilon} = \sqrt{\frac{2(2+R)}{3(1+2R)}}\left[(1+2R)(\varepsilon_1^{\,2} + \varepsilon_2^{\,2}) + (2R^2+R)\ \varepsilon_3^{\,2}\right]^{\frac{1}{2}} \tag{11.4}$$

To find the stress ratios between the principal stresses, plastic stress-strain relationships were used. Dividing two of the equations of (3.19) side by side:

$$\frac{d\varepsilon_2}{d\varepsilon_3} = \frac{x(R+1)-R-k}{2k - x - 1} \tag{11.5}$$

or using the total strains with some degree of approximation:

$$\frac{\varepsilon_2}{\varepsilon_3} = \frac{x(R+1)-R-k}{2k - x - 1} \tag{11.6}$$

and solving for x gives:

$$x = \frac{\varepsilon_2(2k-1) + \varepsilon_3(R+k)}{\varepsilon_2 + \varepsilon_3 \ (R+1)} \tag{11.7}$$

In eqn. (11.7), ε_2, ε_3 and R can be directly determined from the experimental results. An initial approximation for $k = \frac{\sigma_3}{\sigma_1}$ is necessary which could be the value belonging to the previous point on the bulge, either determined from previous calculations or from the boundary conditions. Now an improved value of k can be found from eqn. (3.30), which, for the purpose of the calculation can be written as:

$$k = - \frac{t}{2\rho_1{}'r'} (r + x \ \rho_1 \sin\theta) \tag{11.8}$$

This is the second equation of equilibrium.

The value of k found from eqn. (11.8) can then be used in eqn. (11.7) and the process can be repeated until no significant change in x or k is obtained. This usually is rapidly convergent. The value of x thus found would be approximate if the straining is not uniform. For more accurate results incremental strains should be used in eqn. (11.7) instead of the total strains.

In the determination of the coefficient of friction by the method presented in section 7.2, the value of x found from eqn. (11.7) was used in:

$$\mu = \frac{(1-x)\sin^2\theta}{(1+x)(\theta - \sin\theta\cos\theta)} \qquad \text{(repeated 7-18)}$$

This equation involved another assumption, i.e. $\frac{dp}{dr} = 0$. As explained in section 7.2, this and the use of eqn. (11.7) based on total strain theory, would hold true only at the pole of the bulge in stretch forming. Hence for points further away from the pole the error due to these two factors is expected to increase. To eliminate this error, μ for each point in region one was calculated, and plotted against θ. The extrapolation of this curve to $\theta = 0$ gave the correct value of μ within experimental accuracy.

Using the variables determined so far, it is then possible to determine the following:

(i) The equivalent stress ($\bar{\sigma}$) from the empirical relationship given by eqn. (3.48) using $\bar{\varepsilon}$,

(ii) The meridional stress (σ_1) from the yield criterion given by eqn. (3.18) using $\bar{\sigma}$, x, and k,

(iii) The circumferential stress from $\sigma_2 = x\sigma_1$.

(iv) The interfacial pressure p from eqn. (3.30) which can be expressed as $p = -2\sigma_1 k$.

The analysis of the experimental data using the above formulae and procedure was programmed for the Atlas computer as discussed in the following section.

11.2. Computer Program

The computer program was written for the Atlas computer in the EMA programming language. It processed the experimentally obtained data, e.g. grid, and thickness measurements, and produced the final results used in plotting the curves. It requires the following format for input:

1. Number of sets of data - integer.
2. Code for hemispherical or ellipsoidal punch - integer. Hemispherical: 10, Ellipsoidal: -10.
3. A in the empirical strain hardening law (psi)- decimal.
4. B " " " (dimensionless) - decimal.
5. n " " " " "
6. Radius of curvature (ρ_1') of the hemispherical punch or one of the semi-axes (a) of the ellipsoidal punch in inches - decimal.

7. The second semi-axis of ellipsoidal punch in inches - decimal.

8. Radius at the point of contact of sheet metal with punch, in inches - decimal.

9. Number of directions in which measurements were taken plus one - integer.

10. Number of measurements taken radially - integer.

11. Initial thickness of blank in inches - decimal.

12. Radial measurements of the grid on the outer surface of the specimen, in the following order.

$r_{o,1}$, $r_{o,2}$, $r_{L,1}$, $r_{L,2}$, $r_{T,1}$, $r_{T,2}$, $r_{45,1}$, $r_{45,2}$, $t_{L,1}$, $t_{L,2}$, $t_{T,1}$, $t_{T,2}$, $t_{45,1}$, $t_{45,2}$

....

where the symbols have the usual meanings, and the suffices are:

o - original dimensions

1 and 2 - measured radially out from the pole 180^{o} to each other along the same line, and on the same scribed circle.

L - in the rolling direction.

T - in the transverse direction.

45 - 45^{o} to the rolling direction.

Due to the limited scale of the co-ordinate table of the U-10, the grid measurements were taken from a convenient datum, so that (1.500 - above radii) inches were in fact replaced by the above data. The same convention applies to items 8 and 13.

13. Radial measurements of the grid on the inner surface of the specimen having the same format as the ones in item 12. Thickness measurements are omitted since they are the same as in item 12.

Wherever the grid measurements could not be obtained, the number "100" was inserted. Program could find the unknown value using the co-ordinate of either the known inner or outer grid and the local thickness with the assumption that the normal to an element of sheet metal before the deformation remains normal to the surface of the punch, which was later shown to be true by experiment (See Fig.47).

A print out of the computer program used to analyse the experimental data is presented in Appendix-E with explanatory comments ("≫" sign starts a comment). The "Chapter o" of the program reads the data prepared according to the format given above, punched on a paper tape. Since the grid measurements are (1.500 - radii) inches, the true radii are calculated by subtracting the measurements from 1.500. Then the arithmetic mean of the final radii and thickness are found and stored. The constants and parameters that appear in the formulae presented, are calculated.

In Chapter 1 of the program, the three principal strains, i.e. ε_1, ε_2, ε_3 are calculated using the eqn. (11.1), (11.2), and (11.3). The equivalent plastic strain based on the total strain theory is computed by eqn. (11.4), and the stress ratios by eqns. (11.7) and (11.8) with the iterative method presented in section 11.1.

The program then calculates $\bar{\sigma}$, σ_1, σ_2, p and μ according to the method described in section 11.1 and the steps (i) to (iv) given therein.

The program prints out the results according to the following format. For every point located on a scribed circle in a radial direction:

1. Mean radius of the scribed circle on the outer surface of the specimen before the plastic deformation - inches.
2. Circumferential strain for the outer surface of the specimen - logarithmic.
3. Mean radius of the scribed circle on the inner surface of the specimen before the plastic deformation - inches.
4. Circumferential strain for the inner surface of the specimen - logarithmic.
5. Mean radius, corresponding to the middle surface of the specimen before deformation - inches.
6. Mean circumferential strain corresponding to the middle surface of the specimen - logarithmic.

7. Thickness strain - logarithmic.
8. Meridional strain - logarithmic.
9. Equivalent strain.
10. Stress ratio - x.
11. Stress ratio - k.
12. Equivalent stress - psi.
13. Meridional stress - psi.
14. Circumferential stress - psi.
15. Mean radius of the scribed circle on the outer surface of the specimen after the plastic deformation - inches.
16. Mean radius of the scribed circle on the inner surface of the specimen after the plastic deformation.
17. Mean radius corresponding to the middle surface of the specimen after the plastic deformation.
18. Angle θ, normal to an element of sheet metal makes with the vertical axis - degrees.
19. Interfacial pressure p - psi.
20. The approximation to the coefficient of friction (μ) used in the extrapolation technique.

11.3. Discussion of Results

The bulk of the experimental and theoretical results are presented in the forms of curves and tables in Volume II of the thesis. They will be referred to by Figure and Table numbers in the following discussions.

11.3.1. Erichsen Test

Erichsen numbers obtained were plotted against blank diameter (or strip width), since this variable had most effect. Typical results are shown in Figs. 40 and 41 for soft copper and E.D.D.S. It is seen that the rate of increase of Erichsen number increases by decreasing blank diameters, and the curves tend to infinity around 40 mm blank diameter. The curves also show that the effect of the blank-holder load is less significant but not negligible. Comparing the curves obtained with and without the use of the rough blank-holder, it is seen that appreciable drawing-in takes place over the die especially in the case of copper (Fig.40). However, as will be discussed later, serrated blank holder and die surfaces do not completely eliminate the drawing-in, but can reduce it to a minimum. Hence, if the generally desired accuracy of 0.2 mm on the Erichsen number is to be attained, a careful specification of the test conditions would be necessary.

Typical distributions of circumferential strains are shown in Figs. 42-44. The maximum values are reached away from the pole and near the locations of the fractures. It is observed that the outer fibres of the metal undergo larger strains in the stretch forming zone due to superimposed bending onto stretching.

In the area where the material is in contact with the die curvature there is an inward plastic flow expressed by the negative circumferential strain. This is more for the fibres facing the blank-holder due to the superimposed plastic bending. From the radius 0.65 inches (die bore) onwards, the inner and outer circumferential strains are the same due to the absence of bending. In Fig.42, the effectiveness of the serrated blank-holder is seen in stopping all the drawing-in with E.D.D.S. This was not completely achieved with the non-ferrous materials as typically illustrated in the case of brass in Fig.44. The same figures show that the effect of altering the blank-holder load over a wide range is less significant.

Typical results showing the distributions of thickness strain are presented in Fig.45 for the four materials tested. The curves follow very closely the same pattern and the thinnest zone of the bulge is where the fracture occurs. This is away from the pole due to the friction between the punch and the sheet metal.

A secondary peak occurs, where the material is in contact with the die curvature. This is due to thinning under plastic bending under tension. It is seen that no thinning occurs in the flange of the specimens.

Fig.46 shows typical punch load versus punch travel curves for various thicknesses of brass specimens, under different blank-holder loads. It is seen that under identical conditions, tests carried out at higher blank-holder loads produce higher punch loads for the same punch travel, due to the additional frictional forces induced between the die, blank-holder and the sheet metal. This information is used in the determination of the coefficient of friction according to the method presented in section 7.1. The areas under the curves represent the energy required to produce the plastic deformation.

The actual final disposition of elements in the sheet over the bulge was determined. It was found that line elements originally normal to the plane of the sheet were finally substantially normal to the surface of the punch. This is illustrated typically, for copper in Fig.47. This knowledge is used in finding the circumferential strains on the inner and outer surfaces of a bulge when the circumferential strain in the middle surface together with the shell thickness are known. Calculations of the circumferential strains on the outer and inner surfaces were effected this way in obtaining the theoretical results in stretch forming. Due to slight inaccuracies obtained in the extrapolation of these short line elements towards the centre of curvature of the punch, an "envelope" which bounds the centres of bending of the elements is obtained in Fig.47, instead of a single centre.

The only way of exhibiting the variation of Erichsen number that occurs in the tests is to define a measure of the drawing-in and to plot Erichsen number against this variable. This can be done because, for a given amount of stretching on the onset of fracture, the Erichsen number depends only on the amount of drawing-in that takes place. A suitable quantity to define drawing-in is the circumferential strain that occurs at the inside diameter or bore of the blank-holder. In Figs. 48-51, Erichsen numbers and the corresponding blank-diameters are plotted against drawing-in as defined above. It is clearly seen that drawing-in significantly contributes to the variation of the Erichsen number.

The curves show that the rough blank-holder prevents drawing-in almost completely for steel and aluminium, and that the Erichsen number attains a minimum value in such circumstances. Drawing-in can apparently never be completely prevented without the use of a rough blank-holder, because with a smooth blank-holder the curves of blank diameter against drawing-in are not asymptotic to the zero axis. Higher blank-holder loads do have some effect in reducing drawing-in, but roughening the surface of the blank-holder, is clearly much more effective. Drawing-in, in the case of copper and brass could not be prevented by the rough blank-holder used as seen in Figs. 49, and 50. Later, experiments carried out by

Yokai[*] with rough die, and blank-holder surfaces showed that still it was not possible to prevent drawing-in completely with the non-ferrous materials. The following values of the circumferential strains at the bore of the blank-holder were the minimum ones attained:

Copper :	- 0.005
Brass :	- 0.004
Aluminium :	- 0.0015

Since most of the non-ferrous materials have a low yield stress in shear, this may not have been sufficient to support the radial load in the vicinity of the bore of the blank-holder. Also, since the material around the die curvature undergoes plastic bending under tension, and a consequent thinning, the material in this area tends to pull away from the serrations of the blank-holder. For these reasons it seems that it is not possible to prevent drawing-in completely. Nevertheless much can be gained by the use of serrated die and blank-holder surfaces in the way of reducing scatter in the determination of the Erichsen number in comparison to when smooth surfaces are used with not carefully specified blank-holder loads.

---

* The author thanks Mr.M.Yokai for his permission to quote some of his results which appear in his dissertation for the Diploma of Imperial College, 1965.

A correlation between round and strip specimens may be established on the basis of their giving the same Erichsen number. The results, plotted as strip width against blank diameter, are given in Fig.52. Between 75 and 100 mm, strip width and blank diameter were equivalent for steel, copper, and aluminium within an accuracy of 0.1 mm in Erichsen number. Thus a strip of 16 S.W.G. copper, 80 mm wide, would give the same Erichsen number as a round blank of 80 mm diameter. This is certainly not true for brass. Much larger size of blank must be used in order to obtain the same Erichsen number with a strip specimen. This is because, the round specimen suffers more drawing-in than the brass strip specimen. This difference in behaviour is connected with the differences in stress-strain properties of the materials considered. Reference to Table 8.2 shows that brass with $n = 0.437$, strain-hardens at a higher rate than the other materials. The rate of strain-hardening has an effect on the location of the elastic-plastic boundary in the flat flange of the specimen, between the die and the blank-holder. When the material in the vicinity of the die curvature plastically deforms, i.e. thins or thickens, it strain hardens and thus carries the increased load imposed on it. It also transmits this load to the neighbouring element. An element of material with a high rate of strain-hardening characteristic deforms to a smaller extent to carry the same load. Hence for a given amount of plastic deformation say at the bore of the blank-holder, the elastic-plastic boundary is expected to move further away from the centre for materials with a high rate of strain-hardening. This would be the case for brass specimens. Hence the size and shape of the blank becomes more important, and if a strip is used which imposes more restraint due to the large areas of material remaining elastic on both sides of the indentation, the elastic-plastic boundary will move towards the centre of indentation with less contribution to drawing-in which results in a lower Erichsen number. The distribution of circumferential strains in the flange of the specimen in Figs. 42 and 44 support this view. The same size brass blank suffers more deformation in the flange than a steel blank, and hence the elastic-plastic boundary is further away making the Erichsen number more sensitive to the size and shape of the blank used.

The lubrication in all the tests was constant and the H.T.G. grease was used as recommended in D.I.N.50101. However, a few exploratory tests were carried out using a 0.003 in. P.T.F.E. film. This resulted in a higher Erichsen number, approximately 2 mm higher than that obtained by the H.T.G. grease. There was an appreciable increase in the general thinning of the material over the punch and the fracture took place near the pole due to the decreased coefficient of friction.

Table 11.1 shows the necking and fracture in Erichsen test. It is observed that, although E.D.D.S. and soft aluminium have nearly all round-isotropic fractures, they show significant planar plastic anisotropy as seen from Figs. 21, 24, 25 and 28 which result in appreciable earing in deep-drawing as shown in Table 11.3.

11.3.2. Stretch Forming

Fig.53 shows the specimens, stretch formed by hemispherical and ellipsoidal punches under various lubrication conditions. The stage of plastic deformation reached is that just before the onset of fracture. The distorted grid and the indentations of the die to prevent drawing-in are slightly visible. It is seen that the location of severe necking is significantly dependent on the lubrication conditions. It moves further away from the pole as friction increases. Typical examples being the soft copper specimens one lubricated with a P.T.F.E. film where the necking is very near the pole, the other deformed by a dry and roughened punch, where the location of necking is the furthest away from the pole. For the same material and punch geometry, the bulge depth decreases with increased friction due to less general thinning over the punch. This will be more apparent in the study of the distribution of strains over the bulge in the following sections.

Figs. 54-57 show the distributions of mean true circumferential strain in stretch forming, by the hemispherical punch under H.T.G. grease lubrication. The materials are soft copper, brass, aluminium and E.D.D.S. respectively. To illustrate the development of strain, three stages are shown, the last corresponding to the state just before the onset of fracture. The results for the first and second stages were obtained by using different specimens, prepared and tested under the same conditions. These tests were stopped before fracture to give suitable intervals in general straining. It was found that stretch forming a specimen up to an arbitrary stage before fracture, and taking the necessary measurements and lubricating it again, and then stretch forming it to fracture did not give the same results as in stretch forming a specimen to fracture in one stage. This was due to a lubrication effect and in the former case the relubrication substantially lowered the coefficient of friction which resulted in a deeper and thinner bulge.

A study of the Figs. 54-57 shows that some drawing-in takes place despite the grip of the serrated die and blank-holder surfaces. This can be explained in a similar way as in the case of the Erichsen test, i.e. the shear stresses induced here exceed the yield stresses of the materials in shear; and the materials tend to pull away from the serrations on the blank-holder due to thinning under bending under tension around the die curvature. Fig.62, which will be referred to later, shows that - in support of the above points - the circumferential strain at the clamped periphery on the surface facing the die is zero. Hence at this boundary the material is rotating inwards with respect to a centre at the die corner. Therefore the resultant drawing-in near the clamped periphery depends on the amount of such rotation against the amount of stretching outwards. Since the mean surface of the specimen rotates more than it stretches in the early stages of deformation, the zero and negative circumferential strains are reached at a radius nearer to the pole, than at later stages when more stretching takes place.

In Figs. 54-57, it is observed that the circumferential strains for the first two stages smoothly decrease after an increase. However, for the last stage, this is not the case, and a secondary peak forms in the location where the fracture occurs. This is due to the additional local stretching before fracture.

It may be noted that the tangents to the curves have zero slopes at the pole, supporting the theoretical considerations in section 3.2.3.1.

Figs. 58 and 59 show the distributions of circumferential strains in stretch forming of soft copper by the hemispherical punch using (i) a P.T.F.E. film as lubricant, and (ii) dry and rough punch surface, respectively. It is seen that friction has a very significant influence over the undergoing plastic deformation and the limiting strain before fracture. In the case of the P.T.F.E. lubrication, the average level of the circumferential strain is more than twice as high as that obtained with the H.T.G. grease lubrication. On the other hand, with the dry and rough punch surface, results are about one half of the circumferential strains achieved in the case of the H.T.G. grease lubrication. Also the location of severe necking moves out with increased friction.

Figs. 60 and 61 show the circumferential strains developed, in stretch forming by the ellipsoidal punch. The lubricants used were the H.T.G. grease, and P.T.F.E. film with 18 S.W.G. copper. The trends observed are the same as in stretch forming with the hemispherical punch, but the rates of increase and decrease of the strains are higher due to the increased curvature of the particular ellipsoidal punch used. The peak strains reached, with the ellipsoidal punch are higher than the corresponding ones obtained by the hemispherical punch. This is because, the location of necking is nearer to the pole with the ellipsoidal punch, which implies that necking takes place at a stress ratio nearer to unity, which results in higher strains according to the criteria of plastic instability discussed in Chapter 4.

A typical distribution of the surface circumferential strains is presented in Fig.62 for 18 S.W.G. soft copper, stretch formed by the hemispherical punch, under P.T.F.E. film lubrication. Two stages of straining are shown. In the first stage the differences between circumferential strains on the inner and outer surfaces of the specimen are greater due to the larger thickness. This difference gets less as the specimen deforms more, and gets thinner.

It is also observed that there is no drawing-in on the outer surface at the clamped periphery. On the contrary, there is appreciable drawing-in on the inner surface for reasons already discussed at the beginning of this section.

Figs. 63-70 show the distributions of true thickness strains in stretch forming, corresponding to the cases for which the circumferential strains were presented. Here again, the development of thickness strains are shown in three stages, last one corresponding to that just before the onset of fracture. Figs. 63-66 give the strain distributions for soft copper, brass, aluminium, and E.D.D.S., lubricated by the H.T.G. grease and deformed by the hemispherical punch. In these figures, the developments of strain follow similar trends. The location of maximum thinning in the first stage, gradually moves away from the pole in the further stages. This indicates that there is considerable friction between the sheet and the punch. The frictional force carries part of the load tangential to the punch surface, induced by the plastic deformation of the sheet, and hence prevents to some extent, the thinning of the region over the punch head.

It is observed that the slopes of the curves are zero at the pole, as was shown in section 3.2.3.1, in determining the boundary conditions. In the third stage of the deformation, the point with maximum thinning is the seat of eventual fracture. Comparing this stage with the previous ones it is seen that the thinning in this zone develops rather rapidly, and there is a considerable amount of local plastic deformation just before the onset of fracture.

In Figs. 63-66, for the four different materials with fairly varied basic mechanical properties, namely n, B, A and R, one does not get a similar variation in e.g. maximum thinning, or circumferential strains. The reasons will be discussed later in this Chapter and also in Chapter 13, when comparing these results with the theory.

Figs. 67 and 68 show the thickness strain distributions for soft copper, stretch formed by hemispherical punch under P.T.F.E. lubrication, and with dry and rough punch surface respectively. It is clearly seen when comparing these two figures with the previous ones, that friction is the most significant variable in stretch forming. In the case of the P.T.F.E. lubrication where the coefficient of friction is a minimum, there is considerable general thinning and the location of severe necking is the nearest to the pole. On the other hand, with a dry and slightly roughened punch surface, there is little general thinning, and the location of necking is the furthest away from the pole. In the latter, the polar strains are much less, since most of the induced load is carried by the frictional force, and hence the polar region is protected from severe thinning.

In obtaining the results of Figs. 69 and 70, the ellipsoidal punch was used in the stretch forming of soft copper under H.T.G. grease, and P.T.F.E. lubrication, respectively. Here again the main features are that the levels of general thinning and maximum thinning strains are higher for the P.T.F.E. lubrication. Also the location of necking is nearer to the pole due to decreased friction. The main difference between this and the thickness strains produced by the hemispherical punch is that, here the slopes of the curves are steeper due to the increased curvature of the ellipsoidal punch.

Figs. 71-78 show the distributions of meridional strains corresponding to the cases for which the circumferential and thickness strains were presented before. They in effect, represent the "extensions" of the elements on the bulge, in the meridional direction.

With the increasing radial co-ordinate, meridional strain increases till a maximum is reached. After the maximum, it decreases at a faster rate than its rate of increase. Most of the zone where the decrease takes place, lies in region two.

In Figs. 71-74, for soft copper, brass, aluminium and E.D.D.S. stretch formed by the hemispherical punch under H.T.G. grease lubrication, the distribution of the strains and their maximums do not again vary, nearly in the same ratios as the basic parameters of the materials do. This will be discussed in connection with plastic instability later in this Chapter and also in Chapter 13. However, it is observed that the maximum meridional strain is reached at the location which is the seat of eventual fracture.

The significance of friction is illustrated in

Figs. 75 and 76, where the meridional strains were obtained in stretch forming copper by the hemispherical punch under P.T.F.E. lubrication, and secondly using a dry and rough punch surface. Under P.T.F.E. lubrication where the friction between the sheet and punch is much less than in the latter case, more extension is suffered by every element on the bulge. The location of maximum meridional strain is closer to the pole, also due to the decreased friction.

As illustrated in Figs. 77 and 78, the trends in meridional strains when using the ellipsoidal punch are in general the same as those with the hemispherical punch with the exception that the slopes of the curves are steeper due to the increased curvature of the particular ellipsoidal punch used.

Figs. 79 and 80 present the distributions of equivalent plastic strain for soft copper in stretch forming by the hemispherical punch under H.T.G. grease and P.T.F.E. lubrication respectively. These strains were calculated using the formula (11.4), based on the total strain theory. They are presented for the purpose of comparing them with the theoretical distributions of the equivalent plastic strain, calculated using the incremental theory, taking into account the strain history. The experimental curves clearly show that the equivalent strain of any element on the bulge, is not too different than the absolute value of the thickness strain, the difference being generally within 10%. In a balanced biaxial stress system for isotropic materials the absolute value of the thickness strain is numerically equal to the equivalent plastic strain, as can be seen from eqn. (3.23). However, for the conditions of the tests in Figs. 79 and 80, i.e. plastic anisotropy, slight triaxiality in the stress system, and the planar stress ratio varying from 1.1 to 0.4, the thickness strain still remains the closest in absolute value to the equivalent plastic strain. The figures illustrate the effect of varying frictional conditions for the same material, on equivalent strain, i.e. with reduced friction higher average and peak equivalent strains are achieved, and the location of the peak is nearer to the pole.

Figs. 81 and 82 show the distributions of equivalent stress in stretch forming copper, by the hemispherical punch under H.T.G. grease and P.T.F.E. film lubrication. These curves were obtained by using the equivalent strains presented in Figs. 79 and 80 in eqn. (3.48). Hence they closely follow the pattern followed by the equivalent plastic strains, and therefore most of the discussion for Figs. 79 and 80 also applies here.

The distributions of the meridional stresses are presented in Figs. 83 and 84 for soft copper stretch formed by hemispherical punch under H.T.G. grease, and P.T.F.E. lubrication. It is observed that under P.T.F.E. lubrication, the general level of stress reached is much higher, although the peak stress is about the same as that in the case of H.T.G. grease lubrication. With the H.T.G. grease lubrication, the more localized and highly stressed zone is further away from the pole which becomes the eventual seat of fracture.

Figs. 85 and 86 show that, unlike meridional stresses, the distribution of circumferential stress is not significantly dependent on friction. Generally, at all stages of deformation, the maximum is very near or at the pole. This can be explained by a study of the distribution of the stress ratios for the same conditions.

Figs. 87 and 88 show the distributions of the stress ratios computed using eqn. (11.7) which is derived from the total strain theory, and hence should be regarded as approximate. They were obtained with the view of comparing them with the theoretical results obtained from the incremental strain theory, but the following discussion still applies. It is observed that the stress ratio decreases steadily with the increasing radial co-ordinate, starting from a value near unity.

The decrease is faster in the case of the H.T.G. grease lubrication compared to the P.T.F.E. lubrication. If the straining were proportional, the distributions of the stress ratios for the three stages in each Figure would be identical. Since $\sigma_2 = x\sigma_1$:

$$\frac{d\sigma_2}{dr} = \frac{dx}{dr} + \frac{d\sigma_1}{dr} .$$

Hence it should be noted that the rate of change of the circumferential stress depends on the rates of changes of the stress ratio and the meridional stress. As seen in Figs. 85 and 86, maximum in σ_2 may not coincide with the seat of eventual fracture.

Figs. 89 and 90 show the distributions of interfacial pressure between the hemispherical punch and the sheet, for soft copper under H.T.G. grease and P.T.F.E. film lubrication. It is observed that there is variation of pressure at all stages as a function of the radial co-ordinate. Hence any theoretical solution with the assumption of constant pressure over the bulge would not be sufficiently general and realistic.

In Fig.89, it is seen that, in the vicinity of the eventual seat of fracture under the H.T.G. grease lubrication, the pressure for the third stage drops quite considerably even below that of the second stage. In Fig.90, where the bulge suffers even more thinning, the pressure for most of the third stage is below that of in first stage. This clearly indicates that, maximum pressure cannot be a satisfactory criterion for plastic instability or fracture in stretch forming as was also shown in Chapter 4.

It is also worth noting that for coefficients of friction of up to unity, the shear stresses between the punch and the sheet will remain well less than the yield stresses in shear of the materials. For instance in the case of soft copper the highest interfacial pressure is about 4500 psi, whereas with reference to Fig.23, its yield stress in shear is at least 7000 psi. Hence the shear stresses could not reach their limiting values under the conditions of these experiments.

Figs. 91-93 contain the punch load diagrams obtained for the various materials using the hemispherical and the ellipsoidal punches in stretch forming. In Fig.91, the diagrams for soft copper under H.T.G. grease and P.T.F.E. film lubrication are shown. It is observed that with H.T.G. grease lubrication, for the same punch load less punch travel is obtained, compared to that with P.T.F.E. lubrication. This is due to the higher level of thinning over the punch head with the P.T.F.E. lubrication.

In the same Figure, the punch load diagram for soft copper, stretch formed by the ellipsoidal punch under

P.T.F.E. film lubrication is shown. Comparing this curve with the corresponding one obtained by the hemispherical punch, it is seen that for the same punch travel the punch load for the former is much less. This is mainly due to the smaller value of r at the moving boundary, where sheet metal contacts the punch, and as can be seen by a study of eqn. (3.49), this results in a smaller punch load.

The values of punch loads for different materials are influenced, to a great extent, by their basic material characteristics, i.e. A, B, and n. This phenomenon is apparent in Figs. 92, and 93 for E.D.D.S., soft brass and aluminium.

In most cases, there were no decisive maximums in the punch load diagrams just before the onset of fracture. The explanation for this cannot be very simple, since it depends on the complicated interactions of the variables in eqn. (3.49), as will be discussed in Chapter 13.

In relation to the experimental findings in stretch forming, reported above, one can deduce the following conclusions for the effects of the variables on plastic instability - the state of plastic deformation reached, just before the onset of fracture.

From a study of the results, it is clearly seen that the most significant variable is the friction between the sheet and the punch surface. Increased friction results in less general thinning, and moves the seat of fracture further away from the pole. This is because, the frictional force carries a greater portion of the tangential load induced by the plastic deformation, and hence leaves less load to be carried by the meridional stresses in the material. This in turn, results in the deformation of the material over the punch head to a lesser extent, as compared to the case with less friction. It is observed that the peak value of the thinning strain decreases as friction increases. This would be the case if the plastic instability obeyed the ML criterion as discussed in Chapter 4. With decreased friction, the location of fracture would be nearer to the pole, and it would therefore be taking place at a greater value of x resulting in a higher thinning strain. For the other criteria of instability, it is difficult to show this analytically, and the numerical results in support of this view will be discussed in Chapter 13.

The effects of the variations of the basic material parameters, namely n, B, A, and R, on the thinning strain at plastic instability are very much less than the variations in the parameters themselves for the different materials. That is to say, e.g. if n varies by a factor of two, the variation in the thinning strain at plastic instability will be much less than the factor of two.

Since all the materials were in the soft, annealed condition the constant B was very small in value as can be seen from Table 8.2.

It is therefore difficult to be able to assess its significance from the results presented, but from a study of the criteria of instability in Chapter 4, one can say that an increase in B would decrease the thinning strain at plastic instability in stretch forming.

From studies of results presented, and others not contained in this thesis, it was observed that parameter A influenced the magnitude of the stresses at instability and not the magnitude of the strains.

It is difficult to separate the effects of n and R unless one carries tests on materials which have identical parameters, including friction, except one of the above two. Studying Figs. 63-66, and bearing in mind that although the same lubricant (H.T.G. grease) is used with the different materials, it is not expected to produce the same coefficient of friction, as is shown in section 11.3.4., one can reach the following conclusions:

Comparing Figs. 63 and 64 for copper with $n = 0.37$, $R = 0.8$, and brass with $n = 0.43$, $R = 0.85$, the magnitudes of the peak strains are about the same, but for brass the instability occurs at a slightly greater radius.

From the evidence of Chapter 4, supposing that the magnitude of the thinning strain at plastic instability increases with an increase in n, it is then possible to say that an increase in the magnitude of R decreases the thinning strain at instability. This is more obvious in the case of aluminium (see Fig.65) which has, n = 0.253, and R = 0.55. Here compared to copper, the decrease in n would have reduced the magnitude of the thinning strain at plastic instability if the two R's were the same, but due to the decreased value of R for aluminium, the resulting thinning strain is nearly equal to that for copper. It is more difficult to draw such conclusions in the case of E.D.D.S. because of its more complicated plastic anisotropy in the plane of its sheet, and also due to its higher thickness (16 S.W.G.), which is likely to increase the thinning strain at plastic instability (see Chapter 4, for effect of k on ML instability).

As referred to in section 1.2, a systematic experimental investigation into stretch forming was reported by Keeler and Backofen (50). The authors studied stretch forming under Teflon lubrication, and dry surfaces. They adopted an incremental deformation method, and at each stage their specimens were lubricated after taking the grid measurements. This method of lubrication, in the present author's opinion, would have decreased the friction further compared to the case of lubricating the specimen once at the beginning. Comparing their results, with those obtained using the P.T.F.E. film lubrication in this work, it seems that P.T.F.E. is a much better lubricant, since the location of fracture as a percentage of punch radius is about 38% in the present work, but it is 62% in theirs. The peak thinning strains that the authors obtained with various materials remained nearly constant at about -0.055. In the present work the range was -0.60 to -0.80, which seems close enough considering the possible differences in material parameters and friction. Although no values for the strain-hardening exponent "n" were given in their paper, the authors supported the view that, increases both in n and R-values extended the stretching limits of the materials. The present author does not subscribe to the view that an increase in the R-value would increase the stretching limit, as discussed earlier in this section. Most of the R-values reported by Keeler and Backofen ranged from 0.81 to 0.93 except for steel which had 1.56. The levels of general straining, and peak thinning strains reached with these materials were certainly not in the order of their R-values, e.g. steel with R = 1.56 seemed to have strained to a lesser extent than aluminium with R = 0.81 (the minimum of all).

It is therefore difficult to see how the authors reached the aforesaid conclusion.

11.3.3. Deep-Drawing

The limiting blank sizes which could be drawn without any failure are presented in Table 11.2, together with the diameters of the oversize and undersize blanks. The limiting drawing ratios (L.D.R.) with respect to the punch and mean wall diameters of the cups are also contained in the same table.

A study of the L.D.R's with respect to the punch diameter, considering the average of the L.D.R's belonging to the different thicknesses for the same material give the following rating of the materials, in an ascending order of performance, as far as the L.D.R. is concerned:

(i) Aluminium (ii) E.D.D.S. (iii) Copper (iv) Brass

A similar study based on the L.D.R. with respect to the mean wall diameter, also resulted in the same order of classification, although the increments between the average L.D.R's of the materials were slightly different from the previous case.

This rating of the sheets agrees well with the variation in the n, and R-values of the materials. Referring to Table 8.2, it is seen that L.D.R. for the materials under consideration, increases with increase in the value of n. From a study of Figs. 25-28, it is also observed that L.D.R. increases with increase in the magnitude of the R-value, except in the case of E.D.D.S. The method of choosing the representative R-value might have a bearing on this point for materials such as E.D.D.S., if the R-value varies as a function of direction in the plane of the sheet. For E.D.D.S., if, say the minimum value, rather than the arithmetic mean of those in different directions was used, one would get the expected rating. Another independent evidence, as discussed in Chapter 13, also favours the using of the minimum R-value, as the representative or effective R-value, compared to the use of the arithmetic mean.

In deep-drawing, high n, and R values are desirable, since they increase the L.D.R. as discussed above. With a high value of n, the critical stress and strain levels before fracture which generally takes place over the punch head are increased. At the same time, the radial load induced by the plastic deformation over the die surface increases, but at a smaller rate than the load carrying capacity of the stretch forming region, hence resulting with a net increase in the L.D.R.

The advantage of having a high R-value was shown by Whiteley et al (93). In deep-drawing a high R-value provides more resistance to thinning over the punch head, and thereby increases the load carrying capacity of this region. On the other hand, in the radial drawing region, it similarly reduces the thickening of the flange, hence reducing the punch load. Therefore this combined effect increases the L.D.R. in the case of a material with a high R-value.

In the previous section it was shown that a low R-value is more desirable to have to extend the streching limit in stretch forming, contrary to its effect in deep-drawing.

The rating of the various gauges of the materials presented in Table 11.2, on the basis of their L.D.R's with respect to punch diameter, and mean wall diameter do not produce the same classification. It seems that maximum differences between the results of the two criteria are within three increments; whereas one increment is generally thought to indicate a significant change in L.D.R. in using any one of the criteria.

The photographs of the deep-drawn specimens from the oversize blanks, whose dimensions are given in Table 11.2, are presented in Fig.94. It is seen that fracture or severe necking took place in all cases away from the pole, and in an isotropic, all-round fashion. This is in contrast to the waves shown in the flanges of the E.D.D.S. and the aluminium specimens, due to the planar plastic anisotropy. Therefore, considering the appearance of fracture and necking in deep-drawing, stretch forming and the Erichsen tests, and also the ears obtained in deep-drawing using the same materials, it becomes obvious that one cannot assess the planar anisotropy of the sheet by judging the appearance of the fracture in a stretch forming test.

In Fig.94, the directions of the peaks of the waves for E.D.D.S. and aluminium, correspond to the directions of the maximum R-value in the plane of the sheet as expected. In the case of soft brass and copper, their planar isotropy is confirmed by the round shape of the flanges of the specimens.

Also, one increment undersize blanks were deep-drawn to form hemispherical ended cups to calculate the percentage earing. The results are presented in Table 11.3. It is seen that, in line with the previous results, E.D.D.S. and aluminium show considerable planar plastic anisotropy.

The distributions of the three principal plastic strains are presented in Figs. 95-100 for the four materials, deep-drawn by the hemispherical punch, under H.T.G. grease lubrication. One increment oversize blanks were used, and the tests were carried out up to the state just before the onset of fracture. In the case of brass, fracture occurred, but measurements were taken in a direction to avoid the fracture area.

The distributions of the three principal plastic strains over the punch head in deep-drawing follow a very similar pattern to those obtained in stretch forming. The differences between the corresponding strains in deep-drawing and stretch forming are within the bounds of possible experimental variations. The only definite trend observed is that in all cases the locations of severe necking in deep-drawing are about 10 to 20% further away from the pole compared to those in stretch forming. This is clearly related to the drawing-in, since all of the material properties, and friction are the same in the corresponding tests. With the additional drawing-in in deep-drawing, the same punch load and the load tangential to the middle surface of the sheet are reached at a higher bulge depth or at a larger angle of embrace on the punch, with the result of moving the location of severe necking further out from the pole.

Most of the discussion for stretch forming also applies for the region over the punch head in deep-drawing.

Figs. 95 and 96 show that considerable compressive circumferential strain is suffered in the flanges of the specimens. If the undersize blanks were deep-drawn resulting in full cylindrical cups, the curves for circumferential strain would steadily decrease (in the algebraic sense), instead of curving up due to the partial deep-drawing of the specimen. From Figs.97 and 98 it is observed that appreciable amount of thickening takes place in the flanges of the specimens. Figs. 99 and 100 indicate that the meridional or radial strains are tensile in the flanges of the specimens.

Figs. 91-93 contain the punch load diagrams obtained in deep-drawing. It is clearly seen that, in deep-drawing, for the same punch load, much greater depth of bulge is obtained compared to that in stretch forming. Most of the difference is due to the contribution from drawing-in, in deep-drawing.

It is also observed that unlike those in stretch forming, in deep-drawing of oversize blanks, there are decisive maximums in the punch load curves, and the values of punch loads at these maximums are greater than the highest loads obtained in stretch forming. This is due to the fact that in deep-drawing the angle of embrace on the punch and the corresponding radius are larger than those in stretch forming at the time of the occurrence of fracture. A study of eqn. (3.49) keeping the above consideration in mind, shows that the punch load at fracture will be higher in deep-drawing.

Chung and Swift (6), Yamada (13), Fukui (12), and Woo (15) presented experimental distributions of strains, and punch load diagrams in deep-drawing. The results are not directly comparable due to differences in materials, frictional conditions, and geometry, but the general trends followed by their results are in agreement with those presented by the author.

11.3.4. Coefficients of Friction

The coefficients of friction in the Erichsen Test, under H.T.G. grease lubrication between sheet metal, die, and blank-holder, calculated according to the method given in section 7.1 are presented in Table 11.4. Table 11.5 contains the coefficients of friction operative between sheet metal, die and blank-holder in deep-drawing, under various frictional conditions calculated also by the method of section 7.1.

Comparing the corresponding values of the coefficient of friction in the two tables, it is seen that those in deep-drawing are higher. This is partly because for the loads used, the magnitude of the pressure distribution over the area of the die and blank-holder in deep-drawing is lower than that in the Erichsen test. Hence the peaks of the irregularities on the surface of the metal would be "ironed" more in the Erichsen test, which in effect would reduce friction. The geometry of the dies are different in the two tests. Apart from any direct geometry effects, in deep-drawing, the lubricant would tend to get squeezed out when the sheet slowly embraces the generous die curvature, and this increases the friction.

It is noted that with E.D.D.S., under H.T.G. grease lubrication, in both tests, the coefficients of friction dropped off considerably with increased punch load. This was also observed in the cases of brass and copper, but to a much lesser extent. This variation could be due to fact that E.D.D.S. had initially a rougher surface finish than the rest of the materials. During the course of the deformation, with the increasing punch load, one expects the flattening of the irregularities on the surface of the metal, thereby reducing the friction. Reduction in friction is also augmented by the fact that the shear planes in the graphite particles in the H.T.G. grease gradually line themselves up in the direction of minimum resistance.

The coefficients of friction for the four materials were also obtained for dry and unlubricated surfaces in deep-drawing. These figures, in general are about twice as high as those obtained under H.T.G. grease lubrication.

Only with copper, P.T.F.E. film lubrication, and dry and roughened unlubricated surfaces were tried.

In the case of the former, the coefficient is about 0.01 or less, and in the case of the latter it is about 0.06, which are the extreme cases considered in the experiments.

As can be seen from Table 1.2, the only comparable values seem to be those originally determined by Swift (78), in his investigation of bending under tension. Swift arrived at a value of about 0.04 with graphite and tallow, and 0.12 for dry surfaces using mild steel 0.038 in. thick. The mean value of about 0.05 obtained in deep-drawing with the H.T.G. grease, and 0.11 for dry surfaces, agree well with the Swift's findings. He also quotes 0.13 and 0.022 for brass and 0.11 and 0.027 for aluminium for unlubricated and graphite and tallow lubricated specimens. The corresponding figures from Table 11.5 are 0.06 and 0.03 for brass, 0.043 and 0.015 for aluminium. Considering the differences in material, lubrication, geometry, and the stress system, the agreement seems to be reasonable. The values obtained (about 0.067) by Takahashi and Alexander (81) in the plane-strain compression test for brass without lubrication, are much closer to the present results.

The coefficients of friction operative between punch and sheet metal in stretch forming and deep-drawing are presented in Table 11.6. For all of the four materials, H.T.G. grease lubrication was used. Only for soft copper, coefficients of friction were also found for P.T.F.E. film lubrication, and dry and rough punch surface. The theory for this method of determining the coefficient of friction was explained in section 7.2, and the method of calculation was outlined in sections 11.1 and 11.2.

The coefficients of friction in Table 11.6 are the average and the effective values for the stages of deformation designated by the corresponding polar circumferential strains shown.

The method of extrapolation, as explained in sections 7.2 and 11.1, to find the correct coefficient of friction, is illustrated in Figs. 101 and 102 for copper and brass. The extrapolation of the curves to the zero radius were required, since the total strain theory, and the assumption of $\frac{dp}{dr} = 0$ were used in the derivation of the formulae, used in the computation of the coefficients of friction, and these assumptions would hold true only at the pole. In each of the Figures, the results for three stages of deformation are shown in stretch forming, with one (last) stage of deformation in deep-drawing. It is observed that the results for the third or last stage in stretch forming are very close to the corresponding ones in deep-drawing, and hence only one curve through such points was justified. A study of eqn. (7.18) shows that it is sensitive to inaccuracies near the pole due to the experimentally evaluated stress ratio x, and can cause some scatter in the results in the vicinity of the pole as illustrated in Figs. 101 and 102. Therefore in the extrapolation, points of up to 10°-15° of angle were usually ignored, and the extrapolation was effected by following the trend of the curve.

From a study of the coefficients of friction in Table 11.6, it is observed that they are appreciably higher than the corresponding ones for the same material and lubricants in deep-drawing. This difference in trend may be explained as follows:

(i) In the case of the H.T.G. grease lubrication, most of the lubricant was squeezed out, as soon as the sheet metal contacted the punch. This could be observed visually on the partially deformed specimens. If they were to be relubricated, friction was reduced comsiderably resulting in a deeper and a thinner bulge, with the location of the fracture moving nearer to the pole.

(ii) The relative speed of metal movement over the punch is very small, hence this is not expected to produce as much debris as that produced in the flange of a partially deep-drawn cup where this speed is considerably higher. The debris produced generally reduces the friction considerably as reported by Takahashi and Alexander (81), and the lack of it in stretch forming may not have decreased the coefficient of friction significantly, as compared to that in deep-drawing.

(iii) Figs. 89 and 90, and the corresponding discussion in section 11.3.2. indicate that the surface shear stresses between the punch and sheet metal **remained** always less than the yield stress of the materials in shear, for this particular geometry of the bulge and the stress system in stretch forming. In section 1.7, in connection with the study of the figures in Table 1.2, coefficients of friction in stretch forming would usually be expected to lie in between the cases, where both bodies in contact remain elastic in bulk, and where bulk plastic deformation is caused by stresses acting normal to the interface of the two contacting bodies. Bowden and Tabor's (8) results obtained in slider tests, ranging from 0.1 to 0.8 for metals and alloys on steel can be quoted as an example to the former. For the latter, Whitton and Ford's(94) values obtained in cold rolling, and ranging from 0.025 to 0.124 can be regarded as typical.

Hence the previous experimental evidence points out that the values of the coefficient of friction in stretch forming would be approximately within the above two ranges, as is obtained in the present investigation.

(iv) A visual proof of the effectiveness of a lubricant in stretch forming is the radius at which fracture occurs over the punch. Even with the P.T.F.E. film lubrication, the fracture occurred at 0.2 in. which suggests that the coefficient of friction could be much higher than that found in deep-drawing which is about 0.01.

(v) Possibly the best method of checking the validity of coefficients of friction is to use them in an independent theory and compare the various experimental results found with the corresponding theoretical ones. This was done, and the coefficients of friction given in Table 11.6 were used in the incremental theory presented in Chapters 3, 5 and 6. The agreement of theory with experiment as discussed in Chapter 13 was reasonably good, suggesting that the coefficients of friction found were reasonably accurate.

The coefficients of friction in Table 11.6 show a decrease with increased strain. This could be related to the smoothening of the surfaces in contact by the gradual ironing out of the small surface irregularities.

In Table 11.6, the average value of the coefficient of friction (about 0.32) for copper with H.T.G. grease compares well with those obtained by Rooyen and Backofen (84) in compression test with liquid lubricants. Bearing in mind that, for reasons discussed in section 1.7, values of coefficient of friction in a compression test would normally be lower than those in stretch forming, their values of 0.2 to 0.36 support those obtained in the present investigation. For aluminium and iron they obtained values between 0.2 to 0.57, and 0.11 to 0.28 respectively, which also support the corresponding ones in Table 11.6. The coefficients of friction presented by Rooyen and Backofen are on the whole higher than those presented by Male and Cockroft (63), but they are lower than those given by Schroeder and Webster (73) obtained in compression of rings, although the last two investigations use very similar methods of analysis. The method used by Rooyen and Backofen seems to be more free of errors since it relies on the experimental assessment of shear and normal stresses independent of any theory.

The values of the coefficient of friction found by Littlewood (56) for steel with machine oils in belt friction over a quadrant die range from 0.15 to 0.25. These are closer to the present author's values than Swift's (78), who gave 0.12 for steel with dry surfaces, in also belt friction over a pulley.

The only comparable values for brass were given by Swift (78) which are 0.13 and 0.022 for unlubricated and lubricated surfaces in belt friction. These clearly are much lower than those presented in Table 11.6. However, the location of severe necking in Fig.53 shows that the friction in the case of brass is at least at the same level as that with e.g. copper lubricated by the H.T.G. grease. Hence, it seems very unlikely that the coefficients of friction in these two processes of deformation are of similar magnitudes.

Generally, it seems more reasonable to compare the coefficients of friction for the grease lubricants in Table 11.6 with those obtained under dry conditions in most other processes due to the expulsion of the grease lubricants in stretch forming.

CHAPTER 12 - EMPIRICAL METHOD OF FINDING THE LIMITING DRAWING RATIO

This Chapter presents an empirical method to find the limiting blank diameter in deep-drawing, from which the Limiting Drawing Ratio (L.D.R.) can be computed.

12.1. Formulation of the Method

In deep-drawing, if oversize blanks are used, fracture would occur over the punch head before the drawing of a full cup, at a certain punch travel or bulge depth. These bulge depths, when plotted against initial blank diameters of oversize blanks would produce a smooth curve. A decrease in the initial blank diameter would increase the bulge depth at the onset of fracture, provided that all other conditions such as lubrication and speed of testing are constant.

Similar curves showing the variations in bulge depth (Erichsen number), obtained by altering the size of the initial blank diameter and keeping the other parameters constant, were presented for the Erichsen test in Figs. 40 and 41. Trial experiments in deep-drawing produced similar results to these findings.

A study of the characteristics of these curves such as those presented in Figs. 40 and 41, would indicate that, they can be approximated to an exponential relationship of the following type:

$$D_b = Me^{-Nh} + D_{cr} \tag{12.1}$$

where M, N, and D_{cr} are constants, and the other symbols have their usual meanings. It is observed that when:

$h \rightarrow \infty$ corresponding to a draw without fracture,

$D_b \rightarrow D_{cr}$

In eqn. (12.1), there are three unknowns, namely M, N and D_{cr}. These can be determined if three points are known from experiments, on the characteristic curve. Hence, the three sets of D_b, and h values when substituted in eqn. (12.), produce the following equations:

$$D_{b,1} = Me^{-Nh_1} + D_{cr} \tag{12.2}$$
$$D_{b,2} = Me^{-Nh_2} + D_{cr} \tag{12.3}$$
$$D_{b,3} = Me^{-Nh_3} + D_{cr} \tag{12.4}$$

Subtracting eqn. (12.3) from eqn. (12.2):

$$D_{b,1} - D_{b,2} = M\,(e^{-Nh_1} - e^{-Nh_2}) \tag{12.5}$$

Subtracting eqn. (12.4) from eqn. (12.2):

$$D_{b,1} - D_{b,3} = M\,(e^{-Nh_1} - e^{-Nh_3}) \tag{12.6}$$

Dividing eqn. (12.5) by eqn. (12.6):

$$\frac{D_{b,1} - D_{b,2}}{D_{b,1} - D_{b,3}} = \frac{e^{-Nh_1} - e^{-Nh_2}}{e^{-Nh_1} - e^{-Nh_3}} \tag{12.7}$$

The only unknown in eqn. (12.7) is N. It can be determined by a trial and error solution of the equation. Having calculated N, M can be found from one of eqns. (12.5) and (12.6). With the known values of N, and M, D_{cr} can then be calculated from one of eqns. (12.2), (12.3) and (12.4).

Having thus calculated D_{cr}, L.D.R. can be found by dividing it either by the punch diameter, or by the mean wall diameter, depending on the criterion chosen.

The accuracy of the D_{cr} estimated by this method would depend on how closely eqn. (12.1) represents the actual curve. This is governed by the choice of the range of the sizes of the oversize blanks. Provided that this range is not too large, satisfactory results can be obtained as shown in the next section.

12.2. Experiments, Results and Discussion

To check the validity of the above method, a series of tests were conducted with soft copper, aluminium, brass and E.D.D.S. in each thickness using the hemispherical punch. The experimental procedure followed is the same as that in section 10.2.3. In all tests H.T.G. grease lubrication, and 0.2 Te blank-holder load were used to get comparable results with those reported in section 11.3.3.

Initially, oversize blank diameters of 100, 90 and 80 mm were used, since these could be produced easily by the standard die sets. However, only for aluminium, this range was later found to be too wide, and hence inaccurate. The oversize blank diameters used with each material are shown in Table 11.2.

Initial blank diameters of the specimens were carefully measured by a vernier to within 0.001 in., and they were lubricated with the H.T.G. grease. To obtain an accurate value of the bulge depth at fracture, when a hairline crack occurs, the electronic cut-off mechanism of the sheet metal testing machine was used as in the Erichsen test (See section 10.2.1.).

For each material and thickness, three tests were carried out with the oversize blanks, and the corresponding bulge depths at the initiation of fracture were recorded to within 0.1 mm. This data, together with the initial blank diameters was sufficient to estimate the limiting blank diameters.

The computation of the limiting blank diameter, together with the other constants as explained in section 12.1 were effected by a computer program written for the Mercury computer. A print out of the program is given in Appendix -F.

The input format of the data for this program is:

1) No. of the data - integer.
2) $D_{b,1}$ in inches - decimal.
3) h_1 in mm. -decimal.
4) $D_{b,2}$ in inches - decimal.
5) h_2 in mm. - decimal.
6) $D_{b,3}$ in inches - decimal.
7) h_3 in mm. - decimal.

If there is more than one set of data steps 1 - 7 are repeated.

The program reads the above data and computes the starting values, for the solution of eqn. (12.7) by a successive approximation method. It then enters a loop where the initially estimated value of N is improved until the desired accuracy is reached in the solution of the equation. Having calculated N, it then finds M and D_{cr} from eqns. (12.6) and (12.3), together with the other required quantities as shown below.

The output format is:

1) N - floating point number.
2) M - decimal.
3) D_{cr} - decimal - inches.
4) " - " - mm.
5) L.D.R. - decimal.
6) One increment oversize blank - decimal - inches.
7) " " undersize " - " - " .

8) One increment oversize blank - decimal - mm.

9) " " undersize " - " - ".

10) Residue in successive approximation - floating point number.

Steps 1 - 10 are repeated when more than one set of data is processed.

The results obtained are shown in Table 11.2. The L.D.R.'s presented in this Table were discussed in section 11.3.3., from the standpoint of their relations with the material parameters. Here the discussion will be on the accuracy and the practicability of the proposed method.

The accuracy of the method in predicting oversize and undersize blank sizes given in Table 11.2. were checked by actually deep-drawing blanks of those sizes. As seen from the comments in the Table, except for 18 S.W.G. brass, the other predictions were successful. However, in the case of soft aluminium 85, 80 and 75 mm diameter blanks were used instead of the 100, 90 and 80 mm ones, to obtain the necessary accuracy. With the 20 S.W.G. brass, some scatter was obtained in the h versus D_b function, and the three sets of values for h and D_b were picked from a curve plotted using six points.

Table 11.2 contains the values of the constants M, and N. It is seen that their magnitudes differ considerably, and therefore high accuracy is required in the solution of eqn. (12.7). Although these computations can be attempted by hand using six or seven figure log or exponential tables, it would be more accurate and much faster to obtain the solutions on a computer.

It seems that this method of predicting or estimating the limiting blank diameter and L.D.R. is sufficiently accurate even for a reasonably wide range of sizes of the oversize blanks used. In these experiments, oversize blanks with diameters of 15 - 30% larger than the limiting ones gave satisfactory results. Since this method normally requires three blanks to be deep-drawn, there is saving in material and labour in the determination of the L.D.R. at the expense of solving eqn. (12.7), which can be attempted manually. This method can be used with any shape of punch or die, so long as the only independent variable in testing is the initial blank diameter.

CHAPTER 13 - THEORETICAL RESULTS AND THEIR COMPARISON WITH EXPERIMENT

In this Chapter, theoretical results for stretch forming are presented and compared with the corresponding experimental ones. The basic equations for the theory were given in section 3.2, the numerical analysis in 5.1, and the computer program in Chapter 6.

Although the theory is general and holds for a wide range of conditions, required parameters were chosen to represent the cases for which experimental results were obtained, namely:

(i) Stretch forming of soft copper, brass, aluminium and E.D.D.S. by the hemispherical punch under H.T.G. grease lubrication.

(ii) Stretch forming of soft copper, under P.T.F.E. film lubrication, and also using a rough and dry punch surface, by the hemispherical punch.

(iii) Stretch forming of soft copper by the ellipsoidal punch under P.T.F.E. film and H.T.G. grease lubrication.

(iv) Stretch forming of copper under a constant, and also zero coefficient of friction. The solutions to these two hypothetical cases were found to show the effects of friction.

The parameters required, and their layout for the computer program were given in section 6.3. Values to these parameters were assigned with reference to the following sources:

(i) A, B, and n from Table 8.2.

(ii) Strain ratio R from Figs. 25-28. Arithmetic mean of the average values in each direction were used. With E.D.D.S., a solution was also obtained using the minimum average R-value in one of the directions.

(iii) Coefficients of friction from Table 11.6.

(iv) Geometry of the tools from section 9.4. and Fig.38.

(v) Thicknesses of the materials from Table 8.1.

(vi) For the number of integration steps, 60 was used for all cases, since this gave more than sufficient accuracy in the numerical solution as discussed in Chapter 5.

The computer program produced the results according to the output format given in section 6.3. for every stage of deformation. The maximum difference between the equivalent strains of any point on the bulge for any two consecutive stages was less than 0.045. The computation continued until SP instability, and in some cases ML instability were reached.

In the comparisons with the experimental results, only the stages of deformation from theoretical results which correspond to those obtained in the experiments are presented. The last stage presented is that at plastic instability - just before the onset of fracture.

In Chapter 3, circumferential polar strain in stretch forming was used as a measure of "time" in the deformation process. Consistent with this concept, correspondence of the experimentally and theoretically obtained stages of deformation was made on the basis of their giving the same polar strain. If within a small tolerance, equivalence in the two polar strains were not achieved, then the theoretical results were interpolated to find a theoretical stage, giving the same polar strain as the nearest experimental one.

Most of the theoretical results are plotted with the experimental ones to show their degree of agreement. The location and the types of instability reached are shown on the theoretical curves.

Figs. 54 to 57 show the distributions of circumferential strains for soft copper, brass, aluminium and E.D.D.S. under H.T.G. grease lubrication, for the hemispherical punch, It is seen that for the first two stages, with the above materials, the agreement between theory and experiment is very satisfactory. In the third stage differences between theory and experiment are larger. Theoretical curves do not show the secondary peaks shown by the experimental ones, which are due to the additional local plastic deformation before the onset of fracture. This can be explained as follows:

The theory, since it does not take the variations of the variables along the thickness direction into account, implicitly assumes that the punch is always in contact with the material at every point in region one. It follows that, the frictional stresses tangent to the inner surface of the shell are assumed to act at every point in region one. However, when the materials thins to about half of its original thickness, and if the thinning is not uniform over the punch head, the location with the minimum thickness may not remain in contact with the punch surface any more. Just prior to this state, the interfacial pressure in this zone may be less than what is predicted using the present theory. Hence, elements of the bulge in this zone with little or no frictional stresses tangent to their inner surfaces, would tend to stretch more due to the decreased local friction. Each additional amount of stretching and thinning would reduce the local friction further, resulting in a local accelerated thinning leading to fracture. This phenomenon will be referred to as "boundary separation" in the rest of the thesis.

Hence, the secondary peaks in the experimental curves in the zones of eventual fracture in Figs. 54 to 57 are due to additional local deformations caused by boundary separation. For this reason the general agreement between theory and experiment is less satisfactory in the third stage. However, locations of the seat of eventual fracture and magnitudes of the circumferential strains at the onset of fracture are well predicted by the theory. It is seen that, in most cases results of the ML and SP criteria of instability give very close results to the experiment, but those obtained by the MP criterion are much lower and hence are unsatisfactory.

To a smaller extent some differences between theory and experiment are contributed by:

(i) Taking the coefficient of friction to be constant throughout region one, as a function of the radial co-ordinate.

(ii) Assumption of planar plastic isotropy in the plane of the sheet.

(iii) Assumptions in the basic theory of plasticity and the flow rules as discussed in Chapter 3.

(iv) Using of the average values for A, B, n and R in cases where they showed variations with respect to different directions in the plane of the sheet, and the method of averaging used.

(v) Expressing the strain-hardening behaviour with the exponential law given by eqn. (3.48).

The effects of the above factors do not seem to be too significant, but may account for the small differences between the theory and experiment in some cases. Certainly, no definite trends have been observed except in the case of the R-value. The distribution of circumferential strains for E.D.D.S. in Fig.57 has been obtained using R = 1, the minimum value, instead of R = 1.25, the average value which is the arithmetic mean of the R-values in the rolling and 45° directions. The circumferential strain at the point of SP instability using R = 1.25 came to 0.066 instead of 0.14 obtained by R = 1. This clearly shows that the method of defining the effective R-value is significant in cases where it shows variations as a function of direction in the plane of the sheet. From the evidence of E.D.D.S., it seems more reasonable to use the minimum R-value, but this cannot be regarded as conclusive, and more results are needed to prove it. Since the other materials, for which the theoretical results are presented, did not exhibit widely varying R-values, using the arithmetic mean in their cases was justifiable and gave satisfactory results.

When the boundary separation takes place, since there would be no or little contribution to support the punch load from the zone where it occurs, interfacial pressures and frictional stresses elsewhere in region one must increase. This tends to reduce the plastic deformation, in particular in the region between the pole and the unstable zone, which may account for the differences between theory and experiment in this region, since theory does not take the boundary separation into account.

It may also be mentioned that as data to the computer program, a value of radius slightly less than that of at the clamped periphery was fed at which ε_2 had to be zero. This is in line with the discussion on drawing-in, in section 11.3.2., since in all experiments the radius at which the zero mean strain occurred was before the clamped periphery.

Fig.58 shows the distribution of circumferential strains under P.T.F.E. film lubrication in stretch forming by the hemispherical punch. Agreement between theory and experiment is very satisfactory even for the last stage. This is because, there is little or no boundary separation due to a more uniform thinning. It is observed that in the experimental curve, there is no seconday peak which would confirm the absence of boundary separation.

In the computation of the results shown in Fig.58, SP instability was not obtained. The numerical solution could proceed beyond ML instability if allowed. However, in the author's opinion, there should be a SP instability, occurring most likely soon after the ML instability, but this was not detected by the numerical solution for the following reason:

The numerical solution is usually started at the pole, and proceeds towards the clamped edge as described in section 5.1. The SP instability is detected as illustrated in Fig.13, when the unit force ($\sigma_1 t$) demanded by the equilibrium equation just exceeds that provided by the plasticity laws. Supposing that the thinnest part of the shell is near or at the pole, this will produce a low $\sigma_1 t$ due to the low value of the thickness. It can always be balanced by the unit force of the next element since it has a greater thickness and hence a greater $\sigma_1 t$ (unit force). For this reason the deformation, as calculated by the theory can go on indefinitely. However, if the calculation had been started at the clamped edge and the numerical solution had moved towards the pole, the SP instability would have been detected. This is because, higher values of $\sigma_1 t$ away from the pole would demand higher unit forces in the vicinity of the pole than these elements can provide. Hence, the SP instability would be detected, since there would be no convergence of the numerical solution at such points (See Fig.13). Starting of the numerical solution at the clamped periphery would have no effect on the stress, strain distributions and ML, and MP instabilities, and same results would be obtained as in the case when the solution is started at the pole. It is generally more difficult to start the solution at the clamped periphery due to two unknowns e.g. θ, and ε_3. To eliminate this difficulty, initially the solution can be started from the pole and the results can be obtained for that stage. Then to check for the occurrence of SP instability using the already calculated θ, and ε_3, at the clamped periphery, the solution can be started there, proceeding towards the pole. This was not attempted in the computer program, since it required major changes and additions, and about two fold increase in its execution time.

Fig.59 shows the distribution of circumferential strains in stretch forming of soft copper when using the hemispherical punch with a rough and dry surface. The agreement between experiment and theory is very satisfactory for the first two stages, but in the last stage the experimental curve has a secondary peak due to bounday separation which as discussed before, could not be predicted by the theory. It is seen that only SP instability is obtained, and the solution therefore could not go any further. The predicted SP instability took place at a slightly smaller radius than that obtained experimentally, and also it is associated with a circumferential strain which is about 0.015 less than the experimental one. This is probably partly due to a small inaccuracy in the estimation of the coefficient of friction used, and partly to the effect of boundary separation.

Figs. 60 and 61 present the distributions of circumferential strains in stretch forming of copper by the ellipsoidal punch under H.T.G. grease and P.T.F.E. film lubrication respectively. Here again, the agreement between theory and experiment is very satisfactory for the first two stages, but for the third stage the agreement is not so good. This is because of boundary separation, and also using coefficients of friction which were obtained for the hemispherical punch. It seems that with the ellipsoidal punch coefficients of friction would be slightly higher than those for the hemispherical punch. In both Figures, it is observed that MP instability takes place very early. With the H.T.G. grease, SP instability occurs after ML instability, and both are within 0.02 of the experimental instability strain. With P.T.F.E. film lubrication, for the same reasons as in the case of the hemispherical punch, SP instability could not be detected. ML instability occurred within 0.01 of the experimental instability strain, but slightly nearer to the pole, due to possible differences in frictional conditions.

Fig. 62 shows the distribution of the surface circumferential strains. The agreement between theory and experiment is very satisfactory.

Figs. 63 to 66 present the distributions of thickness strains in stretch forming by the hemispherical punch for the four materials under H.T.G. grease lubrication. The agreement between theory and experiment seems to be very satisfactory for the first two stages. Small differences between theory and experiment can be attributed to the same five factors enumerated in the discussion of the circumferential strains. The author is of the opinion that possible variation in the coefficient of friction as a function of the radial co-ordinate in experiments might be the most important of all. This was not taken into account in the theory.

It is observed that, in the third stages, experimental curves in Figs. 63-66 show sharper peaks than the theoretical ones. Although good agreement is obtained between the polar and instability strains, for the zone in between the two, theory overestimates the thickness strains. This is due to the combined effect of boundary separation, and variations of the coefficient of friction as a function of the radial co-ordinate as explained in the discussion of circumferential strains. It is observed that with copper, the magnitudes of the predicted SP and ML strains are very close, and they are within 0.04 (strain) of the experimental one. In the case of brass ML instability did not occur. With aluminium, and E.D.D.S. the predictions of the SP instability criterion are within 0.1 (strain) of the experimental ones, but ML instability falls shorter unlike in the case of copper. Under similar frictional conditions, the differences between the predictions of the two instability criteria

(ML, and SP) seems to vary as a function of n, and ML instability seems to approach SP instability with increasing n. After a certain value of n, ML instability does not seem to occur and the deformation is limited by the SP instability. In all of the four cases, MP instability occurs much too early in the process, and hence it is an unsatisfactory criterion.

As mentioned earlier, the results shown in Fig.66 for E.D.D.S. were obtained for R = 1 (minimum). For R = 125 (arithmetic mean), the thickness strain at SP instability is -0.33. Compared to -0.55 obtained with R = 1, it is seen that R-value is the next important variable in stretch forming after friction. With a decrease in R-value more thinning is obtained with a consequent increase in bulge depth. This also suggests that the effective R-value for a material which shows plastic anisotropy in the plane of the sheet, may very well be the minimum one, rather than the arithmetic mean.

Fig.67 gives the distribution of thickness strains in stretch forming of soft copper under P.T.F.E. film lubrication by the hemispherical punch. The agreement between theory and experiment for all the stages is very satisfactory. It is evident that there is little or no boundary separation. As explained earlier in connection with the discussion on circumferential strains, SP instability could not be detected in cases such as this when instability occurred very near the pole. It is seen that the magnitude of the predicted ML instability is within 0.02 (strain) of the experimental one.

The effect of friction in stretch forming can clearly be seen by comparing Figs. 67 and 68. In Fig. 68, which shows the thickness strains in stretch forming of copper by the hemispherical punch having a rough and dry surface, the agreement between theory and experiment is not very satisfactory. In all stages, the theory underestimates the thickness strain. This appears to be due to a possible variation (decrease) of the coefficient of friction, in the experiment as a function of the radial co-ordinate. In the numerical calculations for this case the coefficient was taken to be constant both as functions of the radial co-ordinate, and of stages of deformation. Clearly, boundary separation also takes place as indicated by the sharp peak of the curve for the third stage, which is unaccounted for in the theory.

Figs. 69 and 70 show the distributions of thickness strains in stretch forming of soft copper by the ellipsoidal punch under H.T.G. grease and P.T.F.E. film lubrication respectively. The agreement between theory and experiment for the first two stages is quite satisfactory, but the differences are slightly larger in the third stages, due to boundary separation and using of the coefficients of friction obtained for the hemispherical punch. Obviously, the figures indicate that the coefficients of friction would be slightly higher with the ellipsoidal punch for the same lubricants. The magnitudes of the predicted thickness strains at instability are within 0.08 (strain) of the experimental ones. The predictions of the locations of the plastic instability are also very close to those found by experiment. In both cases, MP instability occurred too early, and hence is unsatisfactory as a criterion to predict the onset of fracture. SP instability with the P.T.F.E. lubrication could not be detected in Fig. 70, for the reasons given earlier in this section.

Figs. 71-78 show the distributions of meridional strains in stretch forming for the four materials under various lubrication conditions, when using hemispherical and ellipsoidal punches. The results correspond to the cases for which the circumferential and thickness strains were presented earlier. The Figures will not be discussed in detail, because the discussion given for circumferential and thickness strains also apply here to a large extent.

In most cases, for the first two stages of deformation, agreement between the theory and experiment is satisfactory. Polar and instability strains (meridional) are also well predicted. Beyond the maximums, mainly in region two, theory underestimates the meridional strains in most cases. Previous Figures showed that, circumferential strains were slightly overestimated, and thinning strains were slightly underestimated in this region. Since the meridional strain is derived from the constancy of volume principle, the two sets of differences for the other two strains when added together produce the amplified differences we see in the Figures for meridional strains between theory and experiment.

In the third stages, experimental curves show sharper peaks due to boundary separation, except in the case of the P.T.F.E. film lubrication. In most cases polar strains, and locations of instability are fairly accurately predicted. The differences between theory and experiment for the region between the pole and the zones of instability are larger due to the effects of boundary separation and the variations of the coefficient of friction as a function of the radial coordinate.

It is observed that differences between the predicted magnitudes of the meridional strain at instability for soft aluminium and E.D.D.S., and the corresponding experimental strains are larger than those for copper and brass, due to planar plastic anisotropy shown by the former materials. In the case of stretch forming by the rough hemispherical punch, prediction of the magnitude of the instability strain is unsatisfactory due to the effects of exaggerated local thinning and boundary separation, which has taken place. Also the consequent variations of the frictional stresses which were not taken into account in the theory, have contributed to the difference between experiment and theory.

The order in the occurrence of the three types of instabilities follow the same pattern as with the other strains. Except in the case of the rough hemispherical punch, MP instability occurs followed by ML and SP instabilities. For brass, there is no ML instability. It follows clearly that for the same lubrication conditions with increasing n, ML instability approaches the SP instability. Since ML instability cannot take place after the SP instability, the latter becomes the only one that can occur beyond a certain value of n as in the case of brass.

Figs. 79 and 80 show the distributions of equivalent strains in stretch forming of copper by the hemispherical punch under H.T.G. grease and P.T.F.E. film lubrication respectively. The theoretical curves have been obtained from the computer results based on the incremental plasticity theory, whereas the experimental ones were determined using the total strain theory as described in section 11.3.2. These curves are presented to compare the results of the two theories.

This comparison is not a simple one to make, because the effects of boundary separation and possible variations of the coefficient of friction with the radial co-ordinate in experiments were not taken into account in the theory. However, as discussed earlier in this section, these effects are less significant with the P.T.F.E. film lubrication. In Fig.80, differences between the curves obtained by the incremental and the total strain theories are relatively small, and are comparable to the differences obtained between the theoretical and experimental thickness strain curves for the same lubricant. This would indicate that although there is an approximation introduced by the use of the total strain theory, this does not seem to affect the equivalent strain significantly, when compared with the effects of e.g. boundary separation, and possible variation of coefficient of friction with the radial co-ordinate, as illustrated in Fig.79. Stretch forming certainly does not take place under uniform straining, as confirmed by the variations in the stress ratio x as shown in Figs. 87 and 88, but it appears that such variations have a small effect on the equivalent strain. Woo (95) claimed that the large differences he observed between his theory and experiments for some of his results even at low strain level were due to the use of the total strain theory. The present author is of the opinion that these were mainly due to neglecting the effects of the moving boundary and assuming that the sheet was stretch formed to cover the whole of the punch surface at an early stage in stretch forming. Also, the use of the total strain theory certainly would have contributed to the differences between his theory and experiment but possibly to a smaller extent.

Figs. 81 to 90 present various results corresponding to the cases presented in Figs. 79 and 80. Experimental curves were obtained using the total strain theory, and the theoretical results were computed by the computer program based on the incremental theory. Since the discussion on the occurrence of the three types of instabilities is the same as that given when discussing the three principal strains, they won't be repeated here. Their locations are shown in the Figures. The differences between theoretical and experimental results in these Figures support the view expressed in the discussion for the equivalent strains. That is, they are mainly caused by neglecting the effects of the boundary separation, and the variations of the coefficient of friction across the bulge, more than the approximation introduced by the use of the total strain theory in the processing of the experimental results. However, a true assessment of the approximation introduced by the use of the total strain theory could only be made by computing the theoretical results using each of the theories separately. This was not attempted due to the limitation on the available computer time.

Figs. 81 and 82 show the distributions of the equivalent stresses. Their trends are very similar to those of the equivalent strains. Meridional stresses in Figs. 83 and 84 also show very similar variations. However, distributions of the circumferential stresses presented in Figs. 85 and 86 show that they are less affected by friction. Their maximums do not occur at the zone of instability, but they are located nearer to the pole. It is observed that the theoretical curves show a discontinuity at the moving boundary as explained in section 3.2.3.2., since $\sigma_2 = x\sigma_1$, and σ_2 and x are discontinuous whereas σ_1 is continuous. The discontinuities in x are shown in Figs. 87 and 88. It is observed that variations in the stress ratio (x) of an element of sheet metal through the stages of deformation is less in the case of the H.T.G. grease lubrication, compared to that obtained with the P.T.F.E. film lubrication. This is more so in the vicinity of the moving boundary. If total strain theory is used in the theory of stretch forming, more approximate predictions would be expected in the cases of lower friction between punch and sheet metal.

Figs. 89 and 90 show the distributions of interfacial pressure. It is observed that the theory (incremental strain) and experiment (total strain) agree very closely indicating that the effect of neglecting the strain history on interfacial pressure is very small. As discussed in section 11.3.2, the frictional stresses remain well under the limiting yield stress in shear for up to about $\mu = 1$. The locations of MP instability on the curves clearly show that, fracture takes place after a considerable drop in the interfacial pressure at the unstable zone. In cases of boundary separation, the pressure at this zone would drop down to zero, also eliminating the localeffects of the friction.

In Fig.103, distribution of thickness strains is presented for the same parameters as in Fig.63 (soft copper stretch formed by the hemispherical punch under H.T.G. grease lubrication), except that the coefficient of friction was kept constant throughout the whole process, equal to 0.26, which is the effective value for the last stage in Fig,63. In the experiment (Fig.63), for the previous stages, μ was higher as can be seen from Table 11.6. The results in Fig.103 represent a theoretical case and has no direct experimental comparison. However, to illustrate the effect of keeping μ constant, the stages of deformation in Fig.103 were so chosen that the first three had the same polar strains as those in Fig.63. The last, fourth stage in Fig.103 corresponds to that at SP instability. Comparing the two Figures, it is clearly seen that keeping the coefficient of friction constant, and in this case equal to its minimum value, has increased the general thinning. Polar strain at instability has varied from -0.27 to -0.38, but instability strain changed by only 0.03 in the direction of increased thinning. The location of instability has also moved slightly towards the pole. It therefore appears that, a realistic theory should at least take into account the variation of the average coefficient of friction with the stages of deformation, short of including its variation as a function of the radial co-ordinate. This was achieved in the present work.

Fig. 104 presents the distribution of thickness strains for stretch forming of soft copper with the hemispherical punch with $\mu = 0$ throughout the deformation. This of course has no direct experimental comparison, but the first three stages in Fig.104 were chosen to give the same polar strains as those with the P.T.F.E. film lubrication in Fig.67. It is clearly seen that at all stages, the maximum thinning occurs at the pole, unlike the results in Fig.67. Also the ML instability occurs at -0.87 strain whereas it is at -0.80 in the case of the P.T.F.E. film lubrication. Here also, as with the P.T.F.E. film lubrication no SP instability could be detected, since the numerical solution was not started from the clamped periphery or away from the pole.

Theoretical punch load diagrams, along with the corresponding experimental ones are contained in Figs. 91 to 93. In Fig.91, theoretical predictions of bulge depth are within 0.5 mm of the experimental findings for H.T.G. grease and P.T.F.E. film lubrication for soft copper stretch formed by the hemispherical punch. The slightly higher bulge depths obtained in the experiments compared to those predicted by the theory are due to the contribution from the thinning under bending under tension around the clamped periphery whose effect is not included in the theory. The agreement in the case of the ellipsoidal punch is much better due to the smaller angle that the shell bends at the clamped periphery, which induces less thinning. In all of the above three cases the punch loads are overestimated by the theory throughout the deformation process. This is not very straightforward to explain, but it seems that most of the variables (σ_1, r, θ, t) at the moving boundary were slightly overestimated in eqn. (3.49), and each such difference contributed to the differences seen between theory and experiment.

Punch load diagrams for E.D.D.S. and soft brass are contained in Fig.92. It is observed that bulge depth for E.D.D.S. is underestimated by about 3.5 mm. This is because, the thickness strain distribution at the SP instability was underestimated as shown in Fig. 66. The punch load diagram for aluminium is shown in Fig.93. The agreement between theory and experiment is much better compared to that with E.D.D.S.

The discussion given on punch load diagrams for soft copper also applies to the other materials.

It is observed that SP, and also ML, and MP instabilities take place at increasing punch load in agreement with the experiments. This is governed by the variations of the variables in eqn. (3.49). It therefore appears that, the use of the maximum in the punch load curve as an instability criterion would not lead to satisfactory results.

A typical trace of the moving boundary, on the initial radius versus thickness strain plane is illustrated in Fig.67. Agreement between theory and experiment is very satisfactory. This also shows that, effect of plastic bending is negligible. Plastic bending can only take place when the sheet comes into contact with the punch surface, i.e. at the moving boundary, since from then on the radius of curvature of the shell becomes the same as that of the punch for a hemispherical punch. It is observed that the thickness strain curves have a very smooth transition between regions one and two, which would not have been the case if there was an appreciable thinning due to instantaneous bending under tension.

This justifies the case for having neglected them in the theory, and also shows that deformations throughout the regions one and two are by stretching, and those due to plastic bending are negligible.

In the theory, elastic strains were also neglected. The results show that they are generally about 1% or less, of the plastic strains, and no evidence has come about which can suggest the importance of them in the present context.

The results for the two principal radii of curvature in region two are not presented in detail. In most cases it was found that ρ_1 varied from about -0.8 inch at the moving boundary to -10 inches at the clamped periphery in the early stages of the deformation. However, the value at the clamped periphery reduced to about -1 inch with increased deformation, whereas the other remained fairly stationary. The circumferential radius of curvature, ρ_2 varied from about 0.7 inch to 4 inches, and the value for the later stages of deformation at the clamped boundary was about 0.8. It followed the same trends as ρ_1.

The degree of agreement between theory and experiment suggests that the effective coefficients of friction for the stages of deformation considered in stretch forming of the materials, have been estimated generally fairly accurately by the method of section 7.2.

CHAPTER 14 - CONCLUSIONS

The theory presented in the thesis explains the behaviour of sheet metal in the stretch forming process. Agreement between theoretical predictions and experimental results generally has been very satisfactory for all stages of deformation except the last few. This was because, in cases of non-uniform thinning over the bulge, the thinnest elements over the punch head did not remain in contact with the punch surface or prior to this the interfacial pressure in this area reduced considerably, and hence the effects of friction in such zones were reduced or eliminated. This, so called "boundary separation" resulted in local thinning, and also a redistribution of interfacial pressure and frictional stresses over the punch surface. However, in most cases, the predictions of the polar strains, and the magnitude and location of the instability strains were in good agreement with experiment, but larger differences were found between theory and experiment for the zone between the pole and the instability location in the stages near instability. This could only be eliminated if the variations through the thickness direction of all the variables were taken into account, but it would have resulted in theoretical complications which could not have been resolved by the present computer facilities. Such possible extensions to the theory are discussed in the next Chapter.

The predictions of the three plastic instability criteria showed that the SP criterion was the most realistic of all. In fact, with the theory used no further solution can be obtained beyond the occurrence of SP instability except for certain special cases. This criterion, which is an integral part of the numerical analysis, has not been used by previous researchers in this field. It was found that the ML criterion was the second best, this would correspond to the Swift-Hill (79,35) criterion in stress states with proportional straining. MP instability was generally reached too early in the process and therefore could not suitably be used as a criterion to predict plastic instability which is interpreted as the state just before the onset of fracture, in stretch forming. Both the theory and experiments showed that plastic instability invariably occurred under increasing punch load.

It was found that the predictions of the ML instability criterion approached those of the SP criterion with increasing n, other conditions remaining the same. After a certain value of n, only SP instability could take place.

In cases where the coefficient of friction was low, SP instability could not be detected by the numerical solution if it started from the pole. In such cases the solution would have to start from the clamped periphery and proceed towards the pole. However, the computer program was not modified to follow this alternative procedure.

Both the theoretical and the experimental results showed that friction is the most important variable in stretch forming. With increased value of the coefficient of friction, the location of fracture moved away from the pole and the magnitudes of the strains at instability decreased. For smaller values of coefficient of friction, more general thinning, and hence deeper bulges are obtained.

Two new methods of estimating coefficients of friction in stretch forming, and in radial drawing were developed and used. The results showed that the coefficients of friction between punch and sheet metal in stretch forming were appreciably higher than those between the die, blank-holder, and sheet metal in deep-drawing under similar lubrication conditions. The latter were found to be similar to those obtained in frictional conditions of the type met in e.g. plastic bending under tension. It has not been possible to compare the values for the former, because of the unavailability of other methods to determine the coefficient of friction in stretch forming. However, when used in the theory for stretch forming they led to generally good agreement with the other experimental results. These two methods of estimating the coefficient of friction could predict its variations with the continued plastic deformation. This was particularly valuable in stretch forming, since it was shown that with the assumption of a constant coefficient of friction throughout all stages of deformation, less good agreement with experiment was obtained.

The stretch forming theory took into account plastic anisotropy in the thickness direction, but assumed the sheet to be isotropic in its plane. Soft copper, and brass conformed to this type of anisotropy. With E.D. D.S., which showed large variations in its R-value, use in the theory of the minimum one (an average of the values in one direction with degree of straining) gave a better correlation with experiment, compared to using the arithmetic mean of the R-values in various directions. This suggests that the effective R-value for such materials, can be the minimum, rather than the arithmetic mean of the R-values in various directions. However, more research is required to reach a definite conclusion on that point. It can be concluded that high n and low R-values are desirable in stretch forming from the point of view of obtaining the maximum thinning and the deepest bulge. This is supported by both theory and experiment.

Effects of the parameter B in the empirical strain-hardening equation could not be studied fully in the experiments, since all the materials were in a soft condition. However, theoretical studies indicated that an increase in B would lower the instability strain.

Experimentally obtained strain distributions over the punch head in deep-drawing were quantitatively very similar to those obtained in stretch forming. Hence it may be suggested that stretch forming theory can be used to predict these, but it will not be able to predict the L.D.R. which is generally the desired result. The theory for the complete solution of deep-drawing is given but no numerical results have been obtained. The new empirical method given, to predict the L.D.R. from three oversize specimens produced reliable results. It was observed that L.D.R. increased with increases in n, and R-value, consistent with the findings of the previous researches.

Values of n, B, and A in the empirical strain hardening law were determined by a new computer program based on existing mathematical techniques, so that minimum error was obtained between the experimental points and the curve-fitted empirical law. This gave very satisfactory results.

Also the instability of material subjected to simpler stress systems, such as that in hydraulic bulging, was investigated. Analytical formulae were obtained to express the ML and MP instability strains. It was shown that in contradiction to some previous work, the two criteria led to different results, and could only produce the same results for certain combinations of the parameters, n, R, and B. Instability obtained at decreasing or increasing pressure in hydraulic bulging could be explained by the ML criterion. An original general numerical solution for hydraulic bulging is given but no results have been obtained.

Evidence from experimental and theoretical analyses showed that plastic bending, and elastic strains had negligible effect on the above problems considered, and hence they were neglected.

The study of the variables influencing the Erichsen number revealed that "drawing-in" can never be completely prevented even when both serrated die and blank-holder surfaces are used. Unless drawing-in is reduced to a minimum, considerable scatter may be found in test results, due to variation in lubrication conditions, specimen geometry, blank-holder load, and other factors. The loads necessary to cause indentation of the sheet by the serrated die and blank-holder may be taken as those quoted in the present research for the materials studied. For other materials a load must be chosen which gives a visible impression of the grooves in the material. Care must be taken to modify the zero point to compensate for the indentation.

The Erichsen test should be considered as a stretch forming test, and any uncontrolled drawing-in will lead to scatter in the results. It basically measures the capability of sheet metal to deform up to fracture under a quasi-biaxial tensile stress system. The deformation is significantly influenced by friction between punch and sheet. Although the conditions of lubrication can be changed in an attempt to simulate a practical pressing operation, unless all the other factors influencing the test are changed according to a true scale, effects of friction might be difficult to judge. Therefore it seems to be a better idea to standardise frictional conditions so that they can remain fairly constant in spite of possible errors or differences in e.g. lubrication techniques, surface finish of tools, etc., used by different bodies. It may be suggested that P.T.F.E. film can be used as a lubricant, which fulfils the above requirements. However more research would be needed to determine the consistency of results obtained by its use.

The experimental results in the Erichsen and stretch forming tests showed that planar plastic anisotropy cannot be determined by the appearance of fractures in a stretch forming test. In fact completely misleading predictions would result since in the present experiments, all-round "isotropic" fractures were associated with quite pronounced earing, in the cases of aluminium and E.D.D.S.

CHAPTER 15 - APPLICATIONS, AND RECOMMENDATIONS FOR FURTHER RESEARCH

The theory of stretch forming presented in this thesis can be applied in practice. The feasibility of stretch forming an axisymmetrical shell from a sheet metal with certain material and frictional characteristics can be studied. Also by varying the different input parameters to the computer program, process (e.g. geometry, friction) and material parameters (n, B, A, and R) can be optimized, say to give minimum cost or deepest bulge. The theory can also handle the effects of "differential annealing", or "differential lubrication". Sheet metal need not be flat but it can be of any axi-symmetrical shape, and have any variation of thickness and initial strain, so long as the radius of curvature of the punch remains smaller than that of the initial shell at points of contact. Since in most industrial processes, stretch forming operation is limited by e.g. tolerances on thickness variations or bulge depth, and not by plastic instability, accurate predictions by the theory are expected since there would be less chance of having boundary separation which would lead to larger differences between practice and theory.

A theoretical study of this type however if may be desirable is somewhat costly. On commercial rates the cost of running the stretch forming program once on a large computer would be approximately between £200 - £300. Since a few runs will generally be necessary, it would only be economically justified to carry on such a theoretical study, if the capital cost of the equipment to be installed exceeds a few thousand pounds.

The two methods of estimating coefficients of friction in radial drawing and stretch forming can be used to investigate the effectiveness of various lubricants in these processes, besides providing data for use in metal working theories.

For most theories in plasticity, it is desirable to express the experimentally determined strain-hardening characteristic in a single equation. The method of curve-fitting used in this thesis is fairly general and would apply to even more complicated empirical equations than the one used. There is no theoretical limit on the number of the parameters to be minimized in an equation to be curve-fitted. The method may usefully be employed, say in expressing the creep behaviour of materials.

The empirical method of predicting the L.D.R. from three oversize blanks can find some useful application when the amount of sheet metal for testing purposes is limited. The same method can be used to predict the drawability of a complex pressing if three oversize specimens, preserving the geometrical similartity of the blanks, are used in the same way as the round specimens in deep-drawing.

The conclusions drawn from the results of the investigation into the Erichsen test were given in the last Chapter. It seems that, in an effort to reduce scatter and increase reliability of the Erichsen test, serrated die and blank-holder surfaces should be used, with standard lubrication e.g. a. P.T.F.E. film.

Although researches conducted so far have thrown considerable light upon some of the important aspects of sheet metal deformation, much more needs to be known to satisfy the needs of industry. It is seen that even for the simplest of such processes - plastic deformation of an axisymmetrical shell - a formidable effort is needed to obtain a complete theoretical solution. In an endeavour to elucidate some more of the unknowns in this field, the author may humbly suggest the following extensions to the present work, also with a strong emphasis on the use of computers in their solution:

(i) Writing a computer program for the complete solution of hydraulic bulging for materials anisotropic in the thickness direction. The numerical procedure is given in section 5.4 of this thesis. It will be necessary to check for the SP instability by also starting the solution from the clamped edge, or away from the pole, and proceeding towards the pole. The computer program will probably take about the same time to execute, as that for stretch forming.

(ii) Writing of a computer program for the complete solution of deep-drawing, including the effects of radial drawing and stretch forming. The theory and the numerical procedure is given in section 5.3. of this thesis. The program is envisaged to take at least four to five times the time required to execute the stretch forming program.

(iii) The above problems can be solved including the effects of strain-rate. In this case the equilibrium equations need to be modified to take into account dynamic forces, and the flow rules should allow for strain-rate effects. The method of solution would probably remain the same.

(iv) Plastic deformations of non-axisymmetrical shells in stretch forming, deep-drawing and hydraulic bulging can be studied theoretically. If only a membrane solution is sought, this would lead to the solution of a set of partial differential equations in two independent variables. It is estimated that any computer program on the same basis as the present theory written to solve such a case will require at least about 100 times the time required for stretch forming.

(v) Any of the above problems can be considered also allowing for the variations of the variables through the thickness direction. However, it is envisaged that it will multiply the complexity of the numerical procedure and the computer program by about a factor of 50 at least, compared to the stretch forming problem.

AN INVESTIGATION OF STRETCH FORMING IN RELATION TO DEEP-DRAWING AND TESTING SHEET METAL

by

BİLGİN KAFTANOĞLU, B.Sc. (Eng.)

VOLUME - I

Thesis presented for the Awards of

DOCTOR OF PHILOSOPHY

Degree
in the
Faculty of Engineering
of
University of London

and

DIPLOMA OF IMPERIAL COLLEGE
in the
Department of Mechanical Engineering

Imperial College,
London, S.W.7.

January, 1966

ABSTRACT

A theory has been developed to obtain a general solution for the axisymmetrical stretch forming of sheet metal with clamped boundary. Factors included were plastic anisotropy in the thickness direction, non-linear strain-hardening, pre-strain, variable coefficient of friction, and an approximation to the variation of thickness stress. The effects of strain history, and the moving contact of sheet metal on the punch surface with continued deformation has been incorporated. The numerical solution was programmed for the Atlas computer. Three plastic instability criteria have been studied, one of which is an integral part of the numerical solution and is new in concept.

The theoretical results were compared with the results of stretch forming tests. Agreement was very satisfactory for all but the last few stages of deformation. Near the occurrence of plastic instability greater differences between experiment and theory were observed, but the location of the instability zone and instability strains in most cases could be accurately predicted.

Extensions to the theory to solve the hydraulic bulging and deep-drawing problems have been given, but no numerical results were obtained.

Two methods of estimating the coefficient of friction in stretch forming and in radial drawing were used. It

was found that coefficients of friction in stretch forming are considerably higher than those in radial drawing.

Experimentally obtained strain hardening curves could satisfactorily be curve-fitted to a Swift type empirical law by a computer program.

Limiting Drawing Ratio (L.D.R.) in deep-drawing could be predicted satisfactorily by an empirical method from tests of three oversize blanks.

The effect on the Erichsen number of altering the main variables has been investigated. Equivalent round and strip sizes were determined. Results showed that "drawing-in" could not be completely eliminated when using serrated surfaces on blank-holder and dies. No correlation was found between the appearance of fracture in the Erichsen test and planar plastic anisotropy.

ACKNOWLEDGEMENTS

Firstly I would like to express my gratitude to my supervisor J.M.Alexander, Professor of Engineering Plasticity, Imperial College, London, for his continued attentive interest, encouragement and very useful discussions during the course of the research so freely offered at all times.

I would also like to acknowledge the Department of Technical Co-operation for financing, and The British Council for administring the Award of a CENTO Fellowship without which it would not have been possible to carry out the required study and research.

Many thanks are due to The Institute of Computer Science, University of London for the allocation of a large amount of computer time on the Atlas and the Mercury computers, and for many helpful discussions.

Thanks are also due to I.C.I. Metals Division and the Shell International Petroleum Co., Ltd., for donating some of the sheet metals and lubricant.

CONTENTS

Page No.

Page No.

Page No.

Page No.

Copies of the author's six publications (see references 45 to 49 in BIBLIOGRAPHY) are bound with this thesis.

NOTATION

A, B, n	constants in empirical strain-hardening equation, $X = A(B + \varepsilon_\ell)^n$.
a, b	semi-axes of an ellipsoid of revolution.
C_1, C_2	integration constants.
c	constant in equivalent anisotropic plastic strain-increment equation (eqn. 3.21).
E	Young's modulus.
D	die throat diameter.
D_b	diameter of undeformed blank in deep-drawing.
D_{cr}	critical or limiting blank diameter in deep-drawing.
F, G, H, L, M, N and F_o, G_o, H_o, L_o, M_o, N_o	parameters of plastic anisotropy (See eqns. 3.12 and 3.13).
F_1, F_2	radial frictional forces on a large segment of sheet metal in radial drawing (Fig.17) acting on upper and lower surfaces of the segment.
f	yield function, also a general mathematical function
F^*, $\bar{F}^*$	general mathematical functions.
g	a scalar in plastic stress-strain relationships (eqn. 3.10).
I	Erichsen number

J_1, J_2, J_3	invariants of the stress tensor σ_{ij}.
J_1', J_2', J_3'	invariants of the reduced or deviatoric stress tensor $\sigma_{ij}' = \sigma_{ij} - \sigma\delta_{ij}$.
H	blank-holder load.
h	bulge depth, and also proportionality parameter for yield stresses for anisotropic materials (eqn. 3.13).
K_1, K_2, ... , K_5	constants in equations for plastic instability (eqns. 4.8 to 4.20).
k	stress ratio = σ_3/σ_1.
k_{ro}, k_{r1}, k_{r2}, k_{r3}	intermediate quantities in Runga-Kutta integration.
ℓ	steplength in numerical integration, also distance between two gauge markings on a tensile specimen.
M, N	constants in empirical equation (12.1) used in determining L.D.R.
P	punch load in deep-drawing and stretch forming.
p	interfacial pressure between sheet metal and tool in stretch forming and deep-drawing.
p_1	interfacial pressure between sheet metal and die in deep-drawing.
p_2	interfacial pressure between sheet metal and blank-holder in deep-drawing.

Q	total load transmitted in a direction tangential to the mean surface of a bulge.
R	parameter of plastic anisotropy in tension $= \dfrac{\varepsilon_W}{\varepsilon_t}$.
r_a	current radius of rim of the blank (Fig.1).
r_b	radius to innermost point of flat portion of blank (Fig.1).
r_c	radius to centre of cup wall at point of departure from die (Fig.1).
r_d	radius to centre of cup wall at point of junction with punch profile (Fig.1).
r_e	radius of flat portion of punch head (Fig.1).
r	current radius to centre of shell wall (Fig.3).
r'	current radius to inner face of shell wall (Fig.3).
S_1, S_2, S_3	forces on a segment of sheet metal in radial drawing (See section 7.1).
s	principal stress, also degree of a polynomial.
t	current thickness of element of sheet metal.
T	time.
u	radial displacement.
v	any mathematical variable.

V_1, V_2, V_3	constants in equations for plastic bending under tension (See eqns. G.4, G.5 and G.6).
w	one less than the number of points in a tabular set of data, also width of a tensile specimen.
W	work.
X, Y, Z	yield stresses in principal directions of plastic anisotropy.
X_s, Y_s, Z_s	yield stresses in shear in the principal directions of plastic anisotropy.
x, y, z and 1, 2, 3	orthogonal co-ordinates.
x	stress ratio = $\frac{\sigma_2}{\sigma_1}$, and also independent variable.
y	dependent variable, and also co-ordinate through the thickness direction of an element in plastic bending under tension.
y_n	displacement between neutral and central surfaces in plastic bending under tension.
z	vertical co-ordinate.
α	angle, that normal to element of sheet metal makes with the vertical axis at the point of contact with punch (Fig.2).
β	rate of linear strain-hardening.
γ	angle separating two normals to the shell wall in the plane of ρ_2 (Fig.B.1).

Δ	general error function.
$\bar{\varepsilon}$, $d\bar{\varepsilon}$	total and incremental equivalent strains.
ε_ℓ, ε_w, ε_t	true strains in length, width and thickness directions in tensile test.
ε_1, ε_2, ε_3	and
$d\varepsilon_1, d\varepsilon_2, d\varepsilon_3$	total and incremental principal plastic strains also corresponding to meridional, circumferential, thickness strains in axi-symmetrical sheet metal deformation.
ε_{1b}, ε_{2b}, ε_{3b}	principal strains in plastic bending under tension in meridional, circumferential, and thickness directions.
θ	angle, that normal to an element of shell wall makes with vertical.
$d\lambda, d\lambda', d\lambda''$	scalars in plastic stress-strain relation-ships.
μ	coefficient of friction.
ξ	general function in integration.
ν	Poisson's ratio.
ρ	instantaneous radius of curvature.
ρ_1	meridional radius of curvature of the mean surface of shell wall.
ρ_1'	meridional radius of curvature of the inner surface of shell wall.
ρ_2	radius of curvature in circumferential direction of the mean surface of the shell wall.

ρ_d	radius of curvature of die profile in deep-drawing.
ρ_N	radius of curvature of neutral surface in plastic bending under tension.
$\bar{\sigma}$	equivalent stress.
$\sigma_1, \sigma_2, \sigma_3$	meridional, circumferential, and thickness stresses in axisymmetrical sheet metal deformation.
σ	hydrostatic stress ($\sigma = \frac{1}{3}\sigma_{ii}$).
σ_{1b}	mean stress in plastic bending under tension (Fig.G.1).
φ	angle, that normal to an element of cup wall makes with vertical at contact with die surface in deep-drawing (Fig.1).
ψ	angular co-ordinate in horizontal plane (Fig.3).
τ	shear stress.

<u>Operators</u>:

δ	refers to a finite increment.
d	total differential.
∂	partial differential.
δ_{ij}	Kronecker delta. $\delta_{ij} = 1$ when $i = j$ $\delta_{ij} = 0$ when $i \neq j$.
Δ	increments at a discontinuity.

Abbreviations:

L.D.R.	limiting drawing ratio in deep-drawing.
U.T.S.	ultimate tensile strength in uniaxial tension.
D.R.	drawing ratio in deep-drawing.
F.P.	flat headed punch.
H.P.	hemispherical headed punch.

Suffices:

i, j, k, ℓ	summation convention applies over values 1, 2, and 3.
m, n	designates location of a point in space and time respectively (summation convention does not apply).
u	refers to any discrete point on yield stress curve.
v	refers to total number of points on yield stress curve.
q	number of differential equations in a system.
r	a member of a family of differential equations.

Subscripts:

p	polar values of variables in stretching over punch.

o	initial values of variables.
e	effective values of variables.
m	mean values of variables.
cr	critical values of variables.

<u>Superscripts</u>:

*	increments taken along a strain path following an element.
p	plastic state of stress.

LIST OF FIGURES

PAGE NO.

PAGE NO.

PAGE NO.

In Appendices: PAGE NO.

VOLUME -II.

LIST OF TABLES

PAGE NO.